1-1-2013

Polybenzimidazole Membranes with Enhanced Mechanical Properties for Extended Lifetime Electrochemical Applications

Max Molleo
University of South Carolina

POLYBENZIMIDAZOLE MEMBRANES WITH ENHANCED MECHANICAL PROPERTIES FOR EXTENDED LIFETIME ELECTROCHEMICAL APPLICATIONS

by

Max Molleo

Bachelor of Science
Rensselaer Polytechnic Institute, 2009

Master of Science
Rensselaer Polytechnic Institute, 2009

Submitted in Partial Fulfillment of the Requirements

For the Degree of Doctor of Philosophy in

Chemistry

College of Arts and Sciences

University of South Carolina

2013

Accepted by:

Brian C. Benicewicz, Major Professor

Chuanbing Tang, Committee Member

Michael L. Myrick, Committee Member

Scott R. Crittenden, Committee Member

Lacy K. Ford, Vice Provost and Dean of Graduate Studies

DEDICATION

This dissertation is dedicated to my first educators — My parents, Edward and Marion, my brothers, Edward and Kane, and my grandparents, Jeniveve and Louie. Your unconditional love and support allowed me to pursue my passion for science. Without your guidance and encouragement, none of this would be possible.

I also dedicate this dissertation to my fiancé, Shannon. You inspire me to overcome any obstacle and to achieve my greatest potential. I cannot wait to marry you and begin our journey together as husband and wife.

ACKNOWLEDGEMENTS

I sincerely thank everyone involved with helping me complete my doctorate. Foremost, I would like to thank Dr. Brian Benicewicz for his guidance and support through my graduate studies. Our conversations, both scientific and political, have incredibly broadened my understanding of the world. I would also like to thank the other members of my doctoral committee – Dr. Chuanbing Tang, Dr. Michael Myrick, and Dr. Scott Crittenden – for their advice and encouragement throughout my candidacy.

I am honored to have worked with all of my colleagues, past and present, and appreciative of your support and assistance throughout my time in the graduate program. Darren, Atri, Jordan, and Guoqing -- you help me out beyond measure when I began my research in lab and when I was trying to adjust to life in the South. I would also like to thank Alex, Xin, Anand, and Kayley for our friendship and for keeping me sane while working side-by-side. Chris, Jim, Scott, Onn, and all of my colleagues in the Benicewicz and Tang labs, I thank you for your continuous support and I look forward to continuing our friendships in the future.

I would like to thank BASF Fuel Cells for their financial support of my research and collaborative efforts. In particular, I offer my thanks to Dr. Joerg Belack, Dr. Moritz Ehrenstein, and Dr. Gordon Calundann for their guidance. I also acknowledge DARPA for partial support of this research and the University of South Carolina for use of the HPC cluster funded by the National Science Foundation under Grant No. CHE-1048629.

ABSTRACT

After approximately 20 years of development, polybenzimidazole (PBI) chemistries and the concomitant manufacturing processes have evolved into commercially produced membrane electrode assemblies (MEAs). Commerical PBI MEAs can operate reliably for over two years at elevated temperatures of 120-180°C due to the physical and chemical robustness of PBI membranes. Recently, the Department of Energy has issued a target of 40,000-80,000 hours for stationary (i.e. combined heat and power, back-up power) polymer electrolyte membrane / proton exchange membrane (PEM) fuel cells. It is known through observation that over time, PBI membranes at 180°C creep in a direction perpendicular to compressive forces, thus also changing the composition of the membrane. To reach this goal of 40k hours, enhancement of the mechanical properties of PBI membranes is of great importance to prevent membrane creep. From a manufacturing standpoint, new approaches of improving the long-term mechanical properties of PBI membranes are needed which are cost effective and compatible with current manufacturing processes that have been developed for these unique membrane materials. Herein, we review the history of PBI gel membranes (Chapter 1) and propose multiple novel approaches to enhancing the mechanical properties of PBI membranes and report the in-depth structure-to-property relationships of these modified membranes (Chapters 2-5).

Chapter 2 and Chapter 3 each focus on the synthesis and processing of three new series of polybenzimidazole copolymer membranes (3,5-pyridine-r-2OH-PBI, 3,5-pyridine-r-para-PBI, and 3,5-pyridine-r-meta-PBI; 2,5-pyridine-r-meta-PBI, 2,5-pyridine-r-para-PBI, and 2,5-pyridine-r-2OH-PBI, respectively) using the PolyPhosphoric Acid (PPA) Process. Monomer pairs with high and low solubility characteristics were used to define phase stability-processing windows for preparing membranes with high temperature membrane gel stability. Creep compliance of these membranes (measured in compression at 180°C) generally decreased with increasing polymer content. Membrane proton conductivities decreased in a relatively constant manner with increasing membrane polymer content. Fuel cell performances of some high-solids copolymer membranes (up to 0.66 V at 0.2 A cm^{-2} following break-in) were comparable to para-PBI (0.68 V at 0.2 A cm^{-2}) despite lower phosphoric acid (PA) loadings in the high solids membranes. Long-term steady-state fuel cell studies showed these copolymer MEAs maintained a consistent fuel cell voltage of >0.6 V at 0.2 A cm^{-2} for over 9000 h. Phosphoric acid that was continuously collected from the long-term study demonstrated that acid loss is not a significant mode of degradation for these membranes. The PBI copolymer membranes' reduced high-temperature creep and long-term operational stability suggests that they are excellent candidates for use in extended lifetime electrochemical applications.

Chapter 4 offers an in-depth investigation of the structure-to-function properties of 2,5-py-r-para-PBI, 2,5-py-r-meta-PBI, 3,5-py-r-para-PBI, and 3,5-py-r-meta-PBI high polymer content membranes. Theoretical calculations of dipole strength and ground state geometries of model cmpounds (repeat units) were determined using Spartan'10

software. The complete protonation of each model compound was determined as energetically favorable. Protonation bond energy data indicates that steric hindrance partially impedes the ability of each lone electron pair of nitrogen in an sp2 orbital to bond. Data gathered from the PPA Process of these random copolymers indicate that greater proportions of flexible PBI moieties and stronger dipoles enhance the solubility of polymer chains, which consequently affects their abilities to form stable gels. High temperature creep compliance tests indicated that thermal gel stability decreased with increasing proportions of pyridines, more flexible PBI moieties, or PBIs with stronger dipoles. Higher dipole strengths of the fully protonated model compounds correlate with increased solubility and decreased gel thermal stability in phosphoric acid environments. Electrochemically, membranes composed of more soluble PBIs tend to demonstrate lower anhydrous proton conductivity and fuel cell voltage.

Chapter 5 reports the investigation of alternative approaches at modifying the structures of PBI membranes to enhance the mechanical and electrochemical properties. Research focused on the viability of a PBI polymer blending approach, the synthesis of novel polyetherbenzimidazoles (PEBIs) and polyphosphonobenzimidazoles (phos-PBI), and the inclusion of various small-molecule organic additives to PBI membranes. These efforts demonstrated mixed success and provided valuable insights into the structure-to-property relationships of PBI gel membranes.

TABLE OF CONTENTS

LIST OF TABLES

LIST OF FIGURES

GLOSSARY

Polybenzimidazoles (PBIs): A class of polymers recognized for their excellent thermal and chemical stability, PBIs have historically been spun into fibers and woven into thermal protective clothing. In the past decade, PBIs have been cast into membranes and incorporated into fuel cells.

Polymer Electrolyte Membrane (PEM): Also referred to as Proton Exchange Membranes, PEMs are semi-permeable membranes that conduct and transport protons while preventing the transmission of gases and electrons.

Membrane Electrode Assembly (MEA): A device that is comprised of a PEM that is sandwiched between two electrodes.

Conventional Imbibing: The original process of impregnating polymer membranes with dopants. The pre-cast, fully dense membranes are placed in baths of dopants and allowed to absorb the dopant which assists in proton conductivity.

PPA Process: A recently developed imbibing process, PBIs are polymerized and cast in a polyphosphoric acid (PPA) solvent. Under controlled hydrolysis conditions, Polyphosphoric acid, a good solvent for PBI, is converted into phosphoric acid, a poor solvent for PBI. A mechanically stable PBI gel membrane that is highly

doped with phosphoric acid is produced by means of a sol-to-gel transition.

Proton Conductivity: A measure of how well a material can transfer protons. In fuel cell technology, it is used to gauge the viability of proton exchange membranes.

Polymer Creep: The tendency of a polymer to move slowly or deform under continuous stress.

1. POLYBENZIMIDAZOLE FUEL CELL TECHNOLOGY: THEORY, PERFORMANCE, AND APPLICATION

1.1. INTRODUCTION TO POLYBENZIMIDAZOLE FUEL CELL SUSTAINABILITY

Alternative energy is often defined as any energy derived from sources other than fossil fuels or nuclear fission. These alternative energy sources, which include solar, wind, hydro, and geothermal energy, are considered renewable because they are naturally replenished and their supply is seemingly limitless. In contrast, the Earth's supply of fossil fuels is constantly being diminished. Fossil fuels, which include crude oil, coal, and natural gas, continue to be the dominating sources of energy in the world (Figure 1.1). Fossil fuels provide more than 86% of the total energy consumed globally [1]. In 2008, over two-thirds of the electrical energy and 97% of the transportation energy in the US was produced from these non-renewable sources [2]. It is predicted that the global demand for fossil fuels will continue to increase over the next 10-20 years due to economic growth. One may conclude that the importance of renewable energy will steadily increase as Earth's supply of fossil fuels continues to be depleted.

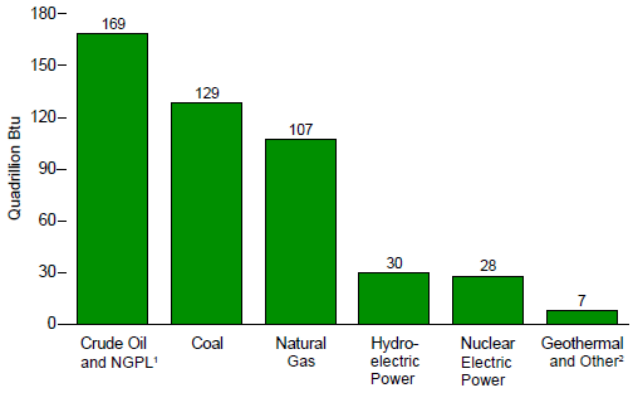

Figure 1.1. Global production of energy in 2006 by source. [1]Natural Gas Plant Liquid. [2]Net electricity generation from wood, waste, solar, and wind [1].

Polymer electrolyte membrane (PEM) fuel cells, also known as proton exchange membrane fuel cells (PEMFCs), are energy conversion devices that could provide the world with clean and efficient energy. Due to their excellent energy production, inexpensive starting materials, and lack of pollutant byproducts, these cells have exponentially gained in popularity over the past decade. Electricity is produced at the heart of the fuel cell by the membrane electrode assembly (MEA), a component that is comprised of a proton exchange membrane sandwiched between two electrodes. Fueled by a hydrogen-based source, a metal catalyst at the anode splits the hydrogen into protons and electrons. As the protons are transported through the proton electrolyte membrane to the cathode, the electrons provide electrical work by traveling around the membrane through an external circuit from the anode to the cathode. The protons and electrons react with an oxidant (typically air or pure oxygen) at the cathode to form water, thereby completing the electrochemical cycle. Hydrogen gas is commonly used as a fuel source for the cells, but other fuels such as methane, methanol, and ethanol have been explored.

PEM fuel cells provide multiple advantages over conventional fossil fuel energy production. Because water is the only byproduct of the electrochemical process, these fuel cells are clean and environmentally friendly. If one considers the tremendous amount of carbon dioxide created by energy production on the global scale (Figure 1.2), PEM fuel cells offer a method to significantly reduce hazardous gas emissions. Minimal moving parts reduces the amount of maintenance of each cell, and the lack of combustion significantly decreases the amount of harmful pollutants such as sulfur oxides and nitrogen oxides. In addition, PEM fuel cells are much more efficient at producing energy (this is discussed in detail in Section 1.3), and much like a combustion engine, the cell can run continuously as long as fuel and oxidant are provided. Although fuel cells are an environmentally friendly energy conversion device, one must consider the manner in which hydrogen is gathered. Both hydrogen production and conversion from chemical to electrical energy need to be sustainable to make the overall process sustainable. Hydrogen production, however, is out of the scope of this chapter.

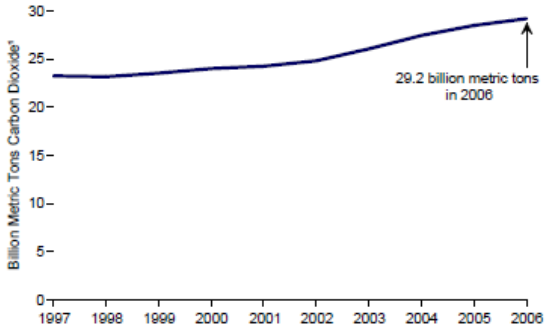

Figure 1.2. Global production of carbon dioxide annually from 1997-2006. [3]

The efficiency of a PEM fuel cell is largely dependent on the materials used and their arrangement in the cell. Fuel cells use an array of different catalysts, electrodes,

membranes, and dopants, each of which function under specific operating conditions. Cells that use low-boiling dopants, such as water, operate at approximately 60-80^{o}C to avoid vaporization of the proton-transfer agent. Large heat exchangers are required to ensure the heat generated by the cell does not vaporize the electrolyte. Consequently, system complexity is increased as extra components and controls are required to ensure that the membrane remains hydrated during operation. Moreover, cell operation at such low temperatures allows trace amounts of reformate byproducts, especially carbon monoxide, to bind to the catalyst. These highly-competitive, non-reversible reactions "poison" the catalyst, thereby decreasing and possibly terminating the functionality of the fuel cell. Therefore, low temperature fuel cells require an extremely pure fuel source.

In contrast to low-temperature cells, high-temperature PEMs use high-boiling dopants, such as phosphoric acid and sulfuric acid, and function at temperatures of 120-200^{o}C. Because the cell is able to run at elevated temperatures, much smaller heat exchangers are required. Operating at higher temperatures allows fuel pollutants to bind reversibly to the catalyst, which helps to prevent catalyst poisoning. Comparatively, high-temperature PEMs can use reformed gases with much higher levels of impurities and lower reformation costs. Furthermore, high temperatures typically improve both the electrode kinetics and operating abilities of the cell. This chapter reports on the chemistries and sustainable usages of PBI-based high temperature PEMFCs.

1.2. History and Technical Information of Polybenzimidazole Membranes

Polybenzimidazoles (PBIs) are a class of polymers recognized for their excellent thermal and chemical stability. PBI is used in multiple applications including matrix

resins, high strength adhesives, thermal and electrical insulating foams, and thermally resistant fibers. PBI fibers were originally synthesized in the early 1960's by a cooperative effort of the United States Air Force Materials Laboratory with Dupont and the Celanese Research Company. One of the first PBIs to be widely investigated was poly(2,2'-*m*-phenylene-5,5'-bibenzimidazole), which is commonly referred to as *m*-PBI (Figure 1.3). Because *m*-PBI is non-flammable, resistant to chemicals, physically stable at high temperatures, and can be spun into fibers, this polymer has been used in astronaut space suits, firefighter's turnout coats and suits, and high temperature protective gloves.

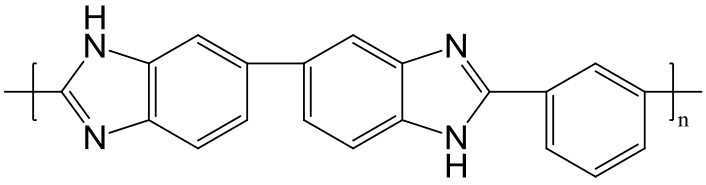

Figure 1.3. Chemical structure of poly(2,2'-*m*-phenylene-5,5'-bibenzimidazole) (*m*-PBI)

Acid-doped polybenzimidazole membranes are excellent candidates for high-temperature fuel cells because of their thermal and chemical stability and proton conducting ability. The stability of PBIs is attributed to its aromatic structure (alternating single and double bonds) and the rigid nature of its bonds [4]. While the acid-doped membrane structure allows protons to flow from one side to the other, it acts as a barrier to the crossover of gases and electrons. The chemical stability of PBIs allows the membranes to withstand the chemically reactive environments of the anode and cathode. Furthermore, the basic nature of the polymer allows it to be highly doped with phosphoric or sulfuric acid. The dopants interact with the polymer matrix and provide a network through which protons can be transported. These acids are used as electrolytes

because of their high conductivity, thermal stability, and enhanced proton-transport capabilities. It is important to note that the proton conductivity of PBI membranes without a dopant is negligible. For liquid phosphoric acid, the proton jump rate is orders of magnitude larger than the diffusion of the phosphoric acid molecule as a whole [5]. Additionally, it has been reported that both protons and phosphate moieties have a substantially decreased diffusion coefficient when blended with basic polymers as opposed to liquid phosphoric acid [6]. Therefore, a heterogeneous, two-phase system in which the PBI membrane is phase-separated and imbibed with phosphoric acid has a higher conductivity than its homogeneous counterpart [7]. The partial charges of the phosphate ions involved with proton transfers increases charge delocalization, which lowers the overall energy barrier of proton transfer [8]. The proton transfer mechanism of large proton vehicle species (such as phosphate ions) can be initiated by local vibrations of the vehicle species. In comparison, the amount of energy required to induce proton transfer small proton vehicle species such as water is comparable to the amount of energy required to diffuse the entire small proton vehicle.

1.2.1. Synthesis of Polybenzimidazoles

One of the first PBIs membranes investigated for fuel cell use was poly(2,2'-*m*-phenylene-5,5'-bibenzimidazole) (*m*-PBI). At the time, there was a vast amount of research previously reported on *m*-PBI and it was renowned for its excellent thermal and mechanical properties [5]. The polymer is synthesized by the reaction of 3,3',4,4'-tetraaminobiphenyl (TAB) with diphenylisophthalate (DPIP) during a melt/solid polymerization (Scheme 1.1). The resulting polymer is extracted and has an inherent viscosity (IVs) between 0.5-0.8 dL g^{-1}, which corresponds to a polymer with low to

moderate molecular weight. The *m*-PBI is further purified by dissolving it in a solution of N,N-dimethylacetamide and lithium chloride (DMAc/LiCl) under 60-100 psi and 250 ^{o}C and then filtering; this step removes any crosslinked *m*-PBI. The polymer is then cast as a film and dried at 140 ^{o}C under vacuum to evaporate the solvent. The *m*-PBI membrane is washed in boiling water to remove any residual DMAc/LiCl solution trapped in the polymer matrix. After the polymer has been dried, an acid bath is used to dope the membrane; the doping level of the membrane can be partially controlled by varying the concentration of acid in the bath. Originally, this conventionally imbibed process created membranes with molar ratios of phosphoric acid/polymer repeat unit (PA/PRU) approximately 6-10 [9]. A "direct acid casting" (DAC) technique was later developed to allow the PBI membrane to retain more PA [10]. Both the conventional imbibing process and DAC were developed following the research performed by Jean-Claude Lassegues, who was one of the first scientists that investigated basic polymeric-acid systems (a summary of his work is reviewed in reference [11]). The DAC technique consists of extracting low molecular weight PBI components from PBI powder, and then dissolving the high molecular weight PBI components in trifluoroacetic acid (TFA). Phosphoric acid is added to the TFA/PBI mixture, which is then cast onto glass plates with a casting blade. One may tune the doping level of the polymer by adjusting the amount of phosphoric acid that is added to the TFA/PBI mixture. However, as one increases the PA doping level of a DAC PBI membrane, its mechanical strength decreases to the point where it can no longer be used in a fuel cell. Modern imbibing processes can increase the PA/PBI ratio to 12-16, and these fuel cell membranes are reported to have proton conductivities as high as 0.08 S cm^{-1} at 150 ^{O}C at various humidities.

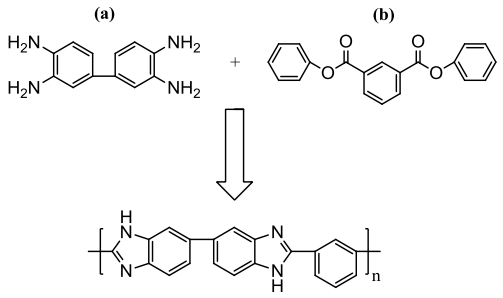

Scheme 1.1. Polymerization of *m*-PBI from (a) 3,3',4,4'-tetraaminobiphenyl and (b) diphenylisophthalate

A novel synthetic process for producing high molecular weight PBIs, the "PPA Process" was developed at Rensselaer Polytechnic Institute with cooperation from BASF Fuel Cell GmbH. This process has previously been discussed by Xiao *et al. [12]*. The general synthesis of PBI by this method requires the combination of a tetraamine with a dicarboxylic acid in polyphosphoric acid (PPA) in a dry environment. The step-growth polycondensation reaction typically occurs around 200^{o}C for 16-24 hours in a nitrogen atmosphere, producing high molecular weight polymer. This solution is cast directly from PPA as a thin film on a substrate, and upon absorption of water, the PPA hydrolyzes *in situ* to form phosphoric acid. Note that PPA is a good solvent for PBI while PA is a poor solvent. Under controlled hydrolysis conditions, a mechanically stable PBI gel membrane that is highly doped with phosphoric acid is produced. The multiple physical and chemical transformations that explain the solution-to-gel phase transition are summarized in Figure 1.4.

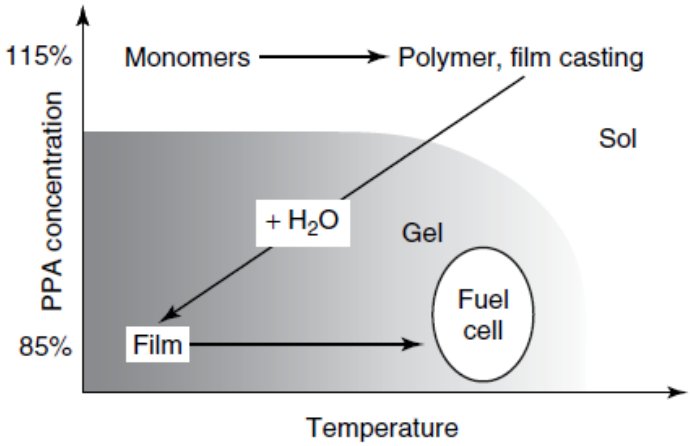

Figure 1.4. State diagram of the PPA Sol-Gel Process [12]

The PA doped *m*-PBI fuel cell membrane maintains thermal and physical stability while operating at high temperature. To illuminate the fundamental differences in polymer film architecture, polymers with similar physical characteristics were prepared by the conventional and PPA Process (Table 1.1). Even though the ratio of phosphoric acid-to-polymer repeat unit (PA/PRU) achieved by both processes were nearly identical, the PPA Process produces membranes with much higher proton diffusion coefficients and conductivities. The higher proton diffusion coefficients of membranes produced by the PPA Process versus conventionally imbibed membranes were confirmed by NMR [13]. One can conclude that the PPA Process creates a membrane with a proton transport architecture superior to that of the conventionally imbibed PBI membrane. In addition, inherent viscosity data indicates that the PPA Process produces polymers of much higher molecular weight [12]. It was subsequently shown that improved membrane morphology and increased molecular weight allow the polymer to retain much more phosphoric acid than traditionally cast PBI membranes. An increased PA doping level typically improves the conductivity of the membrane and may even increase the performance of the cell.

Table 1.1. Comparison of conventionally imbibed *m*-PBI vs. *m*-PBI synthesized from the PPA Process [14]

IV[a] (dl g^{-1})	Film process	Polymer (wt%)	PA (wt%)	Water (wt%)	PA/PBI (molar ratio)	Proton diffusion coefficient[b] ($cm^2\ s^{-1}$)	Conductivity[c] ($S\ cm^{-1}$)
0.89	Conventionally imbibed	15.6	60.7	23.7	12.2	10^{-7}	0.048
1.49	PPA process	14.4	63.3	22.3	13.8	3×10^{-6}	0.13

[a] Inherent viscosity (IV) was measured at a polymer concentration of 0.2 g dl^{-1} in concentrated sulfuric acid (96%) at 30 °C, using a Canon Ubbelohde viscometer
[b] Estimation of upper bound for conventionally imbibed *m*-PBI at 180 °C; PPA-prepared *m*-PBI measured at 180 °C
[c] Measured at 160 °C after an initial heating to 160 °C to remove water

1.2.2. Properties and Performance of Synthetically Modified PBI

In this chapter the synthesis of significant PBI membranes (Figure 1.5) and their use in fuel cells are described. Synthetically modified PBIs are investigated for enhanced thermo-oxidative stability, solubility, and flexibility; these attributes allow for improved processability and production of membranes with good chemical and mechanical properties. All PBI membranes are produced by means of step-growth polycondensation reactions and are generally imbibed by either the conventional technique or made by the PPA Process. To synthesize modified polymers, one may either polymerize modified monomers or use post-polymerization crosslinking or substitution reactions. The following sections briefly detail the syntheses of PBI derivatives and their performances as fuel cell membranes.

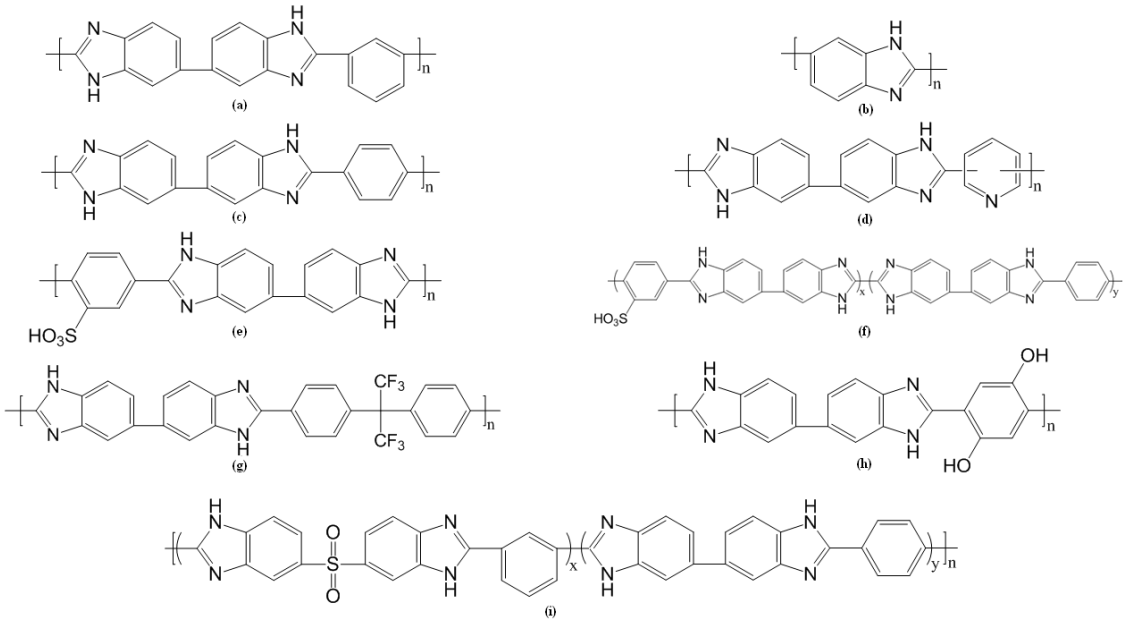

Figure 1.5. Various synthetically-modified polybenzimidazoles for use in fuel cells. (a) *meta*-PBI, (b) AB-PBI, (c) para-PBI, (d) py-PBI, (e) s-PBI, (f) s-PBI/para-PBI random block copolymer, (g) 6F-PBI, (h) 2OH-PBI, (i) meta-SPBI / para-PBI segmented block copolymer

1.2.2.1 Poly(2,2'-(1,3-phenylene)5,5'-bibenzimidazole) – META-PBI

One of the first PBI membranes investigated for fuel cell use was Poly(2,2'-(1,3-phenylene)5,5'-bibenzimidazole) (*m*-PBI, Figure 1.5-a). As previously discussed, the film can be processed by using either the conventional imbibing method or the PPA Process. Using the conventional imbibing method, the inherent viscosity of the membrane is usually between 0.50-1.00 dL g^{-1} at 30 ^{o}C, which indicates polymers of moderate molecular weight. In contrast, *m*-PBI membranes synthesized and doped via the PPA Process have inherent viscosities of approximately 1.00-2.35 dL g^{-1} at 30 ^{o}C, which corresponds to higher molecular weight polymers [9]. Using the PPA process, higher molecular weight polymers have contributed to higher doping levels. Phosphoric acid doping levels for conventionally prepared *m*-PBI ranged from 6-10 moles PA/PRU,

whereas the doping levels for polymer films prepared via the PPA Process range from 14-26 moles PA/PRU [4]. Trends show that the mechanical stability of conventionally prepared membranes decrease as the doping level increases and/or as the molecular weight of the polymer decreases. The doping level, casting technique, temperature, and humidity all influence the conductivity of a *m*-PBI membrane. Under various humidities, conventionally prepared *m*-PBI membranes have been reported having conductivities in the range of 0.04-0.08 S cm^{-1} [15]. Using the PPA Process, the conductivity values of *m*-PBI membranes are typically higher than that of the conventionally imbibed process. One study [16] reported *m*-PBI membranes formed by the PPA process as having a conductivity of 0.13 S cm^{-1} at 160 ^{O}C under non-humidified conditions.

Phosphoric acid doped *m*-PBI membranes that have been formed by the conventional imbibing method have been extensively studied for use in fuel cells. Li et al. [17] demonstrated that a membrane with 6.2 PA/PRU doping level obtains a current density of approximately 0.7 A cm^{-2} at 0.6 V using hydrogen and oxygen gases; these results were promising because the gases were not humidified. Zhai et al. [18] studied the degradation mechanisms of the PA/*m*-PBI system by continuously operating it at 0.640 A cm^{-2} at 150 ^{O}C with unhumidified hydrogen and oxygen for 550 hours; the fuel cell was operated intermittently the last 50 hours with shutoffs every 12 hours. The voltage increased from 0.57 to 0.66 V during the beginning 90 hour activation period, and the following 450 hour period showed a steady decrease to 0.58 V. The performance of the system rapidly decreased in the following 10 hours due to agglomeration of the platinum from the catalyst, leaching of the phosphoric acid, and hydrogen crossover. Kongstein et al. [19] employed use of a dual layer electrode to prevent the oxidation of carbon in the

polymer membrane, which can occur in acidic environments at high voltages. This electrode would improve the structural integrity of the polymer and help prevent hydrogen crossover from occurring. The PA/*m*-PBI membrane had a maximum of 0.6 V at 0.6 A cm^{-2} with a maximum power density of 0.83 W cm^{-2} at 0.4 V. These performances were lower than that of other PEM systems, such as Nafion, but were still impressive because they could be run at much higher temperatures.

1.2.2.2. POLY(2,5-POLYBENZIMIDAZOLE): AB-PBI

Commonly referred to as AB-PBI, poly(2,5-polybenzimidazole) has a much simpler structure than that of *m*-PBI and other polybenzimidizoles (Figure 1.5-b). Whereas *m*-PBI is synthesized from 3,3',4,4'-tetraaminobiphenyl and DPIP, AB-PBI is polymerized from a single monomer, 3,4-diaminobenzoic acid (DABA). This monomer is commercially available and is less expensive than the starting materials of *m*-PBI. The polymer membrane can be cast and imbibed with phosphoric acid by the conventional imbibing method in a mixture of methanesulfonic acid (MSA) and phosphorous pentoxide (P_2O_5) [20] or DMAc. It can also be cast by direct acid casting using trifluoroacetic acid (TFA) [10, 15] or by the PPA Process [10, 21-23]. AB-PBI membranes prepared by the conventional imbibing method had IV values around 2.0-2.5 dL g^{-1} as reported by Asensio et al. [23] and 6-8 dL g^{-1} by Litt et al. [15]. Polymers produced from recrystallized DABA by the PPA Process have IV values greater than 10 dL g^{-1} [24]; however, membranes of AB-PBI could not be easily formed via the PPA Process because of the polymer's high solubility in acids.

Because AB-PBI has a high concentration of basic sites (amine and imine groups), it has a high solubility and affinity to acids. Due to this affinity, it can be doped with phosphoric acid and sulfonated with sulfuric acid. Sulfonation of AB-PBI (sAB-PBI) is performed by soaking the pre-cast polymer in sulfuric acid followed by treating the mixture with heat. Asensio et al. [23] reported sAB-PBI/PA membranes having an enhanced conductivity over that of AB-PBI/PA and to be both mechanically strong and thermally stable. Using the direct casting method from MSA-P_2O_5, Kim et al. [20] produced AB-PBI/PA membranes with conductivities similar that of Asensio, having values ranging from 0.02-0.06 S cm^{-1} at 110 ^{O}C with no humidification. The conductivity values and physical-chemical properties resemble that of *m*-PBI, making it a good candidate for fuel cell use.

Yu [25] synthesized *p*-PBI-block-AB-PBI membranes to lower the membrane's solubility in acids while maintaining a high acid doping level. Different molar ratios of each polymer block were synthesized, and their conductivities and acid doping levels were investigated. As detailed in Table 1.2, the proton conductivities of the segmented block copolymers were enhanced by an order of magnitude over that of native AB-PBI. Stress-strain studies showed that these block copolymers were strong enough to be used in fuel cell tests. Polarization curves (Figure 1.6) of these membranes illustrate that copolymers II, III, and IV have excellent fuel cell properties (approximately 0.6 V at 0.2 A cm^{-2}); polarization curves for copolymer V and VI could not be measured due to poor thermal stability of the membrane (re-dissolution) at 160 ^{o}C.

Table 1.2. Percent composition, acid doping level, and proton conductivity data for various *p*-PBI-block-AB-PBI membranes [25].

	Para-PBI/AB-PBI (mole ratio, x/y)	acid doping level (PA/ 2 benzimidazole)	proton conductivity (S/cm @ 160 °C)	Membrane composition (%)		
				polymer	H_3PO_4	water
I	100/0	42.9	0.25	4.13	60.38	35.11
II	75/25	19.1	0.25	8.68	58.09	33.22
III	50/50	24.1	0.27	6.59	54.53	38.88
IV	25/75	21.8	0.23	7.79	63.31	28.90
V	10/90	17.3	0.15	8.84	63.23	27.94
VI	0/100	N/A	N/A			

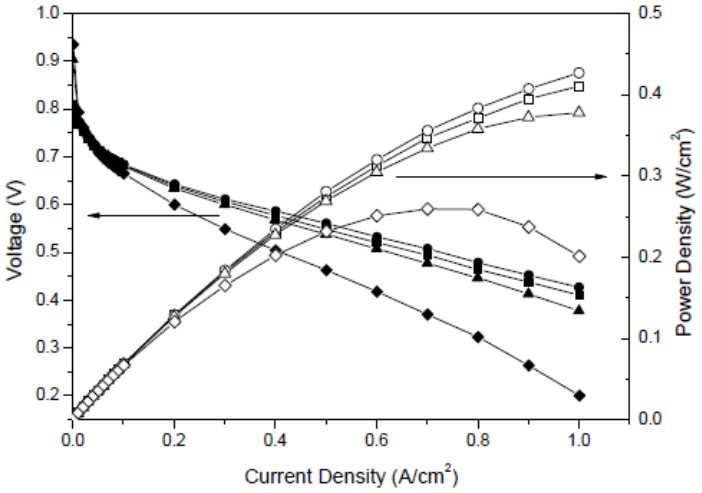

Figure 1.6: Polarization curves (filled symbols) and power density curves (unfilled symbols) of *p*-PBI (Polymer I, ■ □) and *p*-PBI-block-AB-PBI membranes (75/25, Polymer II, ●○, 50/50 Polymer III, ▲Δ, 25/75, Polymer IV, ♦◊) at 160°C with H_2 (1.2 stoichiometry)/Air (2.0 stoichiometry) under atmospheric pressure [25].

1.2.2.3. POLY(2,2'-(1,4-PHENYLENE)5,5'-BIBENZIMIDAZOLE): PARA-PBI

Poly(2,2'-(1,4-phenylene)5,5'-bibenzimidazole) (*p*-PBI, Figure 5-c) is one of the highest performing PBI membranes for high-temperature fuel cell use**.** Due to the rigid nature of *p*-PBI, high molecular weight polymers have typically been difficult to fabricate

or process. The first reported high molecular weight *p*-PBI with an IV value of 4.2 dL g^{-1} was synthesized in 1975 by the United States Air Force Materials Laboratory [26]. Because it could not be spun into fibers as easily as *m*-PBI, *p*-PBI was not investigated further until after the turn of the century. Using the PPA Process, Xiao et al. [12] and Yu et al. [27] synthesized high molecular weight *p*-PBI with IV values as high as 3.8 dL g^{-1}. The PA doping level of the corresponding polymer membranes was >30 mol PA/PRU, allowing the membrane to achieve a conductivity of 0.24 S cm^{-1} at 160 ^{O}C. Xiao and Yu showed that *p*-PBI membrane achieves a much higher acid doping level and conductivity than that of *m*-PBI, which only achieves a doping level of 13-16 mol PA/PRU with a conductivity of 0.1-0.13 S cm^{-1}. Because *p*-PBI had excellent mechanical properties at this high doping level, it was a prime candidate for fuel cell performance tests.

The polarization curves of an MEA using *p*-PBI produced by the PPA Process at various temperatures are shown in Figure 1.7. Hydrogen was used as the fuel and air was used as the oxidant. The *p*-PBI outperformed the *m*-PBI at all temperatures, and the performance of the MEA increased as the temperature increased. Using a load of 0.2 A cm^{-2}, the cell was able to produce a voltage of 0.606 V at 120 ^{O}C; upon raising the temperature to 180^{O}C, the voltage increased to 0.663 V. This was especially promising because the gases were unhumidified.

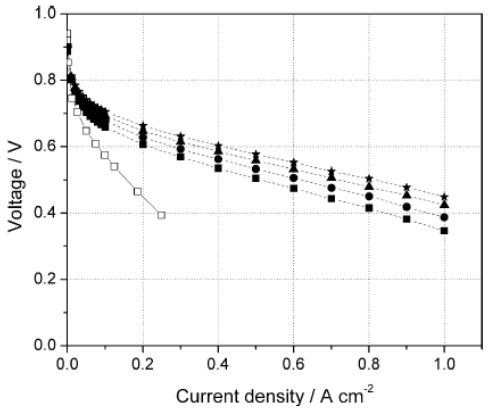

Figure 1.7. Polarization curves of PPA-processed *p*-PBI MEA using hydrogen/air at 120^{O}C (squares), 140^{O}C (circles), 160^{O}C (triangles), and 180^{O}C (stars). Open squares represent DMAc cast *m*-PBI MEA at 150^{O}C [27].

1.2.2.4. PYRIDINE-PBI

Pyridine polybenzimidazoles (py-PBIs, Figure 1.5-d) have been investigated for their use in fuel cells because of their high concentration of basic sites (amine and imine groups). Similar to AB-PBI, the high concentration of basic sites allow these polymers to have a high affinity to acids. The pyridine moiety is commonly combined with the traditional PBI structure by including it as part of the backbone structure.

Xiao et al. synthesized an array of py-PBIs that have the pyridine moiety as part of the polymer backbone [12, 28, 29]. These polymers were synthesized by a reaction of 2,4-, 2,5-, 2,6-, or 3,5-pyridine dicarboxylic acid with 3,3',4,4'-tetraaminobiphenyl (TAB) using the PPA Process. Exceedingly pure monomers were required to polymerize the py-PBIs, and IV values of 1.0-2.5 dL g^{-1} were obtained. The 2,4- and 2,5-py-PBI membranes formed mechanically strong films, whereas the 2,6-py-PBI membrane was mechanically weak and the 3,5-py-PBI was unable to form films due to high solubility in PPA. All of the py-PBI structures were thermally stable in both nitrogen and air in

temperatures up to 420 ^{O}C. The 2,5- and 2,6-py-PBI were reported as having a conductivities of 0.2 S cm^{-1} and 0.1 S cm^{-1} at 160-200 ^{O}C, respectively. The 2,5-py-PBI was found to have the most mechanically robust structure. It was hypothesized that the enhancement of mechanical properties was due to its *para*-orientation as opposed to the other py-PBIs having a *meta*-orientation. In addition, the doping level of 2,5-py-PBI averaged 20 mol of phosphoric acid per polymer repeat unit. Because PPA processed 2,5-py-PBI was an extremely good candidate for fuel cell testing, polarization tests of the MEA were performed (Figure 1.8). The platinum loading on the anode and cathode was 1.0 mg cm^{-2} with 30% Pt in Vulcan XC-72 carbon black. The active area for the MEA was 10 cm^{2}. The membranes used non-humidified H_2/O_2 and higher temperatures improved the performances of 2,5-py-PBI MEA.

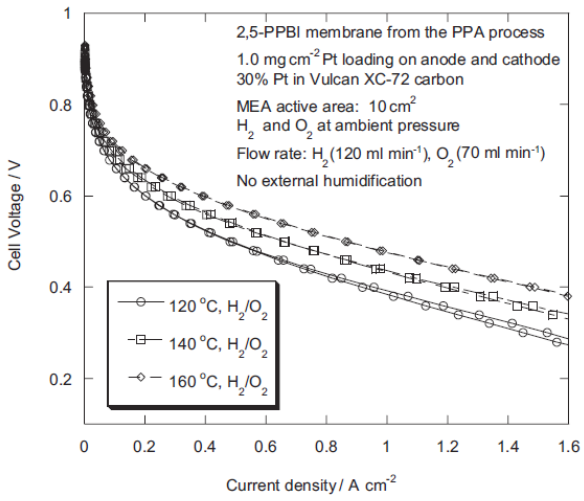

Figure 1.8. Polarization curves under hydrogen and oxygen gases at various temperatures of PA-doped 2,5-py-PBI membranes [30].

There have been studies indicating that blends of PBI polymers with pyridine-containing polymers could prove useful in a high-temperature PEM fuel cell. Kallitsis et

al. [31] combined commercially supplied *m*-PBI with an aromatic polyether that contained a pyridine moiety in the main chain (PPyPO); these polymer blends were then soaked in 85% wt PA. Dynamic mechanical analysis of a 75/25 PBI/PPyPO block copolymer showed reasonable mechanical strength and flexibility. The conductivity of this copolymer was not reported, but the conductivity of 85/15 PBI/PPyPO block copolymer was 0.013 S cm^{-1} at a relatively low PA doping level. Further investigation of these systems is required to prove its utility as a fuel cell membrane.

1.2.2.5. SULFONATED PBI

Sulfonated aromatic polymers have been widely investigated [32-42] for fuel cell use due to their enhanced physical and chemical robustness, acid and water retention, and conductivity over that of Nafion and other perfluorosulfonic acid-type polymers. Thus, due to the enhanced properties of PBI, it was logical to investigate the physical and chemical properties of sulfonated PBI (s-PBI) membranes. Sulfonation of PBI typically occurs by either direct sulfonation of the polymer backbone [23, 43, 44], grafting sulfonated moieties onto the backbone [23, 45], or by a polycondensation reaction that bonds aromatic tetraamines to sulfonated aromatic diacids [46-48]. Compared to other sulfonation methods, polycondensation reactions provide more control over the degree of sulfonation.

Mader investigated the physical and chemical properties of s-PBI with PA as the dopant (Figure 1.5-e) [48]. The polymer was synthesized by two different synthetic pathways; the first was a direct polycondensation reaction of 2-sulfoterephthalic acid (s-TPA) and TAB using the PPA Process, and the second was a post-sulfonation reaction of

p-PBI using concentrated sulfuric acid. The IV values for the polymer membranes derived from the polycondensation reaction ranged from 1-2 dL g^{-1}; these polymers had sufficiently high molecular weights to allow strong films to be cast. In addition, these polymer membranes could achieve doping levels between 28-53 mol PA/PRU, which resulted in significantly high conductivity values (all above 0.1 S cm^{-1} at all temperatures between 100-200 ^{O}C).

Based on the preliminary data, s-PBI polymer membranes were excellent candidates for fuel cell tests. Polarization tests were run using an s-PBI membrane with an IV value of 1.71 dL g^{-1}, a PA doping level of 52.33 mol PA/PRU, and a conductivity of 0.248 S cm^{-1}; the results are depicted in Figure 1.9. The s-PBI membrane exhibited its highest performance at 160 ^{O}C, producing 0.6788 V at a current density of 0.2 A cm^{-2}. This performance compares well to that of other PBIs produced by the PPA Process, which is typically around 0.6-0.7 V at 0.2 A cm^{-2}.

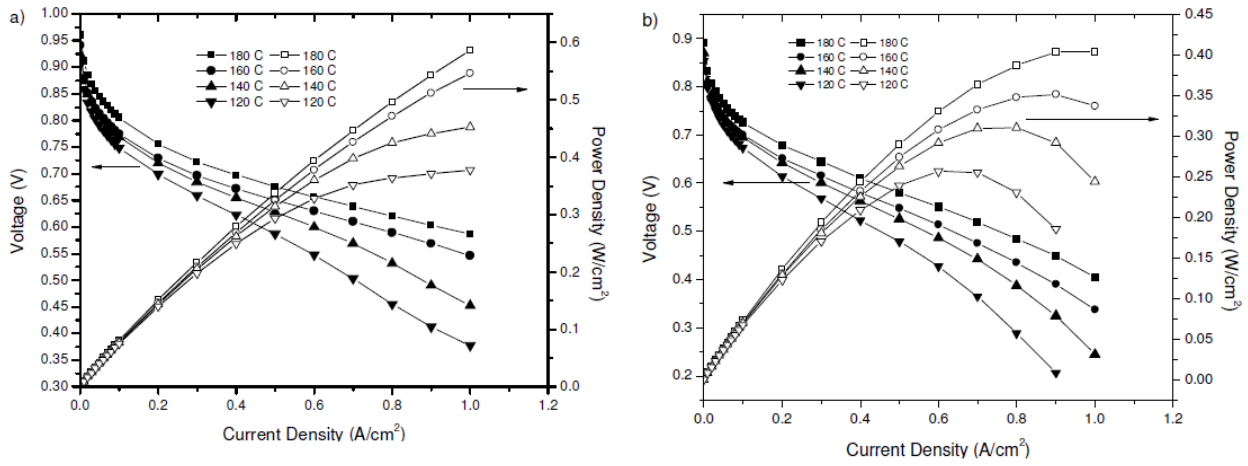

Figure 1.9. Polarization curves (filled symbols) and power density curves (unfilled symbols) of s-PBI using (a) hydrogen and oxygen and (b) hydrogen and air [48].

The s-PBI homopolymer was shown to have both excellent resistance to gas impurities and excellent longevity. A reformate gas composed of 70% hydrogen, 28% carbon dioxide and 2% carbon monoxide was used as the fuel while air was used as the oxidant. As depicted in Figure 1.10, the fuel cell performance increased with increasing temperature; this is explained by the retardation of carbon monoxide poisoning that occurs at high temperatures. The performance loss of s-PBI MEA was measured by holding the MEA at 0.2 A cm^{-2} at 160 ^{O}C for 1200 hours using H_2/O_2. After reaching stabilization at the 343rd hour, the MEA had a voltage loss of 0.024 mV hr^{-1} for the remainder of the test.

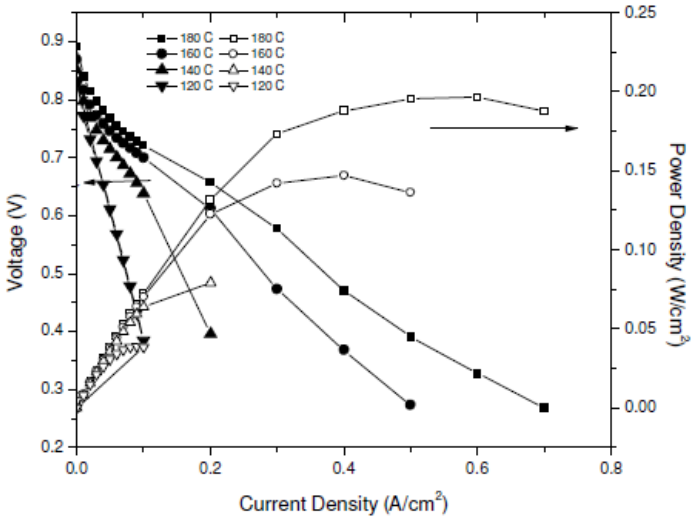

Figure 1.10. Polarization curves (filled symbols) and power density curves (unfilled symbols) of s-PBI using reformate and air [48].

Mader also investigated s-PBI/*p*-PBI random copolymers (Figure 1.5-f) for use in fuel cells [48]. The random copolymer was synthesized by reacting TAB, TPA, and s-TPA in a reaction flask and the membrane was cast via the PPA Process. High molecular weight polymers were achieved with IV values exceeding 1.8 dL g^{-1}; this allowed for

mechanically strong films to be cast. As the ratio of s-PBI/*p*-PBI decreased, the molecular weight of the polymer proportionally increased. Higher PA loading was seen at lower s-PBI/*p*-PBI ratios, indicating a stronger attractive force between PA and *p*-PBI than PA and s-PBI. The PA loading values almost directly corresponded to the conductivity of the membranes. The 75/25 s-PBI/*p*-PBI membrane had a PA loading value of 20.32 mol PA/PBI and a conductivity of 0.157 S cm^{-1}, whereas the 25/75 s-PBI/*p*-PBI membrane had a PA loading value of 40.69 mol PA/PBI and a conductivity of 0.291 S cm^{-1}.

Fuel cell performance tests were conducted on the random copolymers. Even though the 25/75 s-PBI/*p*-PBI random copolymer had a higher conductivity than that of p-PBI homopolymer, it was found that all of the random copolymers showed lower performance than *p*-PBI. The 50/50 and 75/25 s-PBI/*p*-PBI random copolymers had lower performance than the s-PBI homopolymer at all PA doping levels. However, the 25/75 s-PBI/*p*-PBI random copolymer performed comparably to the s-PBI homopolymer at equivalent PA doping levels.

1.2.2.6. PBI-INORGANIC COMPOSITES

For conventionally prepared PBI membranes, as the acid doping levels of PBIs increase, the conductivity and overall performance of the PBI membranes also tend to increase. However, as high acid doping levels are reached for PBI membranes, the mechanical strength of the membrane significantly decreases. Inorganic fillers for PBI membranes have been investigated to improve membrane film strength, thermal stability,

water and acid uptake, and conductivity. These composite membranes have only been examined using *m*-PBI and the conventional casting method.

He et al. investigated the use of zirconium phosphate (ZrP) in a PA/PBI system [49]. The conductivity of *m*-PBI with a doping level of 5.6 PA/PRU increased from 0.068 S cm^{-1} to 0.096 S cm^{-1} with the addition of 15 wt% ZrP at 200 ^{O}C and at 5% relative humidity. As seen in Figure 1.11, the conductivity of the membrane increased as the relative humidity and temperature of its environment increased. Conductivities of other inorganic fillers, such as phosphotungstic acid, silicotungstic acid, and tricarboxylbutylphosphonate, are comparable or lower than that of ZrP. Unfortunately, there have been no fuel cell performance tests published on these systems. Overall, these inorganic fillers improved the conductivity of *m*-PBI membranes.

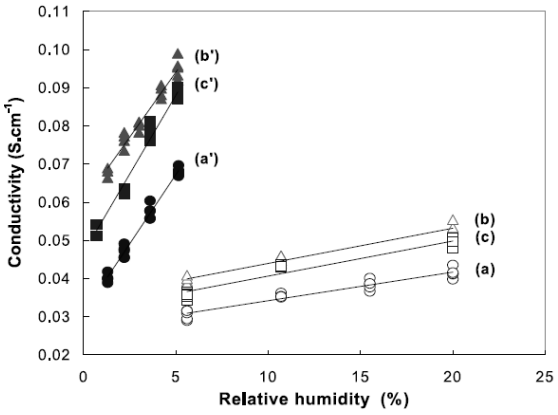

Figure 1.11: Conductivity study of ZrP/*m*-PBI system for (a) *m*-PBI at 140^{O}C, (a') *m*-PBI at 200^{O}C, (b) 15wt% ZrP in *m*-PBI at 140^{O}C, (b') 15wt% ZrP in *m*-PBI at 200^{O}C, (c) 20wt% ZrP in *m*-PBI at 140^{O}C, and (c') 20wt% ZrP in *m*-PBI at 200^{O}C [49].

1.2.2.7. OTHER MODIFIED PBIS

Multitudes of other organically-modified PBI membranes exist that include, but are not limited to, fluorinated PBI, ionically and covalently crosslinked PBI, PBI blends, and a wide variety of PBI copolymers. Because there are far too many to describe, this subsection will highlight select PBI membranes that have not been included in the prior subsections.

Qian et al. investigated the use of hexafluoroisopropylidene-containing polybenzimidazole (6F-PBI, Figure 1.5-g) in fuel cells [50]. The polymer was synthesized via the PPA Process through the reaction of TAB with 2,2-Bis(4-carboxyphenyl) hexafluoropropane in PPA. High molecular weight polymer with an IV value of 0.98 dL g^{-1} was achieved. Although the PA doping level of 6F-PBI was considerably high (30-40 mol PA/PRU), the membrane only achieved a peak conductivity value of 0.09 S cm^{-1} at 180 ^{O}C. This is lower than that of PPA-processed *p*-PBI that achieved approximately 0.25 S cm^{-1} at 160 ^{O}C.

The mechanical strength of 6F-PBI at high PA doping levels was strong enough to fabricate a membrane for fuel cell testing. Polarization and power density curves of 6F-PBI using hydrogen and reformate gases as fuel are illustrated in Figure 1.12. Using hydrogen as fuel and air as the oxidant, the 6F-PBI MEA achieved a steady-state voltage of 0.58 V at a current density of 0.2 A cm^{-2}. When oxygen was used as the oxidant at the same current density, the steady state voltage increased to 0.67 V. Additionally, the MEA showed excellent resistance to carbon monoxide poisoning. When a reformate gas comprised of 40% hydrogen, 40.8% nitrogen, 19% CO_2 and 0.2% CO was used as fuel

and air was used as the oxidant, the CO poisoning effects produced an approximate 3 mV reduction in voltage. This study illustrates that low levels of CO poisoning have little effect on the 6F-PBI MEA operating at this temperature.

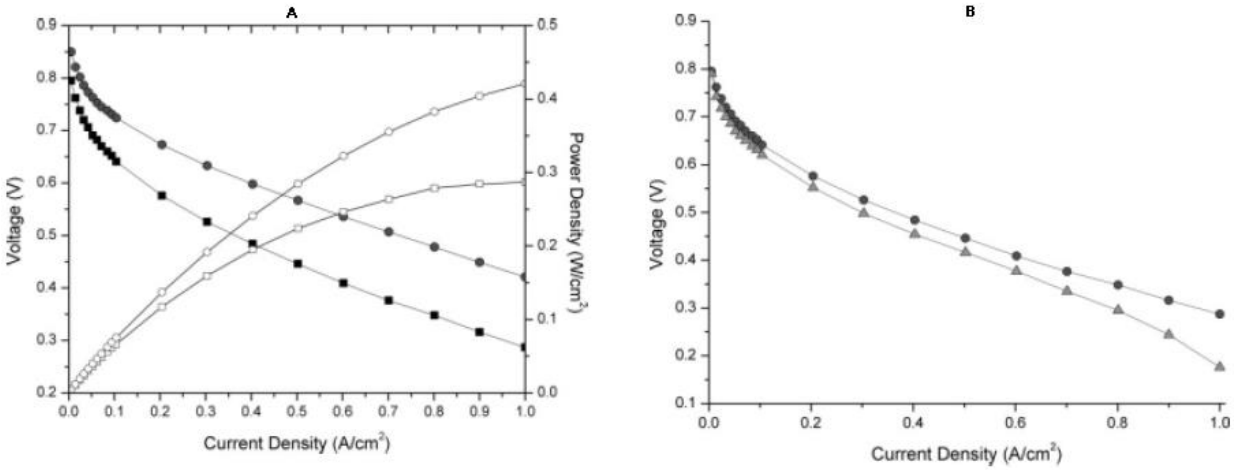

Figure 1.12: Graph (A) Polarization curves (filled symbols) and power density curves (unfilled symbols) of 6F-PBI using H_2/Air (squares) and H_2/O_2 (circles). Graph (B) Polarization curves of 6F-PBI using H_2/air (circles) and reformate/air (triangles) [50].

Commonly known as 2OH-PBI (Figure 1.5-h), poly(2,2'-(dihydroxy-1,4-phenylene)5,5'-bibenzimidazole) is another PBI membrane with extremely promising properties. Yu and Benicewicz [51] synthesized 2OH-PBI homopolymer by combining TAB with 2,5-dihydroxyterephthalic acid (2OH-TPA) in PPA and cast it via the PPA Process. Yu also synthesized the 2OH-PBI/*p*-PBI random copolymer by reacting both 2OH-TPA and TPA simultaneously with TAB; the copolymer membrane was also cast using the PPA Process. It was proposed that the 2OH-PBI homopolymer was significantly crosslinked through phosphoric acid ester bridges. Because of this crosslinking, the polymer was unable to be dissolved and an IV value could not be determined. Upon hydrolysis of the ester bridges by sodium hydroxide, the IV value of

the homopolymer was measured as 0.74 dL g^{-1}. The acid doping level of 2OH-PBI homopolymer was approximately 25 PA/PRU, and its conductivity at 160 ^{O}C was 0.35 S cm^{-1}. It is important to note that at all temperatures between room temperature and 180 ^{O}C, the conductivity of 2OH-PBI homopolymer was greater than that of *p*-PBI. As the ratio of 2OH-PBI/*p*-PBI decreased in the random copolymer, the doping level and conductivity decreased. It was found that the conductivity of the material was highly dependent on the chemical structure of the PBI membrane and not just the doping level.

Using a Pt anode electrode and a Pt alloy cathode electrode, polarization tests were performed on the homopolymer 2OH-PBI MEA (Figure 1.13). The homopolymer produced a voltage of 0.69 V using a load of 0.2 A cm^{-2} at 180 ^{O}C and H_2/air; this is greater than the 0.663 V produced by *p*-PBI under the same conditions. The high acid doping level and the membrane chemistry significantly contribute to the excellent performance of the 2OH-PBI membrane. Overall, the fuel cell performance of 2OH-PBI is comparable to that of *p*-PBI.

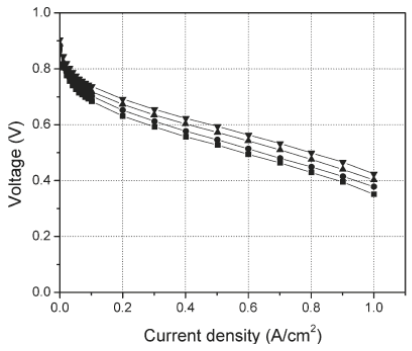

Figure 1.13: Polarization curves of 2OH-PBI using hydrogen as the fuel and air as the oxidant at 120^{O}C (squares), 140^{O}C (circles), 160^{O}C (triangles), and 180^{O}C (down-triangles) [51]

Segmented PBI block copolymers have also been explored for fuel cell use [52]. Scanlon synthesized a 52/48 *p*-PBI/*m*-SPBI (Figure 1.5-i) segmented block copolymer by polymerizing the oligomer of *p*-PBI with that of *m*-SPBI. The oligomers were polymerized in PPA and cast by the PPA Method. Even with an extremely high PA doping level of 91.5 mol PA/PRU, the polymer film had very strong mechanical properties. Under low humidity at 160 ^{O}C, the segmented copolymer achieved a conductivity of 0.46 S cm^{-1}. Because of the great results, a *p*-PBI/*m*-SPBI MEA was constructed for use in fuel cell performance tests. The polarization curves of the segmented copolymer MEA displayed a voltage of 0.62 V at 0.2 A cm^{-2} at 160 ^{O}C and 0.65 V at 0.2 A cm^{-2} at 200 ^{O}C. As implied by the data, these membranes are excellent candidates for high temperature fuel cells.

1.2.2.8. MEMBRANE ELECTRODE ASSEMBLY DURABILITY

As explained in a previous section, a membrane electrode assembly (MEA) consists of the polymer membrane that is sandwiched between an anode and a cathode electrode, respectively. The electrodes are composed of a conductive carbon network that supports a catalyst on a gas diffusion layer. An additive, such as polytetrafluoroethylene (PTFE), helps bind the Pt/C catalyst to the gas diffusion layer. At the anode, the catalyst facilitates the oxidation of hydrogen into its constituent electrons and protons. As the protons are passed through the acid-doped membrane to the cathode, the electrons are passed through an external circuit, thereby creating electricity. Finally, the electrons and protons react with oxygen at the cathode electrode to form water as the final reaction product.

Although PBI membranes are highly resistant to degradation, it is possible for the membranes to fail. Common degradation modes for PBI membranes at operating temperatures of 120 ^{O}C to 200 ^{O}C include membrane thinning and pin-hole formation. If there is too much pressure on the membrane, phosphoric acid could be pushed out of the polymer matrix and "thin out" the membrane. An extreme occurrence of membrane thinning results in pin-hole formations. Both of these occurrences result in increased fuel crossover and reduced fuel cell efficiency. Firm gasket materials help to evenly distribute pressure and prevent over-compression of the membrane [53]

The catalyst-coated electrodes of the MEA must be extremely durable in the presence of harsh physical and chemical environments. The oxidation and reduction processes create immense stress on the electrodes and trigger physical and chemical reactions to occur. A summary of the main MEA and component degradation modes have been previously reported [53, 54]. By means of electrochemical Ostwald ripening, Pt-metal agglomeration causes the loss of electrochemical surface area and decrease of reaction kinetics mainly through a dissolution-recrystallization process [55-57]. Oxidation reactions can also cause corrosion of the gas diffusion layer and carbon components in the electrodes, which would result in acid flooding, an increase in mass transport overpotentials, a decrease reaction kinetics and also, most severely, the loss of the mechanical integrity of the electrodes. Phosphoric acid can dissolve the Pt-metal catalyst and phosphoric acid anions ($H_2PO_4^-$) could adsorb onto the catalyst surface; both of these events would decrease the electrochemical surface area and reaction kinetics. In addition, phosphoric acid evaporation from the catalyst layer would result in similar consequences.

Typical commercial gas diffusion electrodes contain high-surface area carbon supported catalysts, e.g., Pt/Vulcan XC 72. Platinum is typically used as the catalyst at both the anode and cathode electrodes because it facilitates the reduction and oxidation reactions at high efficiency. However, due to the degradation modes previously mentioned, performance of the catalyst is lost over time. Novel platinum-based catalysts have been developed to increase the stability of the electrode catalysts. Compared to a commercial Pt/C (46.6 wt.% TKK), Pt_4ZrO_2/C catalysts have been shown to decrease the overall performance loss of the MEA [58]. The Pt_4ZrO_2/C catalyst showed a higher resistance to Pt-sintering than Pt/C following 3000 cycles of a potential sweep test between 0.6 and 1.2 V versus reversible hydrogen electrode (20 mV s^{-1}). The ZrO_2 is thought to act as an anchor to slow the agglomeration of platinum particles.

In order to improve especially the cathode catalyst kinetics and the catalyst stability, alloying of Pt with a base metal such as nickel or cobalt is widely done. Origins of these alloys date back to early phosphoric acid fuel cell development [59]. These alloys have been reported to typically improve the cathode kinetics for oxygen reduction by roughly 25 to 40 mV [59] or a factor of 1.5 to 4 when considered reaction rates. Commercial MEAs using PBI-based membranes also use Pt-base metal alloy catalyst on the cathode [60, 61]. The origin of the kinetic improvements for the Pt-base metal alloys is discussed manifold in literature [62-70]: i) modification of the electronic structure of Pt (5-d) orbital vacancies); (ii) change in the physical structure of Pt (Pt-Pt bond distance and coordination number); (iii) adsorption of oxygen-containing species from the electrolyte onto the Pt or alloying element; and/or (iv) redox-type processes involving the first-row transition alloying elements. However, as discussed in detail in the recent work

by Stamenkovic et al. [70], the main effect is a shift of the Pt d-band center to lower energy values which induces a surface which adsorbs oxygenated and spectator species to a lower extent and therefore makes more active sites available for the oxygen reduction to proceed.

Other additives to platinum-based electrodes, such as tin-oxide (SnOx) [71], have also been shown to significantly improve the catalytic activity of the oxygen reduction reaction. Using a PPA processed *m*-PBI membrane with a 7 wt.% SnO in $Pt/SnO_2/C$ catalyst under unhumidified H_2/O_2 at 180 ^{O}C, a voltage of 0.58 V under a load of 0.2 A cm^{-2} was produced. Under the same conditions, a *m*-PBI MEA using a Pt/C catalyst produced only 0.4 V at 0.2 A cm^{-2}.

PBI has also been investigated as an additive to platinum-based electrodes. It is thought that incorporation of PBI in the catalyst layer would provide a better interface for proton conduction between the electrode and membrane. Qian [72] incorporated 6F-PBI into the electrodes by four different methods: formation of a PBI bilayer inserting a thin 6F-PBI membrane between an E-TEK cathode and *p*-PBI membrane, casting 6F-PBI/PPA directly onto the E-TEK electrodes and hydrolyzing to form the gel, spraying a 6F-PBI/DMAc solution onto the electrodes, and coating the electrodes with a mixture of 6F-PBI and catalyst (the PBI replaced PTFE). The bilayer method decreased fuel cell performance, and it is proposed that this occurred by creating a large interface resistance between the two PBI membranes. Both the casting method and the spraying method improved electrode kinetics, and it is postulated that this occurred due to a lower interface resistance. In addition, a significant decrease in fuel cell performance showed that 6F-PBI could not be used to replace PTFE.

As an outlook to further improvements of catalyst kinetics and durability in low and high temperature polymer electrolyte fuel cells, several possibilities are currently under investigation [73]: i) extended large scale Pt and Pt-alloy surfaces [70]; ii) extended nanostructured Pt and Pt-alloy films [74]; iii) de-alloyed Pt-alloy nanoparticles [75]; iv) precious metal free catalyst as described by Lefèvre et al. [76], e.g., Fe/N/C catalysts; v) additives to the electrolyte which modify both adsorption properties of anions and spectator species and also the solubility of oxygen [77]. The latter approach is specific to fuel cells using phosphoric acid as electrolyte.

1.3. PBI/PA Fuel Cell Systems and their Applications

Para-PBI is one of the most common polymers used in commercial PBI-based fuel cell systems. A mechanically strong and chemically stable polymer, *p*-PBI has proved to be one of the most reliable PBI polymers for MEA use. Load, thermal, and shutdown-startup cycling tests performed on the *p*-PBI MEA indicated that high temperatures (180 and 190 ^{O}C) and high load conditions slightly increased PA leeching from the MEA system. However, at steady-state fuel cell operation at 80-160 ^{O}C studies showed that PA loss would not be a significant factor in fuel cell degradation [54, 78]. Long term studies showed minimal performance degradation over a two-year span and indicated excellent commercial fuel cell potential [53]. Compared to state-of-the-art phosphoric acid PEMFCs [79], evaporation of phosphoric acid from commercial PBI-based Celtec P1000 MEAs is reduced by a factor of roughly 2 to 3. This is a key factor of long-term stable operation for PBI-based fuel cells.

For the transition of PBI-based fuel cell science into commercial products, the appropriate manufacturing processes need to be developed. Most companies rely on manual operations [80] for PBI-based MEA fabrication. Only recently have significant efforts been devoted to developing automated production lines because simple changes in MEA materials and architecture could necessitate the use of different manufacturing equipment. To accommodate the evolution of fuel cell science, a flexible modular manufacturing line has been developed. Since 2002, BASF Fuel Cell GmbH (previously PEMEAS) has used the line to accommodate three generations of MEAs. The details of this manufacturing process will be further discussed in Section 1.3.2.

Commercial PBI-based high temperature PEMFCs provide energy to a wide array of electronic devices. Hydrogen fuel cell vehicles, both for the private consumer and public transportation, are growing in popularity as pollution and fossil fuel prices continue to increase. Hydrogen offers 2-3 times the overall efficiency in a fuel cell as gasoline does in a typical combustion engine [81]. High temperature fuel cells are also popular as backup generators and combined heat and power devices for stationary use. These types of systems typically produce 1-10 kW, which is enough energy to power a house or a multi-family dwelling. In addition to providing energy, combined heat and power devices use waste heat to heat water and preheat the fuel cell system components, thereby increasing the overall efficiency of the fuel cell system. Fuel cells also offer applications in mobile electronic devices such as laptops and cell phones. Commonly coupled with a methanol reformer, these fuel cell systems are remarkably portable and can power electronics for hours of continuous use.

In addition to producing electricity, these PEMs have been used as a purification device for hydrogen gas. Consider the purification device to have the same basic architecture as a fuel cell. A platinum catalyst splits contaminated hydrogen gas into protons and electrons at the anode. Using an external power source, the electrons are driven through an external circuit to the cathode while the protons are allowed to transport across the membrane from the anode to the cathode. The electrons and protons recombine, thereby creating a higher grade hydrogen gas at the cathode while leaving behind the undesired constituents at the anode. These hydrogen pump devices will be further discussed in Section 1.3.6.

1.3.1 In-Depth Analysis of PPA processed *p*-PBI MEA

PBI-based high temperature MEAs offer many benefits over more well-known perfluorosulfonic acid Nafion PEMs. Unlike low temperature Nafion MEAs, high temperature PA-doped PBI membranes do not need to be hydrated, and therefore, do not require an external humidification of the gases. Additionally, running at high temperatures generally improve electrode kinetics and proton conductivities while requiring smaller heat exchangers. For PBI fuel cell science to transition into commercially available products, the reliability of PBI fuel cell stacks needs to meet specific requirements. The Department of Energy (DOE) specified durability targets of >5,000 h (>150,000 miles) of automotive fuel cell operation and >40,000 h for stationary applications for 2010. Primarily, the durability of the fuel cell stack dictates the durability of the entire system [82]. In depth durability studies of PBI MEAs have been performed [53, 54, 61, 78, 83-85] to evaluate the viability of commercial PBI fuel cells. In addition

to fuel impurity and PA retention tests, load, thermal, and shutdown-startup cycling tests are commonly performed to evaluate the MEAs.

p-PBI MEAs have displayed a relatively high resistance to carbon monoxide and sulfur contaminants [78, 83, 86, 87]. While Nafion and other traditional low-temperature PEM fuel cells are often poisoned by small amounts of carbon monoxide (5-50 ppm) in the fuel or oxidant, *p*-PBI and other PBI membranes have been shown to perform with minimal voltage loss in 10^4 ppm of carbon monoxide. Operating the fuel cell at 180 ^{O}C with a load of 0.2 A cm^{-2} with a reformate gas (70% H_2, 1.0% CO, and 29% CO_2), the voltage loss was only 24 mV as compared to pure hydrogen [27]. This decrease in voltage occurred as a result of fuel dilution and carbon monoxide poisoning. As explained in Section 1.1, the cell is able to resist poisoning because the high operating temperatures allow for reversible binding of carbon monoxide from the catalyst. Details on the CO adsorption isotherms in the presence of hydrogen under fuel cell operation conditions between 150°C and 190°C can be found in literature [87]. Similarly, Garseny et al. [86] reported that a PBI MEA from BASF Fuel Cell GmbH (Celtec-P Series 1000) is 70 times more resistant to sulfur contaminants than Nafion MEAs. Using air contaminated with 1 ppm H_2S or SO_2 as the oxidant, the performance of Nafion decreased by 82.9% while the performance of the Celtec-P MEA decreased by <2%. Garseny et al. proposed that H_2S is converted to SO_2, and that SO_2 adsorbs onto the Pt catalyst surface. At temperatures above 140^{O}C, this SO_2 is desorbed and flushed out of the system. Schmidt and Baurmeister showed that the H_2S tolerance of PBI based Celtec P1000 MEAs is in the range of 10ppm [83], a value significant larger than typical fuel processing catalyst can tolerate. More than 3000 hours operation in reformate with 5ppm

H_2S and 2% CO is proven. Overall, *p*-PBI-based fuel cells can resist contaminant poisoning far better than traditional low-temperature PEM fuel cells, an effect which can mainly be ascribed to the operation temperature between 150°C and 190°C.

Under continuous operation and appropriate stack design and components, the PBI membranes retain phosphoric acid extremely well. Long term performance tests show that *p*-PBI fuel cells can operate for over two years with minimal performance degradation (Figure 1.14). This durability is attributed to the unique nature of PBI membrane formed by the PPA process, which allows it to retain PA under continuous operating conditions. The amount of PA lost from the *p*-PBI MEA per hour was approximately 10 ng h^{-1} cm^{-2}, which is equivalent to a 50 cm^2 cell losing 8.74 mg PA after two years of operation. Such a small loss strongly suggests that the life span of a *p*-PBI PEM fuel cell would not be significantly influenced by PA depletion.

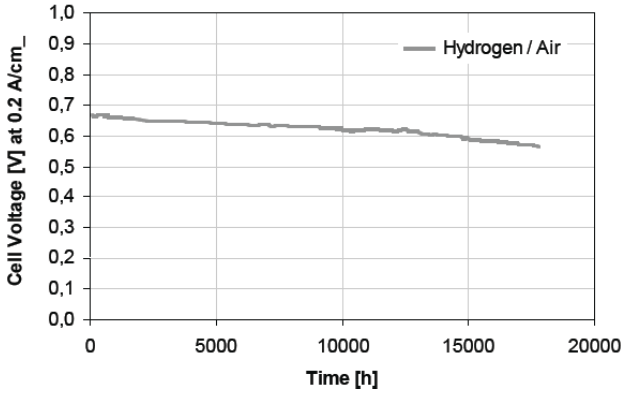

Figure 1.14. Long-term durability test of *p*-PBI MEA at 160^{O}C using hydrogen/air without humidification

Phosphoric acid loss was also monitored during a selection of dynamic durability tests, including load and thermal cycling tests [78]. A single load cycle test involved

measuring the voltage at 160 ^{O}C under at three different loads: open circuit voltage (OCV), 0.2 A cm^{-2}, and 0.6 A cm^{-2}. Air and pure hydrogen were supplied to the MEA as oxidant and fuel, respectively. The voltage of the MEA was measured at OCV for two minutes, followed by 0.2 A cm^{-2} for 30 minutes and then 0.6 A cm^{-2} for 30 minutes. A total of 500 load cycles were performed on a *p*-PBI MEA, and the results indicated that larger loads corresponded to an increased PA loss rate (approximately 20 ng h^{-1} cm^{-2}). Thermal cycling tests were performed by measuring the voltage of the MEA with a constant applied current density of 0.2 A cm^{-2} while either cycling the temperature between 120 ^{O}C and 180 ^{O}C (for a high temperature cycle) or between 80 ^{O}C and 120 ^{O}C (for a low temperature cycle). Both the high and low temperature cycles were performed 100 times each. The results showed that higher temperatures were associated with an increased PA loss rate (almost 70 ng h^{-1} cm^{-2} for the high temperature cycle and 20 ng h^{-1} cm^{-2} for the low temperature cycle). It was proposed that at the higher load and temperature conditions, more water is generated at the cathode. By means of a steam distillation mechanism, an increased amount of PA is lost from the MEA. As indicated by both cycling tests, phosphoric acid loss becomes a significant factor of cell degradation only under extreme conditions.

Shutdown-startup cycling tests have been extensively studied by Schmidt and Baurmeister of BASF Fuel Cell GmbH [54, 61]. Two PBI-based PEFC Celtec-P 1000 MEAs were tested under different operation modes; one was run under shutdown-startup cycling parameters (12 h shutdown followed by operation for 12 h at 160 ^{O}C under a load of 0.2 A cm^{-2}) while the other was continuously operated at 160 ^{O}C under a load of 0.2 A cm^{-2}. Both MEAs were operated for more than 6000 h, during which the shutdown-

startup cycling MEA underwent more than 270 cycles. While the continuously operating MEA had an average voltage degradation rate of roughly 5 $\mu V\ h^{-1}$, the cycling MEA averaged a voltage degradation of 11 $\mu V\ h^{-1}$ or 0.2 $mV\ cycle^{-1}$. This increase in voltage degradation was attributed to an increased corrosion of the cathode catalyst support, thereby significantly increasing the cathodic mass transport overpotential. The observed corrosion was a result of a reverse-current mechanism that occurs under shutdown-startup cycling conditions [88].

Illustrated by the previously discussed durability tests, *p*-PBI MEAs have been shown to be physically and chemically robust. Highly resistant to fuel contaminants, PBI MEAs are resistant to poisoning effects that would typically expunge a low temperature Nafion fuel cell system. Long term steady-state and dynamic durability tests showed that PA loss typically is not a cause of cell degradation. Additionally, Schmidt and Baurmeister showed that PBI MEAs are susceptible to cell degradation under extreme shutdown-startup conditions. Overall, *p*-PBI MEAs have exhibited much potential for use in fuel cell systems.

1.3.2. Advances in PBI MEA Manufacturing

As previously discussed, the manufacturing processes of PBI-based fuel cells need to be improved to make fuel cells a viable commercial product. To put this requirement into perspective, the United States Department of Energy has set a goal of producing 500,000 fuel cell cars each year. If these vehicles are powered using current *p*-PBI membranes, this goal requires the production of seven MEAs per second and approximately 250,000 m^2 of electrode per day. Additionally, the performance of each of

these MEAs would need to be tested; this is a process called "burn-in testing." A typical test stand is 25 ft^2, costs roughly $50,000, and can only test one stack of MEAs at a time. If each stack requires a 24 hour burn-in test, the test facility size would exceed 34,000 ft^2 and house equipment costing over $68.5 million. Existing manufacturing processes need to be improved in order to reach this goal.

The Center for Automation Technologies and Systems (CATS) at Rensselaer Polytechnic Institute has developed a flexible manufacturing process for BASF Fuel Cell GmbH to accommodate the evolving science of fuel cells [89-91]. If one changes the fuel cell type, size, materials, MEA architecture, design, or application, the manufacturing line could be significantly affected. Therefore, a modular manufacturing line was developed by CATS in 2002 that could produce a large range of MEA sizes (1-1000 cm^2), could handle a wide variety of materials (membranes, gaskets, electrodes, etc.), could assemble these materials in different architectures, and could be expanded to integrate additional systems. Each module could be singularly operated or could operate as a subset of the entire process; this modular construction is shown in Figure 1.15. Over the past eight years, this manufacturing line has evolved over three generations of MEA devices.

Figure 1.15. A portion of the 2002 pilot line depicting its modular construction [90].

Members of CATS continue to make great strides in order to reduce costs and improve the overall efficiency of MEA fabrication. Laser cutting and joining of the PBI membranes both uses less power and delivers tighter tolerances than that of conventional cutting and joining. Ultrasonic technology has also been explored to replace the thermal joining of the three components of an MEA. Preliminary results exhibited a significant reduction in pressing time by approximately 90% in addition to using less energy. Additionally, an automated visual inspection of the MEA has been developed using a high precision motion system, multiple cameras and lighting equipment, and software MAT-LAB 7.0 with Image Processing Toolbox [89]. As fuel cell science continues to evolve, so will the manufacturing processes.

1.3.3. Combined Heat and Power

Stationary combined heat and power (CHP) devices are often considered the primary application of high temperature PBI-based fuel cells. These devices are used to provide both electricity and heat (in the form of hot air or water) to small scale residential homes or large scale industrial plants using hydrogen derived from the widely distributed natural gas network. PBI MEAs are ideally situated for combined heat and power devices because they efficiently provide electricity while generating heat as a byproduct. Furthermore, these devices could be used to provide reliable backup power to residential homes, hospitals, servers, etc.

J.-Fr. Hake et al. [92] compared the conventional generation of heat and electricity to that of small scale combined heat and power generation by high temperature fuel cells, and the results of which are shown in Figure 1.16. The small scale CHP

devices studied were used to provide electricity, space heat, and warm water to both residential and commercial buildings. The conventional generation of electricity is much less efficient than that of small scale CHP devices due to the issues of transportation and storage. In addition to efficiently converting chemical energy into electrical energy, CHP fuel cell systems further act as a sustainable energy conversion device by reducing the total amount of greenhouse gas emissions. Hake et al. considered the penetration of small scale CHP fuel cell technology into the US residential sector market starting in 2014 until a saturation point as a logarithmic function. To improve the accuracy of the study, Hake considered the trends of the Japanese small scale CHP market [92, 93]. A typical CHP device in Japan costs roughly $30,000, but analysts expect the price to drop to $5,000 within five years. Analysts also claim that by the year 2050, one in four homes in Japan will run on fuel cells. Also considering current CO_2 emissions, Hake et al. concluded that adoption of this technology in the US could reduce CO_2 emissions by up to approximately 50 million tons by 2050; this corresponds to a 4% reduction in the residential sector.

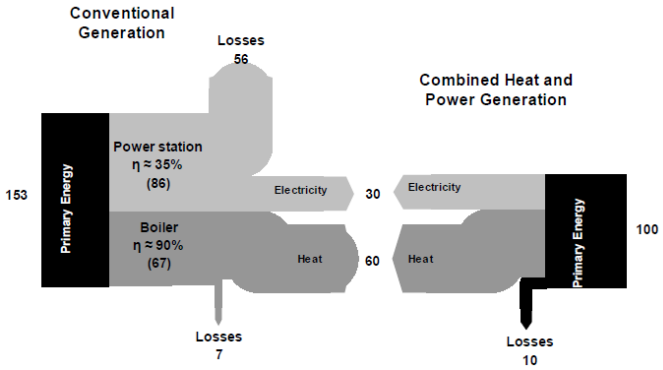

Figure 1.16: Side-by-side comparison of conventional generation of heat and electricity to fuel cell combined heat and electricity generation [92].

As the largest producer of PBI MEAs, BASF Fuel Cell (previously PEMEAS) produces *p*-PBI PEM MEAs for a wide variety of fuel cell applications. The Celtec®-P 1000 PEM MEA is typically integrated into either back-up or auxiliary power units and can produce from 0.25 to 10 kW. The MEA is also advertised as maintaining performance for over 20,000 hours with only a 6 μV h^{-1} voltage drop at 160^{O}C [94]. The Celtec®-P 2100 PEM MEA is used in stationary CHP systems and is capable of producing 0.74 to 10 kW. The MEA has a long term stability of over 20,000 hours under both steady state and cycling conditions (300 shutdown-startup cycles with 13 μ h^{-1} voltage drop). Polarization curves of a Celtec®-P MEA at 160 ^{O}C using an active area of 45 cm^2 are shown in Figure 1.17. PBI-based CHP devices are commercially available from a variety of companies, including Serenergy, Plug Power, and ClearEdge Power. All of these companies assemble a variety of fuel cell devices using commercially available PBI MEAs.

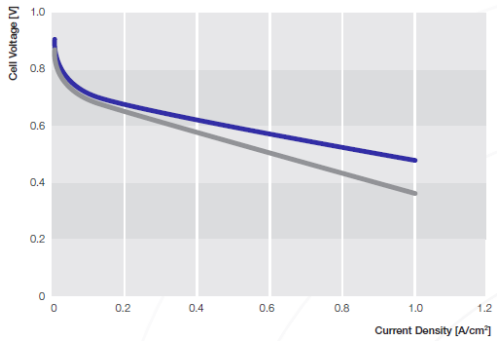

Figure 1.17: Polarization curves of a Celtec®-P MEA [94]. The blue line represents using hydrogen/air as fuel/oxidant. The gray line represents a steam reformate of 70% H_2, 29% CO_2, and 1% CO/Air.

Plug Power of Latham, New York produces a line of PBI-based small scale CHP devices including the GenSys Blue (Figure 1.18) [95]. The GenSys Blue is capable of

producing 0.5 kW to 5 kW of continuous output and is capable of reducing home energy costs by 20-40%. An autothermal (ATR) reformer reacts natural gas (methane) with oxygen and carbon dioxide to produce hydrogen gas that fuels the PEM stack. An inverter is used to improve the efficiency of the CHP device by specifically supplying enough energy to power the home, thereby minimizing energy losses and reducing CO_2 emissions by 25-35%. Additionally, an integrated peak heater ensures proper heating of the entire home.

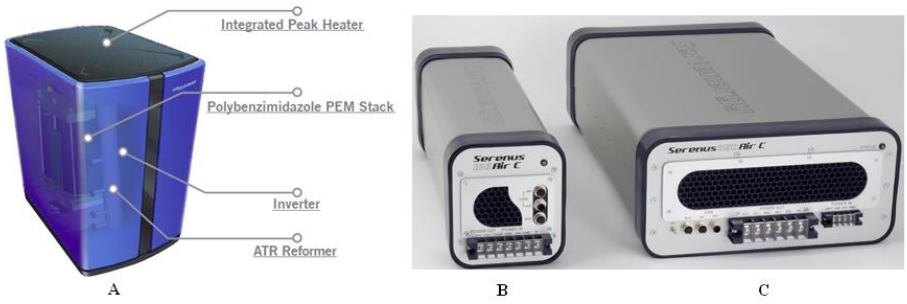

Figure 1.18. Plug Power's GenSys Blue (A), Serenergy's Serenus 166 Air C v2.5 (B), and Serenergy's Serenus 390 Air C v2.5 (C) CHP Fuel Cell Devices [95, 96].

Serenergy, which is based in Hobro, Denmark, also produces PBI-based fuel cell CHP devices [96]. Serenergy's Serenus 166 Air C v2.5 and 390 Air C v2.5 micro-CHP modules nominally produce 1 kW and 3.5 kW, respectively. While the 166 model is comprised of one MEA stack of 65 cells, the 390 model uses three MEA stacks each with 89 cells. Both of these systems are able to tolerate fuel impurities up to 5% CO concentrations and 10 ppm H_2S at 160 ^{O}C. Because the excess energy can be used to heat up air or water, Serenergy claims that over 80% of the total heat and power generated can

be used and that the system efficiency is as high as 57% (the efficiency data was not available). These systems can also be used as auxiliary energy conversion devices.

ClearEdge Power also produces a line of small scale CHP devices, one of which is the ClearEdge5 [97]. Capable of producing 5 kW h^{-1} and up to 20,000 BTU h^{-1} while running at 150 ^{O}C, the ClearEdge5 couples a methane reformer to a PBI fuel cell stack using MEAs provided by BASF Fuel Cell GmbH. ClearEdge advertizes that the CHP device can reduce utility bills by up to 50% and cut CO_2 emissions by over 33%. Annually, the device is capable of producing 43,000 kWh in electricity and 50,000 kWh (equivalent) in heat. Similar to other CHP devices, the ClearEdge5 offers at-home production of energy, thereby eliminating the losses associated with transferring the energy. The device is monitored in real-time by ClearEdge Power and can be monitored directly from the owner's smartphone.

1.3.4. AUTOMOTIVE TRANSPORTATION

Producing 1.9253 billion metric tons of carbon dioxide, which is roughly 33% of the United States' total carbon dioxide emissions, the transportation sector was the largest contributor to pollution in 2008 [98]. According to another 2008 study by the U.S. Department of Energy [2], all transportation in the US consumed approximately 27.8 quadrillion BTUs. Considering both of these facts, one can conclude that a more sustainable energy source could significantly reduce the carbon footprint of the transportation sector. For the transition of fuel cell science into a viable commercial product to occur, the U.S. Department of Energy has set numerous targets for automotive fuel cell systems. Because a typical internal combustion engine costs roughly $25-35/kW,

a fuel cell system will need to cost roughly $30/kW to become competitive enough to penetrate the US market. Furthermore, the system must be durable enough to operate for at least 5,000 hours (or roughly 150,000 miles). Additional issues of system size and management of air, heat, and water will also play a role in automotive fuel cell viability.

Over the past decade, fuel cell technology has been adapted by the major automotive industries as a cleaner, more efficient method of providing energy to vehicles. In addition to the issue of fuel cell automotive viability, issues of hydrogen sources, hydrogen storage, and fueling stations continue to be addressed and solved. The California Fuel Cell Partnership (CaFCP) is a collaboration of auto manufacturers, energy providers, government agencies, and fuel cell technology companies to promote the commercialization of fuel cell vehicles [81]. In 2009, California had only six public hydrogen fueling stations that were used to fuel roughly 200 vehicles. The CaFCP predicts that in 2014, approximately 5,800 kg of hydrogen will be used to fuel roughly 4,310 fuel cell passenger vehicles and 60 fuel cell busses daily. To accommodate the needs of fuel cell vehicle operators, CaFCP proposed the establishment of 46 new fueling stations by the year 2012. Considering each new station would cost in the range of $1.5 to $5.5 million, a predicted $180 million would have to be spent on the fueling station project. Although this "Action Plan" did not specify an amount, this project will provide many new jobs to US residents. The hydrogen used to fuel these stations can be domestically produced as either a low-carbon fuel or potentially as a zero-carbon fuel when produced from renewable sources (such as splitting water into oxygen and hydrogen with solar energy). According to California regulations, at least 33% of the hydrogen must come from such renewable sources.

SunHydro, one of the world's first hydrogen fueling station chains, has set a goal of providing fueling stations along the entire east coast of the US [99]. Using solar cell technology, every SunHydro station will harvest solar energy to electrolytically split water into hydrogen and oxygen gases. This process is extremely sustainable and will create much less greenhouse gas emissions. This hydrogen highway will stretch from Scarborough, ME to Miami, FL and consist of eleven stations. Each station will cost an estimated $2-3 million to construct and will be paid for by private funders.

Over the past decade, many automotive and fuel cell industries have used PBI technology in the development of fuel cell vehicles. In November of 2008, Volkswagen unveiled the VW Passat Lingyu at a Los Angeles Auto Show [100]. The VW Lingyu uses an AB-PBI based fuel cell stack that utilizes a trade-secret coating that helps prevent PA from leeching out of the membrane. Metha Energy Solutions, in cooperation with Serenergy, revealed a hybrid electric/fuel cell vehicle in December of 2009 [101]. In this system, a methanol reformer is used to provide hydrogen to the PBI based fuel cell. It was advertized that this vehicle could travel up to 310 miles on one tank of gas and takes only two minutes to refuel. EnerFuel, a subsidiary of Ener1, has also recently produced a hybrid electric/fuel cell vehicle. The EnerFuel EV uses a reformed methanol PBI fuel cell that works in conjunction with a lithium ion battery. The lithium battery is used to start the vehicle and to power the vehicle while driving, while the fuel cell system produces 3-5 kW to continuously recharge the battery. These fuel cell systems would not generate enough power to drive the vehicle, but would act as a range extender for the battery system. The target market of the EnerFuel EVs is not for those who drive 200+ miles daily, but instead for those with short daily commutes.

In July of 2009, the German Aerospace Center demonstrated that fuel cells have the potential of powering air-transportation vehicles [102, 103]. Designed in cooperation with Lange Aviation, BASF Fuel Cell, DLR Institute for Technical Thermodynamics, and Serenergy, the Antares DLR-H_2 became the world's first piloted aircraft with a propulsion system powered only by PBI-based fuel cells. Besides creating zero CO_2 emissions during flight, the aircraft also generates much less noise than other comparable motor gliders. Using a fuel cell stack capable of producing up to 25 kW, the Antares DLR-H_2 has a cruising range of 750 kilometers (or five hours) and can travel at speeds up to 170 km h^{-1}. Similar fuel cell systems could be coupled with current commercial and military aircrafts as auxiliary power units (APUs) to improve fuel efficiency.

1.3.5. PORTABLE

Microelectricalmechanical (MEM) systems utilizing methanol reformers and PBI fuel cells have been developed for portable use. These devices are generally used to generate power in the range of 5-50 W for laptops, communication systems, and global positioning systems. Compared to batteries that offer equivalent amounts of power, these micro-fuel cell systems are lighter, generate less waste, and are overall more cost effective. Similar to other reformed methanol/PBI fuel cell systems, these MEMS are a sustainable technology by reducing the amount of greenhouse gases produced per unit of electricity generated.

UltraCell of Livermore, CA is a well known producer of PBI MEM fuel cell systems. Funded and field tested by the U.S. Army, the UltraCell XX25 is capable of providing 25 W of continuous maximum power [104]. Depending on the size of the fuel

cartridge, the device is capable of delivering 20 W of continuous power from 9 hours to 25 days. The fuel cartridge weighs less than a pound and The XX25 MEM system has been shown to power radio gear, mobile computer systems, communication devices, and a variety of other electrical devices. The XX25 provides roughly 70% in weight savings when compared to a typical battery on a 72-hour mission (1.24 kg without the cartridge), and is rugged enough to operate in extremely cold or hot environments. In addition, it meets OSHA standards for safe indoor and in-vehicle use. Similar to the XX25, the newly developed UltraCell XX55 is capable of generating 55 W of continuous power for up to two weeks using the largest fuel cartridge [105]. Only 0.36 kg heavier than the XX25, the XX55 has an optional battery module that can provide a peak power output of 85 W. Similar to the XX25, it is a very rugged device that can be used essentially in any conditions.

Larger than the Ultracell devices, the relatively new Serenergy Serenus E-350 is a reformed methanol/fuel cell hybrid with an approximate mass of 11 kg. At nominal power levels, it is capable of producing approximately 350 W [106]. The device is fueled by a 60-40 methanol-deionized water mixture. It takes approximately 45 minutes to start-up, at which point it consumes fuel at a rate of 0.45 L h^{-1}.

1.3.6. H_2 PUMP

Efficient purification of hydrogen is becoming a common interest in both industrial and energy sectors. In particular, technology which can efficiently purify, pump, and pressurize hydrogen at low to moderate flow rates is needed, but is not readily available. Of course, there are existing methods for hydrogen purification which include

various combinations of mechanical compression with cryogenic cleanup, palladium membranes, pressure swing absorption, and passive membrane separators to name a few. However, these technologies are challenged by certain limitations: 1) cryogenic cleanup produces high purity hydrogen, but requires costly refrigeration equipment and is suitable for very large-scale specialty applications; 2) palladium membrane purification can be fairly simple in design and construction, but requires pressurization to drive the hydrogen separation process and suffers from poor utilization when purifying hydrogen from gases containing low fractions of hydrogen; 3) pressure swing absorption (PSA) is widely used in high volume industrial processes and relies on large, mechanical components that are subject to frequent maintenance and inherent inefficiency. Such devices are not easily scaled to smaller sizes or localized generation/purification needs. Furthermore, it is important to state that all of the above processes require expensive, high maintenance, compressors.

Electrochemical pumping is not a new concept and has in fact been utilized as a diagnostic technique within the electrochemical industry for years. General Electric developed this concept in the early 1970's [107]. The use of polymer electrolyte membranes for electrochemical hydrogen compression has been demonstrated in water electrolysis (H_2 generation) devices at United Technologies Corporation, reaching 3000 psi_a [108], as well as studied in academic institutions [109].The electrochemical hydrogen pump, first developed in the 1960's and 1970's, was derived from the original proton exchange membrane fuel cell efforts. The concept is simple, requires little power, and has been shown to pump hydrogen to high pressures. In the original work, the membrane transport medium was a perfluorosulfonic acid (PFSA) material, similar to the material

used in many fuel cells today. The process is quite elegant in that like a fuel cell, molecular hydrogen enters the anode compartment, is oxidized to protons and electrons at the catalyst, and then the protons are driven through the membrane while the electrons are driven through the electrically conductive elements of the cell. The major difference in this cell as compared to a fuel cell is that the pump is operated in an electrolytic mode, not galvanic, meaning that power is required to "drive" the proton movement. Once the protons emerge from the membrane at the cathode, they recombine to form molecular hydrogen. Thus, hydrogen can be pumped and purified in a single step with a non-mechanical device. The pump concept builds upon the understanding of proton transport membranes.

Clearly, the proton conducting membrane properties are critical. Desirable properties include: high proton conductivity, mechanical stability, low solubility and permeability of impurity gases, and sufficient operating temperature to support tolerance to impurities (CO and H_2S) found in reformed gases. The application of the PBI membrane to electrochemical hydrogen pumping provides high proton conductivity (0.2 – 0.4 S/cm), mechanical stability, enhanced gas separation, and up to 180°C operation. The high operating temperature eliminates water management difficulties typically experienced with the low operating temperatures of PSFA membranes while also providing tolerance to poisonous gas species such as CO. As such, the PBI membrane and electrode assembly represents a significant new opportunity and paradigm shift in electrochemical hydrogen pumps as well as in advancing the science of hydrogen separation, purification, and pressurization. This concept has been evaluated and demonstrated in recent work using PBI membranes [110]. The hydrogen pump was

shown to operate with fairly low power requirements, and generally needed less than 100mv when operating at 0.2-0.4 A/cm^2. This was accomplished without the critical water management commonly encountered in low temperature, water-based membranes. The cathodic flow of hydrogen from the device was nearly identical to the theoretical Faradic flows. This suggests that the hydrogen pump could have applications as a hydrogen metering device since the hydrogen flow could be easily and accurately controlled by the current of the power source. The initial work reported devices that could operate for several thousand hours with little change in the operating parameters. This would be expected from the related work on PBI membranes for fuel cells which show outstanding long-term durability. In fuel cell applications, the ability to operate at high temperatures provides benefits for gas cleanup and durability on reformed fuels. In hydrogen pump applications, this tolerance to fuel impurities enables the hydrogen pump to purify hydrogen from hydrogen gas feeds containing such impurities. Figure 1.19 shows the operation of a PBI-based hydrogen pump operating on pure hydrogen, as well as two different synthetic reformates. The flow rates are nearly unaffected by the composition of the gas feed at the various operating conditions (the data points are superimposed for the different gases). The data demonstrates that the pump was capable of operating at high CO levels (1% in this work) and extracting hydrogen from dilute feed streams (<40% hydrogen). Additionally, the hydrogen pump was capable to producing hydrogen with purities greater than 99%, with the final purity dependent on operating conditions. This device could play a prominent role for both the current industrial hydrogen users, as well as in a future economy that is more heavily reliant on hydrogen as an energy carrier. Commercial development of this device is underway.

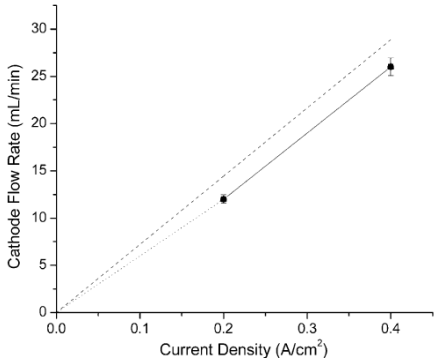

Figure 1.19. The cathodic flow rates of a hydrogen pump operated at 160 ^{O}C and 0% relative humidity and fueled by pure hydrogen (unfilled squares), a reformate gas comprised of 35.8% H_2, 11.9% CO_2, 1906 ppm CO, and 52.11% N_2 (filled circles), and a reformate gas comprised of 69.17% H_2, 29.8% CO_2, and 1.03% CO (filled triangles). The values are nearly identical, and thus, the symbols appear superimposed. The dotted line represents the theoretical flow rate at 100% efficiency [110].

1.4. Motivation for Polybenzimidazole Membrane Research

After approximately 10 years of development, PBI chemistries and the concomitant manufacturing processes have evolved to produce commercially available MEAs. PBI MEAs can operate reliably without complex water humidification hardware and are able to run at elevated temperatures of 120-180 ^{O}C due to the physical and chemical robustness of PBI membranes and the use of PA as a dopant. These higher temperatures improve the electrode kinetics and conductivity of the MEAs and simplify the thermal management of the system. The use of PA as a dopant eliminates the complex water management of the system. Membranes cast by a newly developed PPA Process possessed excellent mechanical properties, higher PA/PBI ratios, and enhanced proton conductivities as compared to previous methods of membrane preparation.

The robustness of *p*-PBI membranes cast by the PPA Process has been tested and characterized by a variety of methods. Under a constant load, *p*-PBI has been shown to

perform for well over two years with very little reduction in performance. Using synthetic reformates, *p*-PBI MEAs have demonstrated excellent resistances to impurities such as CO, CO_2, and SO_2. *p*-PBI membranes have also been shown to retain PA extremely well, and evidence strongly suggests that this small rate of PA loss would not significantly influence the life span of a MEA. Load, thermal, and shutdown-startup cycling tests of *p*-PBI fuel cells have also indicated comparable or improved results over other commercially available fuel cell systems.

Many fuel cell manufacturers are now considering the benefits of high temperature PBI fuel cells. BASF Fuel Cell, the largest producer of PBI MEAs, has been in operation since March of 2007. BASF offers a wide variety of MEAs for stationary systems (combined heat and power, backup generators, etc.) and portable systems (transportation, microelectricalmechanical systems, etc.). Other companies, such as Plug Power, Serenergy, ClearEdge Power, and UltraCell, incorporate commercially available MEAs into their commercial fuel cell systems. Recently, H_2 Pump LLC has developed electrochemical pumping devices that use PBI membranes for the purification of hydrogen gas. Using various reformate gases, the devices have been shown capable of operating at high gas contamination levels and low hydrogen concentrations. Depending on operating conditions, the purity of the extracted hydrogen gas can be greater than 99%. In transportation applications, PBI based fuel cells show great promise as APUs or range extenders for battery powered electric vehicles.

Recently, the Department of Energy has issued a target of 40,000-80,000 hours for stationary (i.e. combined heat and power, back-up power) PEM fuel cells. A thorough understanding of the failure modes of PEM fuel cells is necessary to reach this goal. A

common degradation pathway discussed in Section 1.2.2.8 is membrane thinning, which can result in gas crossover and pinhole formation. This membrane thinning naturally occurs in PBI PEM fuel cells due to the static compressive forces of the fuel cell stack. It is well known that over time, the PBI membrane at 180°C creeps in a direction perpendicular to the compressive forces, thus also changing the composition of the membrane. Studies on the high temperature creep properties in compression have not been reported for PBI membranes, despite the importance of such properties for long-term fuel cell operation. To reach this goal of 40k hours, enhancement of the mechanical properties of PBI membranes is of great importance to prevent membrane creep and enhance the lifetimes of the fuel cell. From a manufacturing standpoint, new approaches to improving the long-term mechanical properties of PBI membranes are needed which are cost effective and compatible with current manufacturing processes that have been developed for these unique membrane materials.

As mentioned throughout this chapter, many attempts have been used to mechanically reinforces or electrochemically improve PBI membranes. To date, chemical crosslinking, inorganic fillers, organic fillers, and alternative processing techniques have only marginally succeeded at improving either of these goals. Dihydroxy-PBI has shown very high anhydrous proton conductivity, but due to its low solubility, cannot be polymerized at high enough polymer contents to improve the mechanical properties of the resulting membranes (discussed in later sections). Sulfonated-PBIs have shown marginal success at improving the chemical robustness of the membranes (stable membranes in sulfuric acid for 3+ years), but have not demonstrated improved durability in fuel cells. Part of the issue at designing more durable PBI membranes is due to a lack

of understanding of PBI membrane structure-to-property relationships, especially the mechanical properties at operational temperatures (120-180°C). Additional investigation of these properties is of utmost importance for the future development of PBI PEMs.

As previously documented with para-PBI membranes, the room temperature tensile strengths of these membranes increased with both polymer inherent viscosity (molecular weight) and polymer content. However, increasing either of these properties dramatically increases the viscosity of the polymerization solution and alters the PPA Process. If the polymer content increases beyond a critical point, the solution becomes unprocessable. Para-PBI, for example, can only be cast with a polymer content up to approximately 5wt%. The initial monomer charge of each polymerization solution and the resulting polymer inherent viscosity are inversely proportional; raising the monomer charge reduces the achievable inherent viscosity of the polymer, and vice versa.

Herein, we propose a thorough investigation of novel structure-to-property relationships for PBI membranes to expand the scope of the PPA Process. By synthesizing functionalized PBI polymers made from more soluble monomers, one can increase polymer solubility and enable film casting from more concentrated solutions. This results in membranes with higher polymer content. Previously investigated pyridine-based polybenzimidazoles (py-PBI) (Section 1.2.2.4) were documented as having higher solubility in polyphosphoric acid (PPA), which was attributed to their higher concentration of basic sites (imidazole and imine groups). By synthesizing random copolymers of pyridine-PBIs with other well-known PBIs, one could potentially achieve highly concentrated polymerization solutions that could be processed into high polymer content membranes.

Chapters 2 and 3 of this dissertation focus on the synthesis of novel PBI copolymers for membranes with high polymer content as well as high thermal stability. Chapter 2 focuses on the incorporation of 3,5-pyridine-PBI (the most soluble pyridine-PBI in PPA) into random copolymers. Specifically, we prepared three sets of copolymers by the PPA Process: 3,5-pyridine-r-2OH-PBI, 3,5-pyridine-r-para-PBI, and 3,5-pyridine-r-meta-PBI copolymers. The highly soluble 3,5-pyridine moiety was used to impart higher polymer solubility in PPA, and therefore, higher polymer content in the membranes. Thus, copolymerizations of 3,5-pyridinedicarboxylic acid and TAB with dihydroxyterephthalic acid, terephthalic acid, and isophthalic acid were conducted to explore the relative solubilities and gel membrane stabilities. Membranes with higher polymer solids than previous work were prepared and characterized with regard to fuel cell performance as well as creep under compressive stress at high temperature. Chapter 3 performs a similar investigation with the incorporation of 2,5-pyridine-PBI (the least soluble pyridine-PBI in PPA) into random copolymers. We prepared three novel sets of copolymers by the PPA Process: 2,5-pyridine-r-2OH-PBI, 2,5-pyridine-r-para-PBI, and 2,5-pyridine-r-meta-PBI copolymers. The structures of each of these copolymers were related to the fundamental membrane properties of tensile strength, proton conductivity, fuel cell performance, and high temperature membrane creep.

A thorough understanding of the relationship between PBI solubility properties and the PPA Process, membrane mechanical properties, and membrane electrochemical properties is critical for the design of next-generation PBI PEM fuel cells. Chapter 4 presents an in-depth investigation of these relationships for the high polymer content PBI random copolymer membranes. It is generally believed that polymer solubility and

membrane properties are strongly influenced by the quantity of dipoles, strength of dipoles, and polymer chain flexibility. Because all of these polymers are wholly-aromatic, rigid-rod systems, we define chain flexibility in terms of persistence length and the projection of the end-to-end vector of the polymer chains (i.e. a measure of how kinked the polymer chain is). In other words, the para-substituted moieties are defined as having less flexible polymer chains than meta-substituted moieties. Herein, four copolymer membrane systems were compared to isolate the effects of these solubility properties in high polymer content membranes: 2,5-py-r-meta-PBI; 2,5-py-r-para-PBI; 3,5-py-r-meta-PBI; and 3,5-py-r-para-PBI. By comparing two systems with equivalent polymer chain flexibilities, one can isolate the influences of dipole strength or dipole quantity on polymer processing and membrane properties. Similarly, comparing two systems with equivalent dipole strength or dipole quantity can isolate the effects of polymer chain flexibility. The solubility to membrane processing and membrane property relationships are critical for the design of next generation PBI PEMs.

Alternative approaches at modifying the structures of PBI membranes were also investigated. Chapter 5 explores the viability of a PBI polymer blending approach, the synthesis of novel polyetherbenzimidazoles (PEBIs) and polyphosphonobenzimidazoles (phos-PBI), and the inclusion of various small-molecule organic additives to PBI membranes. The polymer blending approach involved the incorporation of dried PBI particles of various sizes and chemistries into a PBI polymerization solution. By incorporating PBI particles into the pre-cast PBI solution, we attempted to circumvent the viscosity issues associated with the PPA Process by delaying the solvation / swelling of the particles until after casting the membrane. Novel functionalized PBIs, such as our

proposed PEBIs, could offer alternative routes to more soluble PBIs that retain their physical and chemical robustness. Finally, the incorporation of small-molecule chemical crosslinkers and their effects on structure-to-property relationships was explored. The incorporation of phloroglucinol (Pg), a benzene ring that was tri-substituted with alcohol functional groups, was the focus of this research project. It was hypothesized that this molecule could crosslink in a similar fashion to 2OH-PBI, thereby enhancing both the anhydrous proton conductivity and the mechanical properties of the resulting membrane. A thorough investigation of phloroglucinol's solubility in PPA, as well as the structure-to-property relationships of the processed Pg-PBI membranes, was conducted.

1.5. REFERENCES

[1] 2008, "World Primary Energy Production by Source," Annual Energy Review, U.S. Energy Information Administration.

[2] 2008, "Primary Energy Consumption by Source and Sector," Annual Energy Review, Energy Information Administration.

[3] 2008, "Carbon Dioxide Emissions from the Consumption and Flaring of Fossil Fuels," Annual Energy Review, U.S. Energy Information Administration.

[4] Wainright, J., Wang, J., Weng, D., Savinell, R., and Litt, M., 1995, "Acid-doped polybenzimidazoles: a new polymer electrolyte," J. Electrochem. Soc., 142(7), pp. L121-L123.

[5] Dippel, T., Kreuer, K. D., Lassegues, J. C., and Rodriguez, D., 1993, "Proton conductivity in fused phosphoric acid; a $^{1}H/^{31}P$ PFG-NMR and QNS study," Solid State Ionics, 61, pp. 41-46.

[6] Bozkurt, A., Ise, M., Kreuer, K. D., Meyer, W. H., and Wegner, G., 1999, "Proton-conducting polymer electrolytes based on phosphoric acid," Solid State Ionics, 125, pp. 225-233.

[7] Weber, J., Kreuer, K.-D., Maier, J., and Thomas, A., 2008, "Proton Conductivity Enhancement by Nanostructural Control of Poly(benzimidazole)-Phosphoric Acid Adducts," Adv. Mater., 20, pp. 2595-2598.

[8] Vilciauskas, L., Paddison, S. J., and Kreuer, K.-D., 2009, "Ab Initio Modeling of Proton Transfer in Phosphoric Acid Clusters," J. Phys. Chem. A, 113, pp. 9193-9201.

[9] Mader, J., Lixiang, X., Schmidt, T., and Benicewicz, B. C., 2008, "Polybenzimidazole/Acid Complexes as High-Temperature Membranes," Adv. Polym. Sci., 216(Fuel Cells II), pp. 63-124.

[10] Wainright, J. S., Savinell, R. F., and Litt, M. H., 2003, "High Temperature Membranes," Handbook of Fuel Cells, 3, pp. 436-446.
[11] Colomban, P., 1992, Proton Conductors: Solids, membranes and gels - materials and devices, Cambridge University Press.
[12] Xiao, L., Zhang, H., Scanlon, E., Ramanthan, L. S., Choe, E. W., Rogers, D., Apple, T., and Benicewicz, B. C., 2005, "High-Temperature Polybenzimidazole Fuel Cell Membranes via a Sol-Gel Process," Chem. Mater., 17(21), pp. 5328-5333.
[13] Jayakody, J. R. P., Chung, S. H., Durantino, L., Zhang, H., Xiao, L., Benicewicz, B. C., and Greenbaum, S. G., 2007, "NMR Studies of Mass Transport in High-Acid-Content Fuel Cell Membranes Based on Phosphoric Acid and Polybenzimidazole," J. Electrochem Soc, 154(2), pp. B242-B246.
[14] Seel, D. C., Benicewicz, B. C., Xiao, L., and Schmidt, T. J., 2009, "High-temperature Polybenzimidazole-based Membranes," Handbook of Fuel Cells, 5, pp. 300-312.
[15] Litt, M., Ameri, R., Wang, Y., Savinell, R. F., and Wainright, J. S., 1999, "Polybenzimidazoles/phosphoric acid solid polymer electrolytes: mechanical and electrical properties.," Mater. Res. Soc. Symp. Proc., pp. 313-323.
[16] Zhang, H., December 2004, "Novel Phosphoric Acid Doped Polybenzimidazole Membranes for Fuel Cells," Ph.D. Thesis, Rensselaer Polytechnic Institute, Troy, NY.
[17] Li, Q., Hjuler, H. A., and Bjerrum, N. J., 2001, "Phosphoric acid doped polybenzimidazole membranes: physiochemical characterization and fuel cell applications," J. Appl. Electrochem., 31(7), pp. 773-779.
[18] Zhai, Y., Zhang, H., Liu, G., Hu, J., and Yi, B., 2006, "Performance degradation studies on PBI/H3PO4 high temperature PEMFC and one-dimensional numerical analysis," J. Electrochem. Acta., 52(2), pp. 394-401.
[19] Kongstein, O. E., Berning, T., Borresen, B., Seland, F., and Tunold, R., 2006, "Polymer electrolyte fuel cells based on phosphoric acid doped polybenzimidazole (PBI) membranes," Energy, 32(4), pp. 418-422.
[20] Kim, H., Cho, S. Y., An, S. J., Eun, Y. C., Kim, J., Yoon, H., Kweon, H., and YEW, K. H., 2004, "Synthesis of poly(2,5-benzimidazole) for use as a fuel-cell membrane," Macromol Rapid Commun, 25(8), pp. 894-897.
[21] Asensio, J. A., and Gomez-Romero, P., 2005, "Recent developments on proton conducting poly(2,5-benzimidazole) (AB-PBI) membranes for high temperature polymer electrolyte membrane fuel cells," Fuel Cells, 5(3), pp. 336-343.
[22] Li, Q. F., and Jensen, O. J., 2008, "Membranes for high temperature PEMFC based on acid-doped polybenzimidazoles," Membrane Technology, 2, pp. 61-96.
[23] Asensio, J. A., Borros, S., and Gomez-Romero, P., 2004, "Polymer Electrolyte Fuel Cells Based on Phosphoric Acid-Impregnated Poly(2,5-benzimidazole)," J. Electrochem. Soc., 151(2), pp. A304-A310.
[24] Chen, R., and Benicewicz, B. C., "Unpublished Work."
[25] Yu, S., 2006, "Novel polybenzimidazole derivatives for high temperature PEM fuel cells," Ph.D. Thesis, Rensselaer Polytechnic Institute, Troy, NY.

[26] Delano, C. B., Doyle, R. R., and Miligan, R. J., 1974, "High Strength, Thermally Stable Polymeric Fibers," No. AFML-TR-74-22, United States Air Force Materials Laboratory.
[27] Yu, S., Zhang, H., Xiao, L., Choe, E. W., and Benicewicz, B. C., 2009, "Synthesis of Poly (2,2'-(1,4-phenylene) 5,5'-bibenzimidazole) (para-PBI) and Phosphoric Acid Doped Membrane for Fuel Cells," Fuel Cells, 9(4), pp. 318-324.
[28] Xiao, L., 2003, "Novel polybenzimidazole derivatives for high temperature polymer electrolyte membrane fuel cell application," Ph.D. Thesis, Rensselaer Polytechnic Institute, Troy, NY.
[29] Xiao, L., Zhang, H., Jana, T., Scanlon, E., Chen, R., Choe, E. W., Ramanthan, L. S., Yu, S., and Benicewicz, B. C., 2005, "Synthesis and Characterization of Pyridine-Based Polybenzimidazoles for High Temperature Polymer Electrolyte Membrane Fuel Cell Applications," Fuel Cells, 5(2), pp. 287-295.
[30] Kallitsis, J. K., and Gourdoupi, N., 2003, "Proton Conducting Membranes Based on Polymer Blends for Use in High Temperature PEM Fuel Cells," J. New Mat. Electrochem. Systems, 6(4), pp. 217-222.
[31] Faure, S., Cornet, N., Gebel, G., Mercier, R., Pineri, M., and Sillion, B., 1997, "Sulfonated polyimides as novel proton exchange membranes for H2/O2 fuel cells," Proceedings of the International Symposium on New Materials for Fuel Cell and Modern Battery Systems, 2ndMontreal, pp. 818-827.
[32] Watari, T., Fang, J., Tanaka, K., Kita, H., Okamoto, K. I., and Hirano, T., 2004, "Synthesis, water stability and proton conductivity of novel sulfonated polyimides from 4,4'-bis(4-aminophenoxy)biphenyl-3,3'-disulfonic acid," J. Membr. Sci., 230(1-2), pp. 111-120.
[33] Lufrano, F., Gatto, I., Staiti, P., Antonucci, V., and Passalacqua, E., 2001, "Sulfonated polysulfone ionomer membranes for fuel cells," Solid State Ionics, 145(1-4), pp. 47-51.
[34] Einsla, B. R., Harrison, W. L., Tchatchoua, C., and McGrath, J. E., 2003, "Disulfonated polybenzoxazoles for proton exchange membrane fuel cell applications," Polym. Prepr, 44(2), pp. 645-646.
[35] Gil, M., Ji, X., Li, X., Na, H., Hampsey, J. E., and Lu, Y., 2004, "Direct synthesis of sulfonated aromatic poly(ether ether ketone) proton exchange membranes for fuel cell applications," J. Membr. Sci., 234(1-2), pp. 75-81.
[36] Xing, P., Robertson, G. P., Guiver, M. D., Mikhailenko, S. D., and Kaliaguine, S., 2004, "Sulfonated Poly(aryl ether ketone)s Containing the Hexafluoroisopropylidene Diphenyl Moiety Prepared by Direct Copolymerization, as Proton Exchange Membranes for Fuel Cell Application," Macromolecules, 37(21), pp. 7960-7967.
[37] Gao, Y., Robertson, G. P., Guiver, M. D., Mikhailenko, S. D., and Kaliaguine, S., 2004, "Synthesis of Copoly(aryl ether ether nitrile)s containing sulfonic acid groups for PEM applications," Macromolecules, 37(18), pp. 6748-6754.
[38] Xiao, G. Y., Sun, G. M., Yan, D. Y., Zhu, P. F., and Tao, P., 2002, "Synthesis of sulfonated poly(phthalazinone ether sulfone)s by direct polymerization," Polym. Prepr., 43(19), pp. 5335-5339.
[39] Wang, F., Hickner, M., Kim, Y. S., Zawodzinksi, T. A., and McGrath, J. E., 2002, "Direct polymerization of sulfonated poly(arylene ether sulfone) random

(statistical) copolymers: candidates for new proton exchange membranes," J. Membr. Sci., 197(1-2), pp. 231-242.
[40] Hickner, M. A., Ghassemi, H., Kim, Y. S., Einsla, B. R., and McGrath, J. E., 2004, "Alternative polymer systems for proton exchange membranes (PEMs)," Chem. Rev., 104(10), pp. 4587-4611.
[41] Kim, S., Cameron, D. A., Lee, Y., Reynolds, J. R., and Savage, C. R., 1996, "Aromatic and rigid rod polyelectrolytes based on sulfonated poly(benzobisthiazoles)," J. Polym. Sci., Part A, 34(3), pp. 481-492.
[42] Ariza, M. J., Jones, D. J., and Roziere, J., 2002, "Role of post-sulfonation thermal treatment in conducting and thermal properties of sulfuric acid sulfonated poly(benzimidazole) membranes," Desalination, 147(1-3), pp. 183-189.
[43] Staiti, P., Lufrano, F., Arico, A. S., Passalacqua, E., and Antonucci, V., 2001, "Sulfonated polybenzimidazole membranes - preparation and physico-chemical characterization," J. Membr. Sci., 188(1), pp. 71-78.
[44] Bae, J. M., Honma, I., Murata, M., Yamamoto, T., Rikukawa, M., and Ogata, N., 2002, "Properties of selected sulfonated polymers as proton-conducting electrolytes for polymer electrolyte fuel cells," Solid State Ionics, 147(1-2), pp. 189-194.
[45] Asensio, J. A., Borros, S., and Gomez-Romero, P., 2002, "Proton-conducting polymers based on benzimidazoles and sulfonated benzimidazoles," J. Polym. Sci., Part A, 40(21), pp. 3703-3710.
[46] Sakaguchi, Y., Kitamura, K., Nakao, J., Hamamoto, S., Tachimori, H., and Takase, S., 2001, "Preparation and properties of sulfonated or phosphonated polybenzimidazoles and polybenzoxazoles," J. Polym. Mater. Sci. Eng., 84, pp. 899-900.
[47] Mader J., and Benicewicz B. C., 2010, "Sulfonated Polybenzimidazoles for High Temperature PEM Fuel Cells," Macromolecules, **43**, pp.6706-6715.
[48] He, R., Li, Q., Xiao, G. Y., and Bjerrum, N. J., 2003, "Proton conductivity of phosphoric acid doped polybenzimidazole and its composites with inorganic proton conductors," J. Membr. Sci., 226(1-2), pp. 169-184.
[49] Qian, G., and Benicewicz, B. C., 2009, "Synthesis and Characterization of High Molecular Weight Hexafluoroisopropylidene-Containing Polybenzimidazole for High-Temperature Polymer Electrolyte Membrane Fuel Cells," J. Polym. Sci., Part A, 47(16), pp. 4064-4073.
[50] Yu, S., and Benicewicz, B. C., 2009, "Synthesis and Properties of Functionalized Polybenzimidazoles for High-Temperature PEMFCs," Macromolecules, 42(22), pp. 8640-8648.
[51] Scanlon, E., 2005, "Polybenzimidazole Based Segmented Block Copolymers for High Temperature Fuel Cell Applications," Ph.D. Thesis, Rensselaer Polytechnic Institute, Troy, NY.
[52] Schmidt, T. J., 2006, "Durability and degradation in high-temparature polymer electrolyte fuel cells," ECS Transactions, 1(8), pp. 19-31.
[53] Schmidt, T. J., 2009, "High-Temperature Polymer Electrolyte Fuel Cells: Durability Insights," Polymer Electrolyte Fuel Cell Durability, F. N. Buchi, M. Inaba, and T. J. Schmidt, eds., Springer, New York, pp. 199-221.

[54] Ross Jr., P. N., 1987, Deactivation and poisoning of fuel cell catalysts, Marcel Dekker, New York.
[55] Ferreira, P. J., la O', G. J., Shao-Horn, Y., Morgan, D., Makharia, R., Kocha, S., and Gasteiger, H. A., 2005, "Instability of Pt/C electrocatalysts in proton exchange membrane fuel cells: A mechanistic investigation," J. Electrochem Soc, 152(11), pp. A2256-A2271.
[56] Tang, L., Han, B., Persson, K., Friesen, C., He, T., Sieradzki, K., and Ceder, G., 2010, "Electrochemical Stability of Nanometer-Scale Pt Particles in Acidic Environments," J. Am. Chem. Soc., 132(2), pp. 596-600.
[57] Liu, G., Zhang, H., Zhai, Y., Zhang, Y., Xu, D., and Shao, Z.-g., 2007, "Pt_4ZrO_2/C cathode catalyst for improved durability in high temperature PEMFC based on H_3PO_4 doped PBI," Electrochem. Commun., 9(1), pp. 135-141.
[58] Landsman, D. A., and Luczak, F. J., 2003, Handbook of Fuel Cells - Fundamentals, Technology and Applications, W. Vielstich, A. Lamm, and H. Gasteiger, eds., John Wiley & Sons, Chicester, U.K., pp. 811-831.
[59] Neyerlin, K. C., Singh, A., and Chu, D., 2008, "Kinetic characterization of a Pt-Ni/C catalyst with a phosphoric acid doped PBI membrane in a proton exchange membrane fuel cell," J. of Power Sources, 176(1), pp. 112-117.
[60] Schmidt, T. J., and Baurmeister, J., 2008, "Properties of high-temperature PEFC Celtec-P 1000 MEAs in start/stop operation mode," J. of Power Sources, 176(2), pp. 428-434.
[61] Luczak, F. J., and Landsman, D. A., 1984, "Ordered Ternary Fuel Cell Catalysts Containing Platinum, Cobalt and Chromium."
[62] Luczak, F. J., and Landsman, D. A., 1987, "Ordered Ternary Fuel Cell Catalysts Containing Platinum and Cobalt and Method for Making the Catalyst."
[63] Beard, B., and Ross Jr., P. N., 1990, "The structure and activity of platinum-cobalt alloys as oxygen reduction electrocatalysts," J. Electrochem Soc, 137(11), pp. 3368-3374.
[64] Glass, J. T., Cahen, G. L., and Stoner, G. E., 1987, "The effect of metallurgical variables on the electrocatalytic properties of platinum-chromium alloys," J. Electrochem Soc, 134(1), pp. 58-65.
[65] Mukerjee, S., and Srinivasan, S., 1993, "Enhanced electrocatalysis of oxygen reduction on platinum alloys in proton exchange membrane fuel cells," J. Electroanal. Chem., 357(1-2), pp. 201-224.
[66] Mukerjee, S., Srinivasan, S., and Soriaga, M. P., 1995, "Role of structural and electronic properties of Pt and Pt alloys on electrocatalysis of oxygen reduction. An in situ XANES and EXAFS investigation.," J. Electrochem Soc, 142(5), pp. 1409-1422.
[67] Paulus, U. A., Scherer, G. G., Wokaun, A., Schmidt, T. J., Stamenkovic, V., Radmilovic, V., Markovic, N. M., and Ross, P. N., 2002, "Oxygen Reduction on Carbon-Supported Pt-Ni and Pt-Co Alloy Catalysts," J. Phys. Chem. B, 106(16), pp. 4181-4191.
[68] Stamenkovic, V., Schmidt, T. J., Ross, P. N., and Markovic, N. M., 2002, "Surface Composition Effects in Electrocatalysis: Kinetics of Oxygen Reduction on Well-Defined Pt3Ni and Pt3Co Alloy Surfaces," J. Phys. Chem. B, 106(46), pp. 11970-11979.

[69] Stamenkovic, V., Fowler, B., Mun, B. S., Wang, B., Ross, P. N., Lucas, C. A., and Markovic, N. M., 2007, "Improved Oxygen Reduction Activity on Pt3Ni(111) via Increased Surface Site Availability," Science, 315(5811), pp. 493-497.
[70] Parrondo, J., Mijangos, F., and Rambabu, B., 2010, "Platinum/tin oxide/carbon cathode catalyst for high temperature PEM fuel cell," J. Power Sources, 195(13), pp. 3977-3983.
[71] Qian, G., 2008, "Fluorine-containing Polybenzimidazoles for High Temperature Polymer Electrolyte Membrane Fuel Cell Applications," Ph.D. Thesis, Rensselaer Polytechnic Institute, Troy, NY.
[72] Gasteiger, H., and Markovic, N. M., 2009, "Just a dream - or future reality?," Science, 324(5923), pp. 48-49.
[73] Debe, M. K., Schmoeckel, A. K., Vernstrom, G. D., and Atanasoski, R., 2006, "High voltage stability of nanostructured thin film catalysts for PEM fuel cells," J. Power Sources, 161(2), pp. 1002-1011.
[74] Strasser, P., 2009, Handbook of Fuel Cells: Advances in Electrocatalysis, Materials, Diagnostics, and Durability, W. Vielstich, H. Yokokawa, and H. A. Gasteiger, eds., John Wiley & Sons, New York, pp. 30-47.
[75] Lefevre, M., Proietti, E., Jaouen, F., and Dodelet, J.-P., 2009, "Iron-Based Catalysts with Improved Oxygen Reduction Activity in Polymer Electrolyte Fuel Cells," Science, 324(5923), pp. 71-74.
[76] Remick, R. J., Wheeler, D. J., and Singh, P., 2010, "MCFC and PAFC R&D Workshop Summary Report. US Department of Energy.."
[77] Yu, S., Xiao, L., and Benicewicz, B. C., 2008, "Durability Studies of PBI-based High Temperature PEMFC," Fuel Cells, 8(3-4), pp. 165-174.
[78] Okae, I., Kato, S., Seya, A., and Kamoshita, T., 1990, "Study of the Phosphoric Acid Management in PAFCs," The Chemical Society of Japan 67th Spring Meeting.
[79] 2005, "Manufacturing for the Hydrogen Economy: Manufacturing Research and Development of PEM Fuel Cell Systems for Transportation Application," U.S. Department of Energy, Washington, D.C.
[80] 2009, "Hydrogen Fuel Cell Vehicle and Station Deployment Plan: A Strategy for Meeting the Challenge Ahead," California Fuel Cell Partnership, West Sacramento, CA.
[81] Feitelberg, A. S., Stathopoulos, J., Qi, Z., Smith, C., and Elter, J. F., 2005, "Reliability of Plug Power GenSys fuel cell systems," J. Power Sources, 147(1-2), pp. 203-207.
[82] Schmidt, T. J., and Baurmeister, J., 2006, "Durability and Reliability in High Temperature Reformed Hydrogen PEFCs," ECS Transactions, 3(1), pp. 861-869.
[83] Mocoteguy, P., Ludwig, B., Scholta, J., Barrera, R., and Ginocchio, S., 2009, "Long Term Testing in Continuous Mode of HT-PEMFC Based H3PO4/PBI Celtec-P MEAs for u-CHP Applications," Fuel Cells, 9(4), pp. 325-348.
[84] Mocoteguy, P., Ludwig, B., Scholta, J., Nedellec, Y., Jones, D. J., and Roziere, J., 2010, "Long-Term Testing in Dynamic Mode of HT-PEMFC H3PO4/PBI Celtec-P Based Membrane Electrode Assemblies for Micro-CHP Applications," Fuel Cells, 10(2), pp. 299-311.

[85] Garsany, Y., Gould, B. D., Baturina, O. A., and Swider-Lyons, K. E., 2009, "Comparison of the Sulfur Poisoning of PBI and Nafion PEMFC Cathodes," Electrochemical and Solid-State Letters, 12(9), pp. B138-B140.
[86] Schmidt, T. J., and Baurmeister, J., 2008, "Development Status of PBI based High-Temperature Membrane Electrode Assemblies," ECS Transactions, 16(2), pp. 263-270.
[87] Reiser, C. A., Bregoli, L., Patterson, T. W., Yi, J. S., Yang, J. D., Perry, M. L., and Jarvi, T. D., 2005, "A Reverse-Current Decay Mechanism for Fuel Cells," Electrochem. Sol. Let., 8(6), pp. A273-A276.
[88] Puffer Jr., R. H., and Rock, S. J., 2009, "Recent Advances in High Temperature Proton Exchange Membrane Fuel Cell Manufacturing," J. of Fuel Cell Sci. and Tech., 6(4), pp. 041013/041011-041013/041017.
[89] Puffer Jr., R. H., and Hoppes, G. H., 2004, "Development of a Flexible Pilot High Temperature MEA Manufacturing Line," Fuel Cell Science, Engineering and Technology--2004, pp. 573-579.
[90] Harris, T. A. L., and Walczyk, D., 2006, "Development of a Casting Technique for Membrane Material Used in High-Temperature PEM Fuel Cells," Journal of Manufacturing Processes, 8(1), pp. 19-31.
[91] Hake, J.-F., Birnbaum, U., Haines, M., and Linssen, J., 2008, "Reduction of greenhouse gas emissions through fuel cell combined heat and power applications," 17th World Hydrogen Energy ConferenceBrisbane, Australia.
[92] Schmidtz, R., 2009, "Japan Working Toward Fuel-Cell Reality," Marketplace, p. 1.
[93] 2010, "Celtec MEAs: Membrane Electrode Assemblies for High Temperature PEM Fuel Cells," BASF Fuel Cell GmbH.
[94] 2009, "High-Temperature Fuel Cell System for Residential Applications," Plug Power, Latham, NY.
[95] 2010, "Serenus 166/390 Air C v2.5," Serenergy, Hobro, Denmark.
[96] 2009, "ClearEdge Power, Delivering Smart Energy Today," http://www.clearedgepower.com/.
[97] 2009, "Emissions of Greenhouse Gases Report," U.S. Energy Information Administration, Washington, DC.
[98] Barry, K., 2010, "A Hydrogen Highway for the East Coast," Wired.com.
[99] English, A., 2008, "Driving VW's fuel-cell prototypes," Telegraph.co.uk, Telegraph Media Group Limited.
[100] Dec. 2009, "Innovative Danish technology uses methanol to make fuel cell vehicles competitive," renewableenergyfocus.com.
[101] 2009, "DLR Motor Glider Antares Takes Off in Hamburg - Powered by a Fuel Cell," German Aerospace Center.
[102] Smock, D., Sept. 18, 2009, "What's Next after the Dreamliner? Think Fuel Cells," Design News.
[103] 2008, "UltraCell XX25: Mobile Power for Mobile Applications," Ultracell, Livermore, CA.
[104] 2008, "UltraCell XX55: Extreme Mobile Power for Demanding Applications," Ultracell, Livermore, CA.
[105] 2010, "Serenus Methanol fuel cell module - 350W," Serenergy, Hobro, Denmark.

[106] Maget, H. J. R., Jan. 13,1970, "Process for Gas Purification, U.S. Patent 3489670."
[107] McElroy, J. F., Aug. 1989, "SPE regenerative hydrogen / oxygen fuel cells for extraterrestrial surface applications," Energy Conversion Engineering Conference, IEEE, Washington, DC, USA, pp. 1631-1636.
[108] Rohland, B., Eberle, K., Strobel, R., Scholta, J., and Garche, J., 1998, "Electrochemical Hydrogen Compressor," Electrochem. Acta., 43(24), p. 3841.
[109] Perry, K. A., Eisman, G. A., and Benicewicz, B. C., 2008, "Electrochemical hydrogen pumping using a high-temperature polybenzimidazole (PBI) membrane," J. Power Sources, 177(2), pp. 478-484.

2. High Polymer Content 3,5-Pyridine-Polybenzimidazole Copolymer Membranes with Improved Compressive Properties

2.1. Motivation for Research Project

Polymer electrolyte membrane (PEM) fuel cells, also known as proton exchange membrane fuel cells, have gained much attention over the past several decade as efficient energy conversion devices for both mobile and stationary applications.[1,2] Fueled by a proton source such as hydrogen, a metal catalyst at the anode splits the fuel into its constituent protons and electrons. The electrons pass through an external circuit to the cathode, thereby creating electricity, while the protons are solvated and transported through the membrane to the cathode. The electrons and protons combine with oxygen at the cathode, thus creating water and heat as the only byproducts of the conversion process. State-of-the-art perfluorosulfonic acid (PSFA)-based PEMs, such as DuPont's Nafion, depend on water clusters to transport protons from the anode to the cathode. Since the operational temperature range is limited by the evaporation of water, these fuel cells have a low tolerance to fuel impurities and require a complicated humidification system. In contrast, PA-doped polybenzimidazole (PBI)-based PEMs have been shown to operate at temperatures up to 200˚C with higher tolerances to fuel impurities, smaller heat exchangers, and no humidification requirements.[3–7]

The conventional process for preparing PBI membranes involves PBI film casting from an organic solvent, solvent evaporation, and subsequent imbibing of PA by the membrane.[8–12] In contrast, the PPA Process offers a more facile route to processing PBI membranes.[3,4,13–15] Diacid monomers are polymerized with tetraamines in PPA under nitrogen at typical temperatures of 190-220°C. This simple one-pot reaction produces PBIs of high molecular weight that are completely dissolved in PPA. The polymerization solution can be directly cast to produce films of uniform thickness. The cast polymer films are then placed into a phosphoric acid (PA) bath or a controlled humidity chamber to hydrolyze the PPA into PA. Since PA is a poor solvent for many PBIs, the film undergoes a sol-to-gel transition which produces a gel membrane fully imbibed with PA. This produces a Type 3 Flory gel, one with polymer networks formed by physical aggregation of polymer chains.[16] Excess water and PA generated through the hydrolysis process are drained from the membranes prior to characterization and use of the membranes.

Both the phosphoric acid content and the membrane morphology are influenced by the membrane processing technique. Membranes processed conventionally from organic solvents and subsequently imbibed tend to contain less phosphoric acid than those cast from the PPA Process. Additionally, a comparative study of the two casting techniques showed that two meta-PBI membranes with similar PA content had different proton conductivities.[17] The PPA Process generated a membrane with a higher conductivity, 0.13 S cm^{-1}, compared with 0.048 S cm^{-1} from a conventionally cast membrane. Because these two membranes had the same chemical composition (polymer

type, molecular weight, and phosphoric acid content), this demonstrated that the casting technique plays a fundamental role in the determination of the membrane properties.

Studies over the last decade have shown that PBI membranes have outstanding fuel cell performance.[15,18,19] Fuel cells employing poly(2,2′-(1,4-phenylene)5,5′-bibenzimidazole) (*para*-PBI) cast from the PPA Process has been shown to operate for over 14,000h under steady-state conditions (>0.6 V at 0.2 A cm^{-2}).[5] However, little is known about the membrane's resistance to long-term degradation modes including polymer creep and membrane thinning, which can result in gas crossover, voltage degradation, and the eventual quenching of the fuel cell. For stationary fuel cell applications, the Department of Energy has an operational target of 40,000h for 2014.[20] To reach this goal, enhancement of the mechanical properties of PBI membranes is of great importance to prevent membrane creep and enhance the lifetimes of the fuel cell. One study investigated the mechanical properties of a low polymer content PBI-based MEA at 180°C [21] and confirmed that the contact stress in the MEA decreased with time. Initial creep and compression properties of commercially available Nafion membranes at elevated temperatures (70-90 °C) have been documented; however, these water-based membranes have inherent mechanical issues at elevated temperatures due to dehydration of the polymer matrix.[22–24] Studies on the high temperature creep properties in compression have not been reported for PBI membranes, despite the importance of such properties for long-term fuel cell operation. New approaches to improving the long-term mechanical properties of PBI membranes are needed which are cost effective and compatible with the manufacturing processes that have been developed for these unique membrane materials.

One way to improve the mechanical properties of PBI membranes may be to increase the polymer content of the gel membrane. However, the processability of the PBI/PPA solution into a film is limited by the solubility of the polymer and viscosity of the solution. If the polymer content increases beyond a critical point, the solution becomes unprocessable. Para-PBI, for example, can only be cast with a polymer content up to approximately 5wt%. This limitation can be circumvented by synthesizing functionalized PBI polymers made from more soluble monomers. Increasing polymer solubility enables film casting from more concentrated solutions, leading to membranes with higher polymer content.

A wide variety of soluble PBIs, prepared via the PPA Process, have been investigated as candidates for high temperature fuel cell membranes.[18] Functionalized polybenzimidazoles, such as dihydroxy-PBI (2OH-PBI), were shown to improve proton transport and thermal stability of the gel membrane.[4] Figure 2.1 compares the relative solubility and gel stability of four common functionalized PBIs. Dihydroxy-PBI has a unique network of phosphate branches and crosslinks that both lowers the solubility of the polymer in PPA and increases its chemical stability (inferred from its poor solubility in concentrated sulfuric acid). Pyridine-based polybenzimidazoles (py-PBI) have been investigated because of their higher solubility in polyphosphoric acid (PPA), which was attributed to their higher concentration of basic sites (imidazole and imine groups).[25] Additionally, PBI monomers that have meta-oriented constituents are generally more soluble than para-oriented PBIs due to their improved backbone flexibility. This increased solubility of the PBIs only has minor effects on the thermal stability of the PBI itself, retaining degradation temperatures above 350°C. However, increasing the

solubility of the PBIs has been shown to decrease the gel stability of the film at elevated temperatures. Our previous research has shown that 3,5-pyridine-PBI is too soluble in PA to form a stable gel membrane at room temperature.[25]

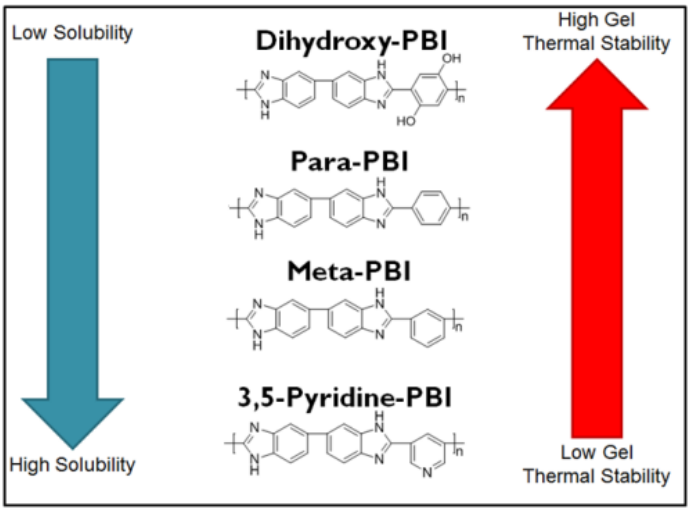

Figure 2.1. Relative comparison of PBI chemistries, gel thermal stabilities, and solubilities in PPA and PA.

Our prior work thus shows a fundamental limitation of PBI homopolymers for preparing gel membranes (Figure 2.1). Increasing monomer solubility leads to higher membrane polymer content, but it has a negative impact on membrane thermal stability. In this work, we report the synthesis of novel PBI copolymers for membranes with high polymer content as well as high thermal stability. Specifically, we prepared three sets of copolymers by the PPA Process: 3,5-pyridine-r-2OH-PBI, 3,5-pyridine-r-para-PBI, and 3,5-pyridine-r-meta-PBI copolymers. The highly soluble 3,5-pyridine moiety was used to impart higher polymer solubility in PPA, and therefore, higher polymer content in the membranes. Thus, copolymerizations of 3,5-pyridinedicarboxylic acid and TAB with dihydroxyterephthalic acid, terephthalic acid, and isophthalic acid were conducted to explore the relative solubilities and gel membrane stabilities. Membranes with higher

polymer solids than previous work were prepared and characterized with regard to fuel cell performance as well as creep under compressive stress at high temperature. The current study reports the relationships between PBI chemical structure and membrane composition with the fundamental properties of gel stability, membrane conductivity, mechanical properties and fuel cell performance.

2.2. Experimental

2.2.1. Chemicals

3,5-Pyridinedicarboxylic acid was purchased from Acros Chemical, TCI America, and Yongyi Chemicals Group Co., Ltd (~98% purity) and purified by recrystallization from a 1:10 dilution of concentrated hydrochloric acid prior to use. 2,5-Dihydroxyterephthalic acid was purchased from Fisher Scientific and Sigma Aldrich, and it was purified by recrystallization from a 3:2 dilution of absolute ethanol to deionized water prior to use. Terephthalic acid (TPA, purified) and isophthalic acid (IPA, purified) were purchased from Amoco Chemicals and used as-received. 3,3',4,4'-Tetraaminobiphenyl (TAB, purified) and polyphosphoric acid (PPA, 115%) were donated by BASF Fuel Cells and used as-received.

2.2.2 Polybenzimidazole Synthesis and Membrane Preparation

To a three-necked flask equipped with nitrogen flow and overhead stirrer, a solution of 3,5-pyridinedicarboxylic acid (py-2COOH), 3,3',4,4'-tetraaminobiphenyl (TAB), polyphosphoric acid (PPA), and either isophthalic acid (IPA), terephthalic acid (TPA), or 2,5-dihydroxyterephthalic acid (2OH-TPA) was stirred and heated to 195-220°C for 3-30 hours. This polymerization scheme is detailed in Scheme 2.1. The polymerization time correlated with both monomer concentration and ratio of the

pyridine monomer to the other diacid monomer. Both the stir-rate and the temperature were adjusted during the polymerization. At the end of the polymerization, the PBI solution was poured onto a pyrex or glass plate and cast at a thickness of 15mil using a Gardner blade. To form a gel membrane, the glass plates with the cast films were immediately placed into a humidity controlled chamber at 55% ± 5% relative humidity (RH), 25 ± 2°C. Complete hydrolysis of the membranes occurred over 12-24h. The final gel membrane thickness was approximately 300-500μm.

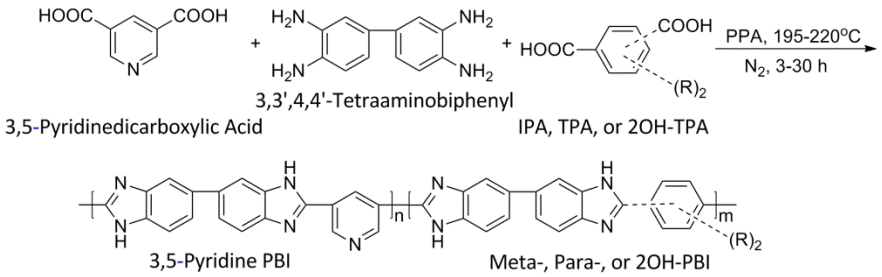

Scheme 2.1. Synthesis of random copolymers using 3,5-pyridinedicarboxylic acid and TAB with terephthalic acid (R=H), isophthalic acid (R=H), or 2,5-dihydroxyterephthalic acid (R= -OH).

2.2.3 Characterization Techniques

The composition of acid-doped PBI membranes was determined by measuring the relative amounts of polymer solids, water, and acid in the film. The phosphoric acid (PA) content was determined by titrating a sample of membrane with standardized sodium hydroxide solution (0.1 N) using a Metrohm 716 DMS Titrino autotitrator. The sample was washed with water and dried in an oven overnight at 120 °C. The dried sample was then weighed to determine polymer solids content for the membrane. The amount of water was calculated by subtracting the weights of polymer and PA from the initial PBI membrane sample weight.

Thermal analysis and inherent viscosity measurements were performed on polymer isolated from the PPA process. Following the polymerization of the random copolymers, the polymer/PPA solution was hydrolyzed in deionized water and the polymer was mechanically blended into small particles. The polymer was filtered and placed in an oven overnight at 120°C to dry the sample. Thermogravimetric analysis (TGA) was performed using a TA Instruments TGA Q-5000 IR with a heating rate of 10 °C min^{-1} under nitrogen. Differential scanning calorimetry (DSC) was conducted using a TA Instruments DSC Q-2000 with a nitrogen flow rate of 20 mL min^{-1} and heating and cooling rates of 10°C min^{-1}. Inherent viscosities (IV's) were measured in concentrated sulfuric acid at 30.0˚C and 0.2 g dL^{-1} concentration using an Ubbelohde viscometer. The following equation was used to calculate the IV:

$$\ln [(t) (t_o)^{-1}] c^{-1} = IV \text{ (dL } g^{-1}) \qquad (2.1)$$

The tensile properties of the membranes were tested at room temperature using an Instron Model 5543A system with a 10 N load cell and crosshead speed of 5 mm/min. Dog-bone shaped specimens were cut according to ASTM standard D683 (Type V specimens) and preloaded to 0.1 N prior to testing.

The compression creep tests were performed using a TA Instruments RSAIII dynamic mechanical analyzer. Discs were cut from polymer membranes with a diameter of 6.3 mm and thickness of approximately 0.9~1.2 mm. Before the compression creep tests, the samples were conditioned by placing them between two parallel smooth Teflon blocks at 180°C for approximately 24 hours. In a typical compression creep test, a step stress was applied to the sample and held constant for 20 hours. The deformation of the

test specimen was recorded as a function of time. To ensure the compression stress was uniaxial, the compression tool surfaces were coated with PTFE to minimize the friction between the sample and the tool. The creep compliance was calculated by dividing the strain with the applied stress, and the compliance as a function of time was fitted with the Maxwell model[26]:

$$J(t) = J_s^0 + t \cdot {\eta_0}^{-1} \qquad (2.2)$$

where J_s^0represents the steady-state (recoverable) compliance, t is time, and η_0 is the extensional viscosity at zero extension rate. All tests were carried out at 180 °C, and the applied stress level was selected to be 0.1 MPa.

Frequency sweep tests were also performed using the TA Instruments RSAIII at various temperatures for characterization of the thermal stability of the gel membranes. Cylindrical compression samples were used with diameter 15mm and thickness ~4mm. Before the tests, the samples were conditioned in vacuo at 80 °C for 24 hours. The storage modulus (E') and loss modulus (E") were recorded as functions of frequency at various temperatures. The test frequency ω spanned from 0.00249 Hz to 9.9 Hz, and a strain amplitude of 0.25% was used.

Ionic conductivities were measured *via* a four-probe through-plane bulk measurement using an AC Zahner IM6e impedance spectrometer that scanned a frequency range from 1 Hz to 100 KHz. A rectangular sample of membrane (3.5 cm x 7.0 cm) was placed in a glass cell with four platinum wire current collectors. Two outer electrodes set 6.0 cm apart supplied current to the cell, while the two inner electrodes 2.0 cm apart on opposite sides of the membrane measured the voltage drop. To ensure a

through-plane bulk measurement of the membrane ionic conductivity, the two outer electrodes were placed on opposite sides of the membrane and the two inner electrodes were arranged in the same manner. The reported conductivities were of preconditioned (dried) membranes that were held at >100°C for at least two hours. Proton conductivity was calculated using the following equation:

$$\sigma = D \cdot (L \cdot B \cdot R)^{-1} \qquad (2.3)$$

where D was the distance between the two test current electrodes, L was the thickness of the membrane, B was the width of the membrane, and R was the measured resistance.

Membrane electrode assemblies consisted of the polymer membrane sandwiched between two electrodes. MEAs were prepared by hot pressing the acid-doped membrane between an anode electrode and a cathode electrode at 150 °C for 90-150 seconds using 4500 lbs of force and compressing to 80% its original width. Prior to compression, the membrane was pretreated with concentrated phosphoric acid (< 10 seconds) to wet its surface, thereby reducing the interfacial resistance of the membrane-catalyst interface. Electrodes were received from BASF Fuel Cell, Inc. with 1.0 mg cm^{-2} platinum (Pt) catalyst loading. Anode electrodes contained only Pt as the catalyst, while the cathode electrodes contained a BASF Fuel Cell standard cathode Pt alloy. The active area of the electrodes was 45.15 cm^2. Fuel cell fabrication was conducted by assembling the cell components as follows: end plate:anode current collector:anode flow field:MEA:cathode flow field:cathode current collector:end plate. Gaskets were used on either side of the MEA to control compression. Following assembly, the cell was evenly clamped to 50 in-lbs of pressure.

Fuel cell performance was measured on 50 cm^2 (active area 45.15 cm^2) single stack fuel cells using test stations obtained from Plug Power or purchased from Fuel Cell Technologies. Polarization curves were obtained at various temperatures (120-180 °C) with hydrogen as a fuel and different oxidants (air or oxygen gas). Fuel cells were operated for at least 100 hours (break-in period) at 0.2 A cm^{-2} at 180 °C before measurement of polarization curves. Long-term stability testing was performed under static current and temperature conditions of 0.2 A cm^{-2} and 180 °C with a constant flow rate of hydrogen and air. Degradation rates of long-term fuel cell operations were calculated by linear fitting of cell voltage data points with respect to time. Product water and PA from the exhaust gases were collected by passing the gases through bottles containing distilled water. The PA loss was determined by analyzing the water in the collection bottles using an ascorbic acid test and UV-Vis absorbance at 880nm wavelength.[27]

2.3 Results and Discussion

2.3.1. Synthesis and Characterization of Random Copolymers

Three series of 3,5-pyridine-r-2OH-PBI, 3,5-pyridine-r-para-PBI, and 3,5-pyridine-r-meta-PBI copolymers were polymerized and cast into membranes using the PPA process. The ratio of pyridine monomer to either isophthalic, terephthalic , or 2,5-dihydroxyterephthalic acid was adjusted for each polymerization. Tables 2.1-2.3 describe the copolymer compositions, mechanical properties, and electrochemical characteristics. Stoichiometric control of diacid:tetraamine was maintained at 1:1 for all polymerizations.

Table 2.1. Chemical, electrochemical, and thermal characterizations of 3,5-pyridine-r-para-PBIs. NFF = Not Film Forming

Notebook #	Monomer Charge (wt%)	Ratio of 3,5-py-PBI to p-PBI	Polymerization Time at 195°C – 220°C (h)	Inherent Viscosity (dL/g)	PA content (%wt)	Polymer contents (%wt)	Water content (%wt)	PA mole ratio to PBI repeat unit	Young's Modulus (MPa)	Strain at Break (mm/mm)	Thickness (mm)	Anhydrous Conductivity at 180°C (S/cm)	Fuel Cell Voltage at 180°C After Break-in @ 0.2A/cm^2 (V)
MM1-103-5	4%	1 to 5	16		58.20%	8.36%	33.44%	21.924	1.298	6.001	0.301	0.234	
MM1-103-3	6%	1 to 5	8		66.31%	9.29%	24.40%	22.475	4.315	0.591	0.284	0.221	
MM1-103-1	8%	1 to 5	4.5		62.67%	11.84%	25.49%	16.735	6.192	0.524	0.322	0.204	
MM1-103-2	10%	1 to 5	4		54.25%	15.25%	30.51%	11.224	8.094	0.111	0.32	0.083	
MM1-36-02	12%	5 to 1	13	1.42	55.00%	14.03%	30.96%	12.377	2.072	5.244	0.683	Failed	
MM1-36-04	12%	3 to 1	13	1.87	60.97%	13.04%	25.99%	11.324	3.902	3.508	0.415	0.05	
MM1-44-4	12%	2 to 1	12		54.53%	15.20%	30.27%	11.32	11.022	1.213	0.379	0.136	0.58
MM1-36-03	12%	2 to 1	13	1.42	53.02%	14.76%	32.21%	14.784	6.705	2.354	0.605	0.162	
MM1-37-01	12%	1 to 1	11	1.25	54.77%	14.91%	30.31%	11.6	6.481	1.734	0.385	0.17	0.57
MM1-39-01	12%	1 to 2	8	1.66	54.74%	17.81%	27.45%	9.68	8.151	1.454	0.39	0.102	0.53
MM1-39-03	12%	1 to 2	6		53.46%	17.69%	28.85%	9.53	10.812	0.401	0.358	0.065	0.45
MM1-39-02	12%	1 to 5	13	1.37	56.00%	14.87%	29.13%	11.86	9.041	0.638	0.294	0.159	0.65
MM1-43-02	12%	1 to 7	9	0.73	NFF	NFF	NFF	NFF	NFF	NFF	NFF	NFF	
MM1-39-04	12%	1 to 11	3		NFF	NFF	NFF	NFF	NFF	NFF	NFF	NFF	
MM1-37-02	16%	5 to 1	11	1.25	17.74%	17.65%	64.61%	3.171	6.778	0.845	0.4	0.094	Failed
MM1-37-03	16%	3 to 1	9	1.18	57.06%	17.11%	25.83%	10.518	10.682	0.284	0.44	0.101	Failed
MM1-37-04	16%	2 to 1	11	1.07	45.91%	18.44%	35.65%	7.887	10.448	0.664	0.412	0.082	0.55
MM1-37-05	16%	1 to 1	11		59.07%	19.54%	21.40%	9.53	5.489	0.085	0.35	0.103	0.58
MM1-41-05	16%	2 to 3	10	0.22	NFF	NFF	NFF	NFF	NFF	NFF	NFF	NFF	NFF
MM1-41-03	16%	1 to 2	5		NFF	NFF	NFF	NFF	NFF	NFF	NFF	NFF	NFF
MM1-39-05	16%	1 to 3	4	0.15	NFF	NFF	NFF	NFF	NFF	NFF	NFF	NFF	NFF
MM1-43-5	20%	15 to 1	3		50.60%	22.85%	26.55%	6.99	20.286	0.203	0.457	0.074	Failed
MM1-41-7	20%	9 to 1	9		52.08%	21.57%	26.36%	7.62	26.389	0.257	0.46	0.074	Failed
MM1-38-01	20%	5 to 1	9		52.84%	20.91%	26.25%	7.97	16.805	0.169	0.492	0.075	Failed
MM1-38-03	20%	3 to 1	13		52.83%	21.51%	25.66%	7.75	17.501	0.095	0.508	0.067	0.51
MM1-38-05	20%	2 to 1	10	0.87	50.28%	22.71%	27.01%	6.98%	42.536	0.141	0.474	0.049	
MM1-38-04	20%	1 to 1	9		NFF	NFF	NFF	NFF	NFF	NFF	NFF	NFF	NFF
MM1-41-04	20%	2 to 3	6		NFF	NFF	NFF	NFF	NFF	NFF	NFF	NFF	NFF

Table 2.2. Chemical, electrochemical, and thermal characterizations of 3,5-pyridine-r-meta-PBIs. NFF = Not Film Forming

Notebook #	Ratio of 3,5-py-PBI to m-PBI	Polymerization Time at 195°C – 220°C (h)	Inherent Viscosity (dL/g)	Monomer Charge (wt%)	PA content (%wt)	Polymer contents (%wt)	Water content (%wt)	PA mole ratio to PBI repeat unit	Young's Modulus (MPa)	Strain at Break (mm/mm)	Thickness (mm)	Anhydrous Conductivity at 180°C (S/cm)	Fuel Cell Voltage at 180°C After Break-in @ 0.2A/cm^2 (V)
MM1-76-6	9 to 1	30	1.15	12%	55.79%	15.55%	28.66%	11.321	11.689	2.657	0.372	0.112	Failed
MM1-76-2	3 to 1	30	1.43	12%	56.81%	20.50%	22.69%	8.748	4.186	5.004	0.34	0.075	0.36
MM1-76-3	1 to 1	30	1.37	12%	54.18%	22.87%	22.95%	7.047	12.8725	7.047	0.345	Failed	
MM1-76-4	1 to 3	30	1.38	12%	63.99%	19.41%	16.60%	10.45	15.274	4.238	0.337	0.139	0.36
MM1-76-5	1 to 9	NFF	0.63	12%	NFF	NFF	NFF	NFF	NFF	NFF	NFF	NFF	NFF
MM1-77-1	9 to 1	30	1.16	16%	57.49%	20.50%	22.04%	8.87	18.266	3.612	0.393	0.062	
MM1-77-2	3 to 1	9	0.88	16%	53.92%	23.20%	22.88%	7.333	18.541	2.191	0.327	0.041	
MM1-77-3	1 to 1	8	0.7	16%	53.94%	27.17%	18.89%	6.257	14.105	1.54	0.324	0.007	
MM1-77-4	1 to 3	6		16%	NFF	NFF	NFF	NFF	NFF	NFF	NFF	NFF	NFF
MM1-77-6	1 to 9	2		16%	NFF	NFF	NFF	NFF	NFF	NFF	NFF	NFF	NFF
MM1-80-1	15 to 1	4	0.81	20%	53.79%	23.91%	22.30%	7.102	7.459	0.561	0.435	Failed	Failed
MM1-80-2	9 to 1	4.5	0.3	20%	54.27%	26.19%	19.53%	6.56	13.044	0.52	0.372	0.037	
MM1-80-3	5 to 1	4	0.79	20%	52.93%	27.05%	20.02%	6.173	23.756	0.839	0.379	0.056	
MM1-80-4	3 to 1	3	N/A	20%	52.04%	26.86%	21.10%	6.11	1.583	1.19	0.33	0.064	
MM1-80-5	2 to 1	4	0.71	20%	48.94%	24.53%	26.52%	6.293	18.51	0.384	0.369	0.091	

Table 2.3. Chemical, electrochemical, and thermal characterizations of 3,5-pyridine-r-2OH-PBIs. NFF = Not Film Forming

Notebook #	Ratio of 3,5-py-PBI to 2OH-PBI	Polymerization Time at 195°C – 220°C (h)	Inherent Viscosity (dL/g)	Monomer Charge (wt%)	PA content (%wt)	Polymer contents (%wt)	Water content (%wt)	PA mole ratio to PBI repeat unit	Young's Modulus (MPa)	Strain at Break (mm/mm)	Thickness (mm)	Anhydrous Conductivity at 180°C (S/cm)	Fuel Cell Voltage at 180°C After Break-in @ 0.2A/cm^2 (V)
MM1-85-1	9 to 1	18	0.76	12 wt%	52.57%	13.61%	33.82%	12.321	8.83	0.352	0.376	0.126	
MM1-85-5	9 to 1	24	1.02	12 wt%	52.12%	14.36%	33.52%	11.575	10.937	1.905	0.401	0.159	
MM1-85-2	5 to 1	18	0.79	12 wt%	52.19%	13.35%	34.46%	12.549	11.156	0.512	0.39	0.194	Failed
MM1-85-3	3 to 1	25	0.75	12 wt%	51.76%	15.15%	33.09%	11.054	10.835	2.993	0.428	0.174	Failed
MM1-85-4	1 to 1	10	0.6	12 wt%	52.37%	14.56%	33.07%	11.923	9.194	0.148	0.371	0.175	0.59
MM1-85-6	1 to 2	3.5		12 wt%	NFF	NFF	NFF	NFF	NFF	NFF	NFF	NFF	NFF
MM1-86-1	9 to 1	18		16 wt%	48.87%	16.91%	34.23%	9.225	17.435	0.164	0.38	0.135	
MM1-86-3	3 to 1	8		16 wt%	48.48%	19.24%	32.28%	8.151	16.21	0.698	0.523	0.127	

Thermal analysis and inherent viscosity (IV) measurements of the copolymers were conducted on polymer samples isolated from the PPA solution as described in the

Experimental Section 2.2.3. Differential scanning calorimetry did not show any transitions up to 300°C and thermal gravimetric analysis showed that decomposition occurred at >500°C in nitrogen for all of the copolymers tested.

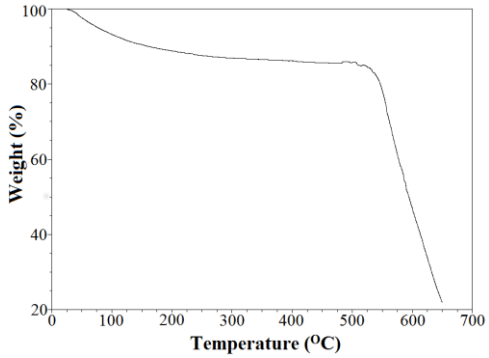

Figure 2.2. A typical thermogravimetric analysis plot of the bulk polymer for the high polymer content PBI membranes under nitrogen and a temperature ramp of 20°C min^{-1}. The decrease in weight-percent below 200°C is attributed to the loss of water. This 3,5-pyridine-r-para-PBI (py:para = 1:1) polymer shows thermal degradation at temperatures above 450°C.

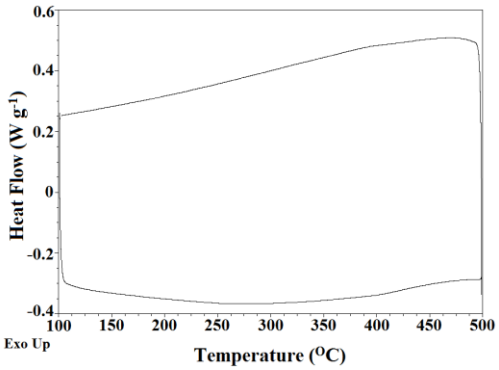

Figure 2.3. The second cycle of a typical differential scanning calorimetry analysis plot of the anhydrous bulk polymer acquired from a high polymer content PBI membranes under nitrogen and a temperature ramp of 10°C min^{-1}. No phase transitions are apparent at temperatures below 300°C.

IV measurements of the copolymers yielded ranges of 1.18-1.87 dL g^{-1} for the 3,5-pyridine-r-para-PBIs, 0.30-1.43 dL g^{-1}, for the 3,5-pyridine-r-meta-PBIs, and 0.60-1.02 dL g^{-1} for the 3,5-pyridine-r-2OH-PBIs. These IVs indicate low-to-moderate

molecular weights for the copolymers. It was apparent that as the initial monomer concentration in the polymerizations increased, the polymerization time to attain a high solution viscosity and the resulting inherent viscosity of the polymer decreased. This trend is shown in Figure 2.4. Additionally, the polymerization time to reach a high viscosity that could still be cast decreased as the ratio of pyridine monomer to either terephthalic, isophthalic, or 2,5-dihydroxyterephthalic acid decreased.

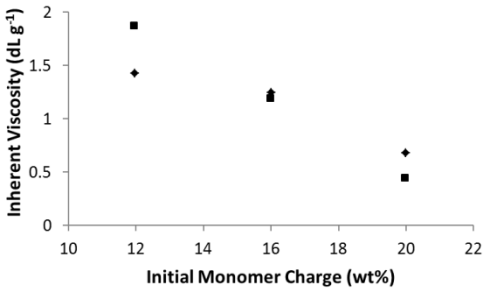

Figure 2.4. The inherent viscosities of a) 5:1 ratio (diamonds) and b) 3:1 ratio (squares) 3,5-pyridine-r-para-PBIs.

2.3.2 GEL FILM FORMATION

As described previously, the PPA Process is a facile route for producing PBI membranes.[3] All copolymers were cast directly from the polymerization solutions at 195-220°C onto glass plates. Higher polymer content membranes needed to be cast thinner than the lower polymer content, traditional PPA processed membranes to produce similar thicknesses of the membranes following hydrolysis of the PPA to PA. All of the high polymer content membranes were cast at 15mil (0.381mm) and produced membranes with thicknesses between 0.3-0.5mm. Following hydrolysis of the PPA to PA and the simultaneous sol-to-gel transition, excess water and PA were drained from the membranes prior to their characterization.

The ability to process high solids-content 3,5-pyridine-r-2OH-PBIs, 3,5-pyridine-r-para-PBIs, and 3,5-pyridine-r-meta-PBIs into gel films was dependent on both the initial monomer charge in the polymerization vessel and the ratio of the two diacid monomers. The amount of time needed to reach a high viscosity suitable for casting (judged visually) was strongly influenced by the ratio of pyridine monomer to the less soluble monomer. This trend is shown in Figure 2.5. Because the introduction of 2OH-, para-, or meta-PBI decreased the solubility of the copolymer in PPA, the polymerization solutions with a higher ratio of dihydroxyterephthalic acid, terephthalic acid or isophthalic acid attained a high viscosity relatively quickly (causing a decrease in the polymerization time) and eventually reaching a viscosity where the solution could not be easily processed into a membrane. It is also important to note that the IV of the copolymers decreased concomitantly with decreasing polymerization time. As shown previously,[3] high IVs are required for membranes to possess suitable mechanical properties. Thus, the low solubility of the copolymer composition, high viscosity of the polymerization solution, and decreased IV all combined to limit the copolymer compositions that could provide suitable membranes.

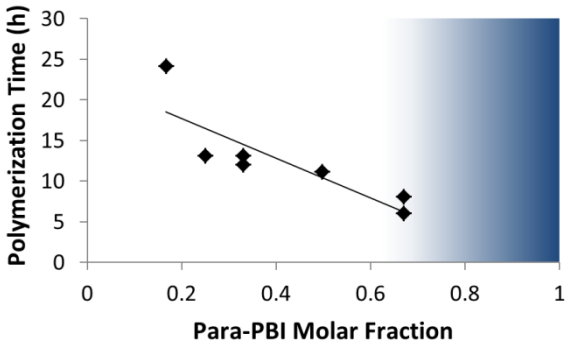

Figure 2.5. Polymerization time to reach a high solution viscosity for 3,5-pyridine-r-para-PBIs at final polymerization temperatures up to 220°C with an initial monomer charge of 12 wt%. The blue region indicates either that the polymerization solution was

too viscous to cast or that the inherent viscosity of the polymer was too low to make a stable membrane.

2.3.3 MEMBRANE PROPERTIES

To investigate the suitability of 3,5-pyridine-r-2OH-PBI, 3,5-pyridine-r-para-PBI, and 3,5-pyridine-r-meta-PBI membranes for fuel cell use, both mechanical properties and proton conductivities were measured.

It was apparent by both physical touch and tensile tests that the room temperature mechanical properties of all copolymers increased with increasing polymer solids content in the membrane. This trend was true for all copolymer series and shown in Figure 2.6 for the 3,5-pyridine-r-para-PBI series. All of the Young's Moduli of the random copolymers were much higher than that of para-PBI (<1.5 MPa at 25°C) which had a 4.5% polymer solids content in the as-cast membrane. [3]

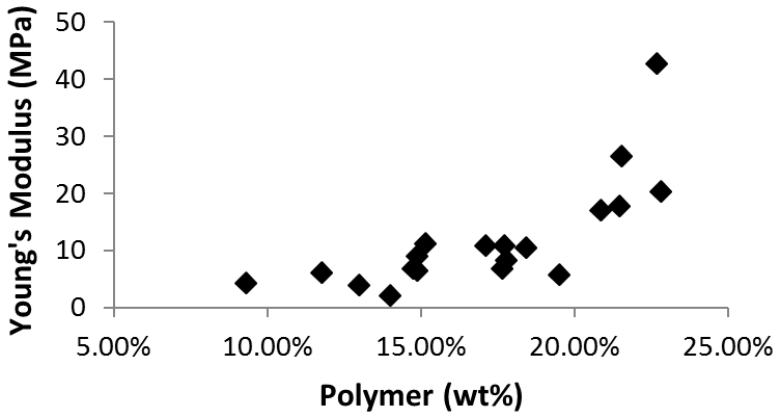

Figure 2.6: 3,5-Pyridine-r-para-PBI Young's modulus (in tension) measured at 25°C on as-cast films.

Upon heating the copolymer films to operating conditions (180°C), it was observed that membranes with a high ratio of 3,5-pyridine-PBI to para-PBI or 2OH-PBI

were thermally unstable [discussed later]. Similarly, almost all of the 3,5-pyridine-r-meta-PBI membranes exhibited similar thermal instability of the gel structure. Visual inspection of the heated membranes confirmed that the gel membrane transitioned to a solution at elevated temperatures. For this reason, 3,5-pyridine-r-meta-PBIs were not processed into MEAs for further high temperature electrochemical studies. Furthermore, it was determined that only specific ratios of 3,5-pyridinedicarboxylic acid to TPA or 2OH-TPA were feasible to polymerize and cast into stable membranes. Two different phenomena were responsible for the observed behavior. At low para-PBI copolymer content, the more soluble 3,5-pyridine monomer allowed for extended polymerization and the ability to cast the polymerization solutions into membranes. However, in this composition range, the more soluble 3,5-pyridine content copolymer membranes were not stable at high temperatures. Conversely, at high para-PBI copolymer content, the less soluble terephthalic acid prevented the polymerization from being conducted to the same extent. Thus, the combination of low solubility and shorter polymerization times (lower molecular weights) resulted in solutions that did not produce membranes or poor ones at best. Figure 2.7 illustrates the phase stability-processing maps for preparing usable membranes at initial monomer charges of 12wt% and 16wt% for 3,5-pyridine-r-para-PBI copolymers. Since 2OH-PBI has lower solubility than para-PBI, the processing window for 3,5-pyridine-r-2OH-PBI was comparatively smaller Table 2.3. The fuel cell performances of the membranes at the mid-composition range at 180°C following break-in are also shown in Figure 2.7. The results indicate that membranes produced within these processing windows are viable for fuel cells.

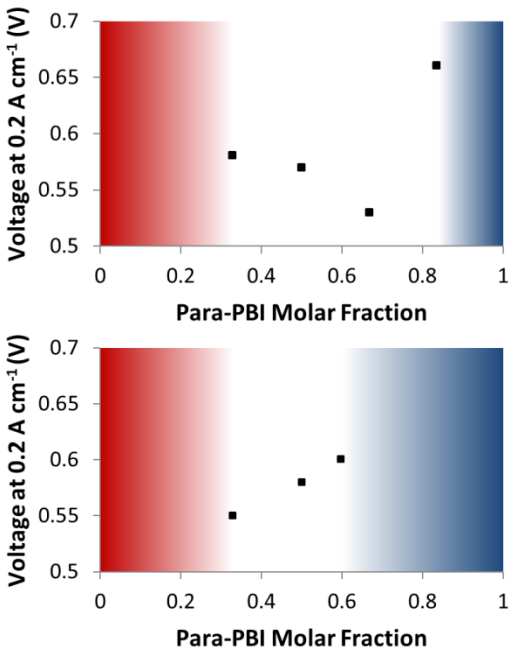

Figure 2.7. Phase stability-processing maps and non-optimized fuel cell performances at 0.2 A cm^{-2} using H_2:Air at a 1.2:2.0 stoichiometric ratio (following break-in) of 3,5-pyridine-r-para-PBI gel films. Membranes were cast from 12 wt% monomer charge (top) and 16 wt% monomer charge (bottom) solutions. The red areas represent membranes with poor thermal gel stability at 180°C, and blue areas represent unprocessable polymerization solutions.

To further investigate the creep resistance of the gel membranes under static compression, creep tests were performed on several high solid content membranes as well as on a commercial para-PBI gel membrane (low solid, ~5wt%) at 180 °C. The membranes were tested under anhydrous conditions to simulate operational fuel cell conditions. Figure 2.8 shows the creep compliance curves for a para-PBI, a 3,5-pyridine-r-para-PBI (py:para = 1:1), and a 3,5-pyridine-r-2OH-PBI (py:2OH = 1:1). Each compliance curve was representative of the average over at least two experimental data sets obtained under the same conditions. In general, the compression compliance of each gel material increased with time as the result of material creep under static compression. After an initial nonlinear transition period (2~4 hours), the increase of the compliance seemed quite linear with time, but the actual compliance slope (rate of increase)

decreased gradually over time due to the compression of the membrane structure and the concomitant composition change. The compression creep tests deliver two important messages, creep compliance and creep rate, which can be used as the metrics for the evaluation of a gel membrane's resistance to creep deformation. A material of good creep resistance should have low values in both creep compliance and creep rate. Comparison of the low polymer content para-PBI gel with the high polymer content pyridine-PBI gels shows that the compliances of the low-solid para-PBI gel was more than twice that of the high-solid PBI gels after 20 hours of static compression at 180 °C. In addition, the average creep rates (change of compliance over a period of time) during the last 12 hours of test for the 3,5-pyridine-r-para-PBI and the 3,5-pyridine-r-2OH-PBI were 0.038 and 0.028 $(MPa \cdot hr)^{-1}$ respectively, also several times smaller than the value of 0.097 $(MPa \cdot hr)^{-1}$for the low-solid para-PBI. Hence the high-solid PBI gel membranes exhibited superior performance to the low-solid PBI gel in terms of creep resistance.

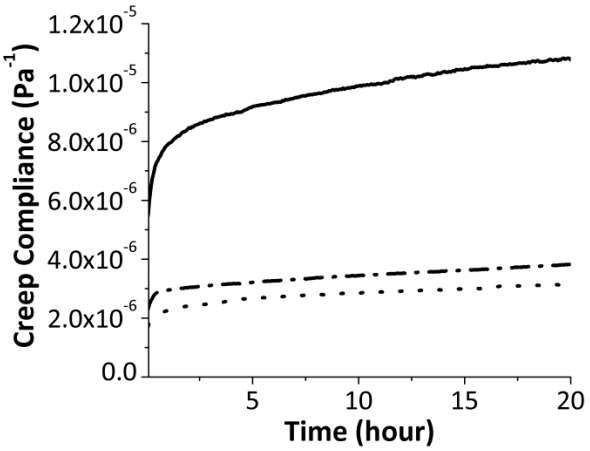

Figure 2.8. Creep compliance curves of a 3,5-pyridine/para-PBI (py:para = 1:1, 19.5 wt% polymer, dotted line), a 3,5-pyridine/2OH-PBI (py:2OH = 1:1, 14.6 wt% polymer, dash-dot line) and para-PBI (<5 wt% polymer, solid line), preconditioned at 180˚C for 24 hours and compressed at 0.1 MPa at 180˚C.

An accurate method of detecting the gel-to-solution transition of thermally unstable membranes was desired to streamline the selection process for high temperature electrochemical characterization. A frequency sweep test at various temperatures was performed on a high polymer content membrane with known thermal instability below 180°C. Figure 2.9 shows the thermal stability study of a 3,5-pyridine-r-para-PBI (py:para=5:1) gel membrane. In Figure 7(a), storage modulus E' and loss modulus E" curves are presented in logarithmic scale. The abscissas (frequency ω) are also presented in logarithmic scale, and they are shifted by an integer number in order to avoid data overlap. At each temperature, as ω decreased, both E' and E" decreased. At temperatures below 140 °C, the storage modulus curve was always above the loss modulus curve in the entire frequency range studied. At temperatures above 150 °C, a cross-over of E' and E" occurred, i.e., tan $\delta = (E'') (E')^{-1} \geq 1$, as frequency decreased. Such a cross-over of E' and E" is indicative of a transition from a solid-like behavior to a liquid-like behavior, as the viscous behavior dominates the elastic behavior in the material. As further shown in Figure 7(b), the transition occurred within the temperature range of 140 °C and 150 °C. The thermal instability of this membrane is attributed to the high percentage of the 3,5-pyridine moiety, as gel-to-solution transitions of similar high polymer content membranes with low 3,5-pyridine proportions are not observed. These measurements support the observation of gel thermal instabilities of select copolymer compositions.

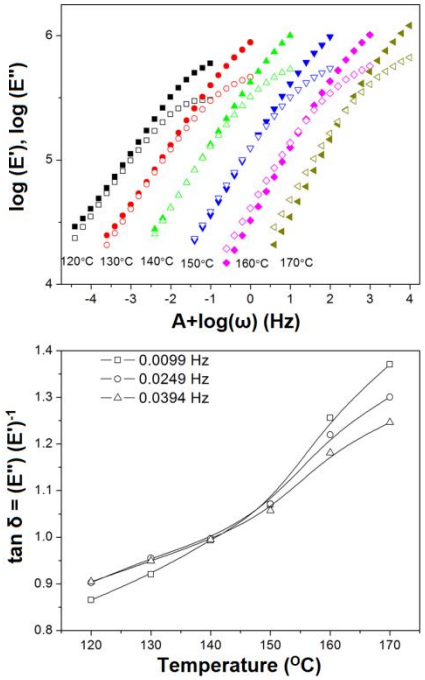

Figure 2.9: (a) Storage modulus E' (filled symbols) and loss modulus E'' (open symbols) of a high polymer content 3,5-pyridine-r-para-PBI (py:para=5:1) gel membrane as functions of oscillation frequency ω (Hz) at various temperatures. The frequency expressed in logarithmic scale for each set of data is shifted by an integer number A (from -2 to +3) to avoid data overlap. (b) Loss tangent tanδ as a function of temperature at various oscillation frequencies.

It is well known that proton conductivity is an important property of a fuel cell membrane. In high temperature PBI fuel cell membranes, proton conductivities have previously been shown as dependent on water content, phosphoric acid content, membrane morphology, and membrane chemistry.[7,11,15,18,19] Because PBI fuel cells are operated at temperatures between 160-180°C, the effects of water on proton transport are considered to be minimal. Therefore, proton conductivities were measured on anhydrous membranes at temperatures ranging from 25-180°C. Proton conductivities generally increase with increasing PA content for PBI membranes, and this trend is shown in Figure 2.10 for the high solids content membranes. By adjusting the initial

monomer wt% in the polymerization, both the PA content of the final membrane and the proton conductivity could be controlled reasonably well. As long as the membrane was thermally stable up to 180°C, there seemed to be no direct correlation between the chemistry of the high solids membranes and their respective conductivities within a copolymer series (Tables 2.1-2.3).

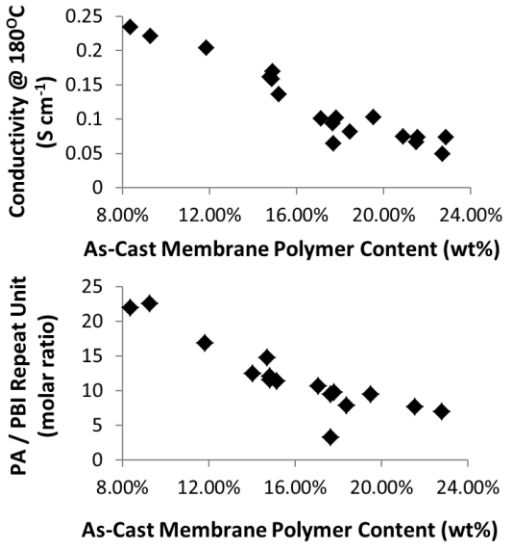

Figure 2.10: Anhydrous proton conductivity of 3,5-pyridine-r-para-PBI membranes at 180°C (top) and their measured PA content (bottom).

A temperature-dependent comparison of the proton conductivities of Nafion, PPA processed para-PBI and a high solids content copolymer made in this study is shown in Figure 2.11. Nafion, a perfluorosulfonic acid-based PEM that relies on water to assist proton conduction, exhibits a conductivity of approximately 0.08 S/cm at 80°C.[3,28] However, its ability to transport protons is drastically reduced at temperatures above 80°C due to the evaporation of water, thus requiring a complicated humidity system for fuel cell operation. In comparison, PPA processed PBI membranes demonstrate much higher anhydrous proton conductivities as the temperature is increased above 100°C. This improvement of conductivities is attributed to the low vapor pressure of PA and the faster

kinetics of the phosphoric acid proton transport.[29–31] Para-PBI membrane exhibits higher proton conductivity than 3,5-pyridine-r-para-PBI membrane due to a higher PA content. While the para-PBI membrane shows a proton conductivity of 0.28 S cm^{-1} with 40 moles of PA/PRU, the copolymer membrane maintains a proton conductivity of 0.16 S cm^{-1} with 11.9 moles of PA/PRU. It is important to note that the anhydrous para-PBI membrane is approximately 10 wt% polymer while the anhydrous copolymer membrane is approximately 20 wt% polymer. Thus, the copolymer compositions described in this study show higher membrane mechanical and compressive properties while maintaining relatively high proton conductivities.

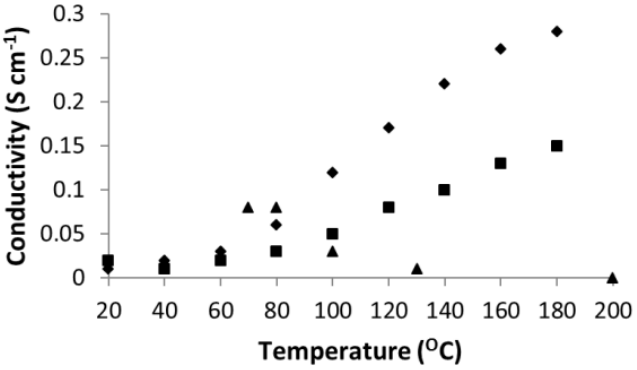

Figure 2.11. Proton conductivities of Nafion (triangle), [1] para-PBI (diamond), and 3,5-pyridine-r-para-PBI (py:para = 1:5) (square) membranes.

It was of interest to further explore the relationship of polymer solids content in the membrane with other important fuel cell properties such as mechanical properties and conductivities. For a single copolymer ratio of 3,5-pyridine-r-para-PBI (py:para = 2:1), three membranes were prepared with varying polymer contents by polymerizing at three different monomer concentrations. Figure 2.12 shows the r.t. stress-strain curves for the three as-cast membranes and Table 2.4 presents the characterization data of these membranes. The data demonstrate that, even for a single copolymer composition that is

sufficiently soluble to be polymerized at high monomer concentration, both polymer content and PA/PBI ratio can be adjusted accordingly to produce membranes with controllable compositions. Most importantly, it was shown that membranes could be produced with much higher moduli than previously reported for the PPA process while maintaining high proton conductivities.

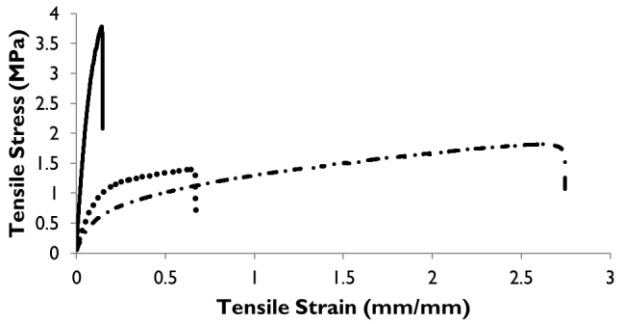

Figure 2.12. Stress-strain curves of three 3,5-py-r-para-PBI as-cast membranes measured at 25˚C (py:para = 2:1). Solid line = MM1-38-5; dotted line = MM1-37-4; dot-dashed line = MM1-36-3.

Table 2.4. Comparison of polymer content in as-cast membranes with PA content, Young's Modulus, and anhydrous proton conductivity of three 3,5-py-r-para-PBIs, where py:para = 2:1.

Membrane Name	**Polymer Content (wt%)**	**PA : PBI Repeat Unit Molar Ratio**	**Young's Modulus (MPa)**	**Proton Conductivity at 180°C (S cm^{-1})**
MM1-36-3	14.76	14.78	6.71	0.16
MM1-37-4	18.44	7.89	10.45	0.08
MM1-38-5	22.71	6.98	42.54	0.05

Steady-state fuel cell tests were performed on many 3,5-pyridine-r-para-PBI and 3,5-pyridine-r-2OH-PBI membranes at 180°C. All MEAs constructed from high polymer

content membranes were surface pretreated (~10 sec) with concentrated phosphoric acid prior to MEA fabrication. This pretreatment wet the surfaces of the membrane and decreased the resistances at the anode and cathode interfaces. Long-term studies were conducted on specific copolymer membranes and the exhaust gases were passed through water bottles to trap PA for subsequent analysis.

Figure 2.13 shows the voltage degradation characteristics and the measured PA loss data for a 3,5-pyridine-r-para-PBI membrane (py:para = 1:5) operated at 180˚C. A very low voltage degradation rate of 5.23 μV h^{-1} was measured at 0.2 A cm^{-2} following a 100h break-in period, which is significantly lower than para-PBI (60 μV h^{-1}) at 190°C.[5] The total PA loss rate (~16.53 ng cm^{-2} h^{-1}) was an order of magnitude less than para-PBI (~110.4 ng cm^{-2} h^{-1}) at 190°C.[5] These differences could partially be attributed to the difference in operating temperatures. PA loss from the cathode was greater than the PA loss from the anode which was likely affected by the water generated at the cathode. This PA loss rate, when compared to the total amount of PA in the copolymer membrane, suggests that PA loss will not be a major factor of fuel cell failure. The long-term cell test in Figure 2.13 failed at 2350h due to a malfunction of the silicon rubber heaters of the cell hardware and subsequent overheating (>200˚C). Failure of the membrane was observed by the decrease in both fuel cell performance and increase in the PA loss rate.

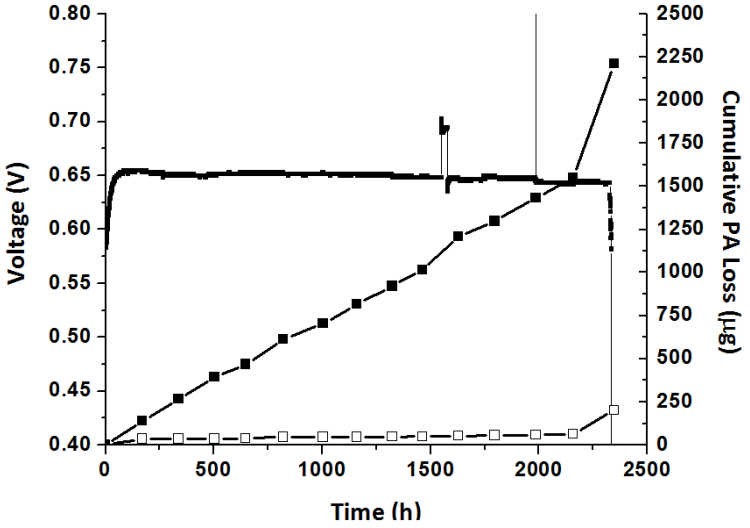

Figure 2.13. Long-term steady-state performance of a 3,5-pyridine-r-para-PBI copolymer membrane at 180°C. The active area of the cell was 45.15 cm^2, the current density was 0.2 A cm^{-2}, and the hydrogen:air ratio was 1.2:2.0 stoichiometric ratio. Anode PA loss (hollow squares) = 0.63 ng cm^{-2} h^{-1}, Cathode PA loss (solid squares) = 15.90 ng cm^{-2} h^{-1}, degradation rate = 5.23 µV h^{-1}.

2.4. CONCLUSIONS

Three series of 3,5-pyridine-r-2OH-PBIs, 3,5-pyridine-r-para-PBIs, and 3,5-pyridine-r-meta-PBIs were polymerized and cast into membranes using the PPA process. The ratio of 3,5-pyridine dicarboxylic acid monomer to isophthalic, terephthalic, or 2,5-dihydroxyterephthalic acid was easily adjusted for each polymerization, thereby allowing a large range of polymers to be produced. Both the initial monomer charge and the ratio of the diacid monomers were used to construct phase stability-processing maps that described copolymer compositions that could be prepared at high solids content solutions and cast into membranes.

Membranes prepared using the 3,5-pyridine-r-meta-PBI copolymers exhibited thermally unstable gel structures due to the high solubility of the copolymers in PA at 180°C or displayed high creep compliance at high temperatures. Membranes prepared

from 3,5-pyridine-r-para-PBIs and 3,5-pyridine-r-2OH-PBIs were stable at high temperatures when the amount of the more soluble 3,5-pyridinedicarboxylic acid was not too high. Copolymer compositions were identified with sufficient solubility and high temperature membrane stability to evaluate the effects of initial monomer polymerization charge on membrane composition, mechanical properties, and proton conductivity.

Long-term fuel cell tests were performed on a 3,5-pyridine-r-para-PBI membrane, and compared to previous results for lower solids content para-PBI membranes. An extremely low voltage degradation rate of 5.23 $\mu V\ h^{-1}$ was measured following a 100h break-in period, which was significantly lower than previous results for para-PBI membrane (60 $\mu V\ h^{-1}$). Phosphoric acid loss measurements indicated that total acid loss rate (16.53 $ng\ cm^{-2}\ h^{-1}$) is not likely to act as a primary failure mode in steady-state operation.

2.5. REFERENCES

[1] Steele B. C. H., and Heinzel A., 2001, "Materials for Fuel-Cell Technologies," Nature, **414**, pp. 345-352.

[2] Dunwoody D., and Leddy J., 2005, "Proton Exhange Membranes: The View Forward and Back," The Electrochemical Society Interface, **3**, pp. 37–39.

[3] Xiao L., Zhang H., Scanlon E., Ramanthan L. S., Choe E. W., Rogers D., Apple T., and Benicewicz B. C., 2005, "High-Temperature Polybenzimidazole Fuel Cell Membranes via a Sol-Gel Process," Chem. Mater., **17**(21), pp. 5328–5333.

[4] Yu S., and Benicewicz B. C., 2009, "Synthesis and Properties of Functionalized Polybenzimidazoles for High-Temperature PEMFCs," Macromolecules, **42**(22), pp. 8640–8648.

[5] Yu S., Xiao L., and Benicewicz B. C., 2008, "Durability Studies of PBI-based High Temperature PEMFC," Fuel Cells, **8**(3-4), pp. 165–174.

[6] Li Q., He R., Gao J., Jensen O. J., and Bjerrum N. J., 2003, "The CO Poisoning Effect in PEMFCs Operational at Temperatures up to 200C," J. Electrochem. Soc., **150**(12), pp. A1599–A1605.

[7] He R., Li Q., Xiao G. Y., and Bjerrum N. J., 2003, "Proton conductivity of phosphoric acid doped polybenzimidazole and its composites with inorganic proton conductors," J. Membr. Sci., **226**(1-2), pp. 169–184.

[8] Wainright J. S., Wang J. T., Weng D., Savinell R. F., and Litt M., 1995, "Acid-doped polybenzimidazoles: a new polymer electrolyte," J. Electrochem. Soc., **142**(7), pp. L121–L123.
[9] Litt M., Ameri R., Wang Y., Savinell R. F., and Wainright J. S., 1999, "Polybenzimidazoles/phosphoric acid solid polymer electrolytes: mechanical and electrical properties," Mater. Res. Soc. Symp. Proc., **548**(Solid State Ionics V), pp. 313–323.
[10] Zhai Y., Zhang H., Liu G., Hu J., and Yi B., 2006, "Performance degradation studies on PBI/H3PO4 high temperature PEMFC and one-dimensional numerical analysis," J. Electrochem. Acta., **52**(2), pp. 394–401.
[11] Li Q., Hjuler H. A., and Bjerrum N. J., 2001, "Phosphoric acid doped polybenzimidazole membranes: physiochemical characterization and fuel cell applications," J. Appl. Electrochem., **31**(7), pp. 773–779.
[12] Kongstein O. E., Berning T., Borresen B., Seland F., and Tunold R., 2006, "Polymer electrolyte fuel cells based on phosphoric acid doped polybenzimidazole (PBI) membranes," Energy, **32**(4), pp. 418–422.
[13] Qian G., and Benicewicz B. C., 2009, "Synthesis and Characterization of High Molecular Weight Hexafluoroisopropylidene-Containing Polybenzimidazole for High-Temperature Polymer Electrolyte Membrane Fuel Cells," J. Polym. Sci., Part A, **47**(16), pp. 4064–4073.
[14] Yu S., Zhang H., Xiao L., Choe E. W., and Benicewicz B. C., 2009, "Synthesis of Poly (2,2'-(1,4-phenylene) 5,5'-bibenzimidazole) (para-PBI) and Phosphoric Acid Doped Membrane for Fuel Cells," Fuel Cells, **9**(4), pp. 318–324.
[15] Mader J., Lixiang X., Schmidt T., and Benicewicz B. C., 2008, "Polybenzimidazole/Acid Complexes as High-Temperature Membranes," Adv. Polym. Sci., **216**(Fuel Cells II), pp. 63–124.
[16] Flory P. J., 1974, "Introductory Lecture," Faraday Discuss. Chem. Soc., **57**, pp. 7–18.
[17] Seel D. C., Benicewicz B. C., Xiao L., and Schmidt T. J., 2009, "High-temperature Polybenzimidazole-based Membranes," Handbook of Fuel Cells, **5**, pp. 300–312.
[18] Molleo M., Schmidt T. J., and Benicewicz B. C., 2012, "Polybenzimidazole-Phosphoric Acid (PBI-PA)-Based Fuel Cells," Encyclopedia of Sustainability, Science and Technology, pp. 391–431.
[19] Wainright J. S., Savinell R. F., and Litt M. H., 2003, "High Temperature Membranes," Handbook of Fuel Cells, **3**, pp. 436–446.
[20] U.S. Dept. of Energy, 2011, An Integrated Strategic Plan for the Research, Development, and Demonstration of Hydrogen and Fuel Cell Technologies. Available at http://www1.eere.energy.gov/hydrogenandfuelcells/pdfs/program_plan2011.pdf
[21] Suvorov A., Elter J., Staudt R., Hamm R., Tudryn G., Schadler L., and Eisman G., 2008, "Stress Relaxation of PBI Based Membrane Electrode Assemblies," International Journal of Solids and Structures, **45**(24), pp. 5987–6000.
[22] Patankar K. A., Dillard D. A., Case S. W., Ellis M. W., Lai Y.-H., and Gittleman C. S., 2012, "Linear Hygrothermal Viscoelastic Characterization of Nafion NRE 211 Proton ExchangeMembrane," Fuel Cells, **12**(5), pp. 787–799.

[23] Lai Y.-H., Mittelsteadt C. K., Gittleman C. S., and Dillard D. A., 2009, "Viscoelastic Stress Analysis of Constrained Proton Exchange Membranes Under Humidity Cycling," J.Fuel Cell Sci. Technol., **6**(2), pp. 021002/1 – 021002/13.
[24] Li Y., Dillard D. A., Case S. W., Ellis M. W., Lai Y.-H., Gittleman C. S., and Miller D. P., 2009, "Fatigue and creep to leak tests of proton exchange membranes using pressure-loaded blisters," J. Power Sources, **194**(2), pp. 873–879.
[25] Xiao L., Zhang H., Jana T., Scanlon E., Chen R., Choe E. W., Ramanthan L. S., Yu S., and Benicewicz B. C., 2005, "Synthesis and Characterization of Pyridine-Based Polybenzimidazoles for High Temperature Polymer Electrolyte Membrane Fuel Cell Applications," Fuel Cells, **5**(2), pp. 287–295.
[26] Ferry J. D., 1980, Viscoelastic Properties of Polymers, 3rd Ed., John Wiley & Sons, New York.
[27] 1999, "Standard Methods for the Examination of Water and Wastewater: 4500-P Phosphorus," pp. 1–24 [Online]. Available: http://www.umass.edu/tei/mwwp/acrobat/sm4500P-E.PDF.
[28] Savinell R. F., Wainright J. S., and Litt M. H., 1998, "High Temperature Polymer Electrolyte Fuel Cells," Proc. Electrochem. Soc, **98-27**, pp. 81–90.
[29] Vilciauskas L., Paddison S. J., and Kreuer K.-D., 2009, "Ab Initio Modeling of Proton Transfer in Phosphoric Acid Clusters," J. Phys. Chem. A, **113**, pp. 9193–9201.
[30] Dippel T., Kreuer K. D., Lassegues J. C., and Rodriguez D., 1993, "Proton conductivity in fused phosphoric acid; a 1H/31P PFG-NMR and QNS study," Solid State Ionics, **61**, pp. 41–46.
[31] Bozkurt A., Ise M., Kreuer K. D., Meyer W. H., and Wegner G., 1999, "Proton-conducting polymer electrolytes based on phosphoric acid," Solid State Ionics, **125**, pp. 225–233.

3. High Polymer Content 2,5-Pyridine-Polybenzimidazole Copolymer Membranes with Improved Compressive Properties

3.1. Motivation for Research Project

Polymer electrolyte membrane / proton exchange membrane (PEM) fuel cells have been recognized for several decades as efficient energy conversion devices for mobile and stationary applications.[1,2] Throughout these years, a variety of materials have been responsible for the conversion of chemical energy to electrical energy as polymer electrolytes. Perfluorosulfonic acid (PSFA) PEMs, such as DuPont's Nafion, depend on water clusters to transport protons from anode to cathode; thus, intricate water-management systems and low operational temperatures (<100°C) are required to keep the membrane properly hydrated. As a result of low operational temperatures, these fuel cells have a low tolerance to fuel impurities.

Polybenzimidazoles (PBIs) have been recognized since the early 1960's as physically, thermally, and chemically robust materials.[3,4] These polymers were commercialized by Celanese (now PBI Performance Products) for high temperature protective clothing including firefighter turnout coats and astronaut space suits. Additionally, PBIs are processed as high-performance engineering thermoplastics under the trade name Celazole for semiconductor and thermal insulation applications. Over the past twenty years, PBIs have been cast into membranes and doped with PA for electrochemical applications.[5-7] PBIs were first used as PEMs for fuel cells by Savinell et al. in the mid-1990's.[5] A series of separate operations was used to prepare

membranes, including polymerization, polymer isolation and dissolution, membrane casting, solvent removal, film washing and drying, and PA doping. This method of membrane fabrication was an extremely time consuming and multistep procedure. [6] In addition, the conventional casting technique produced films with relatively low anhydrous proton conductivities (0.048 S cm^{-1} at 180°C).

The PPA Process provides a concise pathway to obtain high molecular weight PBI membranes that are fully doped with phosphoric acid and has been optimized and commercialized over the past decade.[7-14] Using a standard reaction vessel equipped with a mechanical stirrer and an inert atmosphere, diacid and tetraamine monomers are reacted using PPA as a solvent. Because PPA is a good solvent for many PBIs, higher molecular weight polymers can be achieved. The rate of the polymerization can be easily controlled by adjusting the stir-rate and the time-temperature profile of the reaction. Upon reaching high molecular weights, the polymerization solution is cast directly into films of uniform thickness. Hydrolysis of the PPA (a good solvent for many PBIs) to PA (a poor solvent for many PBIs) causes the film to undergo a sol-to-gel transition, thereby producing a gel membrane fully imbibed with PA. Membranes produced using this method are able to hold higher amounts of phosphoric acid and generate much higher anhydrous proton conductivities (0.10-0.48 S cm^{-1}at 180°C) than membranes produced by conventional imbibing processes.[14] PA-doped PBI PEMs have been shown to operate at temperatures up to 200°C with higher tolerances to fuel impurities, and without the need for humidification control.[7,8,15-17]

Polybenzimidazole (PBI) membranes have garnered much attention over the past decade as viable materials for PEM fuel cells.[7,9,14,18] At high temperatures, PBI-

based MEAs display a high resistance to fuel gas impurities such as carbon monoxide and hydrogen sulfide.[11,19,20] Their electrochemical durability has been established via shut-down/start-up cycling, phosphoric acid (PA) loss measurements, and long-term steady state operation (>18,000h).[11] Applications of PBI MEA's in fuel cells include stationary combined heat and power units, mobile power, and range extenders for electric powered vehicles.[15]

Little is known about the membrane's resistance to long-term degradation modes including polymer creep and membrane thinning, which can result in gas crossover, voltage degradation, and the eventual quenching of the fuel cell. For stationary fuel cell applications, the Department of Energy has set an operational target of 40,000h for 2015.[21] A thorough understanding of the long-term degradation modes of PBI MEAs is crucial to design membranes that are resistant to creep and membrane thinning, and meet lifetime requirements. One study concluded that the contact stress in a PBI MEA decreased with time at 180°C.[22] Investigations of the creep and compression properties of commercially available Nafion membranes at operational temperatures (70-90°C) have been performed although these water-based membranes have fundamentally different mechanical issues due to dehydration of the polymer matrix at elevated temperatures.[23-25] Recently, we have initiated studies to investigate the high temperature creep properties in compression since these properties are critical for long-term fuel cell operation.[26] New approaches for improving the long-term mechanical properties of PBI membranes are needed which are cost effective and compatible with the manufacturing processes that have been developed for these unique membrane materials.

It is well known that the PBI chemistry fundamentally affects the processability of the polymer and the properties of the resulting membrane.[9,18] As described recently,[26] the mechanical properties of PBI membranes can be improved by increasing the polymer content in the gel membrane. However, the solubilities of the copolymers in PPA and viscosities of the resulting PBI/PPA solutions limited the processability of the solutions into films. If the polymer content is too high, the solution becomes unprocessable. This limitation was circumvented by synthesizing functionalized PBI copolymers made from a 3,5-pyridinedicarboxylic acid monomer which imparts higher solubility in the copolymers. Additionally, the effects of chemical structure on both gel thermal stability and electrochemical properties were reported. Figure 3.1 outlines the relationship between the solubility of some common PBIs in polyphosphoric acid (PPA) and PA and the thermal stabilities of the resulting gel membranes. It was observed that a high ratio of the 3,5-py-PBI moiety in the copolymer decreased the thermal stability of the resulting gel membrane. From this work it was hypothesized that a monomer such as 2,5-pyridinedicarboxylic acid (used in place of 3,5-pyridinedicarboxylic acid) could result in copolymer membranes with high polymer content and higher gel thermal stabilities and proton conductivities.

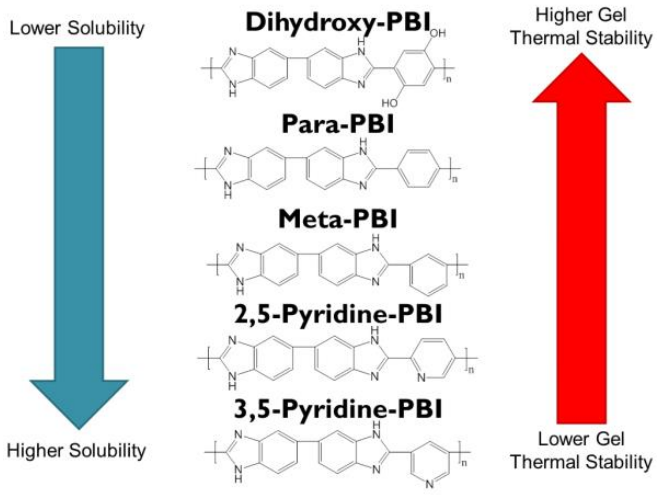

Figure 3.1. Relative comparison of PBI chemistries, gel thermal stabilities, and solubilities in PPA and PA.

In this work, we report our results on the preparation of novel PPA-processed 2,5-pyridine-r-para-PBI, 2,5-pyridine-r-meta-PBI, and 2,5-pyridine-r-2OH-PBI membranes. The highly soluble 2,5-pyridine moiety was used to impart higher polymer solubility in PPA, and therefore, higher polymer content in the membranes. Copolymers of 2,5-pyridine-PBI with either para-, meta-, or 2OH-PBI were prepared and investigated for their relative solubilities and gel membrane stabilities. The high-temperature compressive properties and electrochemical properties of these higher polymer content membranes were measured which expanded our understanding of the relationships between PBI membrane composition and chemical structures with the fundamental properties of gel stability, membrane conductivity, mechanical properties and fuel cell performance.

3.2. EXPERIMENTAL

3.2.1 CHEMICALS

2,5-Pyridinedicarboxylic acid (2,5-py-2COOH) was purchased from Acros Chemical and TCI America (~98% purity) and purified by recrystallization from a 1:1

dilution of concentrated hydrochloric acid. 2,5-Dihydroxyterephthalic acid (2OH-TPA) was purchased from TCI America and Sigma Aldrich (~98% purity) and purified by recrystallization from a 3:2 dilution of absolute ethanol:water. Terephthalic acid (TPA, purified) and isophthalic acid (IPA, purified) were purchased from Amoco Chemicals. 3,3',4,4'-Tetraaminobiphenyl (TAB, purified) was donated by BASF Fuel Cell, Inc. Polyphosphoric acid (PPA, 115%) was obtained from InnoPhos, Inc. and stored under nitrogen.

3.2.2 Polybenzimidazole Synthesis and Membrane Preparation

To a three-necked flask equipped with nitrogen flow and overhead stirrer, a solution of 2,5-py-2COOH, PPA, and either IPA, TPA, or 2OH-TPA was stirred and heated at 195-220^{O}C for 3-30 hours (Scheme 3.1). The polymerization time correlated with the viscosity of the solution, which was dependent on the solids concentration, polymer molecular weight, and the ratio of the 2,5-py-2COOH monomer to the other diacid monomer. Both the stir-rate and the temperature were controlled and adjusted during the polymerization. At the end of the polymerization, the PBI solution was poured onto a Pyrex or glass plate and cast at a thickness of 15mil using a Gardner blade. To form a gel membrane, the glass plates with the cast films were immediately placed into a humidity controlled chamber at 55% ± 5% relative humidity (RH), 25 ± 2^{O}C. Complete hydrolysis of the membranes occurred over a span of 12-24h as previously reported. The final gel membrane thickness was approximately 300-500μm.

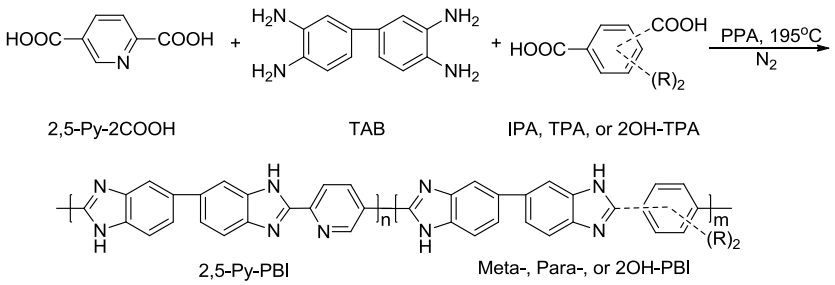

Scheme 3.1. Synthesis of random copolymers using 2,5-pyridinedicarboxylic acid and 3,3',4,4'-tetraaminobiphenyl with terephthalic acid (R=H), isophthalic acid (R=H), or 2,5-dihydroxyterephthalic acid (R= -OH).

3.2.3 CHARACTERIZATION TECHNIQUES

Thermogravimetric analysis, differential scanning calorimetry, and inherent viscosity measurements were performed on polymer isolated from the PPA process. Following the polymerization, the polymer/PPA solution that remained in the reaction vessel was hydrolyzed with deionized water. The precipitated polymer was then pulverized in a commercial Waring blender and neutralized with ammonium hydroxide in 500 mL of distilled water. After heating for 1 hour at 100˚C, the polymer was isolated by filtration and washed thoroughly with water to remove any residual ammonium salts. The powder was then dried for 12 hours at 120-130˚C.Thermogravimetric analysis (TGA) was performed using a TA Instruments TGA Q-5000 IR with a heating rate of 10 °C min^{-1} under nitrogen. Differential scanning calorimetry (DSC) was conducted using a TA Instruments DSC Q-2000 with a nitrogen flow rate of 20 mL min^{-1} and heating and cooling rates of 10°C min^{-1}. Following dissolution of the polymer in 96% sulfuric acid at 0.2 g dL^{-1} concentrations, inherent viscosities (IV's) were measured using an Ubbelohde viscometer in a water bath set at 30.0˚C. Inherent viscosity was calculated according to Equation 1.

$$\ln [(t) (t_o)^{-1}] c^{-1} = \text{Inherent Viscosity (dL g}^{-1}) \quad (1)$$

where t is the solution flow time in seconds, t_o is the solvent (96% sulfuric acid) flow time in seconds, and c is the solution concentration in g dL^{-1}.

The composition of acid-doped PBI membranes was determined by measuring the relative amounts of polymer solids, water, and acid in the film. The phosphoric acid (PA) content was determined by titrating a sample of membrane with standardized sodium hydroxide solution (0.1 N) using a Metrohm 716 DMS Titrino autotitrator. The sample was washed with water and dried in an oven overnight at 120 °C. The dried sample was then weighed to determine polymer solids content for the membrane. The amount of water was calculated by subtracting the weights of polymer and PA from the initial PBI membrane sample weight.

Ionic conductivities were measured via a four-probe through-plane bulk measurement using an AC Zahner IM6e impedance spectrometer that scanned a frequency range from 1 Hz to 100 KHz. A rectangular sample of membrane (3.5 cm x 7.0 cm) was placed in a polysulfone cell with four platinum wire current collectors. Two outer electrodes set 6.0 cm apart supplied current to the cell, while the two inner electrodes 2.0 cm apart on opposite sides of the membrane measured the voltage drop. To ensure a through-plane bulk measurement of the membrane ionic conductivity, the two outer electrodes are placed on opposite sides of the membrane and the two inner electrodes are arranged in the same manner. The reported conductivities were made on preconditioned (dehydrated) membranes that were held at >100°C for at least two hours. Proton conductivity was calculated using the following equation:

$$\sigma = (D) (L \cdot B \cdot R)^{-1} \quad (2)$$

where D was the distance between the two test current electrodes, L was the thickness of the membrane, B was the width of the membrane, and R was the measured resistance.

The mechanical properties of the membranes were measured by cutting dog bone specimens (ASTM D683 Type V) from the bulk membrane using a cutting press. Tensile properties were measured using an Instron Tensile Tester (5543A) with a 10N load cell. All measurements were made at 25°C ± 3°C on samples preloaded to 0.1N with a crosshead speed of 5mm per minute.

The compression creep tests were performed using a TA Instruments RSAIII dynamic mechanical analyzer. Discs were cut from polymer membranes with a diameter of 6.3 mm and thickness of approximately 0.9~1.2 mm. Before the compression creep tests, the samples were conditioned by placing them between two parallel smooth Teflon blocks at 180°C for approximately 24 hours. In a typical compression creep test, a step stress was applied to the sample and held constant for 20 hours. The deformation of the test specimen was recorded as a function of time. To ensure the compression stress was uniaxial, the compression tool surfaces were coated with PTFE to minimize the friction between the sample and the tool. The creep compliance was calculated by dividing the strain with the applied stress, and the compliance as a function of time was fitted with the Maxwell model[27]:

$$J(t) = J_s^0 + t \cdot {\eta_0}^{-1} \qquad (3)$$

where J_s^0represents the steady-state (recoverable) compliance, t is time, and η_0 is the extensional viscosity at zero extension rate. All tests were carried out at 180 °C, and the applied stress level was selected to be 0.1 MPa.

Frequency sweep tests were also performed using the TA Instruments RSAIII at various temperatures for characterization of the thermal stability of the gel membranes. Cylindrical compression samples were used with diameter 15mm and thickness ~4mm. Before the tests, the samples were conditioned in vacuo at 80 °C for 24 hours. The storage modulus (E') and loss modulus (E") were recorded as functions of frequency at various temperatures. The test frequency ω spanned from 0.00249 Hz to 9.9 Hz, and a strain amplitude of 0.25% was used.

Membrane electrode assemblies consisted of the polymer membrane sandwiched between two electrodes. MEAs were prepared by hot pressing the acid-doped membrane between an anode electrode and a cathode electrode at 150 °C for 90-150 seconds using 4500 lbs of force and compressing to 80% its original width. Prior to hot pressing, the membrane was pretreated (dipped into) concentrated PA for less than 10 seconds to wet its surface and thus reduce the interfacial resistance of the membrane-catalyst interface. Electrodes were received from BASF Fuel Cell, Inc. with 1.0 mg/cm^2 platinum (Pt) catalyst loading. Anode electrodes contained only Pt as the catalyst, while the cathode electrodes contain a BASF Fuel Cell standard cathode Pt alloy. The active area of the electrodes was 45.15 cm^2. Fuel cell fabrication was conducted by assembling the cell components as follows: end plate:PTFE insulator:anode current collector:anode flow field:MEA:cathode flow field:cathode current collector:PTFE insulator:end plate. Gaskets were used on either side of the MEA to control compression. Following assembly, the cell was evenly clamped to 50 in-lbs of pressure.

Fuel cell performance was measured in 50 cm^2 (active area 45.15 cm^2) single stack fuel cells using test stations obtained from Plug Power or purchased from Fuel Cell

Technologies. Polarization curves were obtained at various temperatures (120-180 °C) with hydrogen as a fuel and different oxidants (air or oxygen gas). Fuel cells were operated for at least 100 hours (break-in period) at 0.2 A/cm^2 at 180 °C before measurement of polarization curves. Long-term stability testing was performed under static current and temperature conditions of 0.2 A/cm^2 and 180 °C with a constant flow rate of hydrogen and air. Degradation rates of long-term fuel cell operations were calculated by linear fitting cell voltage data points with respect to time. Product water and PA from the exhaust gases were collected by passing the gases through bottles containing distilled water. The PA loss was determined by analyzing the water in the collection bottles using an ascorbic acid test and UV-Vis absorbance at 880nm wavelength.[28]

3.3. Results and Discussion

3.3.1. Synthesis and Characterization of Random Copolymers

A series of 2,5-pyridine-r-meta-PBIs, 2,5-pyridine-r-para-PBIs, and 2,5-pyridine-r-2OH-PBIs were polymerized and cast into gel membranes using the PPA Process. As described in Section 2.2, the polymers were formed via a step-growth polycondensation reaction between aromatic diacids and aromatic tetraamines under acidic conditions. The total amount of diacids was in a 1:1 stoichiometric ratio with the total amount of tetraaminobiphenyl (TAB). The polymerization rate for each copolymer was controlled by adjusting stirring rate and the temperature of the solution. The viscosity of each polymer solution increased as the polymerization proceeded, until an optimal high viscosity for casting was reached.

Inherent viscosity measurements were performed on the polymer isolated from the PPA Process. More accurate molecular weight characterization techniques were

precluded by the insolubility of the polymers in common organic solvents. Inherent viscosities for the random copolymers varied from 0.80 to 2.19 dL g^{-1} for 2,5-py-r-para-PBI, 0.77 to 1.41 dL g^{-1} for 2,5-py-r-meta-PBI, and 0.69 to 1.15 dL g^{-1} for 2,5-py-r-2OH-PBI. This data, along with other polymer and membrane characterization data, can be found in Tables 3.1-3.3. Considering the rigid nature of PBI backbones, these polymers range from low-to-moderate molecular weights. The inherent viscosity measurements of these random copolymers were compared with their respective polymerization time. As observed in Tables 3.1-3.3, shorter polymerization times correlated with lower molecular weights. It is important to note that the solution viscosity determined the polymerization time, and thus, limited the molecular weight of the random copolymers. The relationships between the polymerization solution viscosity with the polymer molecular weight, the chemical composition of the copolymer, and copolymer concentration will be explored in Section 3.2.

Thermal analysis was also performed on the polymer isolated from the PPA Process. Thermogravimetric analysis showed these polymers were stable under an inert atmosphere at temperatures exceeding 600°C (Figure 3.2). This should not to be confused with membrane gel stability, which will be discussed in Section 3.3. Differential scanning calorimetry of a sample of polymers did not show any transitions below 350^{O}C (Figure 3.3). The high temperature stability of these polymers is similar to previously synthesized PBIs, and it suggests that these PBIs should also be stable at fuel cell operation temperatures of 180^{O}C.

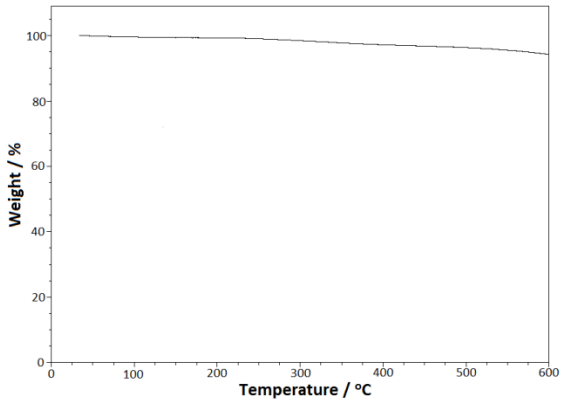

Figure 3.2. A typical thermogravimetric analysis plot of the bulk polymer for the high polymer content PBI membranes under nitrogen and a temperature ramp of 20°C min^{-1}. The decrease in weight-percent below 200°C is attributed to the loss of water. This 2,5-pyridine-r-para-PBI (MM1-40-2, py:para = 3:1) polymer shows thermal degradation at temperatures above 600°C.

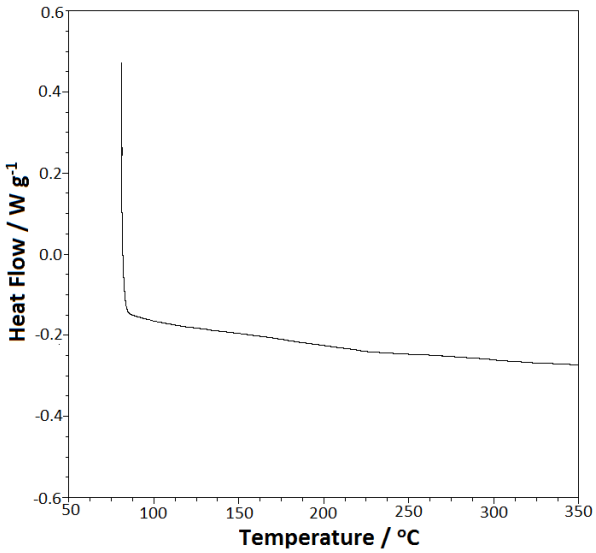

Figure 3.3. The heating ramp of a typical differential scanning calorimetry plot of the anhydrous bulk polymer acquired from a high polymer content PBI membranes under nitrogen and a temperature ramp of 10°C min^{-1}. No phase transitions are apparent at temperatures below 350°C for this 2,5-pyridine-r-para-PBI (MM1-40-2, py:para = 3:1) copolymer.

3.3.2. Copolymer Solution Processing into Gel Films

The polymerization solutions were cast directly into membranes by using the PPA Process, as described previously.[7,26] Upon reaching an optimal casting viscosity, all of

the copolymer solutions were immediately cast onto glass or Pyrex plates using a Gardner blade with a gap space of 15 mil (0.381 mm). These membranes were then placed into a humidity chamber for 12-24 hours to hydrolyze the PPA to PA, which resulted in a membrane that was fully imbibed with PA. All of the chemical compositions of the resulting copolymer membranes (and their respective tensile and electrochemical properties) are listed in Tables 3.1-3.3.

Table 3.1. Chemical, electrochemical, and thermal characterizations for a variety of 2,5-pyridine-r-para-PBIs. NFF = Not Film Forming

Notebook #	Ratio of 2,5-py-PBI to p-PBI	Polymerization Time at 195°C – 220°C (h)	Inherent Viscosity (dL/g)	Monomer Charge (wt%)	PA content (%wt)	Polymer contents (%wt)	Water content (%wt)	PA mole ratio to PBI repeat unit	Young's Modulus (MPa)	Strain at Break (mm/mm)	Thickness (mm)	Anhydrous Conductivity at 180°C (S/cm)	Fuel Cell Voltage at 180°C After Break-in @ 0.2A/cm^2 (V)
MM1-102-3	5 to 1	16	1.22	6 wt%	54.87%	7.65%	37.48%	22.641	2.75	0.479	0.328	0.219	
MM1-102-1	5 to 1	8	2	10 wt%	53.05%	14.37%	32.58%	11.656	8.585	1.804	0.404	0.159	
MM1-102-4	5 to 1	6	1.34	10 wt%	54.33%	13.45%	32.22%	12.745	8.336	0.287	0.362	0.23	
MM1-46-5	15 to 1	10	1.42	12 wt%	51.76%	15.13%	33.11%	10.814	13.052	0.358	0.398	0.158	0.61
MM1-46-6	9 to 1	6	1.60	12 wt%	52.72%	16.25%	31.03%	10.237	12.09	0.292	0.395	0.149	0.62
MM1-40-1	5 to 1	6	2.19	12 wt%	53.04%	17.13%	29.83%	9.768	12.172	0.67	0.364	0.122	Failed
MM1-40-2	3 to 1	13	1.3	12 wt%	54.13%	13.66%	32.21%	12.503	9.054	0.312	0.405	0.129	0.63
MM1-40-3	2 to 1	6	1.70	12 wt%	55.89%	15.93%	28.17%	11.049	25.172	0.529	0.444	0.111	0.65
MM1-46-4	2 to 1	8		12 wt%	52.54%	16.64%	30.83%	9.976	12.01	0.16	0.377	0.14	0.61
MM1-40-4	1 to 1	6	1.08	12 wt%	53.34%	16.33%	30.34%	10.296	9.354	0.163	0.345	0.135	0.55
MM1-46-2	1 to 2	4		12 wt%	NFF	NFF	NFF	NFF	NFF	NFF	NFF	NFF	NFF
MM1-49-2	23 to 1	9	1.27	16 wt%	53.93%	18.81%	27.26%	9.065	20.486	0.108	0.386		0.47
MM1-49-1	15 to 1	5	1.85	16 wt%	51.00%	19.10%	29.90%	8.426	20.211	0.096	0.379		0.59
MM1-47-1	9 to 1	3	0.8	16 wt%	51.49%	20.26%	28.24%	8.02	20.42	0.101	0.409	Failed	0.53
MM1-47-2	5 to 1	5.5	1.62	16 wt%	49.11%	19.54%	31.35%	7.947	17.791	0.158	0.446	0.093 &	0.47
MM1-47-4	2 to 1	3		16 wt%	NFF	NFF	NFF	NFF	NFF	NFF	NFF	NFF	NFF
MM1-47-5	1 to 1	3		16 wt%	NFF	NFF	NFF	NFF	NFF	NFF	NFF	NFF	NFF
MM1-48-1	15 to 1	4		20 wt%	49.03%	26.69%	27.28%	6.534	Brittle	Brittle	Brittle	NFF	NFF
MM1-48-2	9 to 1	2		20 wt%	NFF	NFF	NFF	NFF	NFF	NFF	NFF	NFF	NFF

Table 3.2. Chemical, electrochemical, and thermal characterizations for a variety of 2,5-pyridine-r-meta-PBIs. NFF = Not Film Forming

Notebook #	Ratio of 2,5-py-PBI to m-PBI	Polymerization Time at 195°C – 220°C (h)	Inherent Viscosity (dL/g)	Monomer Charge (wt%)	PA content (%wt)	Polymer contents (%wt)	Water content (%wt)	PA mole ratio to PBI repeat unit	Young's Modulus (MPa)	Strain at Break (mm/mm)	Thickness (mm)	Anhydrous Conductivity at 180°C (S/cm)	Fuel Cell Voltage at 180°C After Break-in @ 0.2A/cm^2 (V)
MM1-72-1	9 to 1	11	1.41	12 wt%	52.33%	13.73%	33.94%	12.025	9.649	0.581	0.386	0.143	0.6
MM1-72-2	3 to 1	11	1.24	12 wt%	55.94%	15.22%	28.85%	11.597	7.219	1.385	0.385	0.22	0.6
MM1-72-3	1 to 1	10	0.8	12 wt%	52.39%	16.69%	30.92%	9.891	6.849	0.209	0.342	0.136	0.34
MM1-72-4	1 to 3	9	0.81	12 wt%	55.00%	19.09%	25.91%	9.085	7.729	0.296	0.306	0.115	0.63
MM1-72-5	1 to 9	9	0.94	12 wt%	52.75%	18.90%	28.35%	8.787	6.548	3.235	0.3	0.112	0.66
MM1-73-1	9 to 1	8	1.08	16 wt%	56.25%	20.27%	23.47%	8.756	19.051	0.353	0.373	0.03	0.48
MM1-73-2	3 to 1	8	1.34	16 wt%	54.69%	18.88%	26.43%	9.165	14.774	0.426	0.476	0.179	0.4
MM1-73-3	1 to 1	6	0.77	16 wt%	51.05%	21.20%	27.75%	7.594	16.4	0.201	0.36	0.117	Failed
MM1-73-4	1 to 3	N/A	N/A	16 wt%	NFF	NFF	NFF	NFF	NFF	NFF	NFF	NFF	NFF
MM1-73-5	1 to 9	N/A	N/A	16 wt%	NFF	NFF	NFF	NFF	NFF	NFF	NFF	NFF	NFF

Table 3.3. Chemical, electrochemical, and thermal characterizations for a variety of 2,5-pyridine-r-2OH-PBIs. NFF = Not Film Forming

Notebook #	Ratio of 2,5-py-PBI to 2OH-PBI	Polymerization Time at 195°C – 220°C (h)	Inherent Viscosity (dL/g)	Monomer Charge (wt%)	PA content (%wt)	Polymer contents (%wt)	Water content (%wt)	PA mole ratio to PBI repeat unit	Young's Modulus (MPa)	Strain at Break (mm/mm)	Thickness (mm)	Anhydrous Conductivity at 180°C (S/cm)	Fuel Cell Voltage at 180°C After Break-in @ 0.2A/cm^2 (V)
MM1-120-3	1 to 5	4	0.69	11 wt%	50.09%	13.62%	36.28%	11.808	10.945	0.031	0.515	0.2	
MM1-92-1	9 to 1	7	0.98	12 wt%	50.73%	13.11%	36.16%	12.34	13.752	0.303	0.367	0.159	
MM1-92-2	5 to 1	6.5		12 wt%	51.68%	14.99%	33.33%	11.064	12.702	0.458	0.509	0.163	0.637
MM1-92-5	5 to 1	6	1.15	12 wt%	51.23%	14.59%	34.17%	11.265	12.948	0.986	0.412	0.148	0.61
MM1-92-3	3 to 1	4.5	1.01	12 wt%	50.05%	13.17%	36.78%	12.329	13.418	0.611	0.4	0.164	0.6
MM1-92-4	1 to 1	4		12 wt%	NFF	NFF	NFF	NFF	NFF	NFF	NFF	NFF	NFF

The viscosity of the final polymerization solution plays a critical role in the casting process. If the polymer content or the molecular weight of the polymers were too high, the polymerization solution would be too viscous to flow and could not be cast into thin films. In contrast, a low solution viscosity was an indication of low molecular weight polymers, which if cast into membranes would form mechanically weak films. Identical to the trends observed in a previous paper, [27] the viscosities of these copolymer

polymerization solutions were directly dependent on the molecular weights of the copolymers, the copolymer ratio, and the concentration of polymer in solution. The relationship between copolymer molecular weight and solution viscosity was visually observed – as the polymerization proceeded, the solution viscosity gradually increased. As the copolymer ratio was changed using monomers with inherently different solubility characteristics, the viscosity increase observed during the polymerization also varied with copolymer ratio. Figure 3.4 highlights this trend by comparing the para-PBI molar fraction with the polymerization time for an initial monomer charge of 12wt%. For copolymers with para-PBI molar fractions less than 0.7, polymerizations could be conducted that reached a high solution viscosity suitable for casting. For copolymers with para-PBI molar fractions larger than 0.7, the insolubility of the copolymer did not allow sufficient time for polymerization to high molecular weights and solidification was observed, rendering the polymerization solution unprocessable. Increasing the initial monomer concentration, which thereby increased the polymer concentration in solution, also decreased the amount of time it took to reach an optimal casting viscosity. This was observed through the polymerization of multiple 2,5-py-r-para-PBIs of identical monomer ratios (2,5-py:para = 5:1) but with initial monomer charges ranging from 6-16 wt% – the polymerization times decreased from 16 h to 5.5 h as the monomer charge increased (Table 3.1). These relationships between polymer content or chemical composition with polymerization time were also observed for the 2,5-py-r-meta-PBI and 2,5-py-r-2OH-PBI compositions (Tables 3.2 and 3.3). Thus, the polymerization time required to reach a high viscosity suitable for casting was dependent on the copolymer molecular weight, chemical composition, and overall polymer concentration.

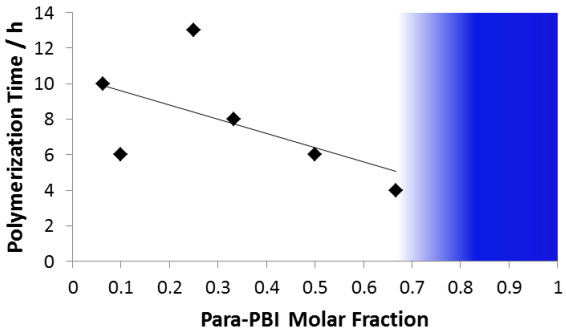

Figure 3.4. The polymerization times of a series of 2,5-pyridine-r-para-PBIs with their respective para-PBI molar fraction. All of the polymerizations had an initial monomer charge of 12 wt%. The blue region indicates either a casting process impeded because the solution was too viscous or that the inherent viscosity of the polymer was too low to make a stable membrane.

3.3.3. MEMBRANE PROPERTIES

The structure-property relationships of the membranes from the three copolymer series, 2,5-pyridine-r-2OH-PBI, 2,5-pyridine-r-para-PBI, and 2,5-pyridine-r-meta-PBI, were investigated using a variety of mechanical and electrochemical characterization techniques. The results of these tests were also used to judge the suitability of using these materials as proton exchange membranes in high temperature fuel cells.

Tensile tests were performed on each series of high polymer content membranes at room temperature and the membranes displayed higher Young's moduli than previously reported for low polymer content para-PBI membranes (<1.5 MPa at 25°C).[7] This trend is shown in Figure 3.5 for 2,5-pyridine-r-para-PBI membranes, which shows a linear correlation between polymer content and Young's moduli. This trend is less distinct for the 2,5-pyridine-r-meta-PBI membranes (Figure 3.6, R^2= 0.35), and 2,5-pyridine-r-2OH-PBI membranes (Figure 3.7). The variations in these trends may be due to both the polymer content in the membrane and the limits in molecular weight that can be attained at higher monomer charges. A copolymer ratio higher in 2,5-

pyridinedicarboxylic acid improved the solubility of the polymer and thus further assisted in attaining high molecular weights. However, all of the data supports the observation that greater polymer contents in the membranes reinforces the tensile properties of PBI membranes.[26]

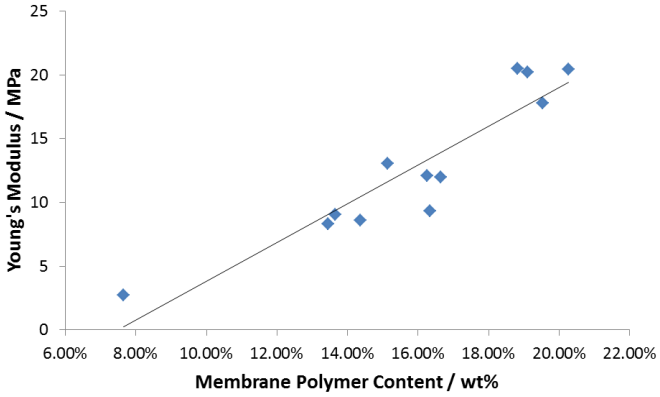

Figure 3.5. The Young's moduli of 2,5-pyridine-r-para-PBIs measured in tension at 25°C ±3°C on as-cast films.

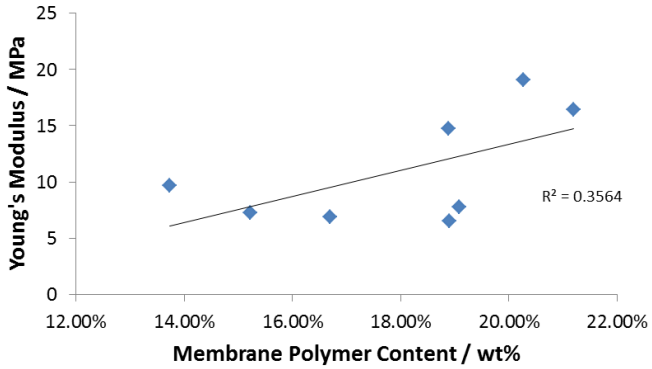

Figure 3.6. The Young's moduli of 2,5-pyridine-r-meta-PBIs measured in tension at 25°C ± 3°C on as-cast films.

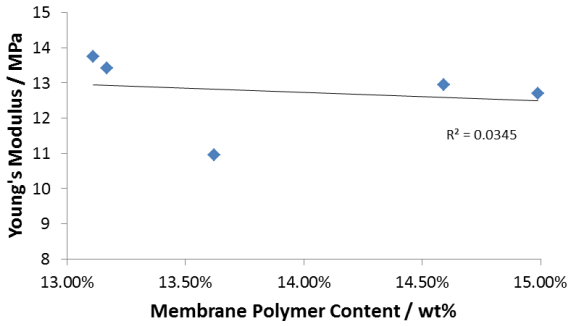

Figure 3.7. The Young's moduli of 2,5-pyridine-r-2OH-PBIs measured in tension at 25°C ± 3°C on as-cast films.

Creep tests were performed on select high polymer content membranes to investigate the high temperature creep resistance of the gel membranes under static compression. The membranes were preconditioned in an oven at 180°C prior to each test to simulate operational fuel cell conditions. Figure 3.8 shows the results of tests for a 2,5-pyridine-r-2OH-PBI membrane, a 2,5-pyridine-r-para-PBI membrane, and a 2,5-pyridine-r-meta-PBI membrane, each composition consisting of a 3:1 ratio of 2,5-pyridine-PBI to its copolymer counterpart. The compliance curves are an average of three experimental data sets under identical preconditioning and testing conditions. As demonstrated in a 20 hour test, the compliance of each membrane increased with time due to material creep under a static compressive force. For each membrane, an initial nonlinear transition period of 1-4 hours was followed by a nearly linear slope compliance period. Upon closer inspection, the compliance slope of the near-linear region gradually decreased over time due to the compression of the gel structure and the resulting composition change. As previously discussed,[26] both the creep compliance and creep rate can be used as points of comparison to distinguish a membrane's resistance to creep under static compressive forces. The creep compliance, J_S^0 and the creep rate, *dJ/dt*, for the high polymer content

membranes were much lower than that of para-PBI (~1.0x10^{-5} Pa^{-1} after 20h and 0.097 MPa^{-1} h^{-1}, respectively).

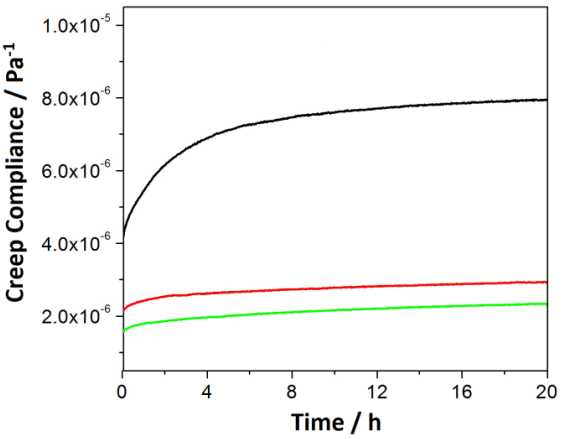

Figure 3.8. Creep compliance, J_s^0, curves of a 2,5-pyridine-r-2OH-PBI membrane (MM1-92-3, 13.17 wt% polymer content, green line), a 2,5-pyridine-r-para-PBI membrane (MM1-40-2, 13.66 wt% polymer content, red line), and a 2,5-pyridine-r-meta-PBI membrane (MM1-72-2, 15.22 wt% polymer content, black line), preconditioned at 180°C for 24 hours and compressed at 0.1 MPa at 180°C. Each copolymer is comprised of a 3:1 ratio of 2,5-pyridine-PBI to its counterpart PBI.

Table 3.4 shows the results of the creep tests for the three copolymer membranes. Interestingly, the 2,5-pyridine-r-meta-PBI membrane has the highest creep compliance and creep rate, even though it had the highest polymer content. This indicates that the creep compliances and rates are not solely based on polymer content, but are also influenced by chemical composition. Based on the results of J_s^0, η_0, and dJ/dt, 2,5-pyridine-r-meta-PBI membranes displayed the lowest creep resistance, while 2,5-pyridine-r-para-PBI membranes and 2,5-pyridine-r-2OH-PBI membranes showed significantly improved resistance. Based on the results of creep compliance at 20h, 2,5-pyridine-r-2OH-PBI membranes showed slightly better creep resistance than 2,5-pyridine-r-para-PBI membranes. At the end of the compression creep test, the J_s^0 and η_0 values of 2,5-pyridine-r-2OH-PBI and 2,5-py-r-para-PBI membranes were comparable

within the range of experimental error, suggesting that adding the 2OH- and para-comonomers have a similar reinforcing effect. The results of these tests correlate with the relative solubility of these membranes in PA (see Figure 3.1) and suggest a correlation with polymers possessing a more extended chain conformation. Thus, the less-soluble PBI components (e.g. 2OH- or para-PBI) impart higher gel thermal stabilities on membranes than more-soluble PBI components (e.g. meta-PBI).

Table 3.4. Creep compliance test results for three different copolymer systems with a 3:1 ratio of 2,5-pyridine-PBI to its counterpart PBI.

Membrane Type	Polymer Content (wt%)	J_s^0 (10^{-6} Pa^{-1})	η_0 (10^{12} Pa s)	J at 20h (10^{-6} Pa^{-1})	$dJ/dt_{8\text{-}20h}$ 10^{-6} Pa^{-1} hr^{-1})
2,5-pyridine-r-2OH-PBI	13.17	1.35±0.20	0.15±0.04	2.33±0.32	0.0180±0.0005
2,5-pyridine-r-para-PBI	13.66	1.34±0.34	0.18±0.06	2.94±0.77	0.0167±0.0002
2,5-pyridine-r-meta-PBI	15.22	2.26±0.63	0.08±0.06	7.94±2.60	0.0384±0.0004

J_s^0 = Steady-state recoverable compliance
η_0 = Extensional viscosity at zero extension rate
J = Compliance
$dJ/dt_{8\text{-}20h}$ = Creep rate (change in compliance over the last 12 hours of the test)

Due to its accuracy and ease of measurement, proton conductivity is a common metric used to compare the relative resistances of proton exchange membranes. Perfluorosulfonic acid-based PEMs, such as DuPont's Nafion, depend on water as a dopant to facilitate proton conduction. Due to hydration issues with the membrane, proton conductivities are generally very low at temperatures exceeding 100°C. In contrast, PA-doped PBI membranes display much higher proton conductivities at elevated temperatures due to the low vapor pressure of PA and the faster proton-transport kinetics of phosphoric acid.[29–31] Prior investigations of high temperature fuel cell membranes have shown that on water content, phosphoric acid content, membrane

morphology, and membrane chemistry all significantly affect the proton conductivity measurements.[9,16,17]

Proton conductivity was measured using four-probe, through-plane a.c. impedance spectrometry. To simulate anhydrous fuel cell operating conditions, as-cast copolymer membranes were dehydrated by preconditioning the membranes at 180°C for at least two hours. Figure 3.9 shows that the as-cast 2,5-pyridine-r-para-PBI membranes had decreasing PA concentrations with increasing polymer content, which results in lower proton conductivities of the membranes. This agrees with the general trends reported in the literature, e.g., that PBI membranes with greater concentrations of phosphoric acid display greater proton conductivities.[14,26] It is important to note that the correlation between polymer content and proton conductivity is only moderate (R^2=0.41) for these high solids membranes, indicating that other factors (i.e. differences in membrane chemistry) may also influence proton conductivity values. Similarly, a moderate correlation (R^2=0.37) was observed between proton conductivity and PA:PRU molar ratio for all 2,5-pyridine high solids copolymer membranes (Figure 3.10). A stronger correlation (R^2=0.70) between PA:PRU molar ratio and proton conductivity was observed when comparing membranes of the same copolymer ratio (Figure 3.11), which supports the claim that polymer membrane chemistry is important in determining proton conductivity. By adjusting the initial monomer concentration in the polymerization solution, both the PA content and the proton conductivity of the final membrane could be moderately controlled.

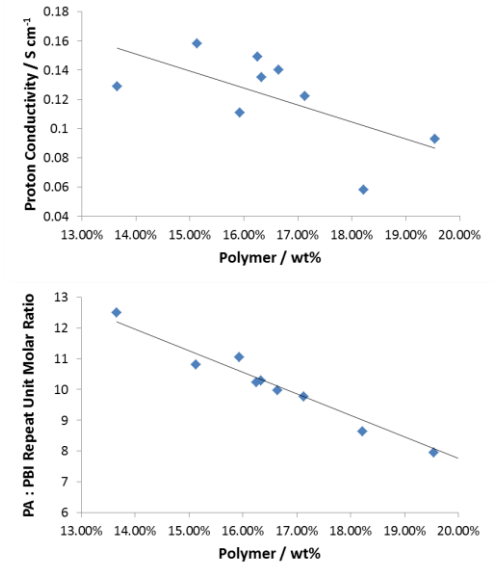

Figure 3.9. The anhydrous proton conductivities of 2,5-pyridine-r-para-PBI membranes measured at 180°C (top) and their respective PA content (bottom).

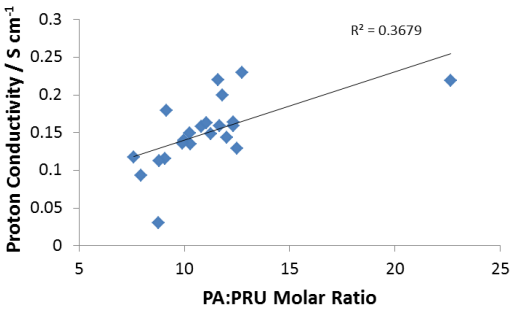

Figure 3.10. The PA:PRU molar ratios plotted against proton conductivities for all 2,5-pyridine high solids copolymer membranes.

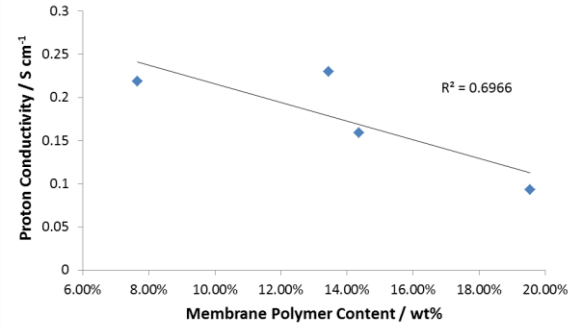

Figure 3.11. A comparison of PA:PRU molar ratios and their respective proton conductivity for a given series of 5:1 2,5-pyridine-r-para-PBI membranes.

A series of non-optimized fuel cell tests were performed to further investigate the electrochemical properties of the 2,5-pyridine high solids MEAs. As-cast films were pretreated with concentrated PA prior to hot-pressing the membranes with the electrodes to reduce interfacial resistances at the three-phase interface. Visual inspection of the hot-pressed MEAs and fuel cell performance indicated that all of the high polymer content 2,5-pyridine membranes were thermally stable at least up to 150°C. This contrasts with high polymer content 3,5-pyridine copolymer membranes, which showed thermal instability at higher copolymer ratios of 3,5-pyridine-PBI.[26] However, it was determined that only specific ratios of 2,5-py-2COOH to IPA, TPA, or 2OH-TPA were feasible to polymerize and cast into membranes. At high copolymer ratios of the meta-, para-, or 2OH- functionalized PBIs, these less-soluble PBIs decreased the polymerization times (Figure 3.4) and thus resulted in membranes with poor mechanical properties or solutions that could not be processed into membranes. Figure 3.12 shows the effects of monomer ratios and polymer solution concentrations with solution processability and fuel cell performance for a series of 2,5-pyridine-r-para-PBI membranes. These performance-processing maps indicate processing windows where membranes could be made with mechanical properties suitable for use in fuel cells.

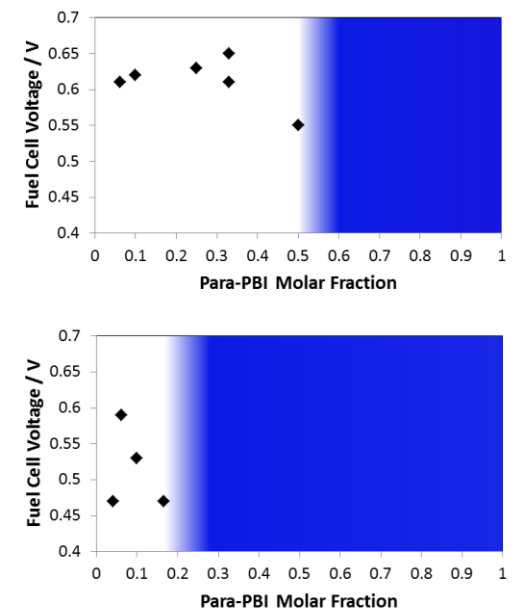

Figure 3.12. Processing map and non-optimized fuel cell performances at 0.2 A cm^{-2} using H_2:Air at a 1.2:2.0 stoichiometric ratio (following break-in) at 180°C of 2,5-pyridine-r-para-PBI gel films. Membranes were cast from 12 wt% monomer charge (top) and 16 wt% monomer charge (bottom) solutions. The blue areas represent copolymers which were too viscous to cast or too low in molecular weight to form viable membranes.

Long-term steady-state fuel cell tests were performed on a membrane of each series of high solids content 2,5-pyridine copolymer membranes. These tests were performed at 180°C, 0.2 A cm^{-2}, and using H_2:Air at a 1.2:2.0 stoichiometric ratio. Figure 3.13 shows the voltage response at constant current density and acid loss data for a 2,5-pyridine-r-meta-PBI membrane (MM1-72-4 in Table 3.2). Following an initial break-in period of 150 h, the fuel cell recorded a voltage degradation rate of 9.45 µV h^{-2} that was much lower than a low-solids para-PBI membrane (60 µV h^{-1}) at 190°C.[11] These differences could partially be due to the differences in operating temperatures. Additionally, the total PA loss rate for this cell (5.55 ng cm^{-2} h^{-1}) is the lowest for any PBI fuel cell recorded to date, and is over an order of magnitude lower than the PA loss rate of para-PBI (110.4 ng cm^{-2} h^{-1} at 190°C). The amount of PA lost from the cathode

was higher than that lost from the anode, which is likely an effect of the water generation process at the cathode. Similarly, Figure 3.14 shows the performance and acid loss of a 2,5-pyridine-r-para-PBI membrane (MM1-46-4). The voltage degradation rate of this MEA was 6.75 μV h^{-1}, which is again much lower than para-PBI at 190°C. However, the total PA loss rate of this membrane (94.73 ng cm^{-2} h^{-1}) was much closer to that of para-PBI. This high PA loss rate was partially attributed to the poor mechanical properties observed in the room temperature tensile tests (the strain-at-break for this membrane occurred at 16% elongation). For both of these fuel cells, the PA loss rate from the high solids content MEA's suggests that PA loss will not be a major factor of fuel cell failure.

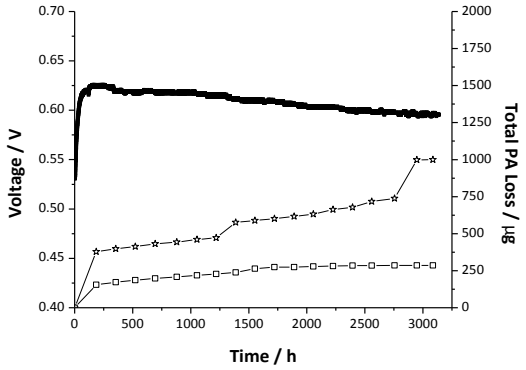

Figure 3.13. Long-term steady-state performance of a 2,5-pyridine-r-meta-PBI (MM1-72-4) copolymer membrane at 0.2 A cm^{-2} , 180^{O}C, and using H_2:Air at a 1.2:2.0 stoichiometric ratio . Solids Content = 19.09 wt%. Anode PA loss = 0.93 ng cm^{-2} h^{-1}, Cathode PA loss = 4.62 ng cm^{-2} h^{-1}, voltage degradation rate = 9.45 μV h^{-1}.

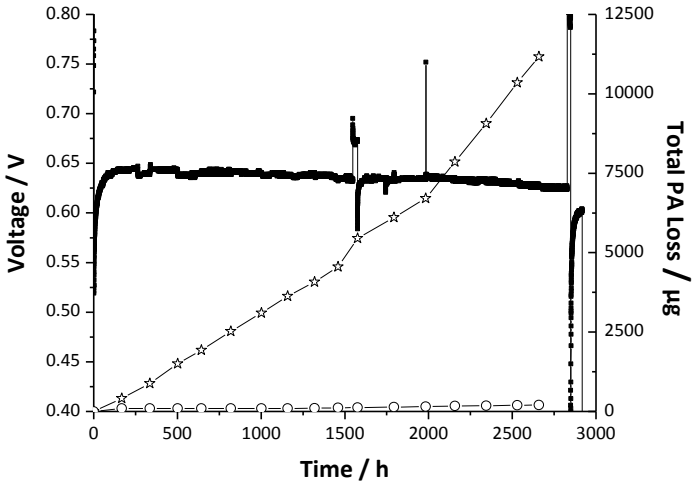

Figure 3.14. Long-term steady-state study of a 2,5-pyridine-r-para-PBI (MM1-46-4) copolymer membrane at 180^{O}C, 0.2 A cm^{-2}, and using H_2:Air at a 1.2:2.0 stoichiometric ratio. Anode PA Loss = 1.69 ng cm^{-2} h^{-1}, Cathode PA Loss = 93.04 ng cm^{-2} h^{-1}, voltage degradation rate = 6.75 µV h^{-1} following 150h break-in. Polarization curve was taken at 1500 h, as shown by the peak in the graph. Significant fuel cell voltage loss (~0.03V) was observed after 2750 h due to an unplanned station event.

Similar testing was conducted on 2,5-pyridine-r-2OH-PBI (MM1-92-2) membrane subjected to a long-term steady-state fuel cell test at 180°C, 0.2 A cm^{-2}, and using H_2:Air at a 1.2:2.0 stoichiometric ratio. This MEA was operated for more than 8600 h and exhibited a voltage degradation rate of 6.15 µV h^{-1}, also supporting the claim that high solids membranes are suited for extended lifetime electrochemical applications.

3.4. CONCLUSIONS

Three series of high polymer content membranes – 2,5-pyridine-r-meta-PBI, 2,5-pyridine-r-para-PBI, and 2,5-pyridine-r-2OH-PBI – were polymerized and cast into membranes using the PPA process. By adjusting the ratio of the more-soluble pyridine monomer to the less-soluble IPA, TPA, or 2OH-TPA counterpart, the solubility of the resulting copolymer, and thus, its processability into a PA-doped membrane could be controlled. Both the monomer concentration and ratio of monomers were used to

construct processing maps to describe copolymer compositions that could form stable membranes for electrochemical applications.

All membranes produced within the defined processing windows were thermally stable at 180°C. Measurement of the compressive creep properties of the membranes at 180˚C showed that membranes consisting of lower solubility copolymers and high solids membrane contents had reduced creep compliances at high temperatures under static loads. Thus, copolymer compositions were identified with sufficient processing capabilities and high temperature gel stability for further investigation. Many high solids compositions were identified that exhibited proton conductivities greater than 0.1 S cm^{-1}, even with reduced PA content.

Long-term steady-state fuel cell tests performed on the high polymer content membranes were compared to previous results for low polymer content para-PBI membranes. Much lower voltage degradation rates ranging from 6.15-9.45 μV h^{-1} were observed for the 2,5-pyridine copolymer membranes at 180°C, as compared with 60 μV h^{-1} for para-PBI reported at 190˚C. PA loss rates were found to be quite low and suggested that PA loss is not likely to act as a primary failure mode during steady-state operation.

3.5. REFERENCES

[1] Steele B. C. H., and Heinzel A., 2001, "Materials for Fuel-Cell Technologies," Nature, **414**, p. 345-352.

[2] Dunwoody D., and Leddy J., 2005, "Proton Exhange Membranes: The View Forward and Back," The Electrochemical Society Interface, **3**, pp. 37–39.

[3] Vogel H. A., and Marvel C. S., 1961, "Polybenzimidazoles, New Thermally Stable Polymers," J. Polym. Sci., **50**, p. 511-539.

[4] Vogel H. A., and Marvel C. S., 1963, "Polybenzimidazoles. II," J. Polym. Sci., Part A1, **1**, pp. 1531-1541.

[5] Wainright J. S., Wang J. T., Weng D., Savinell R. F., and Litt M., 1995, "Acid-doped polybenzimidazoles: a new polymer electrolyte," J. Electrochem. Soc., **142**(7), pp. L121–L123.
[6] Litt M., Ameri R., Wang Y., Savinell R. F., and Wainright J. S., 1999, "Polybenzimidazoles/phosphoric acid solid polymer electrolytes: mechanical and electrical properties.," Mater. Res. Soc. Symp. Proc., pp. 313–323.
[7] Xiao L., Zhang H., Scanlon E., Ramanthan L. S., Choe E. W., Rogers D., Apple T., and Benicewicz B. C., 2005, "High-Temperature Polybenzimidazole Fuel Cell Membranes via a Sol-Gel Process," Chem. Mater., **17**(21), pp. 5328–5333.
[8] Yu S., and Benicewicz B. C., 2009, "Synthesis and Properties of Functionalized Polybenzimidazoles for High-Temperature PEMFCs," Macromolecules, **42**(22), pp. 8640–8648.
[9] Molleo M., Schmidt T. J., and Benicewicz B. C., 2012, "Polybenzimidazole-Phosphoric Acid (PBI-PA)-Based Fuel Cells," Encyclopedia of Sustainability, Science and Technology, pp. 391–431.
[10] Xiao L., Zhang H., Jana T., Scanlon E., Chen R., Choe E. W., Ramanthan L. S., Yu S., and Benicewicz B. C., 2005, "Synthesis and Characterization of Pyridine-Based Polybenzimidazoles for High Temperature Polymer Electrolyte Membrane Fuel Cell Applications," Fuel Cells, **5**(2), pp. 287–295.
[11] Yu S., Xiao L., and Benicewicz B. C., 2008, "Durability Studies of PBI-based High Temperature PEMFC," Fuel Cells, **8**(3-4), pp. 165–174.
[12] Qian G., and Benicewicz B. C., 2009, "Synthesis and Characterization of High Molecular Weight Hexafluoroisopropylidene-Containing Polybenzimidazole for High-Temperature Polymer Electrolyte Membrane Fuel Cells," J. Polym. Sci., Part A, **47**(16), pp. 4064–4073.
[13] Mader J., and Benicewicz B. C., 2010, "Sulfonated Polybenzimidazoles for High Temperature PEM Fuel Cells," Macromolecules, **43**, pp.6706-6715.
[14] Seel D. C., Benicewicz B. C., Xiao L., and Schmidt T. J., 2009, "High-temperature Polybenzimidazole-based Membranes," Handbook of Fuel Cells, **5**, pp. 300–312.
[15] Li Q., He R., Gao J., Jensen O. J., and Bjerrum N. J., 2003, "The CO Poisoning Effect in PEMFCs Operational at Temperatures up to 200C," J. Electrochem. Soc., **150**(12), pp. A1599–A1605.
[16] He R., Li Q., Xiao G. Y., and Bjerrum N. J., 2003, "Proton conductivity of phosphoric acid doped polybenzimidazole and its composites with inorganic proton conductors," J. Membr. Sci., **226**(1-2), pp. 169–184.
[17] Li Q., Hjuler H. A., and Bjerrum N. J., 2001, "Phosphoric acid doped polybenzimidazole membranes: physiochemical characterization and fuel cell applications," J. Appl. Electrochem., **31**(7), pp. 773–779.
[18] Mader J., Lixiang X., Schmidt T., and Benicewicz B. C., 2008, "Polybenzimidazole/Acid Complexes as High-Temperature Membranes," Adv. Polym. Sci., **216**(Fuel Cells II), pp. 63–124.
[19] Schmidt T. J., and Baurmeister J., 2006, "Durability and Reliability in High Temperature Reformed Hydrogen PEFCs," ECS Transactions, **3**(1), pp. 861–869.
[20] Garsany Y., Gould B. D., Baturina O. A., and Swider-Lyons K. E., 2009, "Comparison of the Sulfur Poisoning of PBI and Nafion PEMFC Cathodes," Electrochemical and Solid-State Letters, **12**(9), pp. B138–B140.

[21] U.S. Dept. Energy, An Integrated Strategic Plan for the Research, Development, and Demonstration of Hydrogen and Fuel Cell Technologies, 2011. Available at http://www1.eere.energy.gov/hydrogenandfuelcells/pdfs/program_plan2011.pdf
[22] Suvorov A., Elter J., Staudt R., Hamm R., Tudryn G., Schadler L., and Eisman G., 2008, "Stress relaxation fo PBI based membrane electrode assemblies," International Journal of Solids and Structures, **45**(24), pp. 5987–6000.
[23] Patankar K. A., Dillard D. A., Case S. W., Ellis M. W., Lai Y.-H., and Gittleman C. S., 2012, "Linear Hygrothermal Viscoelastic Characterization of Nafion NRE 211 Proton ExchangeMembrane," Fuel Cells, **12**(5), pp. 787–799.
[24] Lai Y.-H., Mittelsteadt C. K., Gittleman C. S., and Dillard D. A., 2009, "Viscoelastic Stress Analysis of Constrained Proton Exchange Membranes Under Humidity Cycling," J.Fuel Cell Sci. Technol., **6**(2), pp. 021002–021002–13.
[25] Li Y., Dillard D. A., Case S. W., Ellis M. W., Lai Y.-H., Gittleman C. S., and Miller D. P., 2009, "Fatigue and creep to leak tests of proton exchange membranes using pressure-loaded blisters," J. Power Sources, **194**(2), pp. 873–879.
[26] Molleo M., Chen X., Ploehn H., and Benicewicz B. C., 2013, "High Polymer Content 3,5-Pyridine-Polybenzimidazole Copolymer Membranes with Improved Compressive Properties," In Process.
[27] Ferry J. D., 1980, Viscoelastic Properties of Polymers, 3rd Ed., John Wiley & Sons, New York.
[28] 1999, "Standard Methods for the Examination of Water and Wastewater: 4500-P Phosphorus," pp. 1–24 [Online]. Available at: http://www.umass.edu/tei/mwwp/acrobat/sm4500P-E.PDF.
[29] Vilciauskas L., Paddison S. J., and Kreuer K.-D., 2009, "Ab Initio Modeling of Proton Transfer in Phosphoric Acid Clusters," J. Phys. Chem. A, **113**, pp. 9193–9201.
[30] Dippel T., Kreuer K. D., Lassegues J. C., and Rodriguez D., 1993, "Proton conductivity in fused phosphoric acid; a 1H/31P PFG-NMR and QNS study," Solid State Ionics, **61**, pp. 41–46.
[31] Bozkurt A., Ise M., Kreuer K. D., Meyer W. H., and Wegner G., 1999, "Proton-conducting polymer electrolytes based on phosphoric acid," Solid State Ionics, **125**, pp. 225–233.

4. Investigation of Solubility Effects on High Polymer Content Polybenzimidazole Membrane Systems

4.1. Motivation for Solubility Studies

Polymer electrolyte membrane (PEM) fuel cells have demonstrated great potential as energy conversion devices due to their ability to produce high power density, high energy conversion efficiency, and low environmental impact.[1,2] At the heart of these fuel cells, PEM materials facilitate the transport of protons from the anode to the cathode. The most commonly used PEM materials are perfluorosulfonic acid (PFSA) polymer matrices that rely on percolated water/sulfonic acid clusters to facilitate proton transport. These materials have demonstrated excellent mechanical robustness, chemical stability, and high proton conductivity. However, because water is used as the proton conduction media, PFSA-based fuel cells are inherently limited by operation temperatures (<100°C) and water management systems (to keep the film fully hydrated).[3–5] Because these cells are required to operate at relatively low temperatures, high purity fuels are required to prevent non-reversible binding of impurities (e.g. carbon monoxide, hydrogen sulfide) to the platinum catalyst on the electrodes. In contrast, polybenzimidazole (PBI) membranes doped with phosphoric acid (PA) can readily operate at temperatures above 100˚C without the need for water management systems. PBI-based PEM fuel cells typically operate between 160-200°C, and exhibit low degradation rates at these temperatures. Additionally, these cells are able to tolerate greater ranges of fuel impurities because gasses such as carbon monoxide and hydrogen sulfide can reversibly

bind to the catalyst at this temperature range.[6–8] Phosphoric-acid doped PBI membranes have shown excellent fuel cell properties over the past decade.[9–12] Traditionally, PBIs are synthesized in organic solvents and processed into thin films by casting the polymerization solution onto a glass plate and subsequent evaporation of the volatile solvent. It is important to note that the molecular weights of the PBIs are limited due to their inherent solubility issues in organic solvents. Water and PA baths are successively used to respectively wash salts out of the polymer film and swell the film with the PA dopant. This conventional synthesis and imbibing process is an extremely time-consuming, multistep procedure.[13–15] In comparison, the PPA Process offers a facile and concise pathway to achieve PA-doped and high molecular weight PBI membranes.[16] In addition to demonstrating high power densities, physical and chemical stabilities, and high proton conductivities, PBIs have shown much potential for extended lifetime electrochemical applications.[17] Historically, PPA Processed PBI membranes have relatively low polymer contents (<10 wt%).

Inspired by a Department of Energy fuel cell target of 40,000h for stationary applications,[18] we recently investigated the thermal, mechanical, and electrochemical properties of higher polymer content (10-30 wt%) membranes. It is well-known that PEMs under static compressive forces (such as in a fuel cell stack) are susceptible to polymer creep. Over time, polymer creep causes membrane thinning and pinhole formation, thereby decreasing performance of the fuel cell via gas-crossover and electrical shorting.[17,19,20] It was demonstrated that higher polymer content PBI PEMs are less compliant under compressive forces, and therefore, are more resistant to polymer creep. [21,22]

As previously discussed, new polymers chemistries have been explored to cast high polymer content membranes via the PPA Process.[21,22] Traditional PPA Processed PBI membranes, such as poly(2,2′-(1,4-phenylene)5,5′-bibenzimidazole) (para-PBI) or poly(2,2′-(1,3-phenylene)5,5′-bibenzimidazole) (meta-PBI), are limited to lower polymer content membranes due to their low solubility in PPA. Increasing the polymer content in the polymerization solutions increased the viscosity to such an extent that either: 1) only low molecular weight polymer could be achieved, causing poor mechanical properties in the resulting membrane; or 2) the polymer solution no longer flowed and balled-up on the stir-rod (Weissenberg effect), preventing the processing into a thin film.[23] Meanwhile, poly(2,2′-(2,5-pyridine)5,5′-bibenzimidazole) (2,5-py-PBI) or poly(2,2′-(3,5-pyridine)5,5′-bibenzimidazole) (3,5-py-PBI) were known to have higher solubilities in PPA and could be processed into high polymer content membranes.[24] However, these more-soluble py-PBI membranes were known to have lower gel thermal stabilities (not to be confused with polymer thermal stability, which are stable at temperatures exceeding 600°C) as a result of their increased solubilities in both PPA and PA. By synthesizing random copolymers that incorporated thermally (gel) stable meta- or para-PBI's with more soluble 2,5- or 3,5-py-PBI, we achieved membranes with increased polymer contents (>10 wt%) and good thermal gel stability at fuel cell operational temperatures of 180°C. The four PBIs of interest are shown in Figure 4.1 and organized by polymer solubility properties.

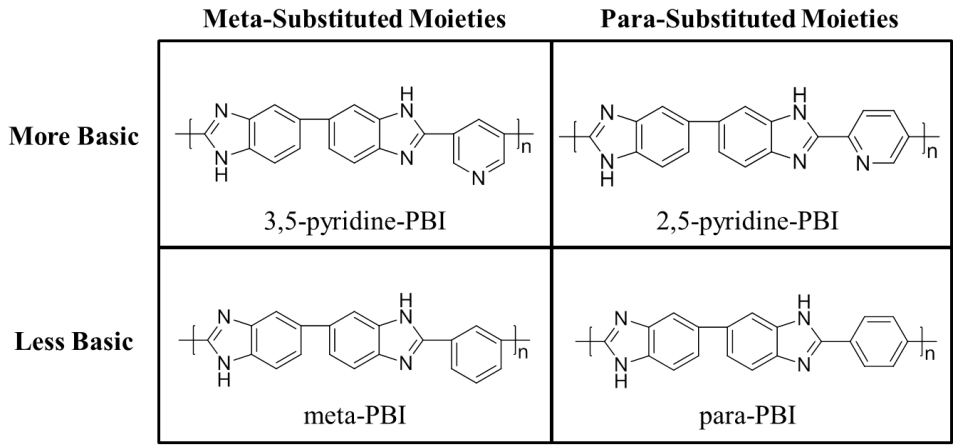

Figure 4.1. Chemical structures of four common PBIs, categorized by characteristics that effect polymer solubility.

Thus, several series of random copolymers were synthesized and cast into membranes with increased polymer content and suitable gel thermal stability for electrochemical applications. Although the 2,5-py-PBI and 3,5-py-PBI copolymer systems have separately been investigated, an in-depth comparison would provide useful information as to how the solubility properties of PBIs affect the fundamental properties of gel thermal stability, proton conductivity, and fuel cell performance. This information is critical for the further development of high polymer content PBI membranes. It is generally believed that polymer solubility and membrane properties are strongly influenced by the quantity or strength of dipoles and polymer chain configuration. We herein propose copolymer membrane systems that isolate the effects of these solubility properties in high polymer content membranes. For example, the two copolymer structures depicted in Scheme 4.1 can be considered to be constitutional isomers given similar monomer ratios of n to m. The theoretical chain persistence lengths would be comparable due to the similarity of the bond lengths and angles of pyridine- and phenyl-

substituted moieties. These two systems were compared to each other to isolate the influences of dipole strength on polymer processing and membrane properties.

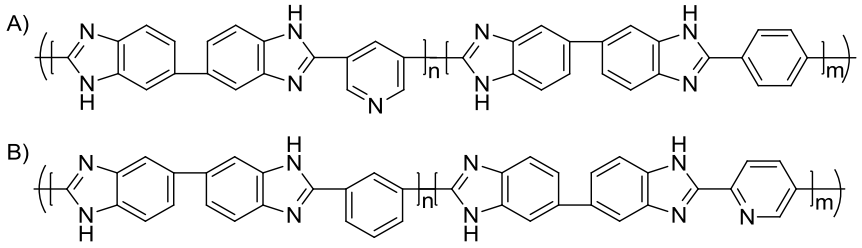

Scheme 4.1. Chemical structures of A) 3,5-py-PBI-r-para-PBI and B) 2,5-py-PBI-r-meta-PBI.

In this work, we report an in-depth investigation of the structure-property relationships of 2,5-py-r-para-PBI, 2,5-py-r-meta-PBI, 3,5-py-r-para-PBI, and 3,5-py-r-meta-PBI high polymer content membranes. Theoretical calculations of dipole strength and ground state geometries of model compounds (repeat units) were determined using Spartan'10 computer software.[25] Careful comparisons of these copolymer systems allowed us to isolate the effects of polymer chain configuration, dipole strength, and pyridine quantity on various aspects of polymer synthesis, membrane processing, thermal gel stability, and electrochemical properties.

4.2. EXPERIMENTAL

4.2.1 CHEMICALS

2,5-Pyridinedicarboxylic acid (2,5-py-2COOH) was purchased from Acros Chemical and TCI America (~98% purity) and purified by recrystallization from a 1:1 dilution of concentrated hydrochloric acid prior to use. 3,5-Pyridinedicarboxylic acid (2,5-py-2COOH) was purchased from Acros Chemical and TCI America (~98% purity) and purified by recrystallization from a 1:10 dilution of concentrated hydrochloric acid

prior to use. Terephthalic acid (TPA, purified), isophthalic acid (IPA, purified) were purchased from Amoco Chemicals. 3,3',4,4'-Tetraaminobiphenyl (TAB, purified) donated by BASF Fuel Cells and used as-received. Polyphosphoric acid (PPA, 116%) were obtained from InnoPhos, Inc.

4.2.2. Polybenzimidazole Synthesis and Membrane Preparation

A solution of 2,5-py-2COOH or 3,5-py-2COOH, PPA, TAB, and IPA or TPA was added to a three-neck flask equipped with nitrogen flow and overhead stirrer, stirred, and heated at 195-220^{O}C for 3-30 hours. This synthesis is depicted in Scheme 4.2. The polymerization time was correlated with the viscosity of the solution, which was dependent on the solids concentration, polymer molecular weight, and the ratio of the pyridine monomer to the other diacid monomer. The rate of the polymerization was controlled by the stir-rate and reaction temperature. When the polymerization solution reached high viscosity (judged visually), the PBI solution was poured onto a pyrex or glass plate and cast at a thickness of 15mil using a Gardner blade. To form a gel membrane, the glass plates with the cast films were immediately placed into a humidity controlled chamber at 55% ± 5% relative humidity (RH), 25 ± 2^{O}C. Complete hydrolysis of the membranes occurred over a span of 12-24h. The as-cast gel membrane generally had a thickness ranging from 300-500µm.

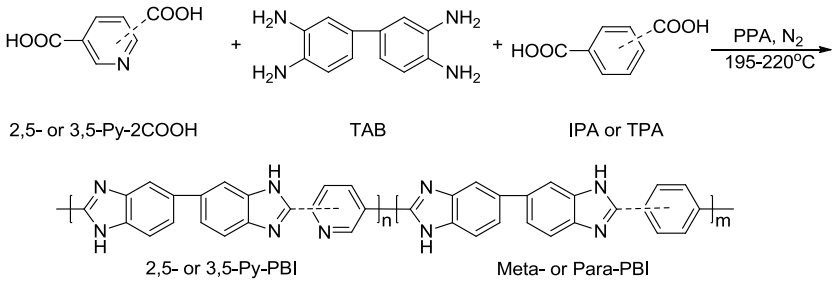

Scheme 4.2. Synthesis of random copolymers using 2,5- or 3,5-pyridinedicarboxylic acid and 3,3',4,4'-tetraaminobiphenyl with isophthalic or terephthalic acid.

2.3 CHARACTERIZATION TECHNIQUES

Thermogravimetric analysis, differential scanning calorimetry, and inherent viscosity measurements were performed on polymer isolated from the PPA process. Following the polymerization of the random copolymers, the polymer/PPA solution that remained in the reaction vessel after casting was hydrolyzed with deionized water. The precipitated polymer was then pulverized in a commercial Waring blender and neutralized with ammonium hydroxide in 500 mL of distilled water. After heating for 1 hour at 100˚C, the polymer was isolated by filtration and washed thoroughly with water to remove any residual ammonium salts. The powder was then dried for 12 hours at 120-130˚C. Thermogravimetric analysis (TGA) was performed using a TA Instruments TGA Q-5000 with a heating rate of 20 °C min^{-1} under nitrogen. Differential scanning calorimetry (DSC) was conducted using a TA Instruments DSC Q-2000 with a nitrogen flow rate of 20 mL min^{-1} and heating and cooling rates of 10°C min^{-1}.

Following dissolution of the isolated polymer in sulfuric acid to make 0.2 g dL^{-1} concentrations, inherent viscosities (IV's) were measured using an Ubbelohde viscometer in a water bath set at 30.0˚C. Inherent viscosity was measured by recording the flow times in the viscometer for the polymer solution and pure sulfuric acid using a suspended level Cannon Ubbelohde viscometer, size 200, at 30.0˚C in a temperature controlled water bath and was calculated according to Equation 1:

$$\ln [(t) (t_o)^{-1}] c^{-1} = \text{Inherent Viscosity (dL g}^{-1}) \qquad (1)$$

where t is the solution flow time in seconds, t_o is the solvent (96% sulfuric acid) flow time in seconds, and c is the solution concentration in g/dL.

The composition of acid-doped PBI membranes was determined by measuring the relative amounts of polymer solids, water, and acid in the film. The phosphoric acid (PA) content was determined by titrating a sample of membrane with standardized sodium hydroxide solution (0.1 N) using a Metrohm 716 DMS Titrino autotitrator. The sample was washed with water and dried in an oven overnight at 120 °C. The dried sample was then weighed to determine polymer solids content for the membrane. The amount of water was calculated by subtracting the weights of polymer and PA from the initial PBI membrane sample weight.

Ionic conductivities were measured via a four-probe through-plane bulk measurement using an AC Zahner IM6e impedance spectrometer that scanned a frequency range from 1 Hz to 100 KHz. A rectangular sample of membrane (3.5 cm x 7.0 cm) was placed in a polysulfone cell with four platinum wire current collectors. Two outer electrodes set 6.0 cm apart supplied current to the cell, while the two inner electrodes 2.0 cm apart on opposite sides of the membrane measured the voltage drop. To ensure a through-plane bulk measurement of the membrane ionic conductivity, the two outer electrodes were placed on opposite sides of the membrane and the two inner electrodes were arranged in the same manner. The reported conductivities were measured on preconditioned (dehydrated) membranes that were held at >100°C for at least two hours. Proton conductivity was calculated using the following equation:

$$\sigma = (D)\,(L \cdot B \cdot R)^{-1} \qquad (2)$$

where D was the distance between the two test current electrodes, L was the thickness of the membrane, B was the width of the membrane, and R was the measured resistance.

The mechanical properties of the membranes were measured by cutting dog bone specimens (ASTM D683 Type V) from the membrane using a cutting press. Tensile properties were measured using an Instron Tensile Tester (5543A) with a 10N load cell. All measurements were made at 25°C ± 3°C on samples preloaded to 0.1N with a crosshead speed of 5mm per minute.

The compression creep tests were performed using a TA Instruments RSAIII dynamic mechanical analyzer. Discs were cut from polymer membranes with a diameter of 6.3 mm and thickness of approximately 0.9~1.2 mm. Before the compression creep tests, the samples were conditioned by placing them between two parallel smooth Teflon blocks at 180°C for approximately 24 hours. In a typical compression creep test, a step stress was applied to the sample and held constant for 20 hours. The deformation of the test specimen was recorded as a function of time. To ensure the compression stress was uniaxial, the compression tool surfaces were coated with PTFE to minimize the friction between the sample and the tool. The creep compliance was calculated by dividing the strain by the applied stress, and the compliance as a function of time was fitted with the Maxwell model[26]:

$$J(t) = J_s^0 + t \cdot {\eta_0}^{-1} \qquad (3)$$

where J_s^0 represents the steady-state (recoverable) compliance, t is time, and η_0 is the extensional viscosity at zero extension rate. All tests were carried out at 180 °C, and the applied stress level was selected to be 0.1 MPa.

Frequency sweep tests were also performed using the TA Instruments RSAIII at various temperatures for characterization of the thermal stability of the gel membranes. Cylindrical compression samples were used with diameter 15mm and thickness ~4mm. Before the tests, the samples were conditioned in vacuo at 80 °C for 24 hours. The storage modulus (E') and loss modulus (E") were recorded as functions of frequency at various temperatures. The test frequency ω spanned from 0.00249 Hz to 9.9 Hz, and a strain amplitude of 0.25% was used.

Membrane electrode assemblies consisted of the polymer membrane sandwiched between two electrodes. MEAs were prepared by hot pressing the acid-doped membrane between an anode electrode and a cathode electrode at 150 °C for 90-150 seconds using 4500 lbs of force and compressing to 80% its original width. Prior to hot pressing, the membrane was pretreated (dipped into) with concentrated PA for less than 10 seconds to wet its surface and thus reduce the interfacial resistance of the membrane-catalyst interface. Electrodes were received from BASF Fuel Cell, Inc. with 1.0 mg/cm^2 platinum (Pt) catalyst loading. Anode electrodes contained only Pt as the catalyst, while the cathode electrodes contain a BASF Fuel Cell standard cathode Pt alloy. The active area of the electrodes was 45.15 cm^2. Fuel cell fabrication was conducted by assembling the cell components as follows: end plate:PTFE insulator:anode current collector:anode flow field:MEA:cathode flow field:cathode current collector:PTFE insulator:end plate.

Gaskets were used on either side of the MEA to control compression. Following assembly, the cell was evenly clamped to 50 in-lbs of pressure.

Fuel cell performance was measured in 50 cm^2 (active area 45.15 cm^2) single stack fuel cells using test stations obtained from Plug Power or purchased from Fuel Cell Technologies. Polarization curves were obtained at various temperatures (120-180 °C) with hydrogen as a fuel and different oxidants (air or oxygen gas). Fuel cells were operated for at least 100 hours (break-in period) at 0.2 A/cm^2 at 180 °C before measurement of polarization curves. Long term stability testing was performed under static current and temperature conditions of 0.2 A/cm^2 and 180 °C with a constant flow rate of hydrogen and air. Degradation rates of long-term fuel cell operations were calculated by linear fitting of cell voltage data points with respect to time. Product water and PA from the exhaust gases were collected by passing the gases through bottles containing distilled water. The PA loss was determined by analyzing the water in the collection bottles using an ascorbic acid test and UV-Vis absorbance at 880nm wavelength.[27]

4.2.4. EQUILIBRIUM GEOMETRY MODELING

Small molecule models of 2,5-pyridine-PBI, 3,5-pyridine-PBI, meta-PBI, and para-PBI repeat units were created and analyzed using Spartan'10 software on a Linux system. The ground state equilibrium geometries were calculated using density functional theory (B3LYP/6-31G*) in a vacuum. Electrostatic potential energy maps and dipole moments were generated using the data obtained from the equilibrium geometry calculations. Bond strengths were calculated by comparing the ground state energy of protonated models to that of non-protonated models.

4.3. Results and Discussion

4.3.1. Modeling Study of PBI Repeat Units

To correlate the solubility properties of the four different PBI systems, each polymer's repeat unit was modeled using Spartan'10 software. Each small molecule consisted of two 2-benzimidazole moieties that were bonded to either a phenyl or pyridine moiety. The ground state equilibrium geometry of each repeat unit was determined by calculating and comparing the minimum potential energy for each individual conformer. Electrostatic potential maps of each lowest energy conformer are depicted in Figure 4.2, and each small molecule's energy values and dipole moments are recorded in Table 4.1. These calculations and comparisons showed that the model compounds containing pyridine moieties possessed a higher dipole moment than the model compounds containing phenyl moieties. The addition of an additional basic site of the pyridine moieties allowed for additional hydrogen-bonding or protonation, which would thereby increase the formal charge of the total molecule. As indicated by the electrostatic potential maps of the non-protonated model compounds, the lower steric hindrance around the pyridine moiety of 3,5-pyridine model compounds should allow greater interactions than the 2,5-pyridine counterpart.

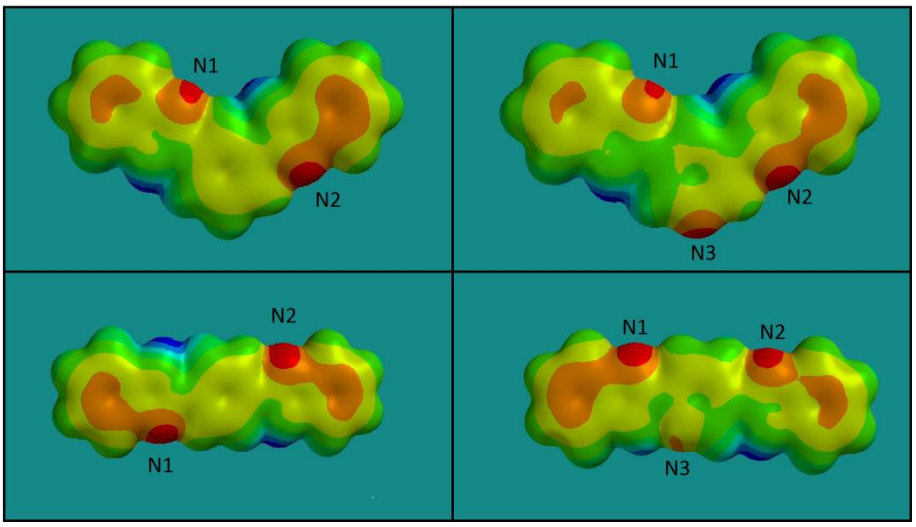

Figure 4.2. Electrostatic potential energy maps of the lowest energy non-protonated model compounds: meta-BI (top left); para-BI (bottom left); 3,5-py-BI (top right); 2,5-py-BI (bottom left).

Additional calculations were performed to understand the relationship between polymer structure and solubility in PPA or PA. Each model compound has either two or three proton accepting sites (nitrogens with an unshared pair of electrons in an sp2 orbital). In a phosphoric acid environment, it is likely that each basic site would become protonated or hydrogen-bonded (the pKa values of the benzimidazolium and pyridinium ions are ~5.5 and ~5.25, respectively).[15,28] The potential energy of protonation and subsequent torsion of the aromatic rings was determined by comparing the energy of the non-protonated model compounds to the energy of each protonated model compound; these values were used to judge the relative favorability of protonating each site. Every combination of protonation was determined, and their energy values are shown as "Δ Energy" in Table 4.1.

The potential energy data indicates that steric hindrance partially hinders the ability of unprotonated nitrogens to become protonated. Generally, the less-sterically hindered benzimidazole nitrogens (i.e. N2 of the meta- or 3,5-py-BI model) were

energetically more favorable to protonate than the more-sterically hindered sites (N1). When considering multiply protonated model compounds, each additional protonation is less energetically favorable which is due to steric hindrance and the subsequent torsion of the aromatic moieties relative to one another.

Table 4.1. The energy levels of each non-protonated and protonated repeat unit model compounds with their respective protonation bond strengths (Δ Energy) and dipole strengths.

Repeat Unit	Energy (Hartree)	Δ Energy (kcal/mol)	Dipole (Debye)
Non-Protonated 3,5-py-BI	-1005.64822	0	3.31
3,5-Py-BI_N1	-1006.03029	-240.7	12.21
3,5-Py-BI_N2	-1006.03696	-244.9	9.11
3,5-Py-BI_N3	-1006.02926	-240.1	7.46
3,5-Py-BI_N12	-1006.32684	-427.5	0.49
3,5-Py-BI_N13	-1006.30244	-412.2	9.62
3,5-Py-BI_N23	-1006.30382	-413	11.22
3,5-Py-BI_N123	-1006.47857	-523.1	7.39
Non-Protonated 2,5-py-BI	-1005.65753	0	4.32
2,5-Py-BI_N1	-1006.05018	-247.4	9.32
2,5-Py-BI_N2	-1006.04654	-245.1	10.92
2,5-Py-BI_N3	-1006.04172	-242	5.32
2,5-Py-BI_N12	-1006.34592	-433.7	1.81
2,5-Py-BI_N13	-1006.30097	-405.4	7.89
2,5-Py-BI_N23	-1006.32154	-418.3	5.18
2,5-Py-BI_N123	-1006.47876	-517.4	2.68
Non-Protonated Meta-BI	-989.61379	0	3.11
Meta-BI_N1	-990.002464	-244.9	11.85
Meta-BI_N2	-990.008143	-248.4	9.54
Meta-BI_N12	-990.3055	-435.8	1.51
Non-Protonated Para-BI	-989.613524	0	0
Para-BI_N1	-990.007866	-248.4	10.58
Para-BI_N12	-990.310353	-439	0

The total energy of the non-protonated repeat units decreased with each additional protonation, signifying that complete protonation of the model compounds was energetically favorable. We propose that the lower energy values of the fully protonated

pyridine-BI model compounds as compared with the phenyl-BI model compounds imbue these compounds with a greater affinity for acidic mediums. Interestingly, the dipole strengths of the fully protonated PBI model compounds was proportional to the solubilities of their parent polymers – the most soluble PBI (3,5-py-PBI) had the highest calculated model compound dipole strength, and the least soluble (para-PBI) had a neutral model compound dipole due to symmetry (Table 4.2). In the following sections, we will discuss the relationship between these calculated dipole strengths and PBI solubility and membrane gel stability in phosphoric acid environments.

Table 4.2. The change in potential energy from the non-protonated to the fully-protonated model (Δ Energy) and the dipole strengths of the fully protonated model compounds.

PBI Type	Δ Energy (kcal/mol)	Dipole of Fully-Protonated Model (Debye)
3,5-py-PBI	-523.1	7.39
2,5-py-PBI	-517.4	2.68
meta-PBI	-435.8	1.51
Para-PBI	-439	0

4.3.2. PBI Chemistry Effects on the Synthesis and Gelation of PBI Membranes

Four random copolymer series (2,5-py-r-para-PBI, 2,5-py-r-meta-PBI, 3,5-py-r-para-PBI, and 3,5-py-r-meta-PBI) were synthesized and cast into membranes using the PPA Process. Previous work on the synthesis and processing of the four copolymer series showed that the solubility of the copolymers in PPA was influenced by their chemical compositions. It was reported that increasing the ratio of the pyridine-containing repeat unit to the phenyl-containing repeat unit increased the solubility of the random copolymers. This trend was observed by the fact that copolymer solutions with greater

ratios of pyridine-PBI could be processed into membranes with higher polymer content. Higher polymer solubilities extended the amount of time it took to reach a high viscosity that was optimal for casting. This phenomenon was previously depicted in phase stability / processing diagrams. However, the isolated effects of backbone rigidity or dipole interactions on the PPA Process were not specifically addressed.

To investigate the influence of polymer chain configuration on the synthesis and processing of high polymer content PBI membranes, two series of 2,5-py-r-para-PBIs and 2,5-py-r-meta-PBIs were synthesized as described in Section 4.2.2 for detailed comparisons. Likewise, two series of 3,5-py-r-para-PBIs and 3,5-py-r-meta-PBIs were also synthesized. By comparing systems that incorporate the same pyridine moiety, the effects of polymer chain configuration on the processability of the polymerization solution could be monitored. Figure 4.3 shows the trends between diacid monomer ratios and the amount of time it took for the polymerization solution to attain a high viscosity suitable for casting for 12 wt% monomer charge polymerization solutions. As previously discussed, the polymerization time increased with an increasing ratio of 2,5-py:para or 2,5-py:meta. Additionally, the polymerization of the 2,5-py-r-meta-PBIs generally take more time to reach a high viscosity solution than the 2,5-py-r-para-PBI counterparts. This trend is more clearly seen in Figure 4.4 for the similar plot of the 3,5-py-r-para-PBIs and 3,5-py-r-meta-PBIs. It is important to note that the polymerizations of 3,5-py-r-meta-PBIs were cast at 30h because the solution viscosity did not appreciably change after 24 hours. One can therefore conclude that para-substituted polymer chains decrease polymer solubility, thereby increasing polymerization solution viscosity for a given polymerization time. This result also indicates that a wider range of copolymer

compositions could be successfully processed into membranes by incorporating more meta-substituted moieties into the polymer. By comparing the polymerization times of the 2,5-py-r-para-PBIs with 3,5-py-r-para-PBIs or 3,5-py-r-para-PBIs with 3,5-py-r-meta-PBIs in Figures 3 and 4, it is evident that the more basic 3,5-pyridine moiety enhances the solubility and processability of the polymer solution to a greater extent than the less basic 2,5-pyridine moiety. Therefore, greater proportions of meta-substituted PBI moieties or stronger dipoles enhance the solubility of copolymers and consequently improve the processability of the copolymer solutions.

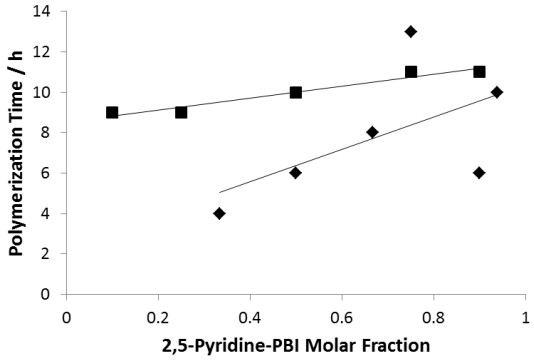

Figure 4.3. Comparison of polymerization times with the ratios of 2,5-py:meta (squares) and 2,5-py:para (diamonds). All of the polymerization solutions had an initial monomer concentration of 12 wt%.

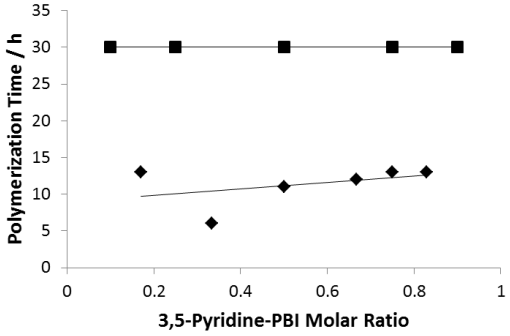

Figure 4.4. Comparison of polymerization times with the ratios of 3,5-py:meta (squares) and 3,5-py:para (diamonds). All of the polymerization solutions had an initial monomer concentration of 12 wt%.

An important part of the PPA Process is the sol-to-gel transition of a PBI/PPA solution to a PBI/PA gel membrane. It was reported that the gelation process was critically dependent on polymer molecular weight, i.e., generally, high molecular weight PBI solutions hydrolyzed into strong gel membranes while low molecular weight PBIs either formed membranes with poor mechanical properties or remained as solutions. Therefore, we briefly explored the effects of polymer solubility on the gelation of PBI membranes. All of the random copolymers of moderate-to-high molecular weights (above 1.0 dL/g) formed good gel membranes with the exception of membranes with a large proportion of 3,5-py-PBI. In these copolymers, the PBI/PPA solutions hydrolyzed to PBI/PA and remained as solutions. We concluded that the higher solubility imparted by the 3,5-pyridine moiety prevented gel film formation for 3,5-py-r-para-PBI compositions with high 3,5-pyridine-PBI concentrations (Table 2.1). Meanwhile, 3,5-py-r-meta-PBIs and 3,5-py-r-para-PBIs that had low proportions of the 3,5-pyridine moiety formed stable films. It is important for the reader to remember that 3,5-pyridine-PBI repeat units are meta-substituted, they each have three protonation sites, and their protonated equilibrium conformations are highly polar (based on the model compounds in Section 4.3.1). Thus, the highly soluble nature of these polymer chains resulted in poor gelation.

An interesting phenomenon was observed during the gelation process of certain PBI/PPA solutions, in which random copolymers appeared to phase separate under low (10-20% RH) humidity levels. To explore the effects of humidity levels on the gelation process, a copolymer solution was cast onto glass plates that were either placed in a humidity chamber at 55% RH or left on a bench-top at 15% RH for a period of 24 h.

Figure 4.5 indicates the visual differences between the two sets of membranes – the solutions that were hydrolyzed under greater humidity levels appeared darker and more translucent, and the solutions that were hydrolyzed under lower levels appeared lighter and more opaque. The tensile properties of the phase separated film could not be measured because our Instron was not sensitive enough to measure any properties before breaking the film into pieces. The non-phase separated film had a Young's Modulus of 10.9 MPa and a strain at break of 3.1%. Given that the two gel films were composed of polymers from the same polymerization solution, we suggest that the differences in appearance and tensile properties arise from a difference in composition and morphology. The non-phase separated membrane was composed of 13.6 wt% polymer, 50.1 wt% PA, and 36.3 wt% water, while the phase separated membrane was composed of 10.5 wt% polymer, 70.5 wt% PA, and 18.7 wt% water. It is evident that the lower relative humidity hindered water absorption for the phase separated membrane. This difference in quenching thereby influenced the solution-to-gel transition, leading to a change in membrane morphology. Molecular dynamics simulations published by Kumar et al. argues that faster quenching rates (i.e. dropping of temperature or the conversion of PPA to PA) arrest phase separation, even though the system is below the bimodal phase transition line.[29,30] In contrast, slower quenching rates give polymer chains enough time at a more-mobile phase to agglomerate, thereby causing phase separation. Our observations of these two polymer membranes are in agreement with this phase separation simulation. However, it is beyond the scope of this paper to investigate whether polymer solubility influences this phase separation at low humidity levels. At elevated humidity levels, all of the PBI/PPA solutions were hydrolyzed into non-phase

separated films, and these were the membranes that were analyzed in the following sections.

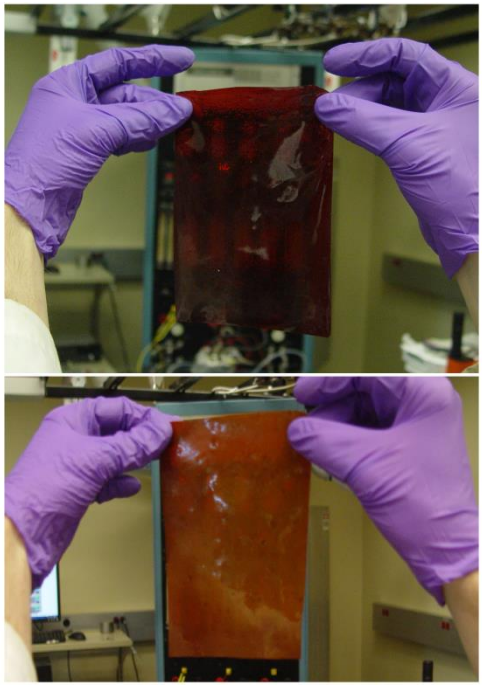

Figure 4.5. Identical high polymer content solutions cast on glass plates and hydrolyzed in the humidity chamber at 55% RH (top) or on the bench-top at 15% RH (bottom).

The compositions of the gel membranes were determined via the titration process described in Section 4.2.2. Generally, the membrane polymer contents decreased as the proportion of either the 2,5-pyridine or 3,5-pyridine moiety increased for a given initial monomer charge (Figure 4.6). Also, this trend correlated with the increased membrane water content and phosphoric acid-to-polymer repeat unit (PA/PRU) molar ratio (Figures 4.7 and 4.8, respectively). The ability of the high pyridine-content PBI membranes to hold greater proportions of water and PA suggests that the pyridine moieties have a greater affinity for both water and PA than their phenyl-substituted polymer counterparts. Interestingly, the 3,5-py-r-meta-PBIs have a relatively low water uptake as compared to the other copolymer series of similar pyridine proportions (Figure 4.9). This low water content may be correlated with the higher solubility of the 3,5-py-r-meta-PBIs in PPA

and PA at room temperature. The effects of pyridine content on membrane mechanical properties will be further explored in Section 4.3.4.

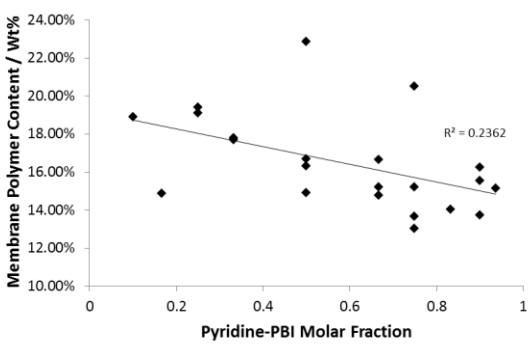

Figure 4.6. The pyridine-PBI molar fraction in 2,5-py-r-para-PBI, 2,5-py-r-meta-PBI, and 3,5-py-r-para-PBI copolymers plotted against the resulting as-cast membrane's polymer content. All polymerization solutions had an initial monomer charge of 12 wt%.

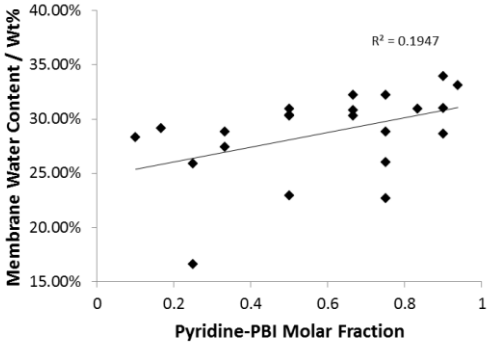

Figure 4.7. The pyridine-PBI molar fraction in 2,5-py-r-para-PBI, 2,5-py-r-meta-PBI, and 3,5-py-r-para-PBI copolymer membranes plotted against the resulting as-cast membrane's water content. All polymerization solutions had an initial monomer charge of 12 wt%.

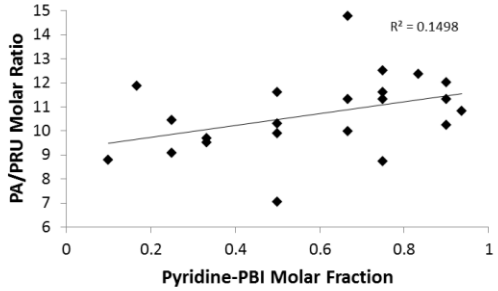

Figure 4.8. The pyridine-PBI molar fraction in 2,5-py-r-para-PBI, 2,5-py-r-meta-PBI, and 3,5-py-r-para-PBI copolymer membranes plotted against the resulting as-cast membrane's phosphoric acid-to-polymer repeat unit molar ratio. All polymerization solutions had an initial monomer charge of 12 wt%.

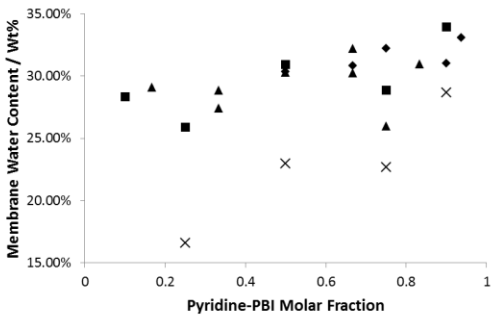

Figure 4.9. The pyridine-PBI molar fraction in random copolymers plotted against the resulting as-cast membrane's water content. X = 3,5-py-r-m-PBIs, Squares = 2,5-py-r-meta-PBIs, Triangles = 3,5-py-r-para-PBIs, Diamonds = 2,5-py-r-para-PBIs. All polymerization solutions had an initial monomer charge of 12 wt%.

4.3.3. Effects of Polymer Chain Configuration on Membrane Properties

Two sets of random copolymers, 2,5-py-r-para-PBI and 2,5-py-r-meta-PBI, were cast into membranes and characterized to investigate the effects of polymer chain configuration on room temperature tensile strength, anhydrous proton conductivity, high temperature creep compliance, and fuel cell performance. Polymers of equivalent 2,5-pyridine PBI content were compared to isolate several structure-property relationships form the influence of pyridine dipole strength or pyridine quantity on membrane properties.

The tensile properties of the 2,5-pyridine random copolymers were investigated as described in Section 4.2.2. As previously discussed, the Young's Modulus of PBI membranes is heavily dependent on the polymer content of the membrane. As the polymer content of the PBI copolymer membranes increased, the Young's modulus also increased. Generally, the 2,5-py-r-para-PBI membranes exhibited higher Young's moduli

than the 2,5-py-r-meta-PBI membranes at equivalent membrane polymer content (Figure 4.10). However, an in-depth comparison that considers polymer chemistry (copolymer ratio) is required to assess the effects of polymer chain configuration on the room temperature tensile properties. Figure 4.11 compares the Young's Moduli of three 2,5-py-r-meta-PBI membranes with three 2,5-py-r-para-PBI membranes that contain equivalent 2,5-pyridine proportions, thus strictly isolating the meta/para influence on membrane properties. Each of the 2,5-py-r-para-PBI membranes showed higher Young's moduli than the 2,5-py-r-meta-PBI membranes regardless of membrane polymer content. This direct comparison of tensile data indicates that PBI polymers with more extended chain conformations result in membranes with high moduli. A direct comparison between the 3,5-py-r-para-PBI and 3,5-py-r-meta-PBI membranes could not be performed because of the large difference in polymer content in these membranes. However, it is noted that the Young's moduli of both of these membrane series scale proportionally with increasing polymer content (Tables 2.1 and 2.2).

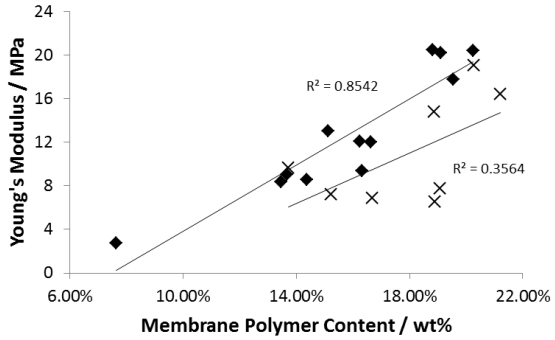

Figure 4.10. Young's moduli of as-cast 2,5-py-r-para-PBI membranes (diamonds) and 2,5-py-r-meta-PBI membranes (X's) at different membrane polymer contents.

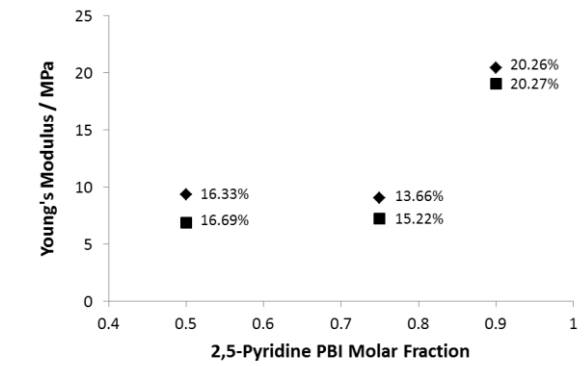

Figure 4.11. A comparison of the Young's Moduli of three 2,5-py-r-meta-PBI membranes (squares) with three 2,5-py-r-para-PBI membranes (diamonds) that contain equivalent 2,5-pyridine proportions. The membrane's polymer content for each sample is listed as a weight percent.

High temperature creep compliance tests were performed as described in Section 4.2.2 to further examine the effects of polymer chain configuration on membrane properties. Measurement of creep compliance at 180°C under an applied static load approximates fuel cell operating conditions and is a facile method of comparing the gel membrane's resistance to creep. All compliance curves are an average of at least two experimental data sets under identical preconditioning and testing conditions. For all of these 24 hour compliance tests, the compliance of each membrane increased over time due to polymer creep under a static compressive load. Following an initial nonlinear compliance over the first four hours, there was a period of seemingly linear compliance over time. After a more-thorough review, it was determined that this linear region gradually decreased over time due to the compression of the gel structure and the resulting composition change.

By comparing copolymers of equal proportions of the 2,5-pyridine moiety, we isolated the effects of the para-oriented vs. meta-oriented repeat units on membrane creep resistance. Figure 4.12 compares a 2,5-py-r-para-PBI and 2,5-py-r-meta-PBI that have

equivalent proportions (3:1) of the 2,5-pyridine moiety. The copolymer with para-PBI (MM1-40-2) was more resistant to polymer creep than the copolymer with meta-PBI (MM1-72-2) based on the values of creep compliance at 20h and creep rate. Considering that the 2,5-py-r-meta-PBI membrane had a much higher polymer content than the 2,5-py-r-para-PBI membrane, the creep results indicate that polymer chemistry (in particular, polymer chain configuration) significantly influenced creep resistance. We propose that PBIs with para-substituted moieties enhance the gel stability of the resulting membranes at elevated temperatures, thereby lowering creep resistances. A comprehensive table of the creep compliance test data can be found in Table 4.3.

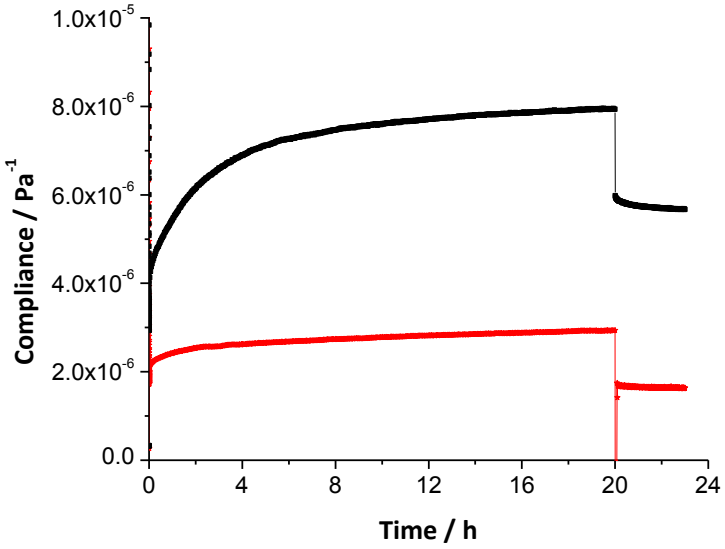

Figure 4.12. Creep compliance tests of a 3:1 2,5-py-r-para-PBI (MM1-40-2, red, lower line) and a 3:1 2,5-py-r-meta-PBI (MM1-72-2, black, upper line) at 180°C under a static load of 0.1 MPa.

The pyridine random copolymer membrane series were also compared to isolate the effects of polymer chain configuration on anhydrous proton conductivity and fuel cell performance. For all of the copolymer membranes, all of the anhydrous proton conductivities increased with increasing PA/PBI repeat unit molar ratio. For the 2,5-

pyridine copolymers, there were no observable trends between chain configuration and either bulk membrane resistance or fuel cell voltage (Tables 3.1 and 3.2). The lack of observable trends could be a result of the influences of many other variables, including polymer inherent viscosity, membrane PA content, or membrane thickness. For these electrochemical studies, a comparison of 3,5-py-r-para-PBI with 3,5-py-r-meta-PBI could not be conducted due to the poor gel thermal stability of 3,5-py-r-meta-PBI membranes. Therefore, we suggest that this poor gel thermal stability is evidence that more flexible PBI moieties result in less physically and thermally stable gel membranes. This observation is consistent with the previous high temperature creep compliance data.

4.3.4 Effects of Dipole Strength and Pyridine Quantity on Membrane Properties

Two sets of random copolymers, 3,5-py-r-para-PBI and 2,5-py-r-meta-PBI, were synthesized to investigate the effects of dipole strength on membrane properties. By comparing copolymers with identical ratios of 3,5-py-PBI:para-PBI to meta-PBI:2,5-py-PBI, one could diminish the effects of polymer chain configuration and roughly isolate the influences of polymer dipole strength on membrane properties. In addition, we can investigate the effects of pyridine quantity by comparing the membrane properties of these random copolymer systems as we adjust the ratio of pyridine-substituted moiety to phenyl-substituted moiety. It is important to note that changing the pyridine quantity changes both polymer dipole strength and polymer chain configuration. Herein, we investigate the effects of dipole strength and pyridine quantity on membrane properties including anhydrous proton conductivity, gel thermal stability, and fuel cell performance.

The Young's Moduli of 2,5-py-r-para-PBIs and 3,5-py-r-para-PBIs were compared to isolate the effect of pyridine dipole strength and configuration on room temperature tensile properties. It was shown that differences between the membranes made from these polymers exhibit different Young's moduli at room temperature, particularly at higher membrane contents (Figure 4.13). Generally, the 2,5-pyridine-containing PBI membranes exhibited higher Young's moduli. In contrast, the effects of the meta/para content or chain configuration are not obvious in this comparison. Figure 4.14 compares 2,5-py-r-para-PBI and 3,5-py-r-para-PBI membranes with equivalent para-PBI molar ratios, and indicates the membrane's total polymer content for each sample. At equivalent (or nearly equivalent) polymer solids content, 2,5-pyr-r-para PBI membranes exhibited higher Young's moduli than the 3,5-pyr-r-para membranes at all pyridine/para ratios.

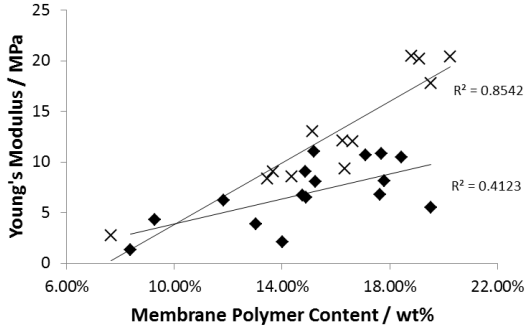

Figure 4.13. The as-cast 2,5-py-r-para-PBIs (Xs) and 3,5-py-r-para-PBIs (diamonds) with their membrane polymer content plotted against their respective Young's Moduli.

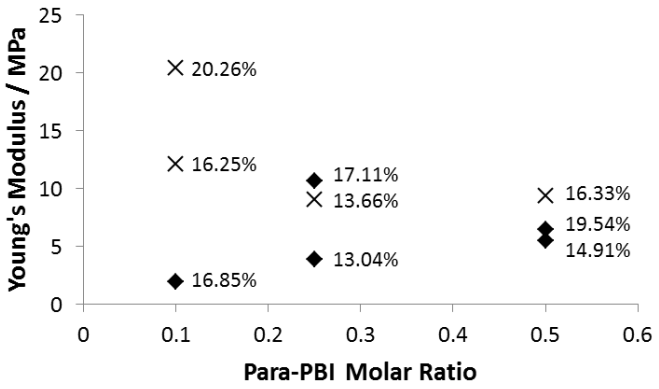

Figure 4.14. Young's moduli of as-cast 2,5-py-r-para-PBIs (Xs) and 3,5-py-r-para-PBIs (diamonds) at different para-PBI molar ratios. The membrane's polymer content (wt%) is also indicated.

Creep compliance tests at 180°C were performed on copolymers to investigate the effects of pyridine quantity and dipole strength on high temperature mechanical properties. These tests were not performed on 3,5-py-r-meta-PBI membranes due to their unstable gel structure at elevated temperatures. Within a copolymer series, a comparison of copolymers with different amounts of pyridine-PBI could distinguish the effects of pyridine quantity on creep compliance. Based on the polymer compliance values at 20h (Table 4.3), there was a strong correlation between high creep resistance and low pyridine content for 3,5-py-r-para-PBI, 2,5-py-r-para-PBI, and 2,5-py-r-meta-PBI membranes. For example, MM1-72-2 has a lower 3,5-py-PBI proportion and lower creep compliance than that of MM1-37-3. Interestingly, the creep rates of the polymers did not seem to decrease with increasing pyridine concentrations. We suggest that the creep rate may be influenced more strongly by other factors (e.g. polymer IV). Overall, membranes with low proportions of pyridine-PBIs were generally more resistant to creep than membranes with high proportions of pyridine-PBIs at elevated temperatures.

To isolate the effects of pyridine dipole strength on polymer creep, the compliance test results of 2,5-py-r-para-PBIs were compared with those of 3,5-py-r-para-PBIs of identical pyridine proportions. In particular, MM1-40-2 was compared with MM1-37-3, and MM1-40-4 was compared with MM1-37-5. For both pairs of copolymers, membrane creep resistance was strongly influenced by the strength of the dipole. The lower dJ/dt and J at 20h of the 2,5-pyridine-r-para-PBI membranes are indicative of a more thermally stable gel structure. Both of the 3,5-pyridine-r-para-PBI membranes have higher polymer content than their 2,5-pyridine counterparts, which suggests that the correlation between low pyridine dipole strength and high creep resistance is not affected by membrane polymer content. Thus, it can be inferred that membranes composed of lower dipole strength PBI moieties possess greater creep resistance than those composed of higher dipole strength PBI moieties.

Table 4.3. Creep compliance test results of all high polymer content pyridine-based copolymer membranes.

Membrane Type	Membrane Name	Inherent Viscosity (dL g^{-1})	As-Cast Membrane Polymer Content (wt%)	J at 20h (10^{-6} Pa^{-1})	$dJ/dt_{8\text{-}20h}$ (10^{-6} Pa^{-1} hr^{-1})
2,5-py/para(3:1)	MM1-40-2	1.30	13.66	2.94 ± 0.77	0.0167 ± 0.0002
2,5-py/para(2:1)	MM1-40-3	1.70	15.93	2.11 ± 0.16	0.0186 ± 0.0002
2,5-py/para(1:1)	MM1-40-4	1.08	16.33	2.47 ± 0.31	0.0182 ± 0.0004
3,5-py/para(3:1)	MM1-37-3	1.18	17.11	3.48 ± 0.35	0.0304 ± 0.0003
3,5-py/para(1:1)	MM1-37-5	0.66	19.54	3.14 ± 0.24	0.0303 ± 0.0003
3,5-py/para(1:5)	MM1-39-2	1.37	14.87	2.65 ± 0.28	0.0347 ± 0.0002
2,5-py/meta(3:1)	MM1-72-2	1.24	15.22	7.94 ± 2.60	0.0384 ± 0.0005
2,5-py/meta(1:9)	MM1-72-5	0.94	18.9	2.88 ± 0.10	0.0292 ± 0.0004

J = Compliance
$dJ/dt_{8\text{-}20h}$ = Creep rate (change in compliance over the last 12 hours of the test)

The 2,5-py-r-para-PBI and 3,5-py-r-para-PBI membrane series were compared to isolate the effects of dipole strength on anhydrous proton conductivity and fuel cell

performance. In addition, the 2,5-py-r-meta-PBI and 3,5-py-r-meta-PBI membrane series were similarly compared. As described previously, there was a clear trend between PA content and proton conductivity. However, the trend between membrane composition and conductivity is much more subtle. Generally, the copolymers composed of the 2,5-pyridine PBI moieties displayed higher conductivities than their 3,5-pyridine counterparts for a given PA/PRU (Figures 4.15 and 4.16). Focusing on the chemistries of the copolymers, it was evident that the membranes with the 3,5-pyridine-PBI moiety were more likely to fail (melt out) during testing at 180°C, especially those with high proportions of this moiety in the random copolymer. In contrast, 2,5-pyridine copolymers of similar pyridine contents did not have a thermally unstable gel. These results were again observed during MEA construction and fuel cell operation, especially in the comparison between the 2,5-py-r-meta-PBIs and the 3,5-py-r-meta-PBIs. The poor fuel cell performances of the 3,5-py-r-meta-PBIs (Table 2.2) again indicates a much lower thermal gel stability, resulting from the high solubility of these copolymers in PA. Overall, membranes composed of more soluble PBIs tend to demonstrate lower electrochemical performance.

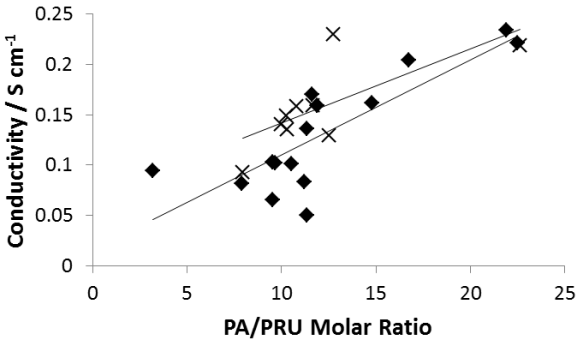

Figure 4.15. The as-cast 2,5-py-r-para-PBIs (Xs) and 3,5-py-r-para-PBIs (diamonds) with their PA/PRU molar ratio plotted against their respective conductivities.

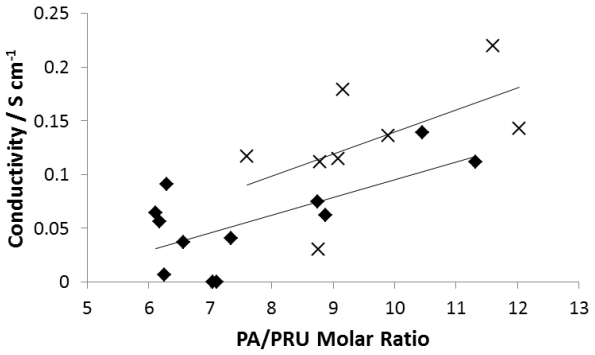

Figure 4.16. The as-cast 2,5-py-r-meta-PBIs (Xs) and 3,5-py-r-meta-PBIs (diamonds) with their PA/PRU molar ratio plotted against their respective conductivities.

4.4. CONCLUSIONS

Ground state geometries for non-protonated and protonated model compounds suggest that it is energetically favorable for the basic sites of PBIs to fully protonate. Protonation bond energy data indicates that steric hindrance partially impedes the ability of each lone electron pair of nitrogen in an sp2 orbital to bond. When comparing the non-protonated models to their multiply-protonated configuration, each additional protonation is less energetically favorable due to steric hindrance and the subsequent torsion of the aromatic moieties relative to each other.

Determined by a comparison of polymerization times, greater proportions of meta-substituted PBI moieties or stronger dipoles enhance the solubility of polymer chains. Consequently, this polymer solubility strongly correlates with a polymer solution's abilities to form stable gels at room temperature. High temperature creep compliance tests indicated that thermal gel stability decreased with increasing proportions of pyridines, more meta-substituted PBI moieties, or PBIs with stronger dipoles. Higher dipole strengths of the fully protonated model compounds correlate with increased solubility and decreased gel thermal stability in phosphoric acid environments.

Electrochemically, membranes composed of more soluble PBIs tend to demonstrate lower anhydrous proton conductivity and fuel cell voltages.

4.5. REFERENCES

[1] Steele B. C. H., and Heinzel A., 2001, "Materials for Fuel-Cell Technologies," Nature, **414**, pp. 345-352.

[2] Dunwoody D., and Leddy J., 2005, The Electrochemical Society Interface, **3**, pp. 37–39.

[3] Appleby A. J., and Foulkes F. R., "Materials Engineering for Solid Oxide Fuel Cell Technology," Fuel Cell Handbook 1989, Van Nostrand Reinhold, New York.

[4] Li Q., He E., Jensen J. O., and Bjerrum N. J., 2003, Chem. Mater., **15**, pp. 4896–4915.

[5] Wainright J. S., Litt M. H., and Savinell R. F., 2003, Handbook of Fuel Cells, Fundamentals, Technology, and Applications, John Wiley & Sons, **3**, p. 436.

[6] Li Q., He R., Gao J., Jensen O. J., and Bjerrum N. J., 2003, "The CO Poisoning Effect in PEMFCs Operational at Temperatures up to 200C," J. Electrochem. Soc., **150**(12), pp. A1599–A1605.

[7] Li Q., He R., Jensen J. O., and Bjerrum N. J., 2004, "PBI-based polymer membranes for high temperature fuel cells - preparation, characterization and fuel cell demonstration," Fuel Cells, **4**(3), pp. 147–159.

[8] Pan C., He R., Li Q., Jensen J. O., Bjerrum N. J., and Hjulmand H. A., 2005, "Integration of High Temperature PEM Fuel Cells with a Methanol Reformer," J. Power Sources, **145**(2), pp. 392–398.

[9] Molleo M., Schmidt T. J., and Benicewicz B. C., 2012, "Polybenzimidazole-Phosphoric Acid (PBI-PA)-Based Fuel Cells," Encyclopedia of Sustainability, Science and Technology, pp. 391–431.

[10] Mader J., Lixiang X., Schmidt T., and Benicewicz B. C., 2008, "Polybenzimidazole/Acid Complexes as High-Temperature Membranes," Adv. Polym. Sci., **216**(Fuel Cells II), pp. 63–124.

[11] Kongstein O. E., Berning T., Borresen B., Seland F., and Tunold R., 2006, "Polymer electrolyte fuel cells based on phosphoric acid doped polybenzimidazole (PBI) membranes," Energy, **32**(4), pp. 418–422.

[12] Wainright J. S., Savinell R. F., and Litt M. H., 2003, "High Temperature Membranes," Handbook of Fuel Cells, **3**, pp. 436–446.

[13] Savinell R. F., Wainright J. S., and Litt M. H., 1998, "High Temperature Polymer Electrolyte Fuel Cells," Proc. Electrochem. Soc, **98-27**, pp. 81–90.

[14] Wainright J. S., Wang J. T., Weng D., Savinell R. F., and Litt M., 1995, "Acid-doped polybenzimidazoles: a new polymer electrolyte," J. Electrochem. Soc., **142**(7), pp. L121–L123.

[15] Wang J. T., Savinell R. F., Wainright J., Litt M., and Yu H., 1996, "A H_2/O_2 Fuel Cell Using Acid Doped Polybenzimidazole as Polymer Electrolyte," Electrochem. Acta., **41**(2), pp. 193–197.

[16] Xiao L., Zhang H., Scanlon E., Ramanthan L. S., Choe E. W., Rogers D., Apple T., and Benicewicz B. C., 2005, "High-Temperature Polybenzimidazole Fuel Cell Membranes via a Sol-Gel Process," Chem. Mater., **17**(21), pp. 5328–5333.
[17] Yu S., Xiao L., and Benicewicz B. C., 2008, "Durability Studies of PBI-based High Temperature PEMFC," Fuel Cells, **8**(3-4), pp. 165–174.
[18] U.S. Dept. of Energy, 2011, An Integrated Strategic Plan for the Research, Development, and Demonstration of Hydrogen and Fuel Cell Technologies. Available at http://www1.eere.energy.gov/hydrogenandfuelcells/pdfs/program_plan2011.pdf
[19] Schmidt T. J., 2009, "High-Temperature Polymer Electrolyte Fuel Cells: Durability Insights," Polymer Electrolyte Fuel Cell Durability, F.N. Buchi, M. Inaba, and T.J. Schmidt, eds., Springer, New York, pp. 199–221.
[20] Schmidt T. J., 2006, "Durability and degradation in high-temparature polymer electrolyte fuel cells," ECS Transactions, **1**(8), pp. 19–31.
[21] Molleo M., Chen X., Ploehn H., and Benicewicz B. C., 2013, "High Polymer Content 3,5-Pyridine-Polybenzimidazole Copolymer Membranes with Improved Compressive Properties," In Process.
[22] Molleo M., Chen X., Ploehn H. J., and Benicewicz B. C., 2013, "High Polymer Content 2,5-Pyridine-Polybenzimidazole Copolymer Membranes with Improved Compressive Properties," In Process.
[23] Yu S., Zhang H., Xiao L., Choe E. W., and Benicewicz B. C., 2009, "Synthesis of Poly (2,2'-(1,4-phenylene) 5,5'-bibenzimidazole) (para-PBI) and Phosphoric Acid Doped Membrane for Fuel Cells," Fuel Cells, **9**(4), pp. 318–324.
[24] Xiao L., Zhang H., Jana T., Scanlon E., Chen R., Choe E. W., Ramanthan L. S., Yu S., and Benicewicz B. C., 2005, "Synthesis and Characterization of Pyridine-Based Polybenzimidazoles for High Temperature Polymer Electrolyte Membrane Fuel Cell Applications," Fuel Cells, **5**(2), pp. 287–295.
[25] Wavefunction, Inc., "Spartan'10." Irvine, CA.
[26] Ferry J. D., 1980, Viscoelastic Properties of Polymers, 3rd Ed., John Wiley & Sons, New York.
[27] 1999, "Standard Methods for the Examination of Water and Wastewater: 4500-P Phosphorus," pp. 1–24. Available at http://www.umass.edu/tei/mwwp/acrobat/sm4500P-E.PDF.
[28] Linnell R., 1960, "Dissociation Constants of 2-Substituted Pyridines," J. Org. Chem, **25**(2), pp. 290-290.
[29] Padmanabhan V., and Kumar S. K., 2011, "Gelation in Semiflexible Polymers," J. Chem. Phys., **134**(17), p. 174902/1 –174902/7.
[30] Padmanabhan V., Kumar S. K., and Yethiraj A., 2008, "Phase Behavior of Semiflexible Polymer Chains," J. Chem. Phys, **128**(12), pp. 124908/1-124908/4.

5. Alternative Approaches to Achieving Polybenzimidazole Membranes with Enhanced Mechanical Properties

5.1. Motivation for Alternative Approaches

For over a decade, polybenzimidazole (PBI) membranes have demonstrated exceptional potential as membranes in energy conversion devices due to their ability to produce high power density, high energy conversion efficiency, and low environmental impact.[1–3] PBI-based proton exchange membranes (PEMs) have been shown to operate for well over 15,000 hours under steady-state conditions and are durable under start/stop cycling operation, thermal cycling, and load cycling.[4] As discussed in prior chapters, it is known that low-polymer content membranes are susceptible to long-term degradation modes including polymer creep and membrane thinning, which can result in gas crossover, voltage degradation, and the eventual quenching of the fuel cell. Recently, the Department of Energy has issued a 40,000-80,000 hour target for stationary fuel cell applications. Furthering our understanding of structure-to-property relationships of PBI membranes will provide us with the information necessary to design PBI PEMs with enhanced longevity for extended use applications.

Multiple attempts have been made to enhance the mechanical and electrochemical properties of PBI-based PEMs. These approaches can be classified into four main categories: the addition of particles (i.e. small organic molecules, inorganic fillers) to the polymer matrix;[5,6] chemically crosslinking the polymer matrix;[7–9] alternative

processing techniques (i.e. conventional imbibing, PPA Process, thermally annealing);[3,10,11] and novel polymer chemistries.[12–14] As discussed in Chapters 2-4 of this dissertation, the exploration of novel chemistries used in conjunction with a modified PPA Process have resulted in PBI membranes with increased resistance to polymer creep at 180°C. These enhanced mechanical properties have resulted in lower voltage degradation rates under steady state conditions and, in some cases, lower phosphoric acid losses by an order of magnitude. Herein, we discuss alternative approaches to enhancing the longevity of PBI-based PEMs, which include a delayed polymer solvation/swelling approach, the addition of small organic molecules to the polymer/acid complex, and novel polyetherbenzimidazole (PEBI) and polyphosphonobenzimidazole (phos-PBI) syntheses.

5.1.1. Delayed Solvation / Swelling of PBI Particles

The delayed polymer solvation / swelling approach is concerned with the addition of dried PBI particles into a PBI/PPA solution and casting the membrane before the PBI particles have fully dissolved or swelled. As previously discussed, increasing the polymer content of a PBI/PPA solution generally increases its viscosity, thereby making the processing of the solution into a thin film much more difficult. Preliminary tests showed that undissolved PBI particles would not substantially increase the viscosity of a stock-solution of para-PBI/PPA, thereby circumventing the increased viscosity issue. The goals of this project were to investigate how PBI particle chemistry, PBI molecular weight (IV), particle size, particle concentration, particle annealing, solution temperature, and

mixing of the particles affected the mechanical and electrochemical properties of the resulting membranes.

Two types of PBI's were investigated in this powder addition study: 2,5-pyridine-PBI and dihydroxy-PBI (2OH-PBI). The pyridine PBIs are well-known for their higher solubilities, and it was thought that incorporation of a more soluble PBI powder could enhance the particle's capabilities for post-processing solvation or swelling. Prior research indicated that 2,5-pyridine-PBI could form physically and chemically stable membranes at fuel cell operational temperatures, making this polymer an ideal candidate for this powder addition study. 2OH-PBI was shown to form chemical crosslinks by means of phosphate ester bridges, thereby lowering its solubility in PPA and increasing the solution viscosity.[7] Therefore, high polymer content membranes of 2OH-PBI are incapable of being formed. It was theorized that inclusion of a 2OH-PBI powder could circumvent the solubility / viscosity issues, and that these crosslinks could enhance the mechanical properties of the resulting films. Random copolymers of 2,5-py-PBI and 2OH-PBI (2,5-py-r-2OH-PBIs) were also synthesized and isolated as powders for the delayed solvation / swelling approach. The concentration of chemical crosslinks was adjusted by varying the ratio of 2,5-py-PBI to 2OH-PBI.

By employing the same delayed PBI particle solvation / swelling approach, 2OH-PBI particles with cleaved phosphate ester bridges could be incorporated into stock solutions of para-PBI/PPA and directly cast into membranes. Crosslinked 2OH-PBI particles are highly insoluble, even in strong solvents such as concentrated sulfuric acid or methanesulfonic acid. However, dissolution of 2OH-PBI can be achieved by cleaving these chemical crosslinks under concentrated basic conditions. The goal of this project

was to incorporate these non-crosslinked 2OH-PBI particles into a para-PBI/PPA stock solution, again using the delayed solvation / swelling approach, to achieve a membrane with increased polymer content. Additionally, this process is likely to restore the chemical crosslinks of 2OH-PBI upon heating, thereby providing additional reinforcement to the membrane. Scheme 5.1 illustrates this reversible crosslinking approach. The relationships between particle chemistry, concentration, mixing time, and mixing temperature and the mechanical and electrochemical properties of the resulting membranes were investigated.

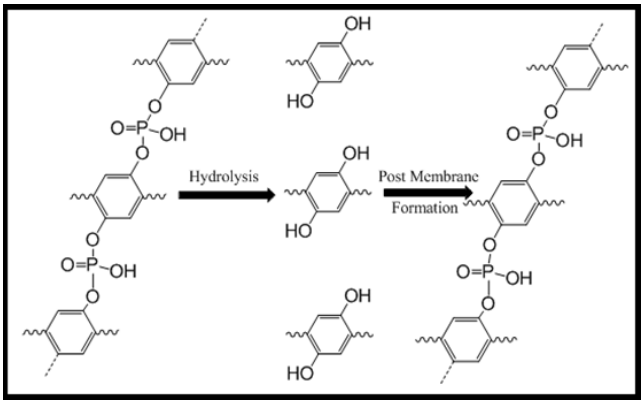

Scheme 5.1. The reversible chemical crosslinking approach of 2OH-PBI particles

5.1.2. Phloroglucinol Addition to PBI Solutions

The addition of small organic molecules or inorganic fillers into PBI gel membranes has had little success at improving the mechanical and electrochemical properties of the resulting films.[5,6] Incorporation of the fillers into the PBI membranes can be conducted in one of three stages of the PPA Process: they can be added to the monomer/PPA solution prior to polymerization; they can be added to the polymer/PPA solution after polymerization prior to casting; or they can be dissolved into a solvent bath and allowed to permeate through an already cast gel film. Generally, if added to the

monomer/PPA solution, fillers can potentially disrupt the polycondensation reaction and prevent high molecular weights from being achieved. It is important to note that PBI membranes are considered Type 3 Flory gels, i.e., gels composed of polymer networks formed by physical aggregation of polymer chains.[15] Addition to either monomer or polymer/PPA solution prior to casting can interfere with proper gelation of PBI membranes, thus weakening their mechanical and thermal stability. Incorporation of fillers into a PA-doped PBI membrane via a solvent bath is often difficult unless the filler can dissolve into PA. If the filler cannot dissolve into PA, then a multi-step process requiring the use of two or more baths is required, which can be both costly and time-consuming.

Herein, we propose the addition of phloroglucinol (1,3,5-trihydroxybenzene) into a PBI membrane cast using the PPA Process. Phloroglucinol was chosen as an additive due to its similarity to 2OH-PBI. Because the 2OH-PBI moiety has demonstrated the ability to form chemical crosslinks by means of phosphate ester bridges, it was theorized that the phloroglucinol could crosslink similarly. Additionally, it was believed that this molecule could enhance the anhydrous proton conductivity of the membrane akin to 2OH-PBI. Unlike previously explored additives, phloroglucinol has the potential to both enhance the mechanical properties and the proton transport capabilities of the resulting membrane. By varying the concentration of the phloroglucinol, one can easily control the amount of crosslinks in the membrane. Furthermore, this molecule is commercially available and requires no purification prior to addition. Thus, multiple addition techniques were employed to incorporate the phloroglucinol into the membrane, and the

membrane composition was correlated with the fundamental properties of membrane conductivity, mechanical properties, and fuel cell performance.

5.1.3. Novel Synthesis of Polyetherbenzimidazoles and Polyphosphonobenzimidazoles

As discussed in Chapter 4 of this dissertation, the solubility properties of PBIs affect the processing, gelation, mechanical and thermal properties, and electrochemical properties of PPA Processed PBI membranes. As an example, pyridine-PBIs (py-PBIs) are well-known to have higher solubilities in PPA and lower gel thermal stabilities as compared to phenyl-based PBIs (e.g. meta-PBI, para-PBI). The development and characterization of new polybenzimidazole derivatives remains of great interest because it could provide us with polymers with enhanced processing characteristics, while potentially maintaining high physical and chemical stability.

As a relatively unexplored class of polymers,[16–19] poly(ether benzimidazoles) (PEBIs) represent a unique combination of PBI chemistry with the chemistry of poly(aryl ethers). Poly(aryl ethers) such as polyether ether ketone (PEEK) and polyether ketone (PEK) are well known thermoplastic materials that have excellent mechanical properties and high chemical resistance. One common method of polymerizing poly(aryl ethers) is by dialkylation reactions of bisphenolate salts. PEEK is synthesized by the repetitive S_N2 reactions between 4,4'difluorobenzophenone with the disodium salt of hydroquinone (Scheme 5.2) in a polar aprotic solvent. Similar to PBIs, most poly(aryl ethers) are highly resistant to thermal degradation. Ether linkages in polymer backbones can also increase polymer backbone chain flexibility. By incorporating an ether linkage into a rigid PBI

backbone, an increase in polymer chain flexibility may imbue new interesting characteristics into the polymer (e.g. solubility, thermal gel stability, tensile properties).

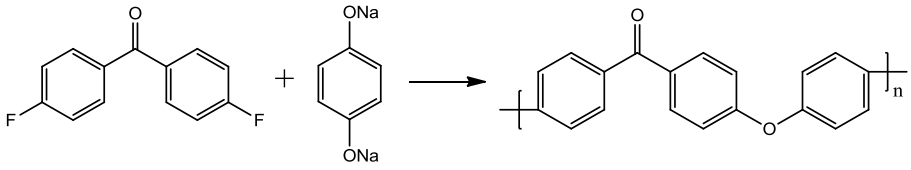

Scheme 5.2: Polymerization of PEEK.

This research project involved the design, synthesis, and characterization of a PEBI, poly(4-(6-methyl-1H-benzo[d]imidazol-2-yl)phenyl) ether (op-PBI). The new PEBI differs from p-PBI by a single ether linkage between the phenyl subunit of the benzimidazole and the other phenyl group. Although this polymer has been prepared, we explored a different method to prepare this polymer.[20] The proposed polymer synthesis will be conducted using an AB-type monomer rather than an AA-BB monomer system.

Whereas PEEK and PEK are commonly polymerized by the combination of two chemical units in solution, this project attempted the polymerization of op-PBI from a single monomer unit (e.g. 4-(6-chloro-1H-benzimidazol-2-yl)phenol). As shown in Scheme 5.3, the proposed polymerization scheme depicts the potassium salt of the op-PBI monomer reacting via an S_N2 mechanism and being stabilized through the formation of an intermediate Meisenheimer-type complex. This complex would be a reaction intermediate stabilized by the delocalization of its negative charge throughout the conjugated monomer system. Similar nucleophilic aromatic displacement polymerizations had previously been performed with aliphatic monomer units,[16] and it motivated us to investigate whether this novel polymerization could proceed using the proposed new monomer.

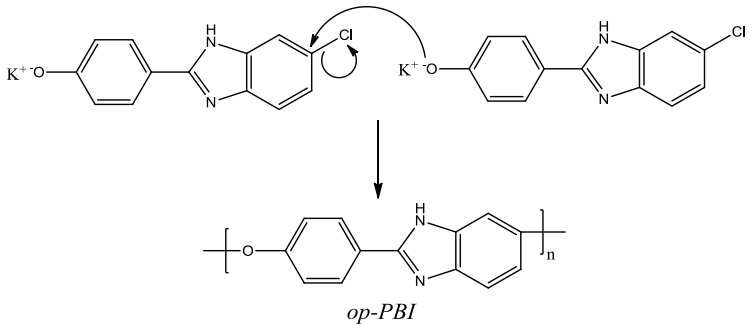

op-PBI

Scheme 5.3: Polymerization of op-PBI by the dipotassium salt of the monomer, 4-(6-chloro-1H-benzo[d]imidazol-2-yl)phenol.

Another class of polybenzimidazoles that is relatively unexplored are the polyphosphonobenzimidazoles (phos-PBI) which have phosphonic acid groups pendant from the polymer backbone and can potentially hydrogen bond or crosslink via phosphate ester bridges in a phosphoric acid environment. PBIs with pendant phosphonic acid groups have previously been synthesized by grafting polyvinylphosphonic acid chains onto the benzimidazole moieties of PBIs, but these have shown little success in low-temperature water-doped PEMs.[21–22] We propose the polymerization of two novel phos-PBIs: a meta- and a para-PBI with phosphonic acid groups substituted on each of the diacid phenyl groups of the repeat unit. The PPA Process could be used to polymerize each polymer via a polycondensation reaction between tetraaminobiphenyl (TAB) and either 1-phosphono-2,5-terephthalic acid or 1-phosphono-3,5-isophthalic acid. These acid monomers are not commercially available and thus need to be synthesized.

We herein propose the synthesis and characterization of two classes of polybenzimidazoles, polyetherbenzimidazoles (PEBIs) and polyphosphonobenzimidazoles (phos-PBI). Following chemical and thermal characterization of each polymer will be conducted and phosphoric acid-doped membranes will be processed via conventional imbibing or the PPA Process. The

relationships between PBI chemical structure and membrane composition with the fundamental properties of gel stability, membrane conductivity, mechanical properties and fuel cell performance will be reported.

5.2. EXPERIMENTAL

5.2.1. CHEMICALS

2,5-Pyridinedicarboxylic acid (2,5-py-2COOH) was purchased from Acros Chemical and TCI America (~98% purity) and purified by recrystallization from a 1:1 dilution of concentrated hydrochloric acid. 2,5-Dihydroxyterephthalic acid (2OH-TPA) was purchased from TCI America and Sigma Aldrich (~98% purity) and purified by recrystallization from a 3:2 dilution of absolute ethanol:water. Terephthalic acid (TPA, purified) and isophthalic acid (IPA, purified) were purchased from Amoco Chemicals. 3,3',4,4'-Tetraaminobiphenyl (TAB, purified) and a stock 1.4 wt% para-PBI solution was donated by BASF Fuel Cell, Inc. Polyphosphoric acid (PPA, 115%) was obtained from InnoPhos, Inc. and stored under nitrogen. All other chemicals were obtained commercially and used as-received.

5.2.2. POLYBENZIMIDAZOLE SYNTHESIS AND ISOLATION OF PBI POWDER

To a three-necked flask equipped with nitrogen flow and overhead stirrer, a solution of PPA and 2,5-py-2COOH and/or 2OH-TPA was stirred and heated at 195-220^{O}C for 3-30 hours. The polymerization time was determined by the viscosity of the solution, which was dependent on the solids concentration and the polymer molecular weight. Both the stir-rate and the temperature were controlled and adjusted during the polymerization. The total amount of diacid was in a 1:1 stoichiometric ratio with TAB.

At the end of the polymerization (at a high viscosity, judged visually), the hot PBI solution was poured into a commercial Waring blender containing deionized water. The cover of the blender was fitted with a funnel so that the polymerization solution could be added to the water while the blender was operating at a high spinning rate. The PBI particles were isolated via vacuum filtration and were neutralized with ammonium hydroxide in 1L of DI water (pH = 7-8). After boiling for approximately one hour, the particles were again isolated via vacuum filtration and dried at 120°C under vacuum for 12-24 h. The texture of the isolated PBI ranged from small particles to fibrillous material, which was dependent on both polymer chemistry and inherent viscosity (molecular weight).

For some 2OH-PBI particles, it was found that the previously described neutralization process did not completely cleave the phosphate ester bridges. In order to cleave these crosslinks, the 2OH-PBI particles that were obtained after being processed in a Waring blender were stirred in concentrated ammonium hydroxide for 2-4 hours at room temperature. These particles were then washed multiple times with boiling water and dried in an oven at 120°C. Cleavage of the phosphate crosslinks was confirmed by FT-IR.

5.2.3. Processing of PBI into Powder / Addition of Powder to PPA/PBI Solution

Bulk PBI material isolated from Section 5.2.2 was further processed into powders via mechanical grinding and/or use of a ball mill. The PBI material was first processed with a Wiley cutting mill, which was able to reduce the size of the PBI particles to a diameter less than 60 mesh (0.251mm). A ball mill was used on the resulting PBI powder

to further reduce the particle size, from which particles smaller than 100 mesh (0.152mm) could be obtained. Dry ice and liquid nitrogen were occasionally used during these mechanical processes to help obtain smaller particles although these cooling techniques did not significantly improve the process. The particles were separated by size using a sieve stack and shaker.

To test the solubility of the PBI particles in PPA, 2.00g of PBI particles were added to 38.00g of PPA (5wt% solution) and stirred under nitrogen for 24 hours at 160°C. Addition to the reaction flask would proceed as follows: 18g of PPA would be added first, followed by 2g of PBI, followed by 20g PPA (this ensured greater homogenization of the solution). Over the course of this test, small samples of solution would be extracted from the reactor and smeared onto a glass slide. The solubility of the particles in PPA would be judged visually.

Addition of the PBI particles to a 1.4wt% stock solution of para-PBI at 180°C would proceed as follows. A clean reaction vessel would be placed on a scale, followed by addition of 50g of stock solution to the vessel. An amount of PBI powder would be added to the flask, followed by addition of (50g – mass of PBI powder) grams of the stock solution. The total mass of the solution would be 100g. These solutions would then be placed in an oil bath at 160°C, stirred under nitrogen for a pre-determined amount of time, and cast onto glass plates using a Gardner blade with an even gap width.

5.2.4. Characterization Techniques

Thermogravimetric analysis, differential scanning calorimetry, and inherent viscosity measurements were performed on polymer isolated from the PPA process.

Following the polymerization, the polymer/PPA solution that remained in the reaction vessel was hydrolyzed with deionized water. The precipitated polymer was then pulverized in a commercial Waring blender and neutralized with ammonium hydroxide in 500 mL of distilled water. After heating for 1 hour at 100˚C, the polymer was isolated by filtration and washed thoroughly with water to remove any residual ammonium salts. The powder was then dried for 12 hours at 120-130˚C. Thermogravimetric analysis (TGA) was performed using a TA Instruments TGA Q-5000 IR with a heating rate of 10 °C min^{-1} under nitrogen. Differential scanning calorimetry (DSC) was conducted using a TA Instruments DSC Q-2000 with a nitrogen flow rate of 20 mL min^{-1} and heating and cooling rates of 10°C min^{-1}. Following dissolution of the polymer in 96% sulfuric acid at 0.2 g dL^{-1} concentrations, inherent viscosities (IV's) were measured using an Ubbelohde viscometer in a water bath set at 30.0˚C. Inherent viscosity was calculated according to Equation 1.

$$\ln [(t) (t_o)^{-1}] c^{-1} = \text{Inherent Viscosity (dL } g^{-1}) \qquad (1)$$

where t is the solution flow time in seconds, t_o is the solvent (96% sulfuric acid) flow time in seconds, and c is the solution concentration in g dL^{-1}.

Proton (^{1}H) and carbon (^{13}C) NMR were performed using a Bruker ARX 300 instrument. Fourier transform infrared spectroscopy (FT-IR) was performed using a Perkin Elmer Spectrum 100 FT-IR Spectrometer. Microwave reactions were performed using a CEM Discover SP-D microwave digestor.

Gas chromatography / mass spectrometry (GC-MS) was performed on samples with solute concentrations in a range of 1-10 ppm. The GC-MS was performed using a Shimadzu GCMS-QP2010 SE equipped with an AOC-20i auto-sampler. The chromatography column was a Shimadzu SHRXI-5MS, 30 meters, with a temperature range of -60-330/350°C. Helium was used as the carrier gas.

The composition of acid-doped PBI membranes was determined by measuring the relative amounts of solids (e.g. polymer, phloroglucinol), water, and acid in the film. The phosphoric acid (PA) content was determined by titrating a sample of membrane of known weight with standardized sodium hydroxide solution (0.1 N) using a Metrohm 716 DMS Titrino autotitrator. The sample was washed with water and dried in an oven overnight at 120 °C. The dried sample was then weighed to determine polymer solids content for the membrane. The amount of water was calculated by subtracting the weights of polymer and PA from the initial PBI membrane sample weight.

Ionic conductivities were measured via a four-probe through-plane bulk measurement using an AC Zahner IM6e impedance spectrometer that scanned a frequency range from 1 Hz to 100 KHz. A rectangular sample of membrane (3.5 cm x 7.0 cm) was placed in a polysulfone cell with four platinum wire current collectors. Two outer electrodes set 6.0 cm apart supplied current to the cell, while the two inner electrodes 2.0 cm apart on opposite sides of the membrane measured the voltage drop. To ensure a through-plane bulk measurement of the membrane ionic conductivity, the two outer electrodes were placed on opposite sides of the membrane and the two inner electrodes were arranged in the same manner. The reported conductivities were made on

preconditioned (dehydrated) membranes that were held at >100°C for at least two hours. Proton conductivity was calculated using the following equation:

$$\sigma = (D)\,(L \cdot B \cdot R)^{-1} \qquad (2)$$

where D was the distance between the two test current electrodes, L was the thickness of the membrane, B was the width of the membrane, and R was the measured resistance.

The mechanical properties of the membranes were measured by cutting dog bone specimens (ASTM D683 Type V) from the bulk membrane using a cutting press. Tensile properties were measured using an Instron Tensile Tester (5543A) with a 10N load cell. All measurements were made at 25°C ± 3°C on samples preloaded to 0.1N with a crosshead speed of 5mm per minute.

Membrane electrode assemblies consisted of the polymer membrane sandwiched between two electrodes. MEAs were prepared by hot pressing the acid-doped membrane between an anode electrode and a cathode electrode at 150 °C for 90-150 seconds using 4500 lbs of force and compressing to 80% its original width. Electrodes were received from BASF Fuel Cell, Inc. with 1.0 mg/cm^2 platinum (Pt) catalyst loading. Anode electrodes contained only Pt as the catalyst, while the cathode electrodes contain a BASF Fuel Cell standard cathode Pt alloy. The active area of the electrodes was 45.15 cm^2. Fuel cell fabrication was conducted by assembling the cell components as follows: end plate:PTFE insulator:anode current collector:anode flow field:MEA:cathode flow field:cathode current collector:PTFE insulator:end plate. Gaskets were used on either side

of the MEA to control compression. Following assembly, the cell was evenly clamped to 50 in-lbs of pressure.

Fuel cell performance was measured on 50 cm^2 (active area 45.15 cm^2) single stack fuel cells using test stations obtained from Plug Power or purchased from Fuel Cell Technologies. Polarization curves were obtained at various temperatures (120-180°C) with hydrogen as a fuel and different oxidants (air or oxygen gas). Fuel cells were operated for at least 100 hours (break-in period) at 0.2 A cm^{-2} at 180°C before measurement of polarization curves. Long-term stability testing was performed under static current and temperature conditions of 0.2 A cm^{-2} and 180°C with a constant flow rate of hydrogen and air. Degradation rates of long-term fuel cell operations were calculated by linear fitting cell voltage data points with respect to time.

5.2.5. Synthesis of Phos-PBI and PEBI Monomers

5.2.5.1. Synthesis of 4-(6-chloro-1H-benzimidazol-2-yl)phenol

The synthesis of the monomer 4-(6-chloro-1H-benzimidazol-2-yl)phenol was first attempted by a condensation reaction between 4-hydroxybenzoic acid and 4-chloro-o-phenylenediamine in PPA at 195°C under nitrogen for 12 hours. The reactants were added in a 1:1 stoiciometric ratio to PPA at a 5wt% total solids concentration. The product was precipitated in deionized water and was neutralized and isolated by multiple washes with ammonium hydroxide and water. Although this reaction proceeded to completion and created the desired product, a more facile route was discovered and is shown in Scheme 5.4. In this reaction, 0.03 mol (3.66g) of 4-hydroxybenzaldehyde and 0.03 mol (4.28g) of 4-chloro-1,2-phenylenediamine were added to 0.033 mol (6.27g)

$Na_2S_2O_5$ in 80 mL DMF (Scheme 5.4). The solution was stirred at 90°C for 2 h, and then gradually cooled down to room temperature. The reaction solution was poured into approximately 1L ice water (2-5°C), and stirred for 4 h. The precipitated product was filtered, washed with cold water, and dried under a vacuum at 120°C. Theoretical yield = 7.34 g. Actual yield = 6.85g (93.3%).

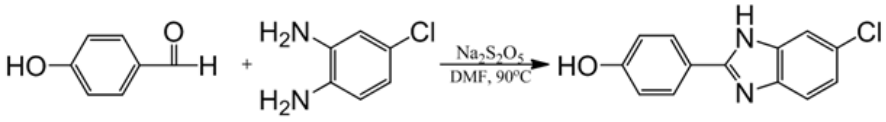

Scheme 5.4: Synthesis of 4-(6-chloro-1H-benzo[d]imidazol-2-yl)phenol.

Formation of the monomer was verified by direct probe mass spectrometry, in which a molecular ion peak of 244 m/z was observed. Carbon and proton NMR spectra also confirmed the identity of the monomer (Figure 5.1 and 5.2, respectively, 300 MHz, D_6-DMSO). Proton shift peaks centered at 7.97 and 6.90 ppm represented the protons on the phenyl ring, 9.99 ppm represented the proton of the hydroxyl group, and 7.52 and 7.14 ppm represent the benzimidazole unit. The small broad peak centered at 12.83 ppm represents the proton bonded to the nitrogen atom. Carbon shift peaks centered at 159.8 and 153.6 represented the carbons adjacent to the hydroxyl and amine/imine groups, respectively. The carbon peak centered at 121.0 ppm represented a carbon of the benzene ring adjacent to the benzimidazole unit, the peaks centered at 122.1 and 126.0 ppm represented carbons of the benzimidazole unit, and the peaks at 128.8 and 116.1 ppm represented carbons of both units. Using DSC analysis, a sharp melting point peak at 273.79°C indicated high monomer purity.

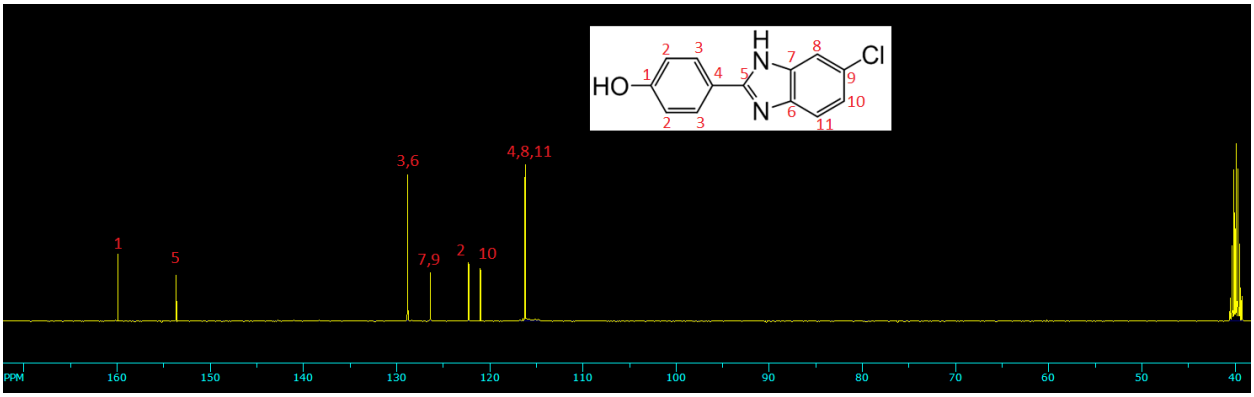

Figure 5.1. The ^{13}C NMR of 4-(6-chloro-1H-benzimidazol-2-yl)phenol in dimethylsulfoxide-d_6.

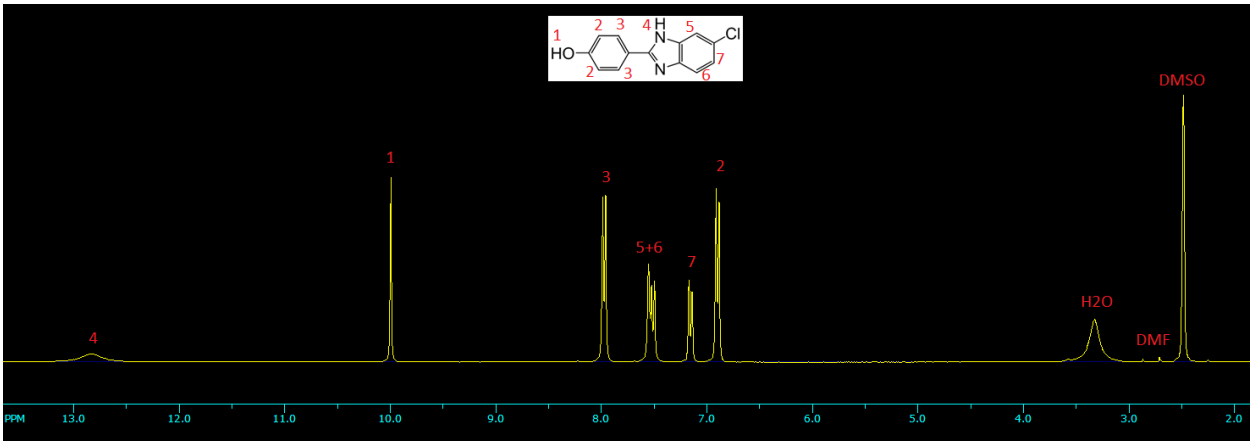

Figure 5.2. The ^{1}H NMR of 4-(6-chloro-1H-benzimidazol-2-yl)phenol in dimethylsulfoxide-D_6

5.2.5.2. SYNTHESIS OF 4-(6-FLUORO-1H-BENZIMIDAZOL-2-YL)PHENOL

In the preferred synthesis, 0.03 mol (3.66g) of 4-hydroxybenzaldehyde and 0.03 mol (3.78g) of 4-fluoro-1,2-phenylenediamine were added to 0.033 mol (6.27g) $Na_2S_2O_5$ in 80 mL DMF. The solution was stirred at 90°C for 2 h, and then gradually cooled down to room temperature. The reaction solution was poured into approximately 1L ice water

(2-5°C), and stirred for 4 h. The precipitated product was filtered, washed with cold water, and dried under a vacuum at 120°C. Theoretical yield = 6.84g. Actual yield = 6.20g (90.6%). Using DSC analysis, a sharp melting point peak at 282.35°C indicated high monomer purity. ^{1}H NMR (300 MHz, D_6-DMSO) δ 12.77 (broad, 1H), 9.96 (s, 1H), 7.97 (s, 1H), 7.94 (s, 1H), 7.50 (m, 1H), 7.30 (m, 1H), 7.01 (m, 1H), 6.94 (m, 2H). ^{13}C NMR (300 MHz, D_6-DMSO) δ 160.4, 159.7, 157.3, 153.6, 128.6, 121.2, 116.2, 110.1, 109.8. MS *m/z* calculated for product [M+] 282, found 282.

5.2.5.3. SYNTHESIS OF 4-(6-NITRO-1H-BENZIMIDAZOL-2-YL)PHENOL

0.03 mol (3.66g) of 4-hydroxybenzaldehyde and 0.03 mol (4.59g) of 4-nitro-1,2-phenylenediamine were added to 0.033 mol (6.27g) $Na_2S_2O_5$ in 80 mL DMF. The solution was stirred at 90°C for 2 h, and then gradually cooled down to room temperature. The product could not be obtained by precipitation into water; thus, the DMF was vacuum-distilled off and the resulting product was then placed in approximately 50mL deionized water, vacuum filtered, washed with cold deionized water, and dried under a vacuum at 120°C. Theoretical yield = 7.65g. Actual yield = 6.20g (81.0%). ^{1}H NMR (300 MHz, D_6-DMSO) δ 12.40 (broad, 1H), 9.90 (s, 1H), 8.30 (s, 1H), 7.95 (s, 2H), 7.72(m, 1H), 7.43 (m, 1H), 6.90 (m, 2H). MS *m/z* calculated for product [M+] 255, found 255.

5.2.5.4. SYNTHESIS OF 4-(6-BROMO-1H-BENZIMIDAZOL-2-YL)PHENOL

0.03 mol (3.66g) of 4-hydroxybenzaldehyde and 0.03 mol (5.61g) of 4-bromo-1,2-phenylenediamine were added to 0.033 mol (6.27g) $Na_2S_2O_5$ in 80 mL DMF. The

solution was stirred at 90°C for 2 h, and then gradually cooled down to room temperature. The product could not be obtained by precipitation into water; thus, the DMF was vacuum-distilled off and the product was then placed in approximately 50mL deionized water, vacuum filtered, washed with cold deionized water, and dried under a vacuum at 120°C. Theoretical yield = 8.67. Actual yield = 6.70g (77.3%). ^{1}H NMR (300 MHz, D_6-DMSO) δ 12.53 (broad, 1H), 9.95 (s, 1H), 7.97 (s, 2H), 7.85 (s, 1H), 7.49(m, 1H), 7.40 (m, 1H), 6.95 (m, 2H). MS *m/z* calculated for product [M+] 288/290, found 288/290.

5.2.5.5. Synthesis of 5-Phosphonoisophthalic Acid

Multiple methods were attempted to synthesize this monomer, of which two were successful.[23,24] The first method began with the bromination of isophthalic acid, followed by subsequent esterification of the carboxylic acids, phosphorylation, and hydrolysis. The second method used the direct phosphorylation of 1-bromo-3,5-dimethylbenzene, oxidation of the methyl groups to carboxylic acids, and reduction of the diethylphosphonic ester moiety to phosphonic acid. The first method produced the greatest yield of product and is described below.

5.2.5.5.1. Method 1: Synthesis of 5-Phosphonoisophthalic Acid

5-Bromo-isophthalic acid was synthesized by combining 30.164g (0.18mol) isophthalic acid in 90mL concentrated (96%) sulfuric acid and heated to 60°C. Slowly, over approximately 30 min, 38.870g 0.218mol, 1.2 equivalents) N-bromosuccinimide was added to the stirring solution. The reaction was stirred overnight (12h), poured into

1L of ice water, and the product was allowed to precipitate over the next hour. The crude product was filtered, washed with 500mL deionized water and 200mL n-hexane, and dried in a vacuum oven at 160°C. A sharp melting point peak was found between 275-277°C. This reaction yielded 40.5g of the product (91.8%).

The methyl ester was synthesized by heating the product with methanol and a catalytic amount of sulfuric acid. The product was neutralized with sodium bicarbonate, filtered, and dried under vacuum. The product was a hard, white solid at room temperature, but it became a liquid around 40°C and was much easier to handle. ^{1}H NMR ($CHCl_3$) δ 8.61 (s, 1H), 8.36 (s, 2H), 3.97 (s, 6H).

5.2.5.5.2. METHOD 2: SYNTHESIS OF 5-PHOSPHONOISOPHTHALIC ACID

Phosphonylation of 5-bromo-isophthalic ester was performed by combining 10.84g (40mmol) of the reactant with palladium acetate (0.90g, 4 mmol), triphenylphosphine (4.2g, 16mmol), diethyl phosphate (6.0g, 44mmol), triethylamine (4.5g, 44mmol) in a round bottom flask equipped with nitrogen inlet and a condenser (that also functioned as a nitrogen outlet). The diethyl phosphate was not commercially available, and so was synthesized by the oxidation of diethyl chlorophosphate. A procedure for this synthesis was found in literature;[25] however, the yield of this reaction was significantly lower than published (18.4% as compared to 92%). After stirring at 90°C for 24h, the product was cooled down to room temperature and purified using a silica-gel column (a gradient hexane:ethyl acetate solution with ratios 5:1 to 1:5 was used). The dimethyl 5-(diethoxyphosphoryl) isophthalate was concentrated under reduced pressure as a clear, viscous liquid. The product was then hydrolyzed in a dilute

HCl solution (18%, 50mL) for 24h, neutralized with sodium bicarbonate, filtered, washed with cold water, and dried at 120°C under vacuum. The reaction yielded 1.2g (12.2%) of an off-white powder. ^{1}H NMR (300 MHz, D_6-DMSO) δ 8.54(s, 1H), 8.44(s, 1H), 8.39 (s, 1H). The acid protons were not observed, and could be due to proton-deuterium exchange with the solvent.

5.2.5.6. Synthesis of 2-Phosphonoterephthalic Acid

The synthesis of this compound had been previously reported by Branion et al.[26] To a solution of 2-bromo-p-xylene (6.00g, 10,80 mmol, 4.50 mL) in anhydrous THF (30 mL) at 78°C (dry ice and acetone) under nitrogen, t-BuLi (32.40 mmol, 19 mL, 1.7M solution in pentane) was added dropwise. The solution was stirred for one hour at -78°C and then allowed to gradually warm up to 0°C over the next hour. The resulting solution was added dropwise to diethyl chlorophosphate (5.58g, 32.40 mmol, 4.65 mL) in anhydrous THF (15 mL) at 0°C, and it was stirred for 12 h and allowed to warm up to room temperature (25°C). This solution was then added to an aqueous solution of ammonium chloride (6.00g in 100 mL of water), followed by addition of diethyl ether (100 mL). After stirring for 5 minutes, the layers were separated, the organic layer was dried ($MgSO_4$), and the solvent was removed under vacuum and heat (roto-vaporized). The crude product was purified using a silica-gel column (a gradient hexane:ethyl acetate solution that ranged from 3:1 to 1:3). The solvents were removed under vacuum to yield a yellowish-oil (3.45g, 44% yield). Small peaks in the NMR suggests that the product was not entirely pure, and that there were trace amounts of ethyl bromide. ^{1}H NMR ($CDCl_3$) δ 1.32 (t, 6H), 2.34 (s, 3H), 2.51 (s, 3H), 4.00-4.20 (m, 4H), 7.14 (dd, 1H), 7.23 (d, 1H),

7.75 (dd, 1H). ^{13}C NMR δ 16.3, 20.6, 20.7, 61.8, 126.4, 131.1, 133.1, 134.5, 134.9, 138.5. The product could not be detected using GC-MS.

This product (3.45g, 14.25 mmol) was dissolved in deionized water (50mL) and t-butanol (7mL) and heated to reflux under a condenser in an oil bath. Potassium permanganate (8.95g, 57mmol) was slowly added over 0.5h, and the solution was allowed to stir and reflux for 2h. The temperature was reduced to 80°C and allowed to stir overnight (approximately 12h). After cooling down to room temperature, the solution was vacuum filtered using a fritted funnel and the filtrate was concentrated under reduced pressure. The solution was cooled to 0-5°C using an ice bath and acidified with concentrated hydrochloric acid (5mL), which was then stirred for three hours at 0-5°C. The precipitate was vacuum filtered, suspended in deionized water (10mL), refluxed for 1 hour, cooled to room temperature, vacuum filtered, and dried at 120°C under vacuum to yield 1.40g (5.69 mmol, 39.9%) of the white product. ^{1}H NMR (DMSO-D_6) δ 7.85 (dd, 1H), 8.03 (dt, 1H), 8.45 (dd, 1H). ^{13}C NMR (DMSO-D_6) δ 131.0, 131.6, 132.3, 133.8, 136.2, 140.3, 167.4, 169.0. Total yield = 17.6%.

5.2.6. Polymerizations of PEBIs

Two different techniques were used to polymerize the PEBIs. One involved the use of a mechanical stirrer, a dean stark trap equipped with a condenser, and nitrogen inlet / outlet. The second involved the use of a microwave reactor under very high heat and pressure conditions. Many variables were altered in each synthetic scheme, including monomer concentration, monomer type, solvent (DMF, DMAc, NMP), base (K_2CO_3,

KOtBu, Cs_2CO_3), temperature, and reaction time. The following are general schemes used during the polymerization reactions of op-PBI.

Polymerization of op-PBI was attempted by combining 0.05mol of monomer, 0.055mol base, 50 mL dry solvent, and 20 mL dry toluene in a two-necked round-bottom flask equipped with a nitrogen inlet and outlet, a mechanical stirrer, and a Dean-Stark trap fitted with a condenser. The reaction solution was mixed at 130°C for 1 h and then at 170-220°C for up to 48 h. The solvent was distilled under reduced pressure, and the residual product was suspended in deionized water, refluxed, cooled to room temperature, vacuum filtered, washed with cold deionized water, and dried at 120°C under vacuum. This polymerization process was similar to a polymerization reaction reported in literature.[23] Analysis of the product involved NMR, GC-MS, and IV measurements. Polymer was not obtained, and the spectra were identical to the starting materials.

Polymerizations involving the use of the microwave reactor were attempted by combining 0.001mol monomer, 0.0011mol base, and 25mL solvent into a sealed reaction vial with a magnetic stir-bar. After purging the vial with nitrogen, the vial was placed in the reactor and stirred at a constant rate. The solution was subjected to the following temperature ramping profile: ramp from 25°C to 150°C for two minutes, isotherm for 30 min, ramp from 150 °C to 250°C for two minutes, isotherm for 30 minutes, ramp from 250°C to 300°C for two minutes, isotherm for 30 minutes. The solutions were then allowed to cool to room temperature, the solvent was distilled under reduced pressure, the residual product was suspended in deionized water, refluxed, cooled to room temperature, vacuum filtered, washed with cold deionized water, and dried at 120°C under vacuum.

Analysis of the product involved NMR, GC-MS, and IV measurements. Polymer was not obtained, and the spectra are identical to the starting materials.

5.3. Results and Discussion

5.3.1. Delayed Solvation / Swelling of PBI Particles

5.3.1.1. PBI Powder Addition

For a successful addition of a PBI powder into a PBI/PPA matrix, the particles needed to remain undissolved / unswelled throughout the mixing process. This is important because undissolved PBI particles would not substantially increase the viscosity of a stock-solution of para-PBI/PPA, thereby circumventing the increased viscosity issue that was previously discussed. Thus, prior to incorporation of the PBI powders into a para-PBI/PPA solution, the solubility or dissolution characteristics of each particle type in PPA were investigated.

Table 5.1 lists the solubility properties of all the PBIs evaluated. It was observed that the 2,5-py-PBI powders were too soluble for the powder addition method, regardless of the PBI powder's inherent viscosity or particle size. Attempts at annealing these powders under nitrogen at elevated temperatures did not affect their solubility/dissolution characteristics. In contrast, 2OH-PBI powders were highly insoluble, even after mixing for up to 24 hours. Random copolymers of 2OH-PBI and 2,5-py-PBI with varying copolymer ratios were synthesized and characterized. It was observed that random copolymers with higher concentrations of 2,5-py-PBI were more soluble, but were still incapable of fully dissolving in PPA. We concluded that the 2,5-py-PBI homopolymers

were too soluble for future research, but that the 2OH-PBI and 2,5-py-r-2OH-PBI particles were possible candidates for powder addition tests.

Table 5.1. Comprehensive list of the solubility properties for PBIs in PPA at a 5wt% polymer powder concentration.

Polymer Type	Inherent Viscosity (dL g^{-1})	Particle Size (mesh)	Annealed?	Solubility in PPA, 1h	Solubility in PPA, 2h	Solubility in PPA, 4h	Solubility in PPA, 8h	Solubility in PPA, 24h
2,5-py-PBI	1.26	60	No	++	+++	+++	+++	+++
2,5-py-PBI	1.05	60	No	++	+++	+++	+++	+++
2,5-py-PBI	2.59	60	No	++	+++	+++	+++	+++
2,5-py-PBI	2.59	60	230 C, 12h	++	+++	+++	+++	+++
2,5-py-PBI	2.51	60	No	++	+++	+++	+++	+++
2,5-py-PBI	2.51	60	350 C, 48h,	++	+++	+++	+++	+++
2,5-py-PBI	1.28	60	No	++	+++	+++	+++	+++
2,5-py-PBI	1.28	60	230 C, 12h	++	+++	+++	+++	+++
2OH-PBI	1.45	60	No	+	+	+	+	+
2OH-PBI	1.45	100	No	+	+	+	+	+
2OH-PBI * Cleaved	1.45	60	No	++	+++	+++	+++	+++
2OH-PBI * Cleaved	1.45	100	No	++	+++	+++	+++	+++
2OH-PBI	1.01	60	No	+	+	+	+	+
75:25 2OH-2,5-py-	0.4	100	No	+	+	+	+	++
50:50 2OH-2,5-py-	1.05	100	No	+	+	+	++	++
25:75 2OH-2,5-py-	0.64	100	No	+	+	++	++	++
10:90 2OH-2,5-py-	0.65	100	No	+	++	++	++	++
75:25 2OH-2,5-py-	1.36	100	No	+	+	+	+	++
50:50 2OH-2,5-py-	1.49	100	No	+	+	+	++	++
25:75 2OH-2,5-py-	1.32	100	No	+	+	++	++	++
10:90 2OH-2,5-dpy-	1.30	100	No	+	++	++	++	++

+: Slight dissolution
++: Substantial dissolution
+++: Complete dissolution

The down-selected PBI powders were added to stock solutions of para-PBI/PPA in various concentrations (2-5 wt%) at 160°C and cast into films. It was observed that all of the cast membranes had lower tensile strengths and lower anhydrous proton conductivity values as compared with membranes cast directly from the stock para-

PBI/PPA solution. The poor tensile and electrochemical properties were attributed to undissolved particles of PBI in the para-PBI/PA matrix. Even after the polymer membranes underwent additional thermal treatment (180-200°C, up to 48 hours, under air or nitrogen), the PBI powders never fully dissolved. Through FT-IR analysis, it was observed that the isolated PBI powders that had a 2OH-PBI component were cross-linked with phosphate ester bridges. We attributed the poor solubility of these particles in the PBI matrices to these chemical crosslinks. Thus, it was concluded that this powder addition was not a viable method for producing membranes with enhanced physical and mechanical properties.

5.3.1.2. Reversible Crosslinking of 2OH-PBI

The 2OH-PBI and 2,5-py-r-2OH-PBI powders were too insoluble in the PBI/PPA solution or PBI/PA matrix to be used in a delayed solvation technique. As previously discussed, we inferred that this insolubility arises due to the phosphate ester bridges that form chemical crosslinks. These chemical crosslinks were cleaved using a concentrated solution of ammonium hydroxide and observed by FT-IR (broad peaks between 1250-1190 cm^{-1} and 1000-850 cm^{-1}, which represented an aromatic phosphate stretch, disappeared). The solubilities of these 2OH-PBI powders with cleaved phosphate bridges were also investigated (Table 5.1). It was determined that these powders were much too soluble for the powder addition process and dissolved too quickly. Thus, we concluded that addition of 2OH-PBIs with cleaved phosphate bridges was not a viable method for producing membranes with enhanced mechanical properties.

5.3.2. Phloroglucinol Addition to PBI Solutions

Incorporation of phloroglucinol (Pg) into PBI membranes was attempted using three different methods: addition of Pg powder to the polymerization solution prior to PBI synthesis; addition of Pg after synthesis of PBI, but prior to casting of membrane; and addition of Pg after PBI membrane formation using an equilibration bath. Initial results indicated that Pg inhibits the polycondensation reaction of PBI polymerizations, and Pg had very poor solubility in acid baths (i.e. phosphoric acid). Thus, a possible method to homogeneously incorporate Pg into a PBI/PA matrix was explored by adding the polymer to a PBI/PPA solution just prior to casting.

The solubility of Pg in PPA was investigated by stirring specific concentrations (1:5 molar ratio, 22.84 wt%; 1:10 molar ratio, 12.89 wt%; 1:20 molar ratio, 6.89 wt%) of Pg in PPA at elevated temperatures (170-250°C) for up to 96 hours. It was found that Pg would dissolve in PPA after approximately 2h at these temperatures, but that the solution would generally have a low viscosity. However, continuing to stir and heat these solutions resulted in highly viscous (gel-like) solutions, some of which could not easily be cast into membranes (indicating a chemically cross-linked solution). When these viscous solutions were cast as thin films and placed on a bench-top, they hydrolyzed to low viscosity solutions within a couple hours. Solutions with greater proportions of Pg took less time to become highly viscous (the 22.84 wt% solution became highly viscous in 18h, as compared to the 6.89 wt% solution that took 96 hours to reach that same viscosity). During the first two hours of these dissolution / cross-linking processes, the Pg/PPA solution turned from yellow to orange, red, brown, and then to black.

The following experiment was used to determine whether incorporation of Pg into a PBI/PA matrix would enhance the mechanical or electrochemical properties of the resulting membrane. A large quantity (400g) of 2 wt% 2OH-PBI was polymerized in PPA under nitrogen. Upon reaching an optimal viscosity (judged visually), part of this solution was immediately cast as a thin film and placed in a humidity chamber. The remainder of this solution was split into two 100mL reaction flasks; the first flask combined 99g of solution with 1g of Pg in one flask and the second flask combined 98g of solution with 2g of Pg in the other flask. Both solutions were then stirred for an additional 3 hours at 170°C to ensure homogenization and dissolution of the Pg into the PBI/PPA solution. These solutions were then cast into membranes and hydrolyzed in the humidity chamber for 24 hours.

The composition, tensile properties, and anhydrous proton conductivities of these membranes are listed in Table 5.2. The molecular weights of these polymers were nearly identical (ranging from 1.07 to 1.10 dL g^{-1}) because the membranes originated from the same polymerization solution. The inclusion of Pg into the membranes caused a significant increase in solids content and decrease in PA:PBI molar ratio. The effects of decreased PA:PBI molar ratio are often associated with decreased proton conductivities, a trend that was also observed with this data. Inclusion of Pg into the 2OH-PBI membranes resulted in an improved Young's modulus in both samples. The fuel cell voltages and voltage degradation rates of these MEAs did not significantly differ (Figure 5.3). Thus, it was determined that addition of Pg to the PBI membranes does not significantly alter the electrochemical properties of the membranes but may form the basis of a method for improving the mechanical properties of PBI membranes.

Table 5.2. The compositions, tensile properties, and anhydrous proton conductivites of three 2OH-PBI membranes.

Type of PBI	Phloro-glucinol (wt%)	PA content (%wt)	Solids contents (%wt)	Water content (%wt)	PA mole ratio to PBI repeat unit	Young's Modulus (MPa)	Strain at Break (mm/mm)	Thickness (mm)	Anhydrous Proton Conductivity at 180^{O}C (S cm^{-1})
2OH-PBI	0%	61.80%	2.92%	35.28%	73.58	0.488	1.111	0.58	0.43
2OH-PBI	1%	59.93%	3.87%	36.20%	53.735	0.754	1.834	0.52	0.31
2OH-PBI	2%	59.39%	3.57%	37.04%	57.965	0.773	1.074	0.52	0.376

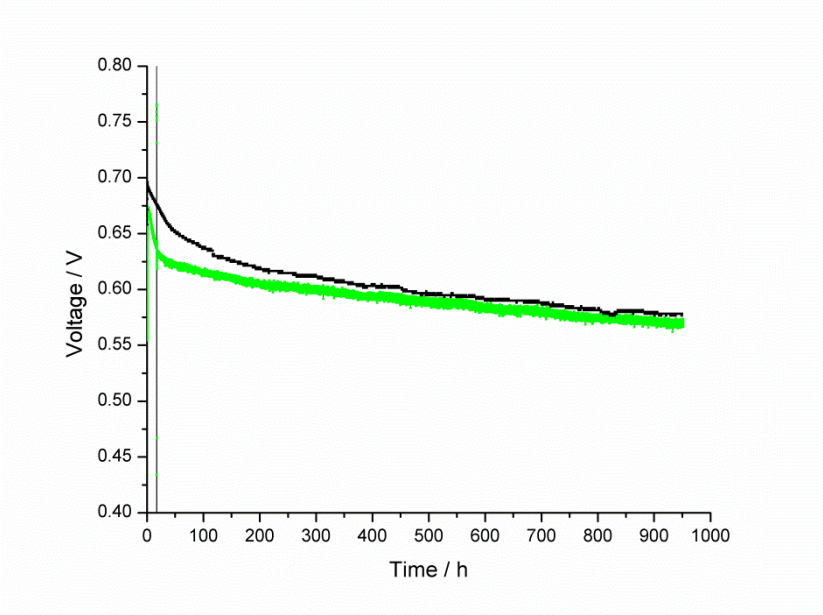

Figure 5.3. Fuel cell performance of 2OH-PBI homopolymer (black, upper line) and 2OH-PBI with 1wt% Pg (green, lower line) operated at 180°C at 0.2 A cm^{-2} with H_2:air 1.2:2.0 stoichiometry.

5.3.3. Synthesis of Polyetherbenzimidazoles and Polyphosphonobenzimidazoles

Multiple strategies were employed for the synthesis of PEBIs (Section 5.2.6). These various strategies involved large changes in monomer type, concentration, solvent, reaction type (e.g. heat, microwave), and type of base used to catalyze the reaction. Following each reaction, the products were isolated, dried, and characterized by means of

GC-MS, NMR, and IV measurements. Data obtained from all tests indicated that large quantities of starting materials remained, and the IVs calculated were below 0.05 dL g^{-1}. This data indicated that monomer degradation or sublimation was not occurring. NMRs of the reaction solution indicate a disappearance of the hydroxyl-proton, indicating that the polymerization is failing due to poor nucleophilic aromatic substitution of the charged monomer. We propose that the monomers could not form a stable Meisenheimer complex for efficient substitution to occur. This theory could be verified by the synthesis and polymerization of a similar monomer with an aliphatic alcohol group. The polymerizations of phos-PBIs were not attempted due to poor monomer yield and monomer impurities.

5.4. CONCLUSIONS

Several methods were employed to enhance the mechanical and electrochemical properties of PBI membranes. Addition of PBI powders into a PBI/PPA solution prior to casting was successfully employed to increase the polymer content of a membrane, meanwhile circumventing solution viscosity / processing issues. However, these undissolved powder particles did not swell nor dissolve in the membrane in any of the attempted post-processing treatments. This method resulted in membranes with lower mechanical and electrochemical properties.

Phloroglucinol addition to PBI membranes enhanced the mechanical properties of the film as shown by the higher room temperature Young's moduli of films containing 1 and 2% levels of Pg. This addition reduced the proportion of phosphoric acid to polymer repeat unit in the imbibed film, thereby causing a slight reduction in the film's anhydrous

proton conductivity. However, there was no substantial change in fuel cell performance between similar films with or without phloroglucinol.

Novel monomers were designed and synthesized for the polymerization of a polyetherbenzimidazole and polyphosphonobenzimidazoles. The synthesis of the former was thoroughly investigated, but ultimately failed due to low monomer reactivity. Polymerization of the latter could not be attempted due to poor monomer yields and purities.

5.5. REFERENCES

[1] Steele B. C. H., and Heinzel A., 2001, "Materials for Fuel-Cell Technologies," Nature, **414**, pp. 345-352.

[2] Dunwoody D., and Leddy J., 2005, "Proton Exhange Membranes: The View Forward and Back," The Electrochemical Society Interface, **3**, pp. 37–39.

[3] Xiao L., Zhang H., Scanlon E., Ramanthan L. S., Choe E. W., Rogers D., Apple T., and Benicewicz B. C., 2005, "High-Temperature Polybenzimidazole Fuel Cell Membranes via a Sol-Gel Process," Chem. Mater., **17**(21), pp. 5328–5333.

[4] Yu S., Xiao L., and Benicewicz B. C., 2008, "Durability Studies of PBI-based High Temperature PEMFC," Fuel Cells, **8**(3-4), pp. 165–174.

[5] He R., Li Q., Xiao G. Y., and Bjerrum N. J., 2003, "Proton conductivity of phosphoric acid doped polybenzimidazole and its composites with inorganic proton conductors," J. Membr. Sci., **226**(1-2), pp. 169–184.

[6] Jin Y. C., Nishida M., Kanematsu W., and Hibino T., 2011, "An H_3PO_4-doped polybenzimidazole/Sn0.95Al0.05P_2O_7 composite membrane for high-temperature proton exchange membrane fuel cells," J. Power Sources2, **196**(15), pp. 6042–6047.

[7] Yu S., and Benicewicz B. C., 2009, "Synthesis and Properties of Functionalized Polybenzimidazoles for High-Temperature PEMFCs," Macromolecules, **42**(22), pp. 8640–8648.

[8] Anis A., and Al-Zahrani S. M., 2012, "Sulfonated PVA/PBI based crosslinked composites towards anhydrous proton conductive polymer electrolyte membranes for fuel cells," Int. J. of Electrochem. Sci., **7**(10), pp. 9174–9185.

[9] Li Q., Pan C., Jensen J. O., Noye P., and Bjerrum N. J., 2007, "Cross-Linked Polybenzimidazole Membranes for Fuel Cells," Chem. Mater.2, **19**(3), pp. 350–352.

[10] Mader J., Lixiang X., Schmidt T., and Benicewicz B. C., 2008, "Polybenzimidazole/Acid Complexes as High-Temperature Membranes," Adv. Polym. Sci., **216**(Fuel Cells II), pp. 63–124.

[11] Wainright J. S., Savinell R. F., and Litt M. H., 2003, "High Temperature Membranes," Handbook of Fuel Cells, **3**, pp. 436–446.
[12] Qian G., and Benicewicz B. C., 2009, "Synthesis and Characterization of High Molecular Weight Hexafluoroisopropylidene-Containing Polybenzimidazole for High-Temperature Polymer Electrolyte Membrane Fuel Cells," J. Polym. Sci., Part A, **47**(16), pp. 4064–4073.
[13] Li Q., Hjuler H. A., and Bjerrum N. J., 2001, "Phosphoric acid doped polybenzimidazole membranes: physiochemical characterization and fuel cell applications," J. Appl. Electrochem., **31**(7), pp. 773–779.
[14] Kerres J., Schoenberger F., Chromik A., Haering T., Li Q., Jensen J. O., Pan C., Noye P., and Bjerrum N. J., 2008, "Partially fluorinated arylene polyethers and their ternary blend membranes with PBI and H3PO4. Part I. Synthesis and characterisation of polymers and binary blend membranes," Fuel Cells, **8**(3-4), pp. 175–187.
[15] Flory P. J., 1974, "Introductory Lecture," Faraday Discuss. Chem. Soc., **57**, pp. 7–18.
[16] Berrada M., Anbaoui Z., Lajrhed N., and Knouzi N., 1997, "Synthesis, Characterization, and Studies of Heat-Resistant Poly(ether benzimidazole)s," Chem. Mater., **9**(9), pp. 1989–1993.
[17] Savall B. M., Fontimayor J. R., and Edwards J. P., 2009, "Selective phenol alkylation for an improved synthesis of 2-arylbenzimidazole H4 receptor ligands," Tetrahedron Letters, **50**(21), pp. 2490–2492.
[18] Connell J. W., Hergenrother P. M., and Smith J. G., 1995, "Polybenzimidazoles via Aromatic Nucleophilic Displacement." US Patent 5412059.
[19] Connell J. W., Hergenrother P. M., and Smith J. G., 1997, "Polybenzimidazoles via Aromatic Nucleophilic Displacement." US Patent 5637670.
[20] Leikin A. Y., Rusanov A. L., Begunov R. S., and Fomenkov A. I., 2009, "Synthesis and Properties of Poly[2(4'oxyphenylene)5benzimidazole] and a ProtonExchange Membrane Produced on Its Basis," Polym. Sci. Series C, **51**(7), pp. 12–16.
[21] Sinigersky V., Budurova D., Penchev H., Ublekov F., and Radev I., 2013, "Polybenzimidazole-graft-polyvinylphosphonic acid—proton conducting fuel cell membranes," J. Appl. Polym. Sci., **129**(3), pp. 1223–1231.
[22] Sukumar P., Uw W., Markova D., Unsal O., Klapper M., and Mullen K., 2007, "Functionalized Poly(benzimidazole)s as Membrane Materials for Fuel Cells," Macro. Chem. and Phys., **208**(19-20), pp. 2258–2267.
[23] Bauer S., and Stock N., 2007, "Synthesis and characterization of four new metal 5-phosphonoisophthalates discovered by high-throughput experimentation," J. Solid State Chem., **180**(11), pp. 3111–3120.
[24] Liao T.-B., Ling Y., Chen Z.-X., Zhou Y.-M., and Weng L.-H., 2010, "A rutile-type porous zinc(II)-phosphonocarboxylate framework: local proton transfer and size-selected catalysis," Chem. Comm., **46**, pp. 1100–1102.
[25] Santschi N., Geissbuhler P., and Togni A., 2012, "Reactivity of an electrophilic hypervalent iodine trifluoromethylation reagent with hydrogen phosphates-A mechanistic study," J. Fluorine Chem., **135**, pp. 83–86.

[26] Branion S., and Benin V., 2007, “Preparation of Some Substituted Terephthalic Acids,” Synth. Comm., **36**(15), pp. 2121–2127.

FUTURE WORK

The investigation of novel high polymer content polybenzimidazole (PBI) membranes revealed several characteristics that were advantageous to high temperature proton exchange membrane fuel cells, including enhanced creep resistance and decreased fuel cell voltage degradation. Optimization of each random copolymer series (i.e. monomer concentration, monomer ratio) could further our understanding of the structure-property relationships of these membranes and offer insights for the future processing and commercialization of membrane electrode assemblies (MEAs). A study of the morphologies of low and high polymer content PBI membranes would provide useful information to understand the mechanisms of proton conduction and membrane creep resistance. Nuclear magnetic resonance studies are required to better understand the proton conduction mechanism in PBI MEAs. Small angle X-ray spectroscopy could be used to investigate the effects of PBI substituents or PBI concentration on polymer aggregation that occurs during the PPA Process. Wide angle X-ray spectroscopy of the high polymer content membranes developed in this dissertation could show how the substituents of PBIs affect d-spacing measurements. These measurements can then be correlated with phosphoric acid content, high temperature creep resistance, proton conductivity, and fuel cell performance. The investigation of novel PBI chemistries, such as polyphosphonobenzimidazoles, should be continued to add to the body of literature concerning structure-property relationships in gel membranes. Furthermore, understanding these relationships can provide insights as to how to achieve membrane

with enhanced polymer processing, membrane thermal gel stability, and MEA fuel cell performance.

REFERENCES

[1] 2008, "World Primary Energy Production by Source," Annual Energy Review, U.S. Energy Information Administration.

[2] 2008, "Primary Energy Consumption by Source and Sector," Annual Energy Review, Energy Information Administration.

[3] 2008, "Carbon Dioxide Emissions from the Consumption and Flaring of Fossil Fuels," Annual Energy Review, U.S. Energy Information Administration.

[4] Wainright, J., Wang, J., Weng, D., Savinell, R., and Litt, M., 1995, "Acid-doped polybenzimidazoles: a new polymer electrolyte," J. Electrochem. Soc., 142(7), pp. L121-L123.

[5] Dippel, T., Kreuer, K. D., Lassegues, J. C., and Rodriguez, D., 1993, "Proton conductivity in fused phosphoric acid; a $^{1}H/^{31}P$ PFG-NMR and QNS study," Solid State Ionics, 61, pp. 41-46.

[6] Bozkurt, A., Ise, M., Kreuer, K. D., Meyer, W. H., and Wegner, G., 1999, "Proton-conducting polymer electrolytes based on phosphoric acid," Solid State Ionics, 125, pp. 225-233.

[7] Weber, J., Kreuer, K.-D., Maier, J., and Thomas, A., 2008, "Proton Conductivity Enhancement by Nanostructural Control of Poly(benzimidazole)-Phosphoric Acid Adducts," Adv. Mater., 20, pp. 2595-2598.

[8] Vilciauskas, L., Paddison, S. J., and Kreuer, K.-D., 2009, "Ab Initio Modeling of Proton Transfer in Phosphoric Acid Clusters," J. Phys. Chem. A, 113, pp. 9193-9201.

[9] Mader, J., Lixiang, X., Schmidt, T., and Benicewicz, B. C., 2008, "Polybenzimidazole/Acid Complexes as High-Temperature Membranes," Adv. Polym. Sci., 216(Fuel Cells II), pp. 63-124.

[10] Wainright, J. S., Savinell, R. F., and Litt, M. H., 2003, "High Temperature Membranes," Handbook of Fuel Cells, 3, pp. 436-446.

[11] Colomban, P., 1992, Proton Conductors: Solids, membranes and gels - materials and devices, Cambridge University Press.

[12] Xiao, L., Zhang, H., Scanlon, E., Ramanthan, L. S., Choe, E. W., Rogers, D., Apple, T., and Benicewicz, B. C., 2005, "High-Temperature Polybenzimidazole Fuel Cell Membranes via a Sol-Gel Process," Chem. Mater., 17(21), pp. 5328-5333.

[13] Jayakody, J. R. P., Chung, S. H., Durantino, L., Zhang, H., Xiao, L., Benicewicz, B. C., and Greenbaum, S. G., 2007, "NMR Studies of Mass Transport in High-Acid-Content Fuel Cell Membranes Based on Phosphoric Acid and Polybenzimidazole," J. Electrochem Soc, 154(2), pp. B242-B246.

[14] Seel, D. C., Benicewicz, B. C., Xiao, L., and Schmidt, T. J., 2009, "High-temperature Polybenzimidazole-based Membranes," Handbook of Fuel Cells, 5, pp. 300-312.
[15] Litt, M., Ameri, R., Wang, Y., Savinell, R. F., and Wainright, J. S., 1999, "Polybenzimidazoles/phosphoric acid solid polymer electrolytes: mechanical and electrical properties.," Mater. Res. Soc. Symp. Proc., pp. 313-323.
[16] Zhang, H., December 2004, "Novel Phosphoric Acid Doped Polybenzimidazole Membranes for Fuel Cells," Ph.D. Thesis, Rensselaer Polytechnic Institute, Troy, NY.
[17] Li, Q., Hjuler, H. A., and Bjerrum, N. J., 2001, "Phosphoric acid doped polybenzimidazole membranes: physiochemical characterization and fuel cell applications," J. Appl. Electrochem., 31(7), pp. 773-779.
[18] Zhai, Y., Zhang, H., Liu, G., Hu, J., and Yi, B., 2006, "Performance degradation studies on PBI/H3PO4 high temperature PEMFC and one-dimensional numerical analysis," J. Electrochem. Acta., 52(2), pp. 394-401.
[19] Kongstein, O. E., Berning, T., Borresen, B., Seland, F., and Tunold, R., 2006, "Polymer electrolyte fuel cells based on phosphoric acid doped polybenzimidazole (PBI) membranes," Energy, 32(4), pp. 418-422.
[20] Kim, H., Cho, S. Y., An, S. J., Eun, Y. C., Kim, J., Yoon, H., Kweon, H., and YEW, K. H., 2004, "Synthesis of poly(2,5-benzimidazole) for use as a fuel-cell membrane," Macromol Rapid Commun, 25(8), pp. 894-897.
[21] Asensio, J. A., and Gomez-Romero, P., 2005, "Recent developments on proton conducting poly(2,5-benzimidazole) (AB-PBI) membranes for high temperature polymer electrolyte membrane fuel cells," Fuel Cells, 5(3), pp. 336-343.
[22] Li, Q. F., and Jensen, O. J., 2008, "Membranes for high temperature PEMFC based on acid-doped polybenzimidazoles," Membrane Technology, 2, pp. 61-96.
[23] Asensio, J. A., Borros, S., and Gomez-Romero, P., 2004, "Polymer Electrolyte Fuel Cells Based on Phosphoric Acid-Impregnated Poly(2,5-benzimidazole)," J. Electrochem. Soc., 151(2), pp. A304-A310.
[24] Chen, R., and Benicewicz, B. C., "Unpublished Work."
[25] Yu, S., 2006, "Novel polybenzimidazole derivatives for high temperature PEM fuel cells," Ph.D. Thesis, Rensselaer Polytechnic Institute, Troy, NY.
[26] Delano, C. B., Doyle, R. R., and Miligan, R. J., 1974, "High Strength, Thermally Stable Polymeric Fibers," No. AFML-TR-74-22, United States Air Force Materials Laboratory.
[27] Yu, S., Zhang, H., Xiao, L., Choe, E. W., and Benicewicz, B. C., 2009, "Synthesis of Poly (2,2'-(1,4-phenylene) 5,5'-bibenzimidazole) (para-PBI) and Phosphoric Acid Doped Membrane for Fuel Cells," Fuel Cells, 9(4), pp. 318-324.
[28] Xiao, L., 2003, "Novel polybenzimidazole derivatives for high temperature polymer electrolyte membrane fuel cell application," Ph.D. Thesis, Rensselaer Polytechnic Institute, Troy, NY.
[29] Xiao, L., Zhang, H., Jana, T., Scanlon, E., Chen, R., Choe, E. W., Ramanthan, L. S., Yu, S., and Benicewicz, B. C., 2005, "Synthesis and Characterization of Pyridine-Based Polybenzimidazoles for High Temperature Polymer Electrolyte Membrane Fuel Cell Applications," Fuel Cells, 5(2), pp. 287-295.

[30] Kallitsis, J. K., and Gourdoupi, N., 2003, "Proton Conducting Membranes Based on Polymer Blends for Use in High Temperature PEM Fuel Cells," J. New Mat. Electrochem. Systems, 6(4), pp. 217-222.
[31] Faure, S., Cornet, N., Gebel, G., Mercier, R., Pineri, M., and Sillion, B., 1997, "Sulfonated polyimides as novel proton exchange membranes for H2/O2 fuel cells," Proceedings of the International Symposium on New Materials for Fuel Cell and Modern Battery Systems, 2ndMontreal, pp. 818-827.
[32] Watari, T., Fang, J., Tanaka, K., Kita, H., Okamoto, K. I., and Hirano, T., 2004, "Synthesis, water stability and proton conductivity of novel sulfonated polyimides from 4,4'-bis(4-aminophenoxy)biphenyl-3,3'-disulfonic acid," J. Membr. Sci., 230(1-2), pp. 111-120.
[33] Lufrano, F., Gatto, I., Staiti, P., Antonucci, V., and Passalacqua, E., 2001, "Sulfonated polysulfone ionomer membranes for fuel cells," Solid State Ionics, 145(1-4), pp. 47-51.
[34] Einsla, B. R., Harrison, W. L., Tchatchoua, C., and McGrath, J. E., 2003, "Disulfonated polybenzoxazoles for proton exchange membrane fuel cell applications," Polym. Prepr, 44(2), pp. 645-646.
[35] Gil, M., Ji, X., Li, X., Na, H., Hampsey, J. E., and Lu, Y., 2004, "Direct synthesis of sulfonated aromatic poly(ether ether ketone) proton exchange membranes for fuel cell applications," J. Membr. Sci., 234(1-2), pp. 75-81.
[36] Xing, P., Robertson, G. P., Guiver, M. D., Mikhailenko, S. D., and Kaliaguine, S., 2004, "Sulfonated Poly(aryl ether ketone)s Containing the Hexafluoroisopropylidene Diphenyl Moiety Prepared by Direct Copolymerization, as Proton Exchange Membranes for Fuel Cell Application," Macromolecules, 37(21), pp. 7960-7967.
[37] Gao, Y., Robertson, G. P., Guiver, M. D., Mikhailenko, S. D., and Kaliaguine, S., 2004, "Synthesis of Copoly(aryl ether ether nitrile)s containing sulfonic acid groups for PEM applications," Macromolecules, 37(18), pp. 6748-6754.
[38] Xiao, G. Y., Sun, G. M., Yan, D. Y., Zhu, P. F., and Tao, P., 2002, "Synthesis of sulfonated poly(phthalazinone ether sulfone)s by direct polymerization," Polym. Prepr., 43(19), pp. 5335-5339.
[39] Wang, F., Hickner, M., Kim, Y. S., Zawodzinksi, T. A., and McGrath, J. E., 2002, "Direct polymerization of sulfonated poly(arylene ether sulfone) random (statistical) copolymers: candidates for new proton exchange membranes," J. Membr. Sci., 197(1-2), pp. 231-242.
[40] Hickner, M. A., Ghassemi, H., Kim, Y. S., Einsla, B. R., and McGrath, J. E., 2004, "Alternative polymer systems for proton exchange membranes (PEMs)," Chem. Rev., 104(10), pp. 4587-4611.
[41] Kim, S., Cameron, D. A., Lee, Y., Reynolds, J. R., and Savage, C. R., 1996, "Aromatic and rigid rod polyelectrolytes based on sulfonated poly(benzobisthiazoles)," J. Polym. Sci., Part A, 34(3), pp. 481-492.
[42] Ariza, M. J., Jones, D. J., and Roziere, J., 2002, "Role of post-sulfonation thermal treatment in conducting and thermal properties of sulfuric acid sulfonated poly(benzimidazole) membranes," Desalination, 147(1-3), pp. 183-189.

[43] Staiti, P., Lufrano, F., Arico, A. S., Passalacqua, E., and Antonucci, V., 2001, "Sulfonated polybenzimidazole membranes - preparation and physico-chemical characterization," J. Membr. Sci., 188(1), pp. 71-78.
[44] Bae, J. M., Honma, I., Murata, M., Yamamoto, T., Rikukawa, M., and Ogata, N., 2002, "Properties of selected sulfonated polymers as proton-conducting electrolytes for polymer electrolyte fuel cells," Solid State Ionics, 147(1-2), pp. 189-194.
[45] Asensio, J. A., Borros, S., and Gomez-Romero, P., 2002, "Proton-conducting polymers based on benzimidazoles and sulfonated benzimidazoles," J. Polym. Sci., Part A, 40(21), pp. 3703-3710.
[46] Sakaguchi, Y., Kitamura, K., Nakao, J., Hamamoto, S., Tachimori, H., and Takase, S., 2001, "Preparation and properties of sulfonated or phosphonated polybenzimidazoles and polybenzoxazoles," J. Polym. Mater. Sci. Eng., 84, pp. 899-900.
[47] Mader J., and Benicewicz B. C., 2010, "Sulfonated Polybenzimidazoles for High Temperature PEM Fuel Cells," Macromolecules, **43**, pp.6706-6715.
[48] He, R., Li, Q., Xiao, G. Y., and Bjerrum, N. J., 2003, "Proton conductivity of phosphoric acid doped polybenzimidazole and its composites with inorganic proton conductors," J. Membr. Sci., 226(1-2), pp. 169-184.
[49] Qian, G., and Benicewicz, B. C., 2009, "Synthesis and Characterization of High Molecular Weight Hexafluoroisopropylidene-Containing Polybenzimidazole for High-Temperature Polymer Electrolyte Membrane Fuel Cells," J. Polym. Sci., Part A, 47(16), pp. 4064-4073.
[50] Yu, S., and Benicewicz, B. C., 2009, "Synthesis and Properties of Functionalized Polybenzimidazoles for High-Temperature PEMFCs," Macromolecules, 42(22), pp. 8640-8648.
[51] Scanlon, E., 2005, "Polybenzimidazole Based Segmented Block Copolymers for High Temperature Fuel Cell Applications," Ph.D. Thesis, Rensselaer Polytechnic Institute, Troy, NY.
[52] Schmidt, T. J., 2006, "Durability and degradation in high-temparature polymer electrolyte fuel cells," ECS Transactions, 1(8), pp. 19-31.
[53] Schmidt, T. J., 2009, "High-Temperature Polymer Electrolyte Fuel Cells: Durability Insights," Polymer Electrolyte Fuel Cell Durability, F. N. Buchi, M. Inaba, and T. J. Schmidt, eds., Springer, New York, pp. 199-221.
[54] Ross Jr., P. N., 1987, Deactivation and poisoning of fuel cell catalysts, Marcel Dekker, New York.
[55] Ferreira, P. J., la O', G. J., Shao-Horn, Y., Morgan, D., Makharia, R., Kocha, S., and Gasteiger, H. A., 2005, "Instability of Pt/C electrocatalysts in proton exchange membrane fuel cells: A mechanistic investigation," J. Electrochem Soc, 152(11), pp. A2256-A2271.
[56] Tang, L., Han, B., Persson, K., Friesen, C., He, T., Sieradzki, K., and Ceder, G., 2010, "Electrochemical Stability of Nanometer-Scale Pt Particles in Acidic Environments," J. Am. Chem. Soc., 132(2), pp. 596-600.
[57] Liu, G., Zhang, H., Zhai, Y., Zhang, Y., Xu, D., and Shao, Z.-g., 2007, "Pt_4ZrO_2/C cathode catalyst for improved durability in high temperature PEMFC based on H_3PO_4 doped PBI," Electrochem. Commun., 9(1), pp. 135-141.

[58] Landsman, D. A., and Luczak, F. J., 2003, Handbook of Fuel Cells - Fundamentals, Technology and Applications, W. Vielstich, A. Lamm, and H. Gasteiger, eds., John Wiley & Sons, Chicester, U.K., pp. 811-831.
[59] Neyerlin, K. C., Singh, A., and Chu, D., 2008, "Kinetic characterization of a Pt-Ni/C catalyst with a phosphoric acid doped PBI membrane in a proton exchange membrane fuel cell," J. of Power Sources, 176(1), pp. 112-117.
[60] Schmidt, T. J., and Baurmeister, J., 2008, "Properties of high-temperature PEFC Celtec-P 1000 MEAs in start/stop operation mode," J. of Power Sources, 176(2), pp. 428-434.
[61] Luczak, F. J., and Landsman, D. A., 1984, "Ordered Ternary Fuel Cell Catalysts Containing Platinum, Cobalt and Chromium."
[62] Luczak, F. J., and Landsman, D. A., 1987, "Ordered Ternary Fuel Cell Catalysts Containing Platinum and Cobalt and Method for Making the Catalyst."
[63] Beard, B., and Ross Jr., P. N., 1990, "The structure and activity of platinum-cobalt alloys as oxygen reduction electrocatalysts," J. Electrochem Soc, 137(11), pp. 3368-3374.
[64] Glass, J. T., Cahen, G. L., and Stoner, G. E., 1987, "The effect of metallurgical variables on the electrocatalytic properties of platinum-chromium alloys," J. Electrochem Soc, 134(1), pp. 58-65.
[65] Mukerjee, S., and Srinivasan, S., 1993, "Enhanced electrocatalysis of oxygen reduction on platinum alloys in proton exchange membrane fuel cells," J. Electroanal. Chem., 357(1-2), pp. 201-224.
[66] Mukerjee, S., Srinivasan, S., and Soriaga, M. P., 1995, "Role of structural and electronic properties of Pt and Pt alloys on electrocatalysis of oxygen reduction. An in situ XANES and EXAFS investigation.," J. Electrochem Soc, 142(5), pp. 1409-1422.
[67] Paulus, U. A., Scherer, G. G., Wokaun, A., Schmidt, T. J., Stamenkovic, V., Radmilovic, V., Markovic, N. M., and Ross, P. N., 2002, "Oxygen Reduction on Carbon-Supported Pt-Ni and Pt-Co Alloy Catalysts," J. Phys. Chem. B, 106(16), pp. 4181-4191.
[68] Stamenkovic, V., Schmidt, T. J., Ross, P. N., and Markovic, N. M., 2002, "Surface Composition Effects in Electrocatalysis: Kinetics of Oxygen Reduction on Well-Defined Pt3Ni and Pt3Co Alloy Surfaces," J. Phys. Chem. B, 106(46), pp. 11970-11979.
[69] Stamenkovic, V., Fowler, B., Mun, B. S., Wang, B., Ross, P. N., Lucas, C. A., and Markovic, N. M., 2007, "Improved Oxygen Reduction Activity on Pt3Ni(111) via Increased Surface Site Availability," Science, 315(5811), pp. 493-497.
[70] Parrondo, J., Mijangos, F., and Rambabu, B., 2010, "Platinum/tin oxide/carbon cathode catalyst for high temperature PEM fuel cell," J. Power Sources, 195(13), pp. 3977-3983.
[71] Qian, G., 2008, "Fluorine-containing Polybenzimidazoles for High Temperature Polymer Electrolyte Membrane Fuel Cell Applications," Ph.D. Thesis, Rensselaer Polytechnic Institute, Troy, NY.
[72] Gasteiger, H., and Markovic, N. M., 2009, "Just a dream - or future reality?," Science, 324(5923), pp. 48-49.

[73] Debe, M. K., Schmoeckel, A. K., Vernstrom, G. D., and Atanasoski, R., 2006, "High voltage stability of nanostructured thin film catalysts for PEM fuel cells," J. Power Sources, 161(2), pp. 1002-1011.
[74] Strasser, P., 2009, Handbook of Fuel Cells: Advances in Electrocatalysis, Materials, Diagnostics, and Durability, W. Vielstich, H. Yokokawa, and H. A. Gasteiger, eds., John Wiley & Sons, New York, pp. 30-47.
[75] Lefevre, M., Proietti, E., Jaouen, F., and Dodelet, J.-P., 2009, "Iron-Based Catalysts with Improved Oxygen Reduction Activity in Polymer Electrolyte Fuel Cells," Science, 324(5923), pp. 71-74.
[76] Remick, R. J., Wheeler, D. J., and Singh, P., 2010, "MCFC and PAFC R&D Workshop Summary Report. US Department of Energy.."
[77] Yu, S., Xiao, L., and Benicewicz, B. C., 2008, "Durability Studies of PBI-based High Temperature PEMFC," Fuel Cells, 8(3-4), pp. 165-174.
[78] Okae, I., Kato, S., Seya, A., and Kamoshita, T., 1990, "Study of the Phosphoric Acid Management in PAFCs," The Chemical Society of Japan 67th Spring Meeting.
[79] 2005, "Manufacturing for the Hydrogen Economy: Manufacturing Research and Development of PEM Fuel Cell Systems for Transportation Application," U.S. Department of Energy, Washington, D.C.
[80] 2009, "Hydrogen Fuel Cell Vehicle and Station Deployment Plan: A Strategy for Meeting the Challenge Ahead," California Fuel Cell Partnership, West Sacramento, CA.
[81] Feitelberg, A. S., Stathopoulos, J., Qi, Z., Smith, C., and Elter, J. F., 2005, "Reliability of Plug Power GenSys fuel cell systems," J. Power Sources, 147(1-2), pp. 203-207.
[82] Schmidt, T. J., and Baurmeister, J., 2006, "Durability and Reliability in High Temperature Reformed Hydrogen PEFCs," ECS Transactions, 3(1), pp. 861-869.
[83] Mocoteguy, P., Ludwig, B., Scholta, J., Barrera, R., and Ginocchio, S., 2009, "Long Term Testing in Continuous Mode of HT-PEMFC Based H3PO4/PBI Celtec-P MEAs for u-CHP Applications," Fuel Cells, 9(4), pp. 325-348.
[84] Mocoteguy, P., Ludwig, B., Scholta, J., Nedellec, Y., Jones, D. J., and Roziere, J., 2010, "Long-Term Testing in Dynamic Mode of HT-PEMFC H3PO4/PBI Celtec-P Based Membrane Electrode Assemblies for Micro-CHP Applications," Fuel Cells, 10(2), pp. 299-311.
[85] Garsany, Y., Gould, B. D., Baturina, O. A., and Swider-Lyons, K. E., 2009, "Comparison of the Sulfur Poisoning of PBI and Nafion PEMFC Cathodes," Electrochemical and Solid-State Letters, 12(9), pp. B138-B140.
[86] Schmidt, T. J., and Baurmeister, J., 2008, "Development Status of PBI based High-Temperature Membrane Electrode Assemblies," ECS Transactions, 16(2), pp. 263-270.
[87] Reiser, C. A., Bregoli, L., Patterson, T. W., Yi, J. S., Yang, J. D., Perry, M. L., and Jarvi, T. D., 2005, "A Reverse-Current Decay Mechanism for Fuel Cells," Electrochem. Sol. Let., 8(6), pp. A273-A276.
[88] Puffer Jr., R. H., and Rock, S. J., 2009, "Recent Advances in High Temperature Proton Exchange Membrane Fuel Cell Manufacturing," J. of Fuel Cell Sci. and Tech., 6(4), pp. 041013/041011-041013/041017.

[89] Puffer Jr., R. H., and Hoppes, G. H., 2004, "Development of a Flexible Pilot High Temperature MEA Manufacturing Line," Fuel Cell Science, Engineering and Technology--2004, pp. 573-579.
[90] Harris, T. A. L., and Walczyk, D., 2006, "Development of a Casting Technique for Membrane Material Used in High-Temperature PEM Fuel Cells," Journal of Manufacturing Processes, 8(1), pp. 19-31.
[91] Hake, J.-F., Birnbaum, U., Haines, M., and Linssen, J., 2008, "Reduction of greenhouse gas emissions through fuel cell combined heat and power applications," 17th World Hydrogen Energy ConferenceBrisbane, Australia.
[92] Schmidtz, R., 2009, "Japan Working Toward Fuel-Cell Reality," Marketplace, p. 1.
[93] 2010, "Celtec MEAs: Membrane Electrode Assemblies for High Temperature PEM Fuel Cells," BASF Fuel Cell GmbH.
[94] 2009, "High-Temperature Fuel Cell System for Residential Applications," Plug Power, Latham, NY.
[95] 2010, "Serenus 166/390 Air C v2.5," Serenergy, Hobro, Denmark.
[96] 2009, "ClearEdge Power, Delivering Smart Energy Today," http://www.clearedgepower.com/.
[97] 2009, "Emissions of Greenhouse Gases Report," U.S. Energy Information Administration, Washington, DC.
[98] Barry, K., 2010, "A Hydrogen Highway for the East Coast," Wired.com.
[99] English, A., 2008, "Driving VW's fuel-cell prototypes," Telegraph.co.uk, Telegraph Media Group Limited.
[100] Dec. 2009, "Innovative Danish technology uses methanol to make fuel cell vehicles competitive," renewableenergyfocus.com.
[101] 2009, "DLR Motor Glider Antares Takes Off in Hamburg - Powered by a Fuel Cell," German Aerospace Center.
[102] Smock, D., Sept. 18, 2009, "What's Next after the Dreamliner? Think Fuel Cells," Design News.
[103] 2008, "UltraCell XX25: Mobile Power for Mobile Applications," Ultracell, Livermore, CA.
[104] 2008, "UltraCell XX55: Extreme Mobile Power for Demanding Applications," Ultracell, Livermore, CA.
[105] 2010, "Serenus Methanol fuel cell module - 350W," Serenergy, Hobro, Denmark.
[106] Maget, H. J. R., Jan. 13,1970, "Process for Gas Purification, U.S. Patent 3489670."
[107] McElroy, J. F., Aug. 1989, "SPE regenerative hydrogen / oxygen fuel cells for extraterrestrial surface applications," Energy Conversion Engineering Conference, IEEE, Washington, DC, USA, pp. 1631-1636.
[108] Rohland, B., Eberle, K., Strobel, R., Scholta, J., and Garche, J., 1998, "Electrochemical Hydrogen Compressor," Electrochem. Acta., 43(24), p. 3841.
[109] Perry, K. A., Eisman, G. A., and Benicewicz, B. C., 2008, "Electrochemical hydrogen pumping using a high-temperature polybenzimidazole (PBI) membrane," J. Power Sources, 177(2), pp. 478-484.
[110] Steele B. C. H., and Heinzel A., 2001, "Materials for Fuel-Cell Technologies," Nature, **414**, pp. 345-352.

[111] Dunwoody D., and Leddy J., 2005, "Proton Exhange Membranes: The View Forward and Back," The Electrochemical Society Interface, **3**, pp. 37–39.
[112] Vogel H. A., and Marvel C. S., 1961, "Polybenzimidazoles, New Thermally Stable Polymers," J. Polym. Sci., **50**, p. 511-539.
[113] Vogel H. A., and Marvel C. S., 1963, "Polybenzimidazoles. II," J. Polym. Sci., Part A1, **1**, pp. 1531-1541.
[114] Li Q., He R., Gao J., Jensen O. J., and Bjerrum N. J., 2003, "The CO Poisoning Effect in PEMFCs Operational at Temperatures up to 200C," J. Electrochem. Soc., **150**(12), pp. A1599–A1605.
[115] Zhai Y., Zhang H., Liu G., Hu J., and Yi B., 2006, "Performance degradation studies on PBI/H3PO4 high temperature PEMFC and one-dimensional numerical analysis," J. Electrochem. Acta., **52**(2), pp. 394–401.
[116] Li Q., Hjuler H. A., and Bjerrum N. J., 2001, "Phosphoric acid doped polybenzimidazole membranes: physiochemical characterization and fuel cell applications," J. Appl. Electrochem., **31**(7), pp. 773–779.
[117] Flory P. J., 1974, "Introductory Lecture," Faraday Discuss. Chem. Soc., **57**, pp. 7–18.
[118] Molleo M., Schmidt T. J., and Benicewicz B. C., 2012, "Polybenzimidazole-Phosphoric Acid (PBI-PA)-Based Fuel Cells," Encyclopedia of Sustainability, Science and Technology, pp. 391–431.
[119] U.S. Dept. of Energy, 2011, An Integrated Strategic Plan for the Research, Development, and Demonstration of Hydrogen and Fuel Cell Technologies. Available at http://www1.eere.energy.gov/hydrogenandfuelcells/pdfs/program_plan2011.pdf
[120] Suvorov A., Elter J., Staudt R., Hamm R., Tudryn G., Schadler L., and Eisman G., 2008, "Stress Relaxation of PBI Based Membrane Electrode Assemblies," International Journal of Solids and Structures, **45**(24), pp. 5987–6000.
[121] Patankar K. A., Dillard D. A., Case S. W., Ellis M. W., Lai Y.-H., and Gittleman C. S., 2012, "Linear Hygrothermal Viscoelastic Characterization of Nafion NRE 211 Proton ExchangeMembrane," Fuel Cells, **12**(5), pp. 787–799.
[122] Lai Y.-H., Mittelsteadt C. K., Gittleman C. S., and Dillard D. A., 2009, "Viscoelastic Stress Analysis of Constrained Proton Exchange Membranes Under Humidity Cycling," J.Fuel Cell Sci. Technol., **6**(2), pp. 021002/1 – 021002/13.
[123] Li Y., Dillard D. A., Case S. W., Ellis M. W., Lai Y.-H., Gittleman C. S., and Miller D. P., 2009, "Fatigue and creep to leak tests of proton exchange membranes using pressure-loaded blisters," J. Power Sources, **194**(2), pp. 873–879.
[124] Ferry J. D., 1980, Viscoelastic Properties of Polymers, 3rd Ed., John Wiley & Sons, New York.
[125] 1999, "Standard Methods for the Examination of Water and Wastewater: 4500-P Phosphorus," pp. 1–24 [Online]. Available: http://www.umass.edu/tei/mwwp/acrobat/sm4500P-E.PDF.
[126] Savinell R. F., Wainright J. S., and Litt M. H., 1998, "High Temperature Polymer Electrolyte Fuel Cells," Proc. Electrochem. Soc, **98-27**, pp. 81–90.

[127] Molleo M., Chen X., Ploehn H., and Benicewicz B. C., 2013, "High Polymer Content 3,5-Pyridine-Polybenzimidazole Copolymer Membranes with Improved Compressive Properties," In Process.
[128] Appleby A. J., and Foulkes F. R., "Materials Engineering for Solid Oxide Fuel Cell Technology," Fuel Cell Handbook 1989, Van Nostrand Reinhold, New York.
[129] Li Q., He E., Jensen J. O., and Bjerrum N. J., 2003, "Approaches and Recent Development of Polymer Electrolyte Membranes for Fuel Cells Operating above 100°C" Chem. Mater., **15**, pp. 4896–4915.
[130] Li Q., He R., Jensen J. O., and Bjerrum N. J., 2004, "PBI-based polymer membranes for high temperature fuel cells - preparation, characterization and fuel cell demonstration," Fuel Cells, **4**(3), pp. 147–159.
[131] Pan C., He R., Li Q., Jensen J. O., Bjerrum N. J., and Hjulmand H. A., 2005, "Integration of High Temperature PEM Fuel Cells with a Methanol Reformer," J. Power Sources, **145**(2), pp. 392–398.
[132] Wang J. T., Savinell R. F., Wainright J., Litt M., and Yu H., 1996, "A H_2/O_2 Fuel Cell Using Acid Doped Polybenzimidazole as Polymer Electrolyte," Electrochem. Acta., **41**(2), pp. 193–197.
[133] Molleo M., Chen X., Ploehn H. J., and Benicewicz B. C., 2013, "High Polymer Content 2,5-Pyridine-Polybenzimidazole Copolymer Membranes with Improved Compressive Properties," In Process.
[134] Wavefunction, Inc., "Spartan'10." Irvine, CA.
[135] Linnell R., 1960, "Dissociation Constants of 2-Substituted Pyridines," J. Org. Chem, **25**(2), pp. 290-290.
[136] Padmanabhan V., and Kumar S. K., 2011, "Gelation in Semiflexible Polymers," J. Chem. Phys., **134**(17), p. 174902/1 –174902/7.
[137] Padmanabhan V., Kumar S. K., and Yethiraj A., 2008, "Phase Behavior of Semiflexible Polymer Chains," J. Chem. Phys, **128**(12), pp. 124908/1-124908/4.
[138] Jin Y. C., Nishida M., Kanematsu W., and Hibino T., 2011, "An H_3PO_4-doped polybenzimidazole/Sn0.95Al0.05P_2O_7 composite membrane for high-temperature proton exchange membrane fuel cells," J. Power Sources2, **196**(15), pp. 6042–6047.
[139] Anis A., and Al-Zahrani S. M., 2012, "Sulfonated PVA/PBI based crosslinked composites towards anhydrous proton conductive polymer electrolyte membranes for fuel cells," Int. J. of Electrochem. Sci., **7**(10), pp. 9174–9185.
[140] Li Q., Pan C., Jensen J. O., Noye P., and Bjerrum N. J., 2007, "Cross-Linked Polybenzimidazole Membranes for Fuel Cells," Chem. Mater.2, **19**(3), pp. 350–352.
[141] Kerres J., Schoenberger F., Chromik A., Haering T., Li Q., Jensen J. O., Pan C., Noye P., and Bjerrum N. J., 2008, "Partially fluorinated arylene polyethers and their ternary blend membranes with PBI and H3PO4. Part I. Synthesis and characterisation of polymers and binary blend membranes," Fuel Cells, **8**(3-4), pp. 175–187.
[142] Berrada M., Anbaoui Z., Lajrhed N., and Knouzi N., 1997, "Synthesis, Characterization, and Studies of Heat-Resistant Poly(ether benzimidazole)s," Chem. Mater., **9**(9), pp. 1989–1993.

[143] Savall B. M., Fontimayor J. R., and Edwards J. P., 2009, "Selective phenol alkylation for an improved synthesis of 2-arylbenzimidazole H4 receptor ligands," Tetrahedron Letters, **50**(21), pp. 2490–2492.
[144] Connell J. W., Hergenrother P. M., and Smith J. G., 1995, "Polybenzimidazoles via Aromatic Nucleophilic Displacement." US Patent 5412059.
[145] Connell J. W., Hergenrother P. M., and Smith J. G., 1997, "Polybenzimidazoles via Aromatic Nucleophilic Displacement." US Patent 5637670.
[146] Leikin A. Y., Rusanov A. L., Begunov R. S., and Fomenkov A. I., 2009, "Synthesis and Properties of Poly[2(4'oxyphenylene)5benzimidazole] and a ProtonExchange Membrane Produced on Its Basis," Polym. Sci. Series C, **51**(7), pp. 12–16.
[147] Sinigersky V., Budurova D., Penchev H., Ublekov F., and Radev I., 2013, "Polybenzimidazole-graft-polyvinylphosphonic acid—proton conducting fuel cell membranes," J. Appl. Polym. Sci., **129**(3), pp. 1223–1231.
[148] Sukumar P., Uw W., Markova D., Unsal O., Klapper M., and Mullen K., 2007, "Functionalized Poly(benzimidazole)s as Membrane Materials for Fuel Cells," Macro. Chem. and Phys., **208**(19-20), pp. 2258–2267.
[149] Bauer S., and Stock N., 2007, "Synthesis and characterization of four new metal 5-phosphonoisophthalates discovered by high-throughput experimentation," J. Solid State Chem., **180**(11), pp. 3111–3120.
[150] Liao T.-B., Ling Y., Chen Z.-X., Zhou Y.-M., and Weng L.-H., 2010, "A rutile-type porous zinc(II)-phosphonocarboxylate framework: local proton transfer and size-selected catalysis," Chem. Comm., **46**, pp. 1100–1102.
[151] Santschi N., Geissbuhler P., and Togni A., 2012, "Reactivity of an electrophilic hypervalent iodine trifluoromethylation reagent with hydrogen phosphates-A mechanistic study," J. Fluorine Chem., **135**, pp. 83–86.
[152] Branion S., and Benin V., 2007, "Preparation of Some Substituted Terephthalic Acids," Synth. Comm., **36**(15), pp. 2121–2127.